Technical Report Documentation Page

1. Report No.	2. Government Accession No.	3. Recipient's Catalog No.
FHWA/TX-95+1175-7F		

4. Title and Subtitle	5. Report Date
Evaluation of Flexible Pavements and Subgrades Using the Spectral-Analysis-of-Surface-Waves (SASW) Method	August 1993
	6. Performing Organization Code
7. Author(s)	8. Performing Organization Report No.
Marwan Fouad Aouad, Kenneth H. Stokoe, II, and Jose M. Roesset	Research Report 1175-7F
9. Performing Organization Name and Address	10. Work Unit No. (TRAIS)
Center for Transportation Research The University of Texas at Austin 3208 Red River, Suite 200 Austin, Texas 78705-2650	11. Contract or Grant No. Research Study 2/3-18-88/1-1175
	13. Type of Report and Period Covered
12. Sponsoring Agency Name and Address	Final
Texas Department of Transportation Research and Technology Transfer Office P. O. Box 5051 Austin, Texas 78763-5051	14. Sponsoring Agency Code

15. Supplementary Notes

Study conducted in cooperation with the U.S. Department of Transportation, Federal Highway Administration. Research study title: "Development of Dynamic Analysis Techniques for Falling Weight Deflectomer Data"

16. Abstract

In this research study, Spectral-Analysis-of-Surface Waves (SASW), Falling Weight Deflectometer (FWD), and compression wave (P-wave) tests were employed at flexible pavement sites at the Texas Transportation Institute's (Texas A&M University) test facility in Bryan, Texas, at a newly constructed site on Loop 1 in Austin, Texas, and at pavement sites in Districts 1, 8, 11, and 21 in Texas. The objective was to improve field testing capabilities in relation to testing flexible pavement systems, and to compare SASW results with other in-situ techniques, including the FWD method. The elements primarily investigated included the selection and performance of high-frequency sources and receivers on asphalt concrete (AC) pavements, the effect of temperature and frequency on SASW and FWD measurements of AC pavements, and the effect of shallow depth to bedrock on the backcalculated moduli of the subgrade layer from each method.

17. Key Words	18. Distribution Statement
Spectral-Analysis-of-Surface-Waves tests, Falling Weight Deflectomer, nondestructive testing, pavement testing	No restrictions. This document is available to the public through the National Technical Information Service, Springfield, Virginia 22161.

19. Security Classif. (of this report)	20. Security Classif. (of this page)	21. No. of Pages	22. Price
Unclassified	Unclassified	283	

EVALUATION OF FLEXIBLE PAVEMENTS AND SUBGRADES USING THE SPECTRAL-ANALYSIS-OF-SURFACE-WAVES (SASW) METHOD

by

Marwan F. Aouad
Kenneth H. Stokoe, II
Jose M. Roesset

Research Report 1175-7F

Research Project 2/3-18-88/1-1175
Development of Dynamic Analysis Techniques for Falling Weight Deflectometer Data

conducted for the

Texas Department of Transportation

in cooperation with the
U.S. Department of Transportation
Federal Highway Administration

by the

CENTER FOR TRANSPORTATION RESEARCH
Bureau of Engineering Research
The University of Texas at Austin

August 1993

IMPLEMENTATION STATEMENT

As the need for more cost-effective pavement designs increases and as the need to monitor the performance of pavements increases, the degree of accuracy in estimating and measuring the properties of the pavement materials increases. In-situ seismic testing has the potential to improve our knowledge of the stiffnesses of the surface, base and subgrade layers used in designing and monitoring pavement systems. Spectral-Analysis-of-Surface-Wave (SASW) testing has been shown to be well suited for the seismic testing of flexible pavements. Piezoelectric sources can be used to implement this testing technique. A frequency adjustment curve is presented which can be used to relate SASW- and (Falling Weight Deflectometer) FWD-determined moduli of asphalt concrete (AC) surface layers. A strain adjustment factor is also presented which can be used to relate subgrade moduli determined by SASW and FWD testing of flexible pavements. Finally, simplified procedures for finding the depth to bedrock and the subgrade moduli from SASW testing of flexible pavements are proposed for implementation.

Prepared in cooperation with the Texas Department of Transportation and
the U.S. Department of Transportation, Federal Highway Administration

DISCLAIMERS

Kenneth H. Stokoe, II (Texas No. 49905)
Research Supervisor

PREFACE

Project 1175 is a joint project between the Center for Transportation Research at The University of Texas at Austin and the Texas Transportation Institute of Texas A&M University. The project is concerned with the investigation of the application of the Falling Weight Deflectometer (FWD) to various types of roads in order: 1) to determine the elastic moduli of the pavement, base and subgrade; 2) to determine optimum ways to use the equipment and interpret the experimental data; and 3) to explore other techniques which could complement the Falling Weight Deflectometer and enhance the reliability of the results. This work builds on Project 1123, where the effect of the finite width of the pavement and the position of the equipment with respect to the edge was investigated and the results obtained with the Falling Weight Deflectometer were compared to those which can be obtained using the Spectral-Analysis-of-Surface-Waves (SASW) method. This report is the fifth of five reports from the Center for Transportation Research. In this report, an experimental investigation of parameters affecting SASW testing of asphalt concrete pavements is presented, along with correlations between SASW and FWD results from 24 flexible pavement sites around the state of Texas. Mr. Bob Briggs was the supervisor of the effort at the Texas State Department of Highways and Public Transportation (now the Texas Department of Transportation).

LIST OF REPORTS

(Note: Report Nos. 1175-1 and 1175-2 have been submitted through the Texas Transportation Institute of Texas A&M University on their part of the joint Project 1175. The reports listed below are the reports submitted through the Center for Transportation Research at The University of Texas at Austin.)

Report No. 1175-3, "Nonlinear Effects on Dynamic Response of Pavements Using Non Destructive Testing Techniques," by Der-Wen Chang, Jose M. Roesset, and Kenneth H. Stokoe, II, presents the results of analytical studies to assess the occurrence and potential importance of nonlinear material behavior in a pavement system under the impact resulting from application of the Falling Weight Deflectometer.

Report No. 1175-4, "Analytical Study and Inversion for the Spectral Analysis of Surface Waves Method," by Rafael Foinquinos Mera, Jose M. Roesset, and Kenneth H. Stokoe, II, presents the results of analytical studies comparing two different

procedures to determine the dynamic displacements caused by an impact load acting on the surface of a pavement and proposes a semi-automated inversion procedure to backfigure the elastic moduli of the pavement, base and subgrade from the dispersion curves.

Report No. 1175-5, "Effect of Depth to Bedrock on the Accuracy of Backcalculated Moduli Obtained with Dynaflect and FWD Tests," by Chia-Ray Seng, Kenneth H. Stokoe, II, and Jose M. Roesset, presents the results of analytical studies in which the importance of depth to bedrock on the backcalculated moduli from Dynaflect and Falling Weight Deflectometer (FWD) tests was evaluated using four typical in-service Texas highway pavement profiles.

Report No. 1175-6, "Development of An In-Situ Method for Continuous Evaluation of the Resilient Modulus of Pavement Subgrade," by Michael P. Rits, Kenneth H. Stokoe, II, and Jose M. Roesset, presents the results of a field experiment in which geophones embedded in the subgrade of an in-service pavement are used to evaluate the resilient modulus of the subgrade at various times during the life of the pavement.

Report No. 1175-7F, "Evaluation of Flexible Pavements and Subgrades Using the Spectral-Analysis-of-Surface-Wave (SASW) Method," by Marwan Aouad, Kenneth H. Stokoe, II, and Jose M. Roesset, presents the results of field experiments to evaluate the applicability of the SASW method to testing flexible pavements and to compare the method with other in-situ techniques, in particular the FWD method, where different frequencies are involved in the measurements.

ABSTRACT

An experimental investigation was undertaken to determine the material properties of asphalt concrete (AC) pavement systems, including the AC surface layer, base and subgrade. The Spectral-Analysis-of-Surface-Waves (SASW) method was the primary field method used in testing. This method is a seismic method which is based on the measurement of surface waves, which can be generated and sensed with instrumentation placed solely on the pavement surface. The objectives of this study included the investigation of the following aspects in relation to the SASW method. First, a variety of surface sources and receivers was studied in the field. The performance of each component was evaluated under various climatic and pavement conditions. The importance of the sources and receivers in SASW testing is that they should be carefully selected according to their frequency range to adequately characterize the material properties of the system.

Second, an experimental program at the test facility of the Texas Transportation Institute (TTI) in Bryan, Texas, was employed to study the effect of some parameters on SASW measurements. Parameters such as the temperature and thickness of the surface layer and the frequency content of the surface wave were studied. At high temperatures (temperatures above 140° F), results showed that energy could not be generated at high frequencies (frequencies above 15 kHz) due to the viscous nature of the AC surface layer. As a result, only thick surface layers (thickness, $H \geq 5$ in. (12.7 cm)) can be measured directly with the SASW method at temperatures as high as 140° F. However, at temperatures lower than about 100° F, AC pavement layers with thicknesses greater than 3 in. (7.6 cm) can easily be evaluated with the SASW method.

Finally, a series of tests was conducted at a newly constructed site in Austin, Texas, and at 24 pavement sites around the state of Texas to understand the effect of the above parameters on the SASW measurements and to correlate moduli determined by the SASW tests with moduli determined with Falling Weight Deflectometer (FWD) tests.

Key words: field testing, seismic measurements, asphalt concrete pavements, SASW testing, FWD testing, subgrades, backcalculated moduli

METRIC (SI*) CONVERSION FACTORS

APPROXIMATE CONVERSIONS TO SI UNITS

Symbol	When You Know	Multiply by	To Find	Symbol
		LENGTH		
in	inches	2.54	centimeters	cm
ft	feet	0.3048	meters	m
yd	yards	0.914	meters	m
mi	miles	1.61	kilometers	km
		AREA		
in^2	square inches	645.2	millimeters squared	mm^2
ft^2	square feet	0.0929	meters squared	m^2
yd^2	square yards	0.836	meters squared	m^2
mi^2	square miles	2.59	kilometers squared	km^2
ac	acres	0.395	hectares	ha
		MASS (weight)		
oz	ounces	28.35	grams	g
lb	pounds	0.454	kilograms	kg
T	short tons (2,000 lb)	0.907	megagrams	Mg
		VOLUME		
fl oz	fluid ounces	29.57	milliliters	mL
gal	gallons	3.785	liters	L
ft^3	cubic feet	0.0328	meters cubed	m^3
yd^3	cubic yards	0.0765	meters cubed	m^3

NOTE: Volumes greater than 1,000 L shall be shown in m^3.

		TEMPERATURE (exact)		
°F	Fahrenheit temperature	5/9 (after subtracting 32)	Celsius temperature	°C

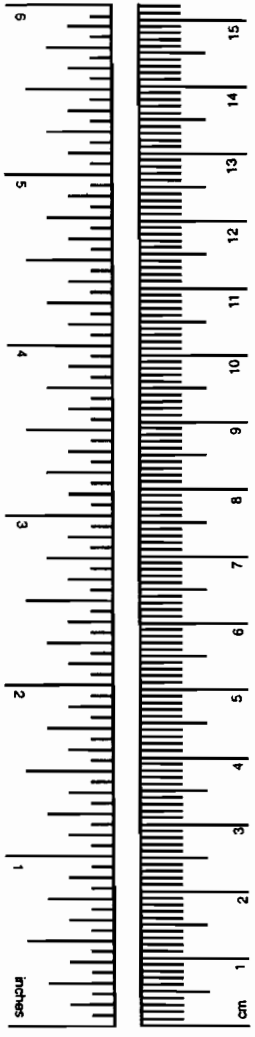

APPROXIMATE CONVERSIONS FROM SI UNITS

Symbol	When You Know	Multiply by	To Find	Symbol
		LENGTH		
mm	millimeters	0.039	inches	in
m	meters	3.28	feet	ft
m	meters	1.09	yards	yd
km	kilometers	0.621	miles	mi
		AREA		
mm^2	millimeters squared	0.0016	square inches	in^2
m^2	meters squared	10.764	square feet	ft^2
m^2	meters squared	1.20	square yards	yd^2
km^2	kilometers squared	0.39	square miles	mi^2
ha	hectares (10,000 m^2)	2.53	acres	ac
		MASS (weight)		
g	grams	0.0353	ounces	oz
kg	kilograms	2.205	pounds	lb
Mg	megagrams (1,000 kg)	1.103	short tons	T
		VOLUME		
mL	milliliters	0.034	fluid ounces	fl oz
L	liters	0.264	gallons	gal
m^3	meters cubed	35.315	cubic feet	ft^3
m^3	meters cubed	1.308	cubic yards	yd^3
		TEMPERATURE (exact)		
°C	Celsius temperature	9/5 (then add 32)	Fahrenheit temperature	°F

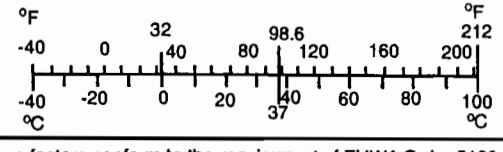

These factors conform to the requirement of FHWA Order 5190.1A.

* SI is the symbol for the International System of Measurements

TABLE OF CONTENTS

LIST OF FIGURES

LIST OF TABLES

SUMMARY

An experimental study dealing with nondestructive testing of flexible pavements was conducted. The test methods of concern were the Spectral-Analysis-of-Surface-Waves (SASW) method, a seismic wave propagation method, and the Falling Weight Deflectometer (FWD) method, a deflection basin method. The thrust of this work revolved around use of these methods as reliable tools to evaluate the stiffnesses of the surface, base, and subgrade layers.

SASW, FWD and compression wave (P-wave) tests were employed at the following flexible pavement sites: 1) the Texas Transportation Institute test facility in Bryan, Texas, 2) a newly constructed site on Loop 1 in Austin, Texas, and 3) 24 pavement sites in Districts 1, 8, 11 and 21 in Texas. The elements which were primarily investigated were: 1) the selection and performance of high-frequency sources and receivers for SASW testing of asphalt concrete (AC) pavements, 2) the effect of temperature and frequency on the SASW and FWD measurements of AC pavements, and 3) the effect of shallow depth to bedrock on the backcalculated moduli of the subgrade layer from each type of test method.

The SASW was found to be sensitive to the variation in stiffness of the AC surface layer. The method can be applied to evaluate the in-place stiffness of the AC layer at selected times during differing climatic conditions. High-frequency sources are required to perform measurements, and piezoelectric sources (V-meter and WR Model F-7 shaker) were found to perform well, especially at elevated pavement temperatures ($T > 80°$ F). The one limitation is that the SASW method can not be used to evaluate the stiffness of thin (thickness < 2 in. (5.1 cm)) AC surface layers. In those cases, it is recommended that compression wave tests be performed to evaluate the stiffnesses of the AC surface layer.

Comparison of Young's moduli (E) of the AC material from SASW and FWD tests in the field and from resonance tests on cylindrical specimens in the laboratory showed that the stiffness of the AC material is frequency (f) dependent. A log(E)-log(f) plot showed a nearly linear relationship between the stiffness of the AC material and the measurement frequency, with the stiffness becoming more frequency dependent at higher temperatures. A potential frequency adjustment curve is proposed. Corrected values of moduli from the SASW tests compare closely to normalized moduli suggested by the AASHTO guide (1986) at temperatures less than 100° F. However, at temperatures above 100° F, the AASHTO guide underestimates the in-place moduli evaluated by the SASW test (correction for frequency). The difference is thought to result from a strain effect which is inherent in the tests used to develop the AASHTO guide.

The subgrade moduli determined from SASW tests are usually higher than those which have been determined from FWD tests. The subgrade moduli from the two techniques compare reasonably well if the moduli are adjusted for the effect of strain (nonlinear effect). The suggested adjustment factor for SASW moduli is equal to 0.75, to represent moduli at a strain of about 0.007% associated with FWD tests, as proposed by Miner (1991).

The depth to bedrock can be predicted from SASW measurements as was the case for measurements on Loop 1 in Austin. The depths to bedrock determined from SASW tests compare reasonably well with the depths determined from the FWD tests using the procedure suggested by Chang (1992) and Seng (1992). However, the depth to bedrock can be determined from the FWD time histories provided the shear wave velocity of the subgrade is known and the FWD time history is recorded for about 200 ms; both of these are not usually the case. As a result, SASW tests can be employed as an independent measurement for predicting the depth to bedrock which is sometimes required in the analysis of FWD data.

Experience gained with SASW testing in this study show that the fundamental mode of vibration is often not the one measured in testing pavements. As a result, it is recommended that a three-dimensional (3-D) model developed by Chang, 1991, and Foinquinos, 1991, be used in the forward modeling of the field measurements to obtain the stiffness profile. The 3-D model takes into account all waves generated during SASW testing, and more realistically models the field setup.

Finally, based on the authors' experience in SASW testing of flexible pavements, a simplified procedure is suggested to obtain the average subgrade stiffness without performing the forward modeling process. In the simplified procedure, the measured wave velocities of the subgrade from receiver spacings of 10, 20 and 30 ft (3, 6.1 and 9.1 m) are averaged and reasonably represent the shear wave velocity of the subgrade layer.

CHAPTER ONE
INTRODUCTION

1.1 General Background

Various types of in-situ tests are used in engineering practice to determine shear modulus profiles of soil sites and Young's modulus profiles of pavement systems. The shear modulus is an important parameter in evaluating the response of foundations under dynamic loadings, in predicting the response of sites under earthquake loadings and in predicting the deformations of many soil and soil-structure systems under working static and cyclic loads. On the other hand, Young's modulus plays an important role in predicting and evaluating the performance of pavement systems under static and repetitive traffic loads.

In-situ methods used to evaluate the shear moduli of geotechnical material are typically based on wave propagation theory. These methods include the crosshole and downhole seismic methods and the newly developed Spectral-Analysis-of-Surface-Waves (SASW) method. For the evaluation of Young's moduli of pavement systems, highway engineers rely on nondestructive techniques so that the integrity of the system under evaluation is preserved. Traditionally, the State Departments of Transportation have adopted the Falling Weight Deflectometer (FWD) as a standard method of determining Young's moduli of the surface, base and subgrade layers. In the last decade, the SASW method has also begun to be used in determining stiffness profiles of pavement systems. This work has shown the SASW test to be a viable tool for testing pavements due to its nondestructive nature and its sound theoretical basis.

The overall goals of this work are: 1) to improve application of the SASW method in pavement evaluations and 2) to develop a framework relating SASW and FWD measurements of flexible pavements.

1.2 Nondestructive Testing of Pavements

In pavement engineering, the FWD and Dynaflect methods are used extensively to determine the modulus of elasticity (Young's modulus) of layered systems. The two methods are based on measuring a deflection basin due to an applied load at the pavement surface. Moduli of the surface, base and subgrade layers are backcalculated using layered linear elastic theory by matching the measured basin with a theoretical one. The following are some of the problems associated with deflection basin methods (Hiltunen and Woods, 1990).

1) Previous knowledge of the thicknesses of the layers is required in the backcalculation procedure (Alexander et al., 1989). Determination of the thicknesses of layers from cores is considered a disadvantage as it makes the methods destructive and increases the costs.

2) Nonlinear behavior is expected in the vicinity of the loaded area in the FWD test when large-magnitude loads are used to simulate the level of strain and stress caused by heavy truck wheels (Nazarian and Stokoe, 1986; Chang et al., 1992). These nonlinearities should be taken into account for a proper interpretation of the data.

3) The presence of shallow bedrock affects the deflection basins measured by the FWD and Dynaflect methods due to the reflection of waves from the rigid boundary. In addition, the applied load is dynamic in nature. The evaluation of the modulus of elasticity assuming an equivalent static load could lead to erroneous results if dynamic effects are not considered in the backcalculation procedure (Mamlouk, 1985; Roesset and Shao, 1985; Chang et al., 1992; Seng, 1992).

4) In the case of thin pavements or the absence of the base layer as can be the case for secondary roads (as Farm-to-Market roads in Texas), the backcalculation procedure is insensitive to the variation of the stiffness of the surface layer. This makes it impossible to determine the stiffness of the surface layer from deflection basin methods in these instances (Rwebangira et al., 1987; Lee et al., 1988).

The drawbacks associated with the deflection basin methods have led to the search for an alternative procedure to nondestructively test pavement systems. The SASW method has proved effective in that regard and has been under development at The University of Texas at Austin for about the past decade.

1.3 Statement of the Problem

The SASW method is a newly developed nondestructive technique for the evaluation of material properties of both pavement and soil sites. The method was introduced at The University of Texas at Austin in the early 1980's by Stokoe and his co-workers (Heisey et al., 1982; Nazarian, 1984). The method is based on the generation and detection of surface seismic waves as illustrated in Fig. 1.1. The waves are generated by an impact applied to the pavement surface. The propagation of these waves past two or more receivers placed on the pavement surface is then measured. One of the strengths of the SASW method is the evaluation of material properties of soils and pavements at small shearing strains ($\gamma < 0.001$ %). At shearing strains smaller than 0.001%, the assumption of linear elastic behavior is realistic in these materials. This is supported by laboratory results obtained from samples subjected to a wide range of loading conditions and stress states. A typical variation of shear modulus with shearing strain is shown in Fig. 1.2 (Stokoe et al., 1980). Thus, by performing SASW measurements, one can eliminate the nonlinear effects associated with large loads in the FWD technique and the difficulty with analyzing the nonlinear results. Another strength of the SASW method is that it provides an estimate of the layer thicknesses which have to be known for the backcalculation procedure in the analysis of the data of the deflection basin methods.

As discussed in Section 1.2, the backcalculation procedure in deflection basin methods is insensitive to the variation in stiffness of the pavement surface layer. On the other hand, the SASW method is very sensitive and easily applied to measuring the surface layer (Nazarian et al., 1983; Roesset et al., 1990). The SASW method was employed as a part of the experimental program herein to characterize the pavement surface layer under different climatic conditions. In

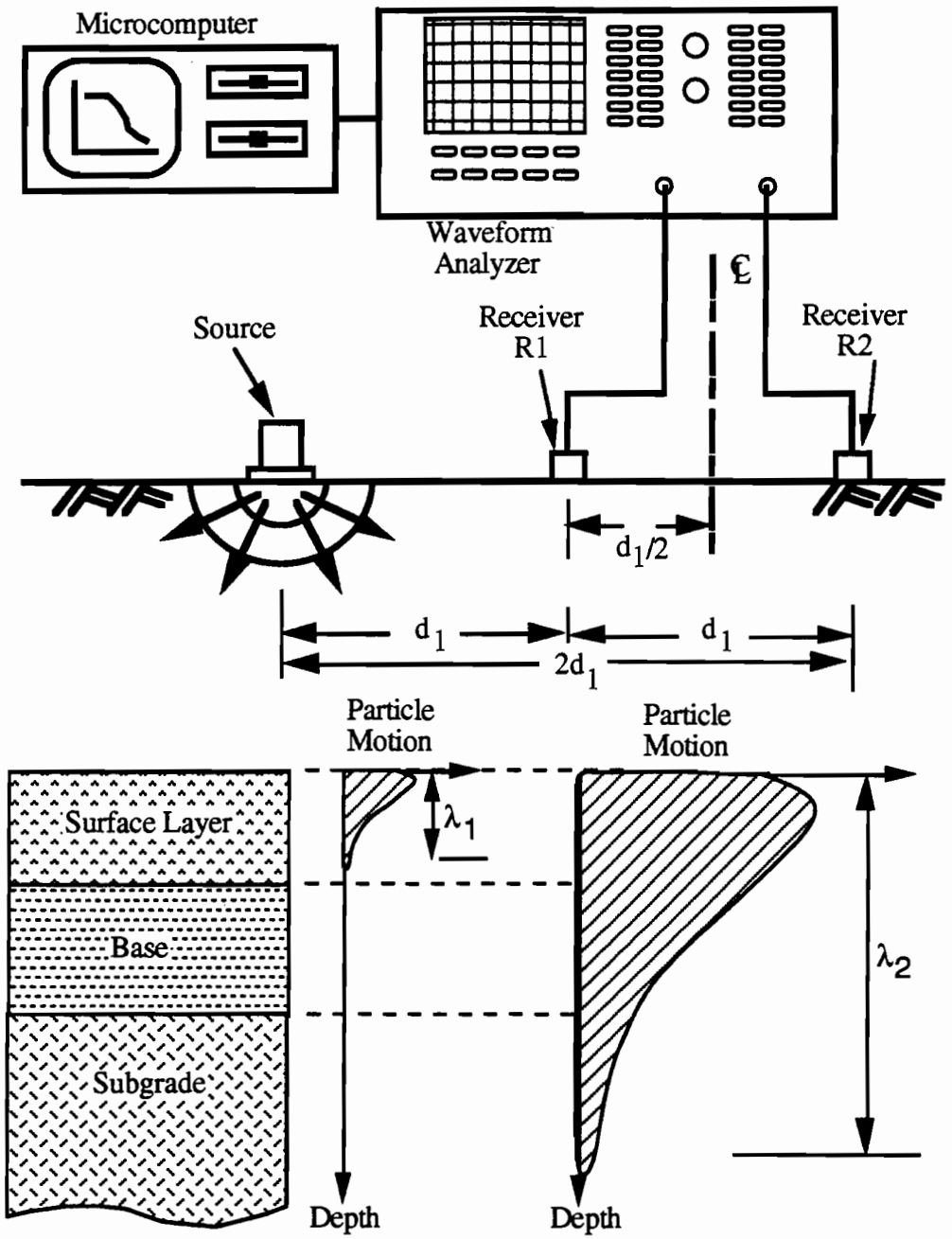

a. Material Profile b. Shorter Wavelength, λ_1 c. Longer Wavelength, λ_2

Fig 1.1. Layout of the In-Situ Instrumentation and Theoretical Features of the Spectral-Analysis-of-Surface-Waves Test.

a. Shear Modulus

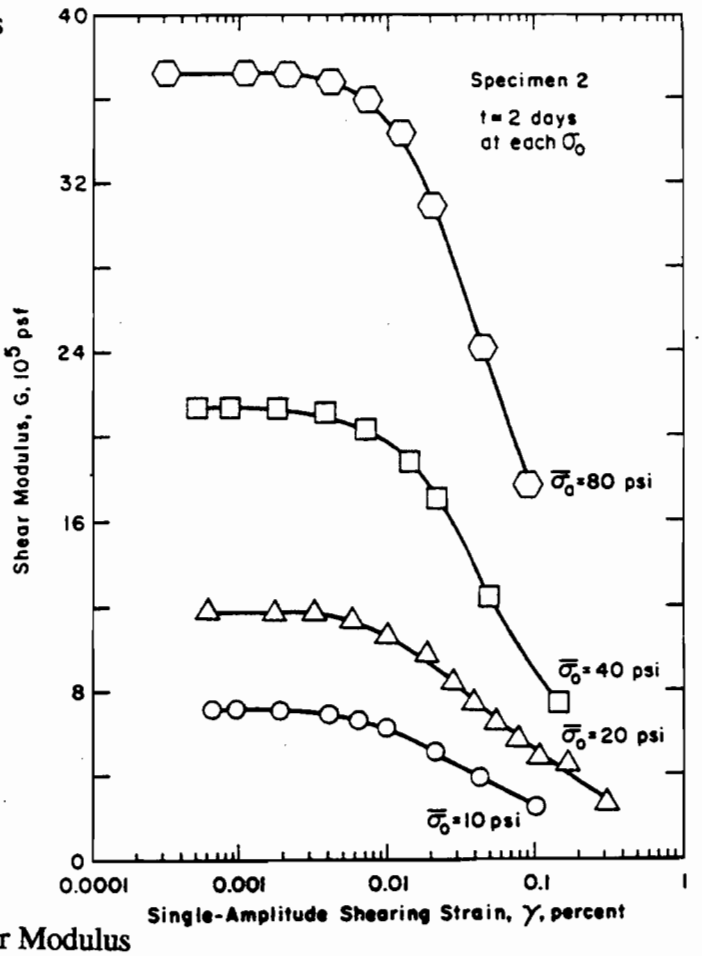

b. Normalized Shear Modulus

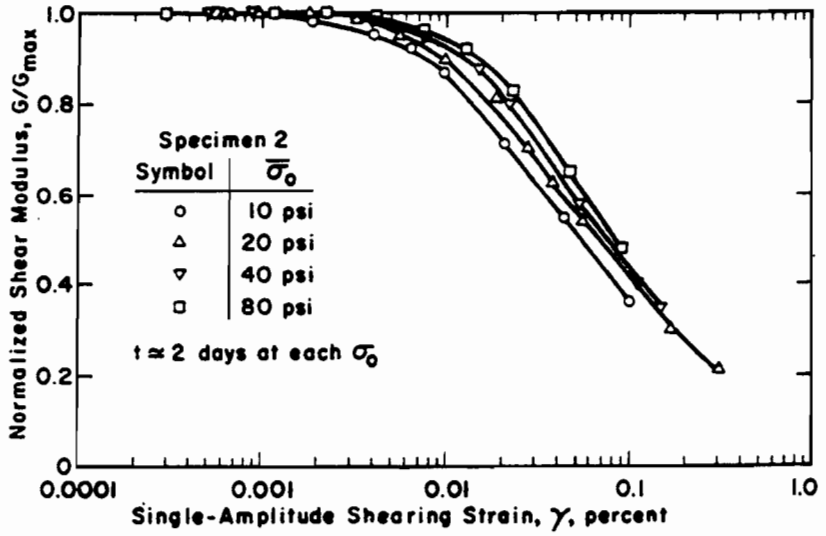

Fig 1.2. Variation in Shear Modulus and Normalized Shear Modulus with Shearing Strain and Effective Confining Pressure (Stokoe et al., 1980).

addition, compressional body wave (P-wave) measurements were performed in conjunction with the SASW measurements in an effort to evaluate the variation of Poisson's ratio of in-place AC materials with temperature. One of the problems encountered with SASW measurements is the high frequency required to sample the top asphalt layer. Typically, impact sources such as small hammers have been used as high frequency sources (Nazarian, 1984). Such sources did not perform adequately for frequencies higher than 15 kHz, especially when the temperature of the surface layer rose above about 27° C (80° F) due to solar warming. Two new sources, the WR Model F-7 shaker and the V-meter, have been employed in the field. Evaluation of the performance of each component is presented.

Values of moduli of pavement materials from SASW measurements were often thought to be high in comparison with moduli obtained by deflection basin methods by many engineers involved in the design and testing of pavements. To understand this discrepancy, the frequency content of measured time signals associated with each technique was studied. Sousa and Monismith (1988) evaluated the variation of the dynamic moduli of AC material with frequency as shown in Fig. 1.3. However, the frequency range used by Sousa and Monismith was from 0.5 Hz to 20 Hz, which was slightly below the 30 Hz dominant frequency in the FWD test and several orders of magnitude below the 5,000 to 25,000 Hz range used in the SASW test. Therefore, the frequency effect on AC material was studied in this research over a wider range of frequencies to cover the high frequencies generated by the SASW testing.

Determination of the depth to bedrock is an essential element in analyzing FWD and Dynaflect data (Chang, 1991; Seng, 1992) if bedrock is within about 18.3 m (60 feet) of the surface. The SASW and the FWD methods were used simultaneously to characterize the material properties of a newly constructed site in Austin, Texas. The site represented an excellent case study in determining the effect of the bedrock depth on measured moduli due to the variation of the thickness of a ramp fill which resulted in bedrock depth varying along the ramp connecting Loop 1 (Mopac Expressway) with Highway 183.

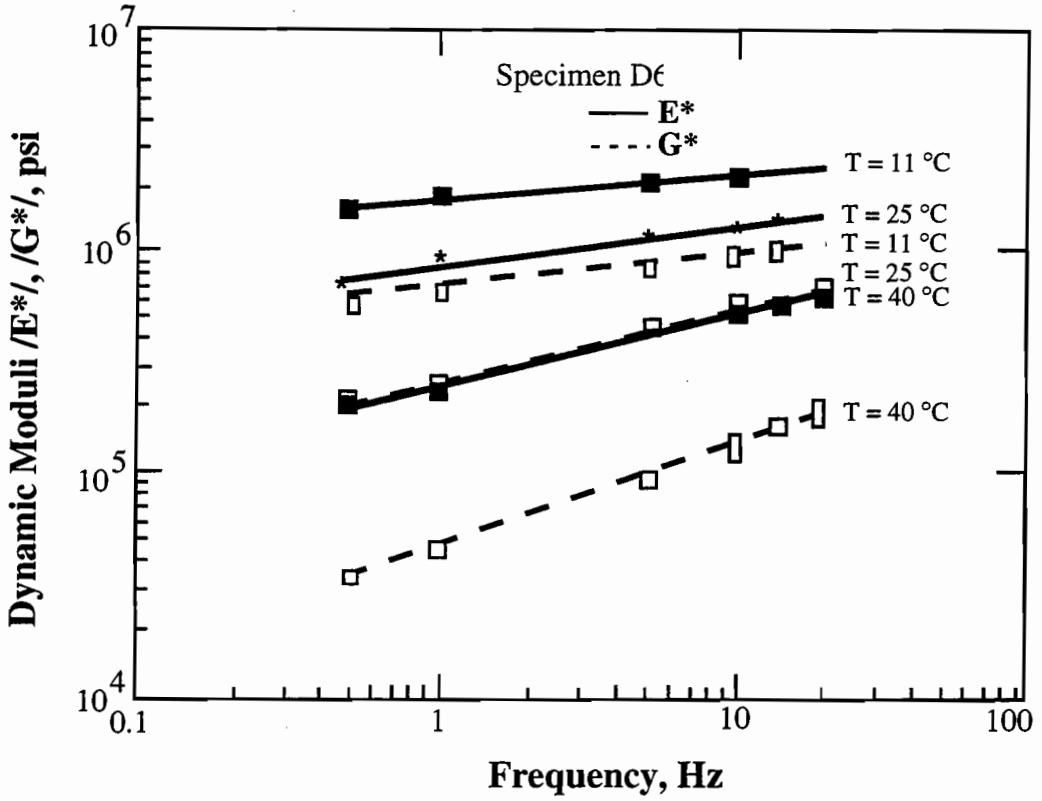

Fig 1.3. Influence of Frequency and Temperature on the Dynamic Moduli of Asphalt Concrete (Sousa and Monismith, 1988).

The ultimate goal of performing SASW measurements on pavement systems is to construct a representative shear wave velocity profile from which shear modulus and Young's modulus profiles can be evaluated. This is done through a forward modeling process in which the field measurements (discussed in Chapter 3) are matched with a theoretical model. The matching process is done by trial-and-error and does not involve apriori knowledge of the layer thicknesses. Two theoretical models were investigated (Chang, 1991; Foinquinos, 1991) in this study. The first one is a simplification of the more comprehensive second model. The second model takes into account all of the types of waves that are generated in SASW testing and represents more realistically the actual setup of an SASW test. The applicability and limitations of each model were investigated in relation to testing pavement systems where the stiffest layer is generally encountered at the surface.

Finally, the SASW method was employed to determine the material properties of pavement sites located in Districts 1, 8, 11 and 21 in the State of Texas. This is a part of a project sponsored by the Texas Department of Transportation. The objective is to evaluate the performance of a variety of nondestructive techniques in determining the material profiles of pavement systems. It should be noted that FWD measurements were performed at these sites by personnel from Texas A&M University, and only the results of their analyses are presented herein for comparison purposes.

1.4 Purpose and Organization

The primary goals of this work were: 1) to develop a better understanding of the SASW method in relation to testing pavement systems, and 2) to investigate the relationship between evaluations of pavement systems by the SASW and FWD methods. These goals were achieved through an experimental program designed to improve the existing capabilities and to identify the limitations associated with the SASW method and through correlations of SASW and FWD measurements.

In Chapter Two, an overview of the most commonly used seismic methods and deflection basin methods to evaluate material stiffnesses is presented. A brief description of wave propagation theory in elastic media is also presented in this chapter so that an appreciation of the measurements involved with seismic methods is developed.

Chapter Three is devoted to a detailed description of the SASW method, since this work deals primarily with SASW measurements on pavement systems. The discussion includes improvements in testing capabilities, mainly in terms of the employment of new sources. The ultimate result of performing SASW measurements is to obtain a shear wave velocity profile (forward modeling). The performance of a 2-D model based on the propagation of plane Rayleigh waves was compared to that of a 3-D model developed by Roesset and his students at The University of Texas. Results from the two models are presented in this chapter along with a discussion of the modeling process.

Chapter Four contains a description of the TTI test facility in Bryan, Texas, and the results obtained from performing SASW measurements at the test facility under various climatic conditions.

Chapter Five includes a presentation of SASW, FWD and crosshole measurements at a newly constructed site in Austin, Texas. Parameters studied at this site included the effect of bedrock depth on the measurements and the effect of frequency on the stiffness of a new asphalt concrete

Chapter Six includes case studies of SASW measurements at pavement sites located in four districts in the State of Texas. This is a part of a project by The Texas Department of Transportation which is designed to investigate the applicability and shortcomings of various nondestructive techniques in evaluating the stiffness profiles under pavement systems for maintenance and rehabilitation purposes.

Chapter Seven provides a summary and the conclusions of this research. It also provides recommendations for future work.

CHAPTER TWO
OVERVIEW OF SEISMIC AND DEFLECTION BASIN METHODS

2.1 Introduction

In-situ techniques are used in engineering practice to characterize material behavior through the determination of material stiffnesses in shear and in compression. In-situ techniques, in relation to testing pavement systems, can be classified into two major categories: 1) seismic methods and 2) deflection basin methods. In-situ methods provide two major advantages over laboratory methods. First, material properties are determined under the actual state of stress, and second, disturbances associated with sample extraction for laboratory testing are eliminated when the in-situ methods are nonintrusive.

Seismic methods are based on introducing stress waves in a body of material and monitoring the response of the media to the propagated waves. The material stiffnesses are then calculated from the measured wave velocities through simple mathematical equations (assuming linear elasticity) that are discussed in Section 2.2. Seismic methods include surface and borehole methods. In most seismic methods, the moduli characterize the material behavior in the elastic range, where the material is subjected to very small strains. On the other hand, deflection basin methods are based on loading the surface of the pavement with transient and steady-state forcing functions and measuring a deflection basin with the aid of geophones placed on the pavement surface. Then, the moduli are determined by an iterative backcalculation procedure. The most commonly used deflection basin methods are the FWD and Dynaflect methods.

It is the purpose in this chapter to present a review of in-situ methods for the determination of Young's and shear moduli. A brief discussion of wave propagation theory in elastic media precedes the presentation of the seismic

methods to provide one with an understanding of the quantities measured in each test.

2.2 Brief Discussion of Wave Propagation in Elastic Media

Disturbances in the interior of a whole space are manifested by stress (seismic) waves being propagated within the body of the medium. Two kinds of waves are recognized and designated by: P-waves (compression) and S-waves (shear). These waves are termed body waves because they propagate within the body (interior) of the whole space. In addition, Lord Rayleigh, in 1885, identified a third type of wave that propagates along the surface of a uniform half-space. This wave is denoted as a surface or Rayleigh wave. Each of the above waves has its characteristics such as its wave propagation velocity and the associated particle motion.

2.2.1 Body Waves

Two different kinds of body waves can be propagated in an unbounded isotropic medium called a whole space. They are P- and S-waves. Solids are usually deformed in two different ways. The first form of deformation results in a volume change without rotation. The second form results in a rotation without any change of volume. Hence the waves are called compressional, longitudinal, dilatational or P- (Primary) waves and shear, transverse, distortional or S- (Secondary) waves, respectively.

In longitudinal waves, the particle motion is in the same direction as the direction of the propagated wave as shown in Fig. 2.1a. The velocity of the compression waves, V_P, is related to the elastic constants and the density as follows:

$$V_P = \sqrt{\frac{M}{\rho}} = \sqrt{\frac{E}{\rho}\,\frac{(1-\nu)}{(1-2\nu)\,(1+\nu)}} \qquad (2.1)$$

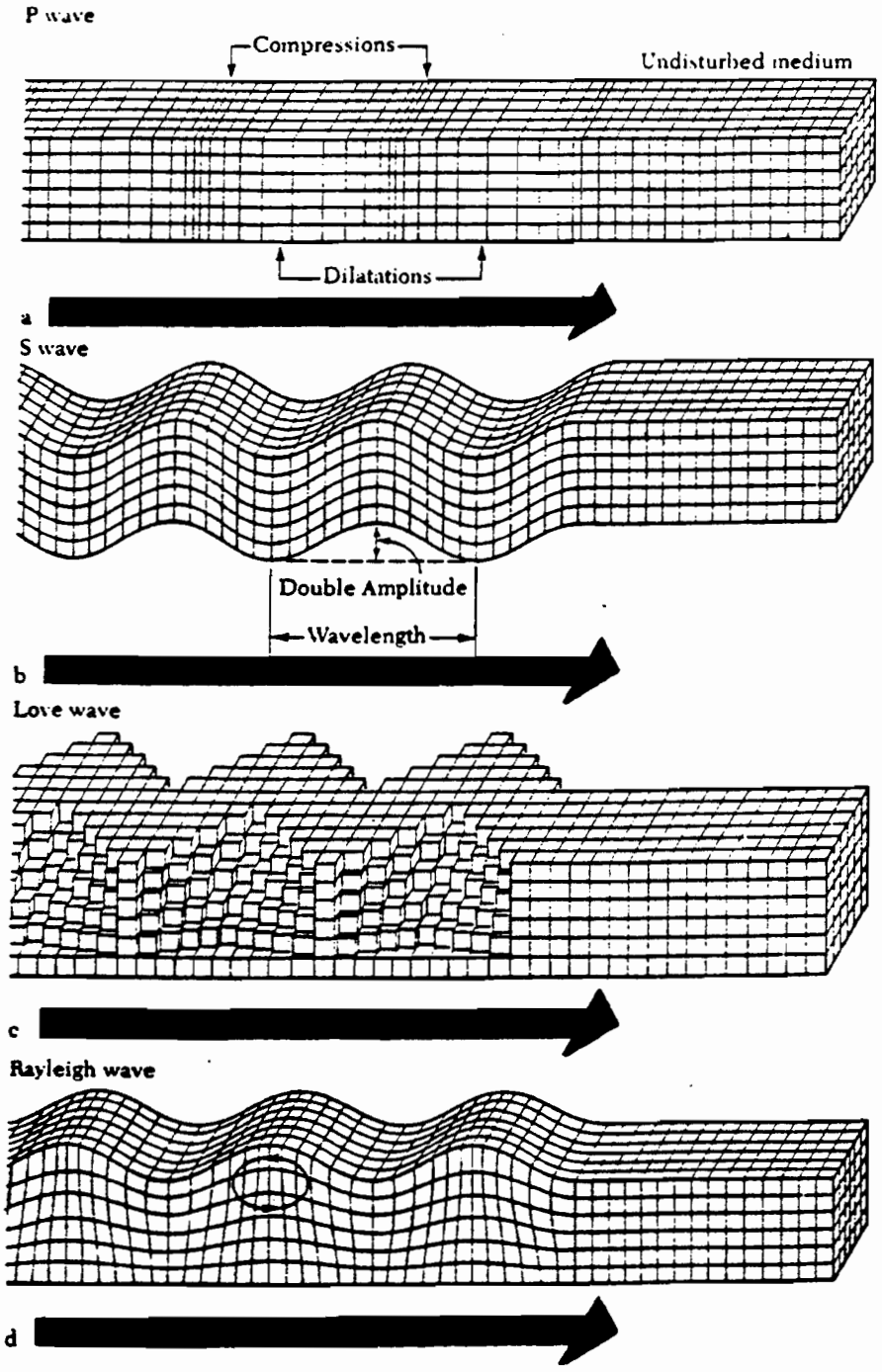

Fig 2.1. Forms of Wave Motion in an Elastic Half-Space (Bolt, 1976).

where

M = constrained modulus,
E = Young's modulus,
ν = Poisson's ratio, and
ρ = mass density (total unit weight divided by gravitational acceleration).

The P-wave velocity is mainly controlled by the modulus of elasticity due to the small changes in Poisson's ratio and mass density for earth material. In media with no constraints on lateral deformations (such as rods and bars), the unconstrained compression wave velocity, V_C, can be calculated as:

$$V_C = \sqrt{\frac{E}{\rho}} \tag{2.2}$$

In transverse waves, the particle motion is in a direction perpendicular to the direction of wave propagation, as shown in Fig. 2.1b. The velocity of the shear waves, V_S, is related to the elastic constants and the density as follows:

$$V_S = \sqrt{\frac{G}{\rho}} = \sqrt{\frac{E}{\rho}\frac{1}{2(1+\nu)}} \tag{2.3}$$

where G is the shear modulus.

Shear waves can be vertically (SV) or horizontally (SH) polarized. For SV waves, the particle motion and the propagated wave are in a vertical plane. For SH waves, the particle motion is in a horizontal plane, whereas the wave is contained in a vertical plane.

Dividing Eq. (2.1) by Eq. (2.3), the following relationship can be obtained:

$$\frac{V_P}{V_S} = \sqrt{\frac{2(1-\nu)}{1-2\nu}} \tag{2.4}$$

Equation 2.4 shows that compression waves propagate faster than shear waves and appear first in travel time records.

2.2.2 Surface Waves

In addition to compression and shear waves that travel within the body of the elastic medium, surface waves can be generated along the surface of the half-space.

There are two kinds of surface waves. First, Rayleigh (1885) identified waves that propagate along the surface of a uniform half-space. These waves decay exponentially with depth and diminish in amplitude with travel distance due to cylindrical spreading of the energy. The velocity of Rayleigh waves is a function of Poisson's ratio, but it can be approximated as being equal to nine-tenths of the shear wave velocity for practical applications. Figure 2.1d shows the particle motion associated with Rayleigh waves. The particle motion describes an elliptical motion as a result of longitudinal and transverse vibrations. Near the surface, the vertical and horizontal components of the particle motion describes a retrograde ellipse in contrast to a prograde ellipse below a depth of approximately two-tenths of the wavelength. In an ideal half-space, the Rayleigh wave velocity does not change with frequency; i.e., waves with different wavelengths travel at the same speed. However, in a layered half-space, Rayleigh wave velocities vary with frequency. This characteristic is called dispersion and constitutes the core of the SASW method.

The other kind of wave which propagates along the surface is called Love waves. This wave exists only if a low-velocity surface layer overlies a medium of higher velocity. Love (1911) demonstrated that these waves are the result of multiple reflections between the top and bottom of the low-velocity layer. The particle motion, being horizontal and transverse to the direction of wave propagation, is shown in Fig. 2.1c. It should be noted that Love waves are normally not detected during seismic prospecting because detectors are normally used to respond to vertical ground motion.

In an elastic, isotropic medium, only two elastic constants need to be known. Others can be determined from simple manipulation of Eqs. 2.1 through 2.4. The propagation velocities of compression and Rayleigh waves relative to shear wave velocities as a function of Poisson's ratio are shown in Fig. 2.2.

The phenomenon of wave propagation is much more complex than what is presented in this section. The simple discussion, presented herein, is intended to give an insight into some of the aspects that are dealt with during the course of this work. For more in-depth treatment of wave propagation theory, the reader is advised to consult available books on this subject (Ewing, Jardetsky, and Press, 1957; Elmore and Heald, 1969; etc).

2.3 Seismic Methods

2.3.1 Surface Methods

Surface seismic methods can be classified into two categories: 1) methods based on body wave propagation and 2) methods based on Rayleigh wave propagation. The reflection and refraction methods belong to the first category. The steady-state Rayleigh wave and the Spectral-Analysis-of-Surface-Waves (SASW) methods belong to the second category. Since most of this research deals with the SASW method, seismic surface methods based on Rayleigh wave propagation are discussed in detail in Chapter Three. A brief description of the reflection and refraction methods is presented below.

In the seismic reflection method, energy is imparted at or just below the ground surface to generate the seismic waves and an array of receivers is used in capturing the direct and reflected waves, mainly compression waves. A typical test configuration used in the reflection method for a simple two-layered system is

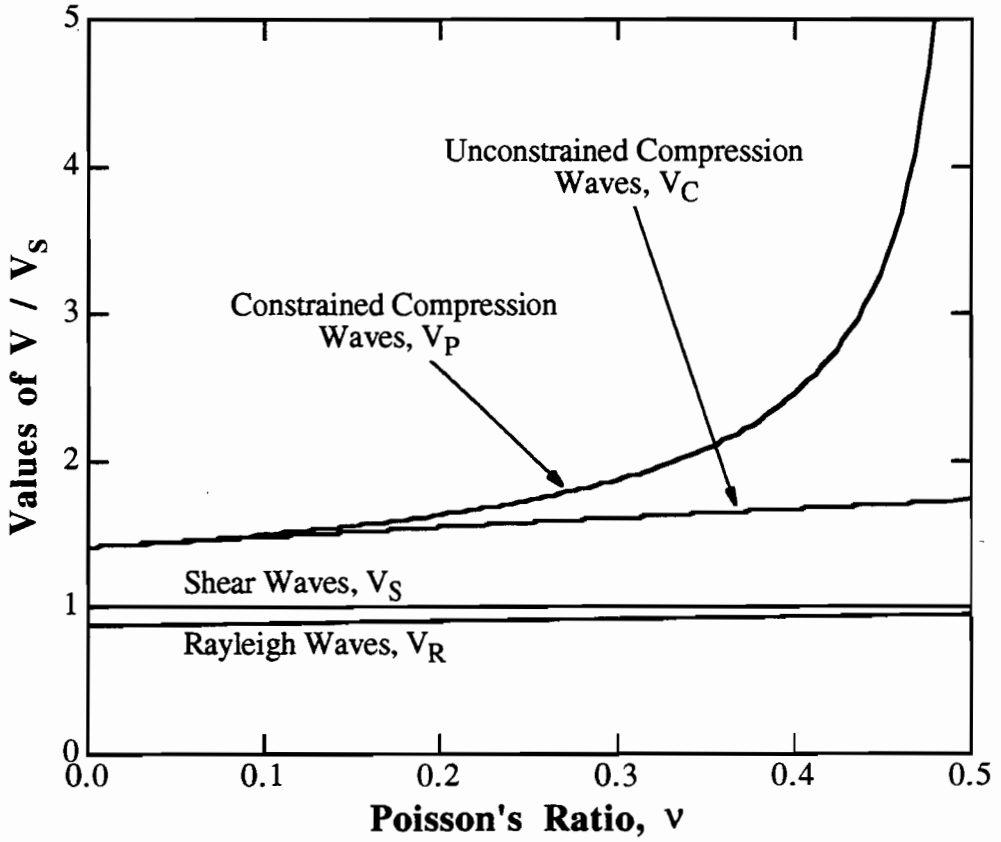

Fig 2.2. Relationship between Poisson's Ratio and Wave Velocities in an Elastic Half-Space (adopted from Richart et al., 1970).

shown in Fig. 2.3. The upper layer has a thickness of H and a wave velocity (either compression or shear) of V_1. The lower layer is really a half-space which has a wave velocity (for the same wave type as in the upper layer) of V_2. One of the strengths of the reflection method is that slow-velocity layers underneath higher-velocity layers can be detected; i.e. V_2 could be less than V_1. However, identification of the reflected waves can sometimes be difficult due to the presence of direct and refracted waves, especially for near-surface profiling. It is important to note that reflected waves never appear as the first arrivals in time records.

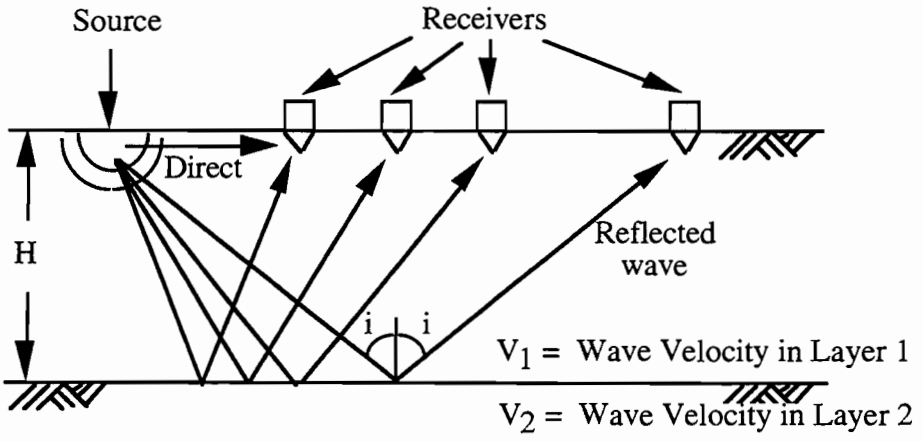

Fig 2.3. Typical Test Configuration Used in the Seismic Reflection Method (Rix, 1988).

The surface refraction method is more often used among civil engineers than the reflection method. The refraction method is based on the first arrival of refracted waves from boundaries between slow-velocity layers underlain by higher-velocity layers. Usually vertical receivers are used to capture the refracted compression waves. However, horizontal receivers can be used to detect horizontally polarized refracted shear waves when sources capable of generating shear energy are used. In a typical refraction test, receivers are placed at known distances from an explosive or impulsive source, as shown in Fig. 2.4. The close-by receivers measure the direct wave arrivals and the far receivers measure the refracted waves arrival.

Figure 2.5 shows a travel time plot from a refraction survey at a simple, two-layered site. The velocities of layers 1 and 2 (V_1 and V_2, respectively) and the

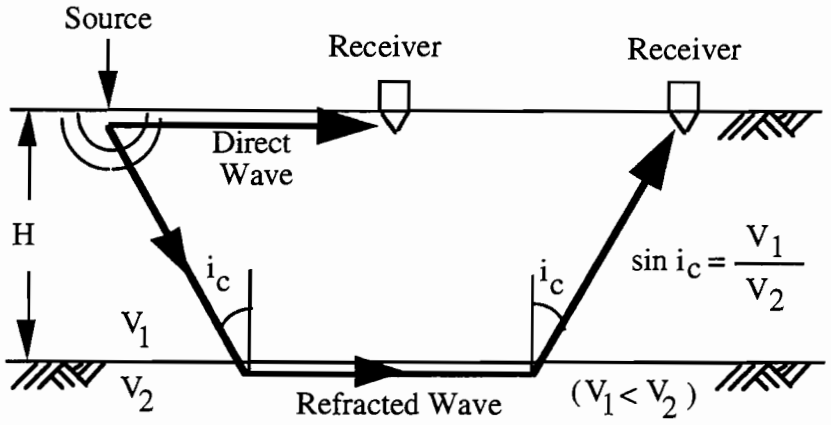

Fig 2.4. Typical Test Configuration Used in the Seismic Refraction Method (Rix, 1988).

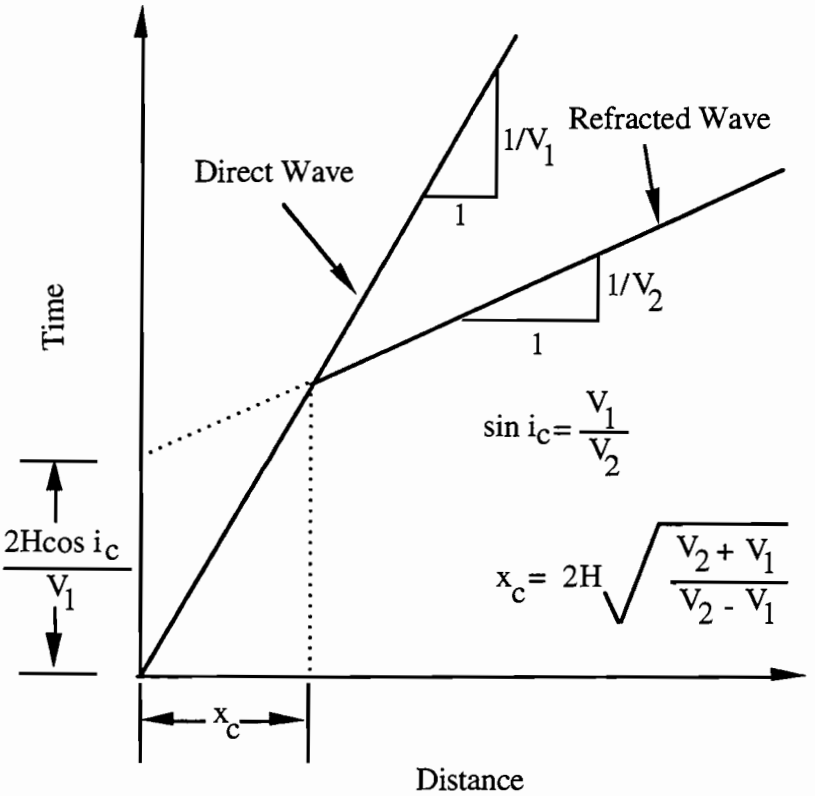

Fig 2.5. Typical Travel Time Plot from a Seismic Refraction Test at a Site Composed of Two Horizontal Layers (Rix, 1988).

thickness of the slower-velocity, upper layer (H) can be determined from this plot. The layer thickness, H, is typically determined from the crossover distance, x_c, as illustrated by the equations inserted in Fig. 2.5. Note that the refraction method cannot be used on pavement sites where, in most instances, the surface layer is stiffer than the layers underneath it. For additional information on the reflection and refraction methods, the reader should consult available books on this subject (for instance, Sharma, 1986; Dobrin, 1988).

2.3.2 Borehole Methods

The borehole methods include the crosshole, downhole, uphole, in-hole and bottom-hole methods (Hoar, 1982). The most commonly used borehole methods are the crosshole and downhole methods. A brief description of these two methods follows.

Crosshole Method

Figure 2.6 shows a typical field setup for crosshole measurements (Stokoe and Hoar, 1978b). In the crosshole test, two or more boreholes are drilled to the desired depth. A source capable of generating compression waves is lowered to the measurement depth in one of the boreholes. A receiver or two are lowered to the same depth in the other one or two boreholes. If one receiver is used, the travel time from source to receiver is measured. This is referred to as a direct travel time measurement. If two receivers are used, the travel time between the receivers is measured. This is referred to as interval travel time measurements. Typical distances between adjacent boreholes are in the order of 3 m (10 ft). The wave velocities at the measurement depth are simply calculated by dividing the travel distances by the measured travel times. The travel distances are determined after the verticality of the boreholes is evaluated (inclinometers are typically used).

Typically, the receiver consists of a three-component geophone (velocity transducer). The vertical geophone is used to capture the vertically propagating shear waves (SV). The radial geophone senses the propagating compression

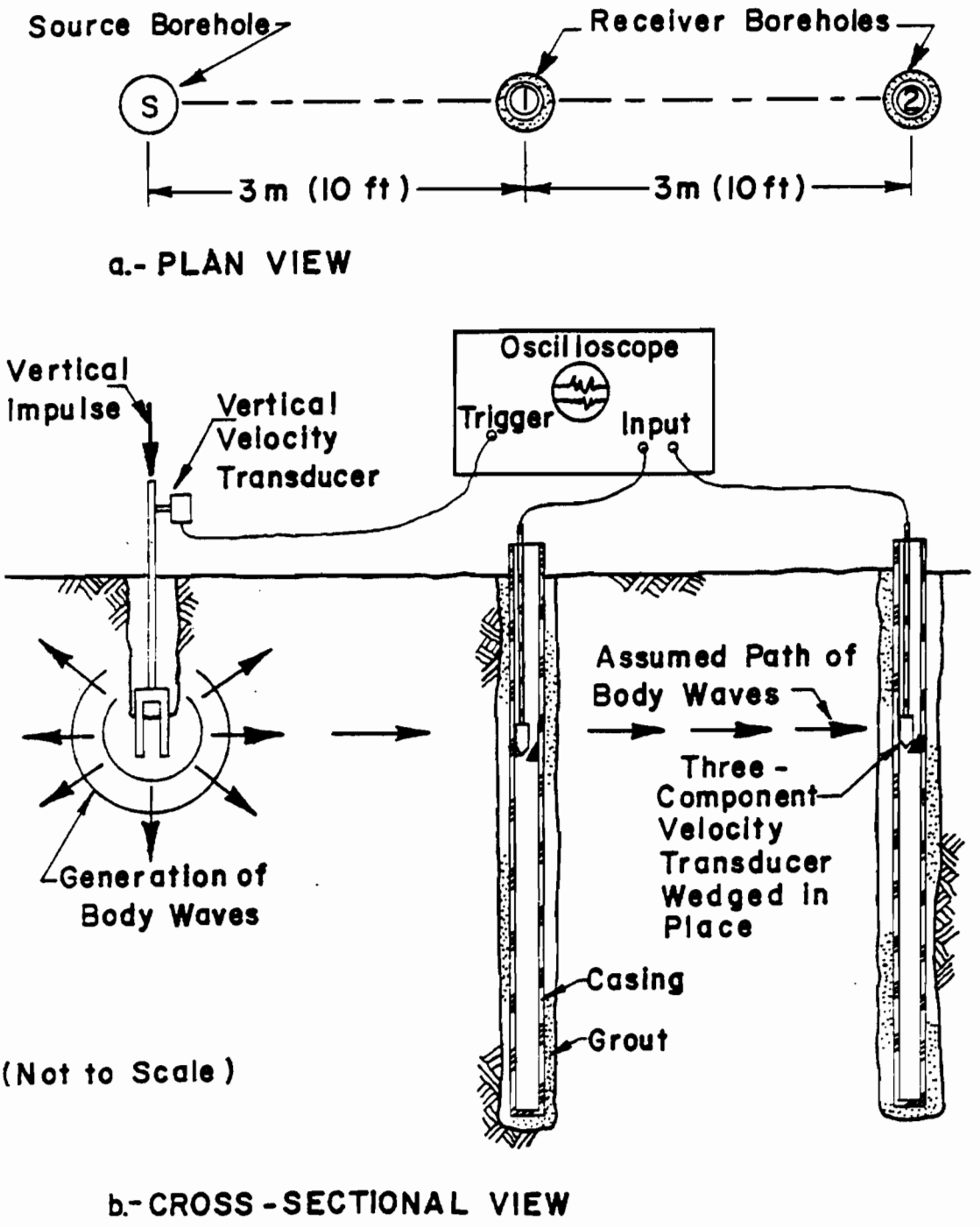

Fig 2.6. Schematic Diagram of Crosshole Seismic Testing with Associated Equipment (Stokoe and Hoar, 1978b).

waves (P) and the tangential geophone senses the horizontally propagating shear waves (SH).

A key element in crosshole testing is the use of sources rich in generating the wave energy of concern. Stokoe and his students at The University of Texas at Austin developed various types of sources to generate P-, SV- and SH-waves energy. An in-hole source (Mok, 1987) was developed to generate the SV-wave energy. The in-hole source is clamped against the borehole walls and a drop weight is used to generate the wave energy. This source allows the operator to hit upwards and downwards to reverse the polarity of the SV-waves. This is important in identifying the arrival of shear waves at the receivers (butterfly shape when traces from upward and downward hits are overlapped). Recently, a source rich in generating P- and SH-wave energy was developed at The University of Texas at Austin (Fuhriman, 1993). Other sources can also be used in crosshole tests as documented by Hoar (1982).

The crosshole method is the most accurate and versatile method for determining shear wave velocity profiles of geotechnical sites. The strength of the crosshole method is appreciated when low-velocity layers trapped between high-velocity layers are to be identified. However, the method can be costly and time-consuming, especially for deep soil profiling.

Downhole Method

A schematic diagram of the downhole seismic test is shown in Fig. 2.7 (Mok, 1987). A source is placed on the ground surface to generate the wave energy, and a receiver is lowered to the measurement depth in a borehole to capture the arrival of the propagating waves. Since only one borehole is needed for the downhole test, the cost of drilling is reduced as compared with that of the crosshole method.

Analysis of the downhole data is not as straightforward as in the case of the crosshole method. Direct travel times can be readily used to obtain an average

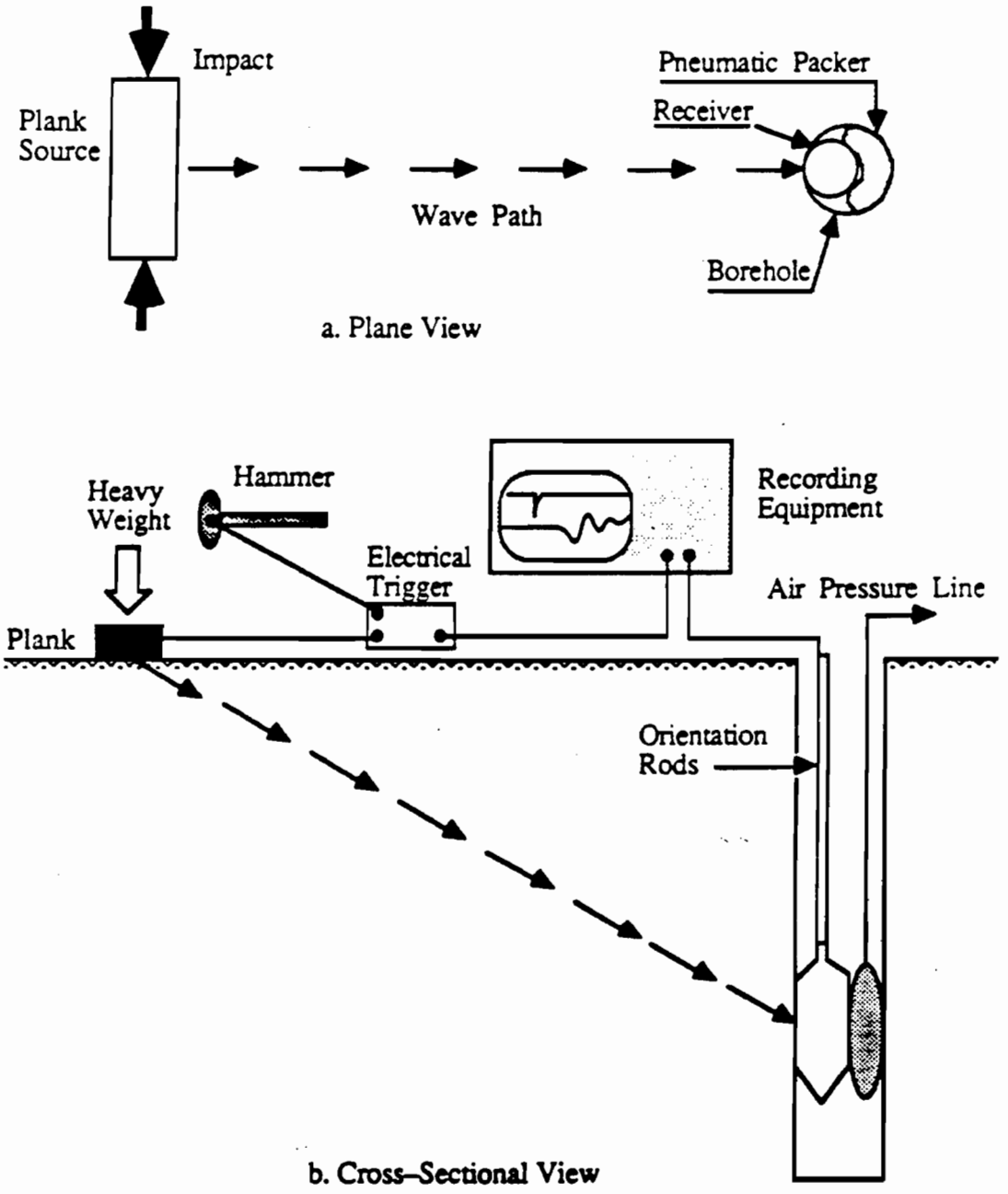

Fig 2.7. Schematic Diagram of Downhole Seismic Testing with Associated Equipment (Mok, 1987).

wave velocity profile. A more refined profile can be obtained from a true interval measurement where two receivers (in the same borehole) are lowered to two different depths. The wave velocities are then determined from the difference in the measured travel times between the two receivers (Patel, 1981; Mok, 1987). For a detailed wave velocity profile using only one receiver, inversion of the downhole data should be performed (Patel, 1981; Mok, 1987).

2.4 Deflection Basin Methods

The most commonly used deflection basin methods on pavement sites are the Dynaflect and the Falling Weight Deflectometer (FWD) methods.

In the Dynaflect test, a trailer-mounted unit generates a steady-state vibratory force of a peak-to-peak magnitude of 4.5 kN (1,000 lbs) at a frequency of 8 Hz. The response of the pavement to the applied force is measured by five geophones placed on the pavement surface. A schematic of the Dynaflect system in operation is shown in Fig. 2.8 (Uddin et al., 1983).

In the FWD test, the pavement surface is loaded with a transient force obtained from a drop weight. Seven geophones are placed on the pavement surface to monitor the response of the pavement to the applied force. The peak magnitudes of the FWD load are controlled by the drop weight and drop height. Typically, peak loads range from 6.7 to 107 kN (1,500 to 24,000 lbs). The frequency content of the load signal ranges from 0 to 60 Hz. A schematic of the FWD system is shown in Fig. 2.9 (Uddin et al., 1983).

The peak deflections measured by the geophones in Dynaflect and FWD tests form what is called deflection basins. Linear elastic layered theory (Bermister, 1945) is then used to analyze the Dynaflect and FWD data. A set of Young's moduli of the existing layers is assumed, and a theoretical deflection basin is computed using available computer programs such as MODULUS (Uzan et al., 1988). The measured deflection basin is compared to the theoretical deflection basin. If the two basins reasonably match, the assumed Young's moduli are

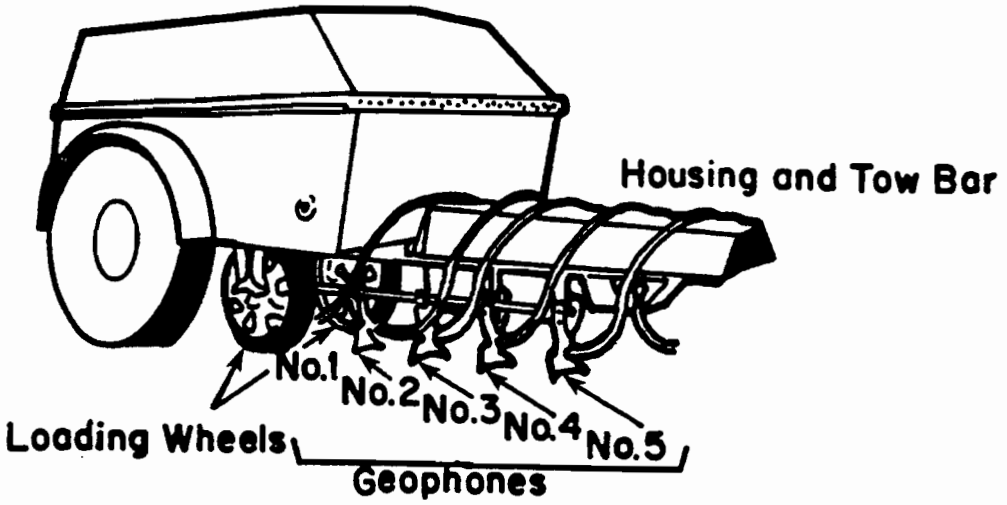

(a) The Dynaflect system in operating position

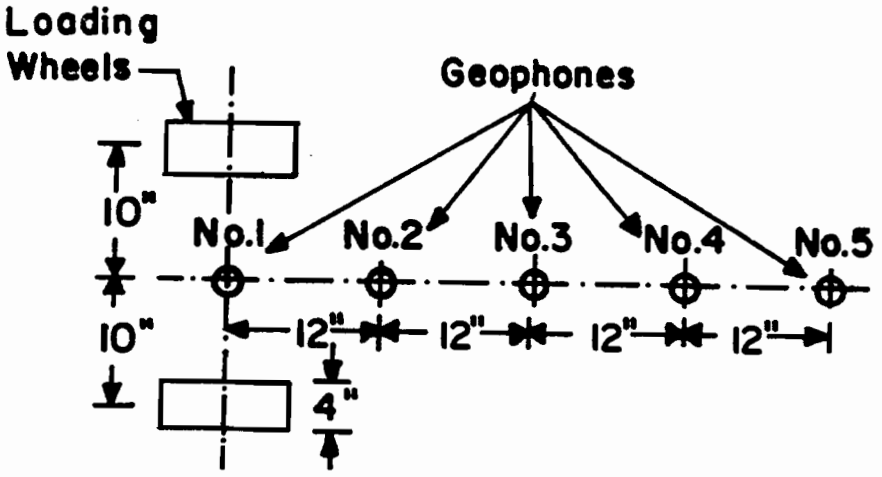

(b) Configuration of load wheels and geophones.

Fig 2.8. Layout of the In-Situ Instrumentation and Geometrical Configuration of the Load and Stations of the Dynaflect Test (Uddin et al., 1983).

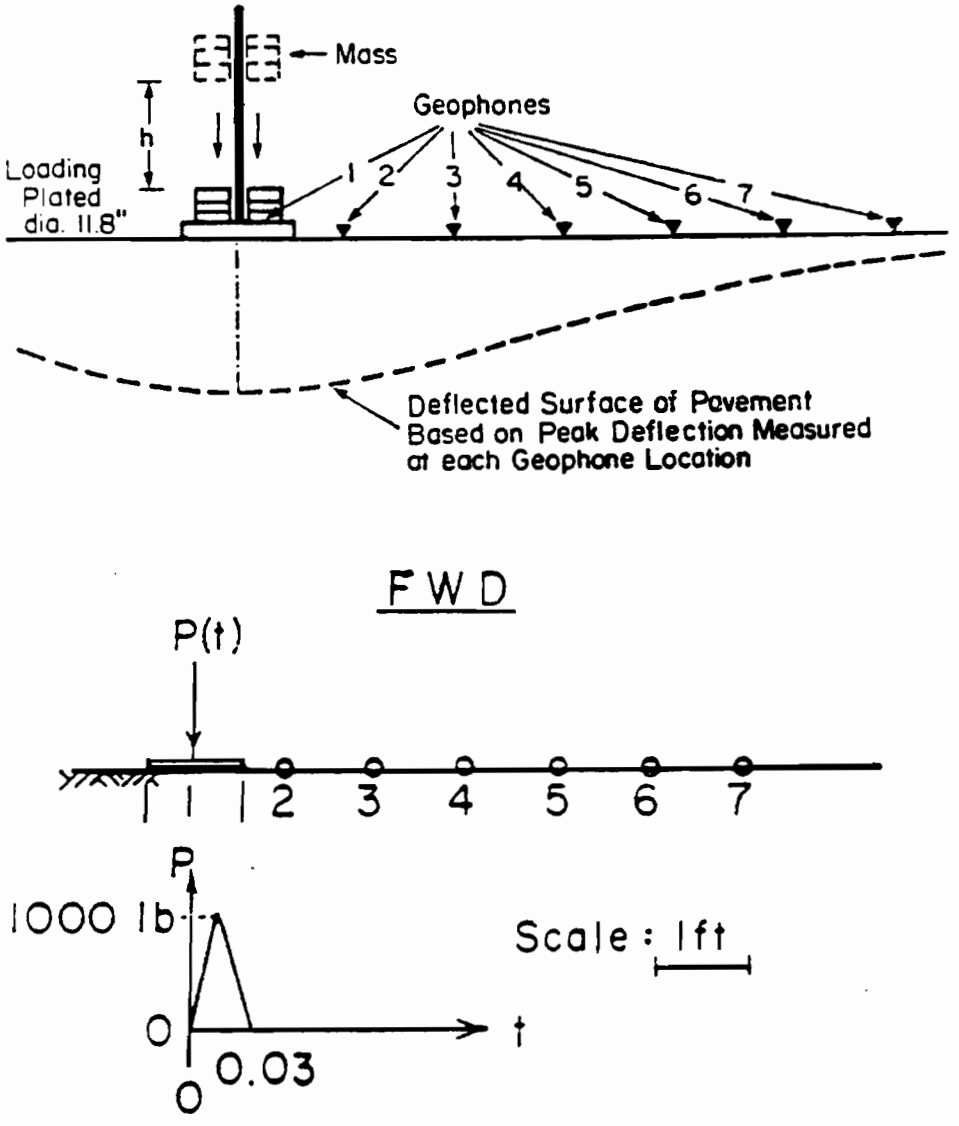

Fig 2.9. Layout of the In-Situ Instrumentation and Geometrical Configuration of the Load and Stations of the Falling Weight Deflectometer Test (Uddin et al., 1983).

considered to be representative of the field moduli. If the two basins do not match, the assumed moduli are adjusted and the process is repeated until a reasonable match between the measured and computed deflection basins occurs.

Program MODULUS and most other available programs generate deflection basins based on static analysis (an equivalent static force replaces the actual dynamic force in the Dynaflect and FWD tests). The static analysis is considered to be satisfactory when the subgrade layer extends to a large depth. However, if bedrock exists at a shallow depth, the dynamic effect should be taken into account for a proper backcalculation of Young's moduli (Mamlouk, 1985; Roesset and Shao, 1985; Chang, 1991; Miner, 1991; Seng, 1992). Dynamic amplification occurs due to shallow bedrock existence. Figures 2.10 and 2.11 show a comparison of the ratio of dynamic (W_d) to static (W_s) deflections versus depth to bedrock for a variety of assumed pavement profiles for Dynaflect and FWD tests, respectively (Chang et al., 1992). As shown in Figs. 2.10 and 2.11, the effect of bedrock extends to a depth of approximately 21 m (70 ft) for typical pavements in Dynaflect testing and approximately 9 m (30 ft) in FWD testing.

2.5 Summary

A variety of in-situ techniques are used to determine the material stiffness of soil sites and pavement systems. These techniques can be classified in two categories: 1) techniques based on wave propagation theory and 2) techniques based on deflection basin measurements. In testing pavement systems, the SASW, FWD and Dynaflect tests can be used to evaluate the stiffness profiles. All of these methods are nondestructive and nonintrusive. A review of the reflection, refraction, crosshole, downhole, Dynaflect and FWD methods is presented in this chapter. A more detailed review of the SASW method is presented in Chapter Three because most of this study deals with the SASW method.

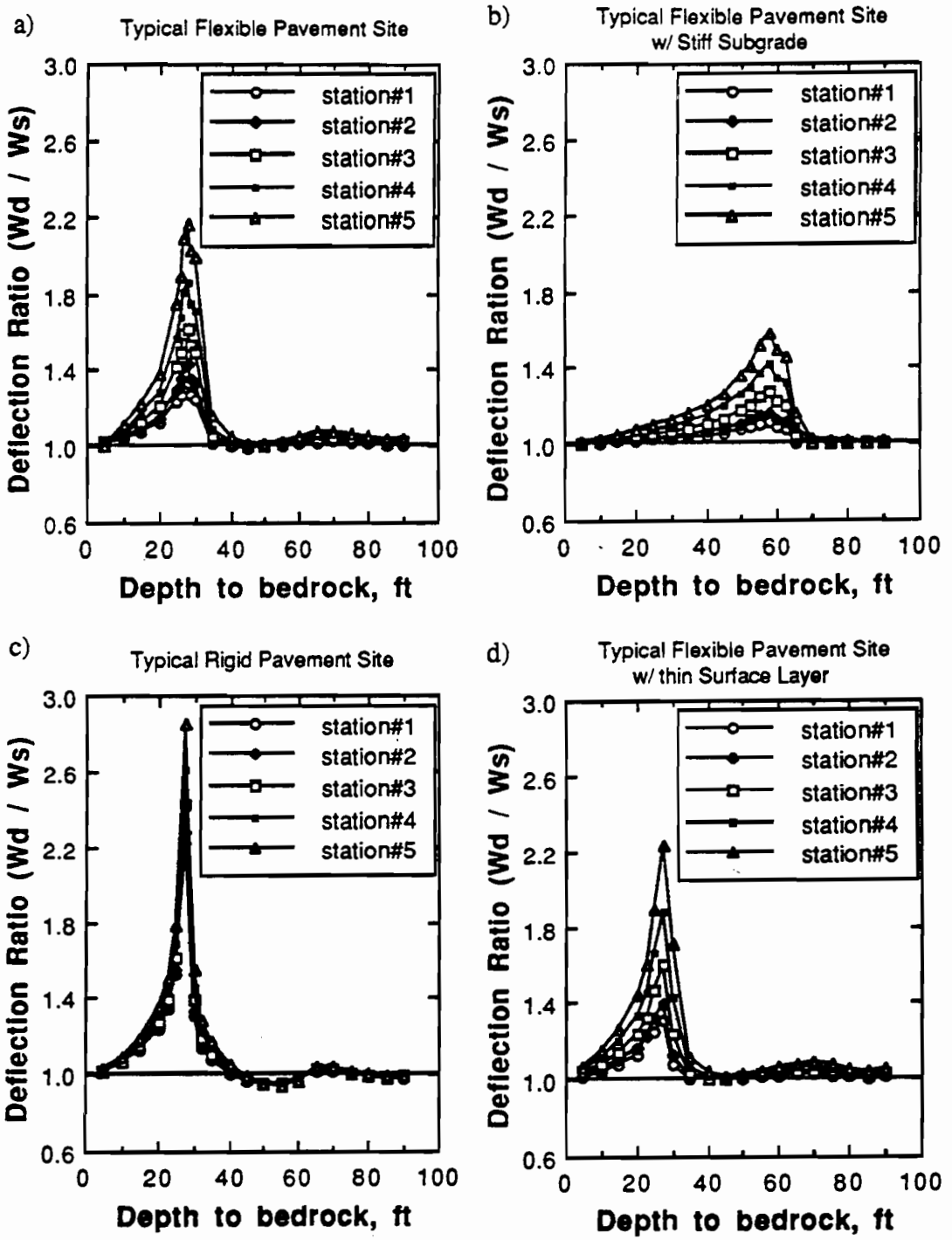

Fig 2.10. Variation of the Ratio of Dynamic (W_d) to Static (W_s) Deflections with the Depth of Bedrock for the Dynaflect Test at Various Pavement Sites (Chang et al., 1992).

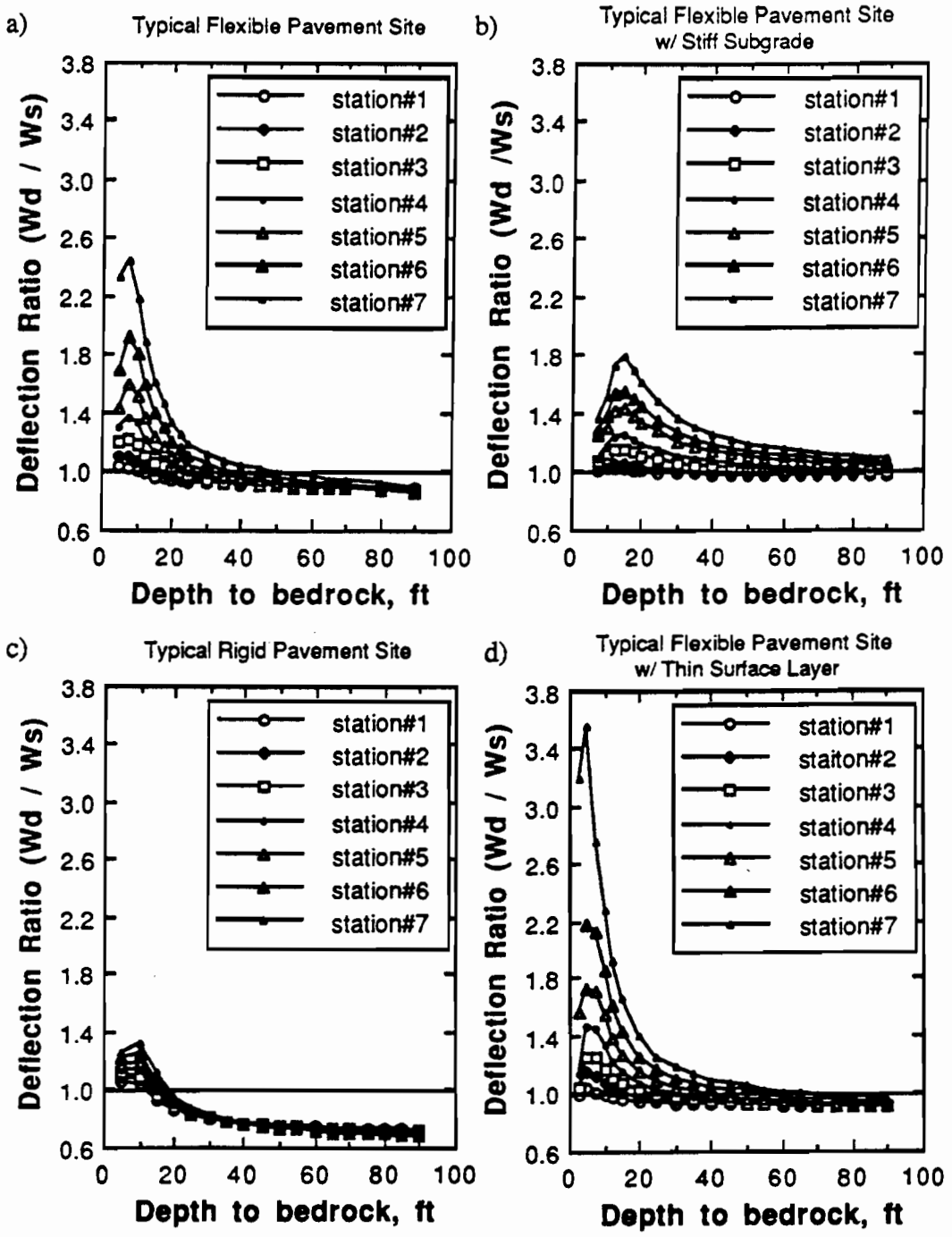

Fig 2.11. Variation of the Ratio of Dynamic (W_d) to Static (W_s) Deflections with the Depth of Bedrock for the FWD Test at Various Pavement Sites (Chang et al., 1992).

CHAPTER THREE
THE SPECTRAL-ANALYSIS-OF-SURFACE-WAVES (SASW) METHOD

3.1 Historical Development

The SASW method is a nondestructive technique used to evaluate shear moduli of soil sites and Young's moduli of pavement sites. The method relies on the generation and detection of stress waves propagating along the pavement surface. The SASW method is a modification of the steady-state Rayleigh wave (SSRW) technique introduced in the 1950's.

In the original SSRW technique, a vibrator is placed on the ground surface and a receiver is moved along the surface until the harmonic input of the vibrator and the vertical motion at the receiver are moving in phase. Figure 3.1 shows the vibrator and the receiver moving in phase for two different frequencies. As the receiver is moved away from the source, wave numbers (n) for a fixed receiver location can be determined. A plot of the wave number versus distance for the two discrete frequencies is shown in Fig. 3.2. An average wavelength corresponding to each frequency can be determined from Fig. 3.2. Then, the phase velocity of the Rayleigh-type surface wave is calculated as:

$$V_R = \lambda_{avg} \bullet f \tag{3.1}$$

where

V_R = Rayleigh wave phase velocity,
λ_{avg} = average wavelength, and
f = input frequency.

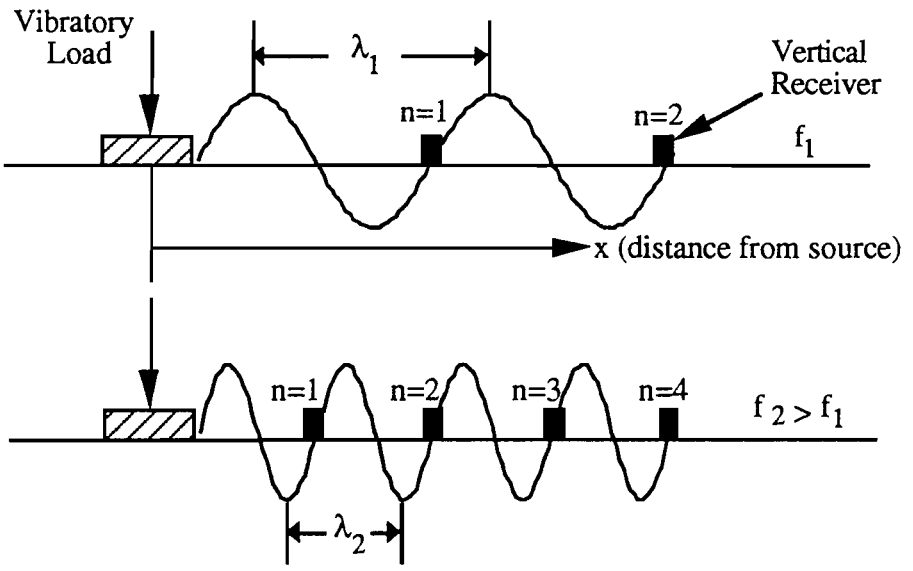

Fig 3.1. Schematic Illustration of the Vibrator and Vertical Receiver Moving in Phase for Two Discrete Frequencies.

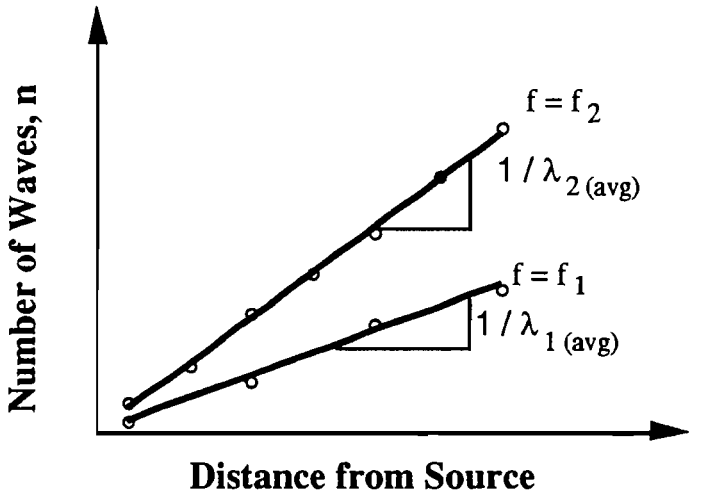

Fig 3.2. Determination of the Average Wavelength (Richart et al., 1970).

The relationship between the phase velocity and wavelength (or frequency) is termed dispersion, and a plot of V_R versus λ_{avg} or f is called a dispersion curve. After a dispersion curve is obtained, a crude inversion procedure is used in the SSRW technique to obtain the variation of the shear wave velocity with depth. The inversion process is performed by scaling the vertical and horizontal axes of the dispersion curve plot according to the following equations:

$$V_S = 1.1 \bullet V_R \tag{3.2}$$

$$Z = \lambda_{avg} / 2 \quad \text{or} \quad \lambda_{avg} / 3 \tag{3.3}$$

where

V_S = shear wave velocity, and
Z = sampled depth.

Many researchers (Jones, 1958; Heukelom and Foster, 1960; Heukelom and Klomp, 1962; Ballard, 1964; Fry, 1965) have used the SSRW technique to evaluate material properties. However, the technique did not gain acceptance in engineering practice because of the time required to complete the test over a range of discrete frequencies, and the empirical inversion procedure.

In recent years, sophisticated electronic equipment has become available where complex data analysis can be performed easily and rapidly. For example, the Hewlett-Packard (HP) Model 3562A dynamic signal analyzer has the capability of performing spectral analyses on time-domain signals through the employment of a Fast Fourier Transform (FFT) algorithm. As a result, the field time consumed in using discrete frequencies is nearly eliminated. These new developments have encouraged researchers to reconsider the applicability of surface waves in determining material profiles. Consequently, the SASW method was introduced at The University of Texas at Austin in the late 1970's by Stokoe and his research assistants, and has been under development since then.

3.2 Description of the SASW Method

The SASW method was first introduced at The University of Texas at Austin by Heisey, 1981, Heisey et al., 1982a, and Heisey et al., 1982b. A key element in SASW testing is the generation and detection of surface waves using a source and two receivers placed on the ground surface. Two major advantages of the SASW method are: 1) all measurements are made from the ground surface (nondestructive) and 2) the time needed to perform a set of measurements is relatively short. These two advantages make the SASW method attractive for testing pavement systems where the pavement surface layer remains intact and the inconvenience resulting from the diversion of traffic is minimized. In the last ten years, active research has been conducted at The University of Texas at Austin to improve the theoretical and practical aspects of the method (Nazarian, 1984; Nazarian and Stokoe, 1985 and 1986; Sheu, 1987; Sánchez-Salinero, 1987; Rix, 1988).

The SASW method is not only effective in the determination of the thicknesses and stiffnesses of pavement systems (Nazarian et al., 1983; Roesset et al., 1990), but the method can also be applied as effectively to soil sites using low-frequency sources and receivers and to pavement sites during construction (before the surface layer is placed, for instance) as well as to potential pavement subgrades before any highway construction has started. A practical application of the SASW method is the determination of shear wave velocities of hard-to-sample soils and pavement subgrades (Stokoe et al., 1988). Another application of the SASW method is the assessment of the stiffness of curing concrete with time (Rix et al., 1990; Bay and Stokoe, 1990 and 1992). A review of the SASW method is presented in the subsequent sections.

3.2.1 Field Testing

The general configuration of equipment in SASW testing is shown in Fig. 3.3. Two receivers are placed on the ground or pavement surface. The two receivers capture the passage of waves generated by a source placed on the surface

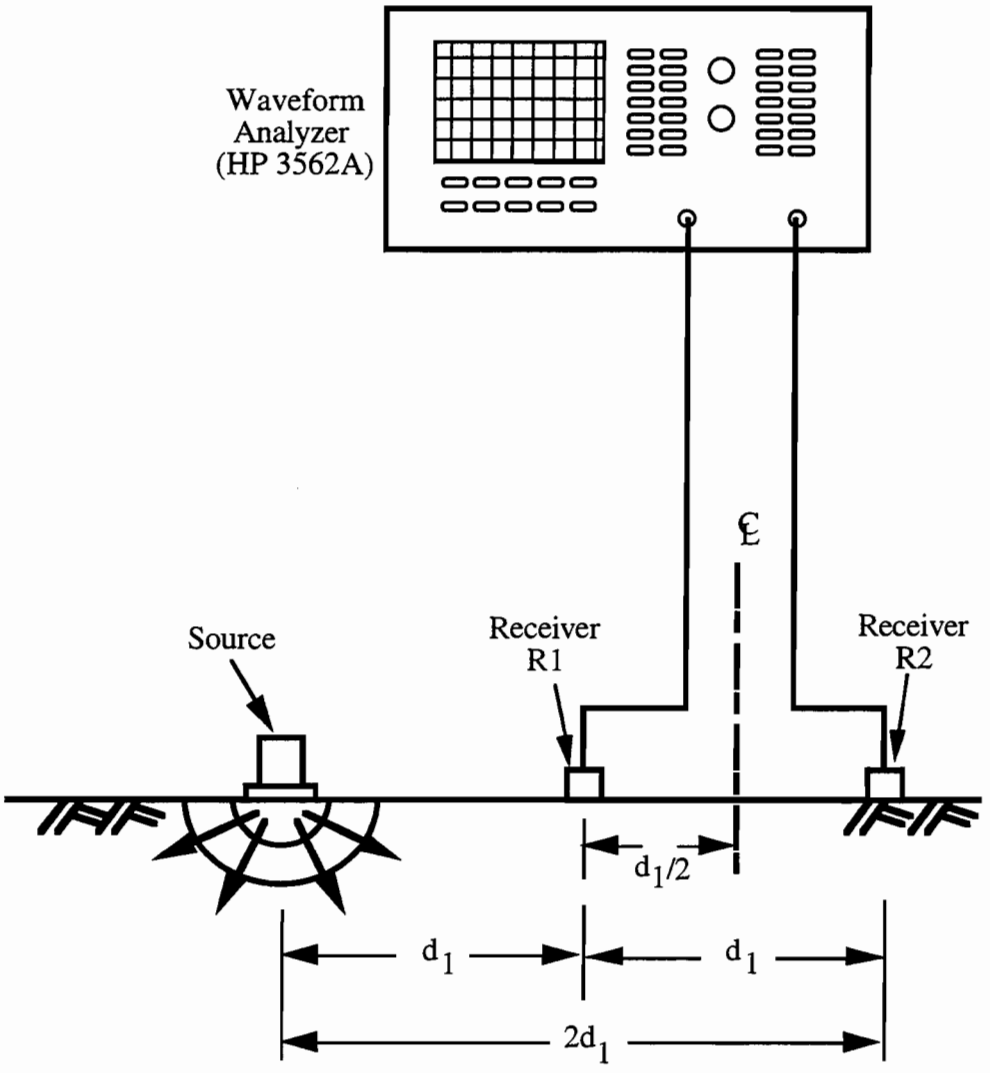

Fig 3.3. Field Arrangement of Source, Receivers and Recording Equipment for Typical SASW Testing.

such that the distance from the source to receiver 1 (d_1) is equal to the distance between the two receivers. A survey of the sources and receivers employed during the course of this research is presented in Section 3.2.3.

The time-domain signals captured by the two receivers are recorded by a dynamic signal analyzer (an HP 3562A was used in this research) capable of performing spectral analyses on the time-domain signals. The performance of spectral analyses in the field represent a crucial part of testing, as it gives the operator an opportunity to check the quality of data and to modify the test procedure to improve the field measurements when necessary. In addition, the HP 3562A model has built-in time-windowing functions such as Hanning and exponential windows. A Hanning window can be employed during testing when random noise is used as the input motion. The Hanning window ensures periodicity in the time domain, which is a requirement for the discrete Fourier transform to avoid leakage in the frequency domain. Exponential windows can be used in situations where reflections from close-by boundaries contaminate the SASW measurements (Bay and Stokoe, 1990). The exponential decay of the window can be controlled by the operator to eliminate the unwanted reflections without altering the signal from the directly propagating waves.

In a typical SASW test, the two receivers are placed at spacing d_1 on the ground/pavement surface. The source is placed on the surface to one side of receiver 1 at spacing d_1, and a measurement is made with this arrangement. This measurement is referred to as forward-profile measurement. With the two receivers kept in place, the source is moved to the other side on the same line connecting receiver 1 to receiver 2 and another measurement is made. This measurement is referred to as reverse-profile measurement. Next, the two receivers are moved away from an imaginary centerline such that the distance between them (d_1) is doubled. Two measurements are made with the source being at a spacing d_1 from receiver 1 and then receiver 2. Doubling the distance between the receivers is continued until measurements to evaluate a site (shallow or deep profiling) are complete. The above described procedure is called the Common Receiver Midpoint (CRMP) Geometry (Nazarian et al., 1983), and is illustrated in

Fig. 3.4. Other source/receiver arrangements can be used. However, the CRMP arrangement was used exclusively in all SASW testing pertaining to this report. At pavement sites, the distance between receivers typically ranges from 0.15 m (0.5 ft) to 9.8 m (32 ft). In testing soil sites, the distance between receivers ranges from 0.61 m (2 ft) up to 61 m (200 ft).

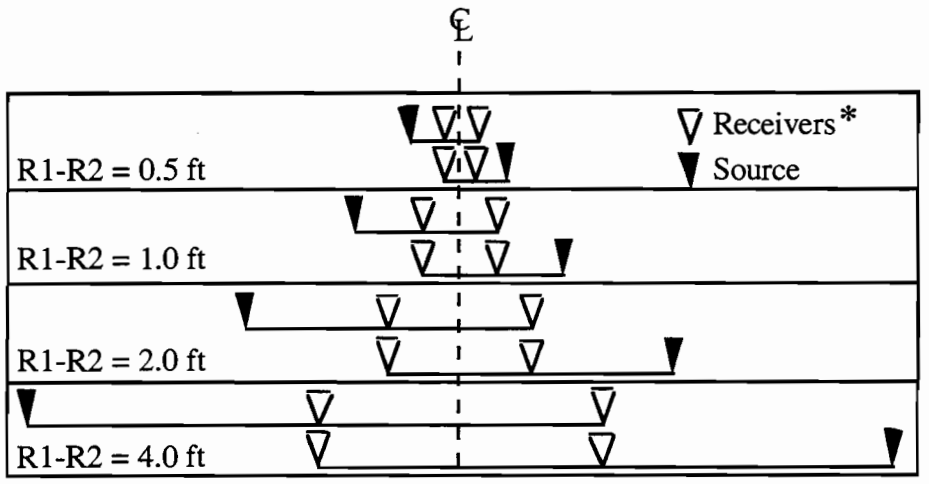

* Sequence is continued up to the desired receiver spacing

Fig 3.4. Common Receivers Midpoint (CRMP) Geometry Used in Typical SASW Testing (Nazarian et al., 1983).

For each receiver spacing, surface waves are generated by an appropriate source. The passage of surface waves is sensed by the two receivers and the time signals captured by the two receivers are displayed on the screen of the dual-channel analyzer. At this stage, the operator has the option to either accept the data or reject it. Once the data is accepted, an FFT is employed by the dynamic signal analyzer to transform the time-domain receiver outputs (denoted by x(t) and y(t)) for receivers 1 and 2, respectively to the frequency domain. The transformed signals are denoted by X(f) and Y(f) for receivers 1 and 2, respectively. X(f) and Y(f) are used to calculate the following spectral functions:

$$G_{XX} = X(f)^* \bullet X(f) \quad (3.4)$$

$$G_{YY} = Y(f)^* \bullet Y(f) \quad (3.5)$$

$$G_{XY} = X(f)^* \bullet Y(f) \quad (3.6)$$

$$\gamma^2(f) = |G_{XY}|2 / (G_{XX} \bullet G_{YY}) \quad (3.7)$$

where

G_{XX} = auto power spectrum of receiver 1,
G_{YY} = auto power spectrum of receiver 2,
G_{XY} = cross power spectrum between receivers 1 and 2,
$\gamma^2(f)$ = coherence function between receivers 1 and 2,
* denotes the complex conjugate, and
| | denotes the magnitude of the cross power spectrum.

Note that spectral functions are real functions of frequency, except the cross power spectrum, which is a complex function of frequency and contains both phase and magnitude information.

Of the above spectral functions, the cross power spectrum (more specifically the phase shift of the cross power spectrum between the two receivers) and the coherence function are the most important functions in SASW testing. The phase shift of the cross power spectrum, ϕ_{XY} (f), is calculated as follows:

$$\phi_{XY}(f) = \tan^{-1}(\mathrm{Im}(G_{XY}) / \mathrm{Re}(G_{XY})) \quad (3.8)$$

where

Im = imaginary part of the cross power spectrum at each frequency, and
Re = real part of the cross power spectrum at each frequency.

The phase shift is used in the calculation of the dispersion curve as discussed in Section 3.2.3. The coherence function is an indicator of the signal-to-noise ratio and is used as one way of judging the quality of the data obtained from SASW

tests. The coherence is equal to unity where the input and the output signals are correlated (noise-free measurement).

Typical functions for ϕ_{XY} and γ^2 are shown in Fig. 3.5 for two different sites, a pavement site and a deep soil deposit. The upper of the two figures corresponds to the smallest receiver spacing used in SASW tests (0.15 m (0.5 ft)), and the lower figure corresponds to one of the largest receiver spacings used in SASW testing (61 m (200 ft)). Note the high frequencies involved with the short receiver spacing (up to 50 kHz), as opposed to the low frequencies involved with the large receiver spacing (0-20 Hz). To generate the appropriate frequencies, different sources and receivers were employed as discussed in Section 3.2.2.

3.2.2 Sources and Receivers

A key element in the SASW testing is the selection of the appropriate sources and receivers for the frequency range of interest. In testing pavement sites, high frequencies are of interest to sample the shallow layers of a pavement system. Accelerometers cover the domain of high-frequency measurements in SASW testing. In testing soil sites, exposed pavement subgrades or uncemented exposed pavement bases/subbases, low frequencies are of greater interest to sample deep layers of soil. Geophones (velocity transducers) cover the domain of low-frequency measurements.

High-Frequency Measurements

Accelerometers are usually used as receivers in testing pavement systems where the distance between the two receivers (R1-R2) ranges from 0.15 m (0.5 ft) to 1.22 m (4 ft). Two types of accelerometers were used at pavement sites presented in this work: PCB model 308B02 accelerometers, and WR model 736 accelerometers. The PCB accelerometers have a resonant frequency of 25 kHz

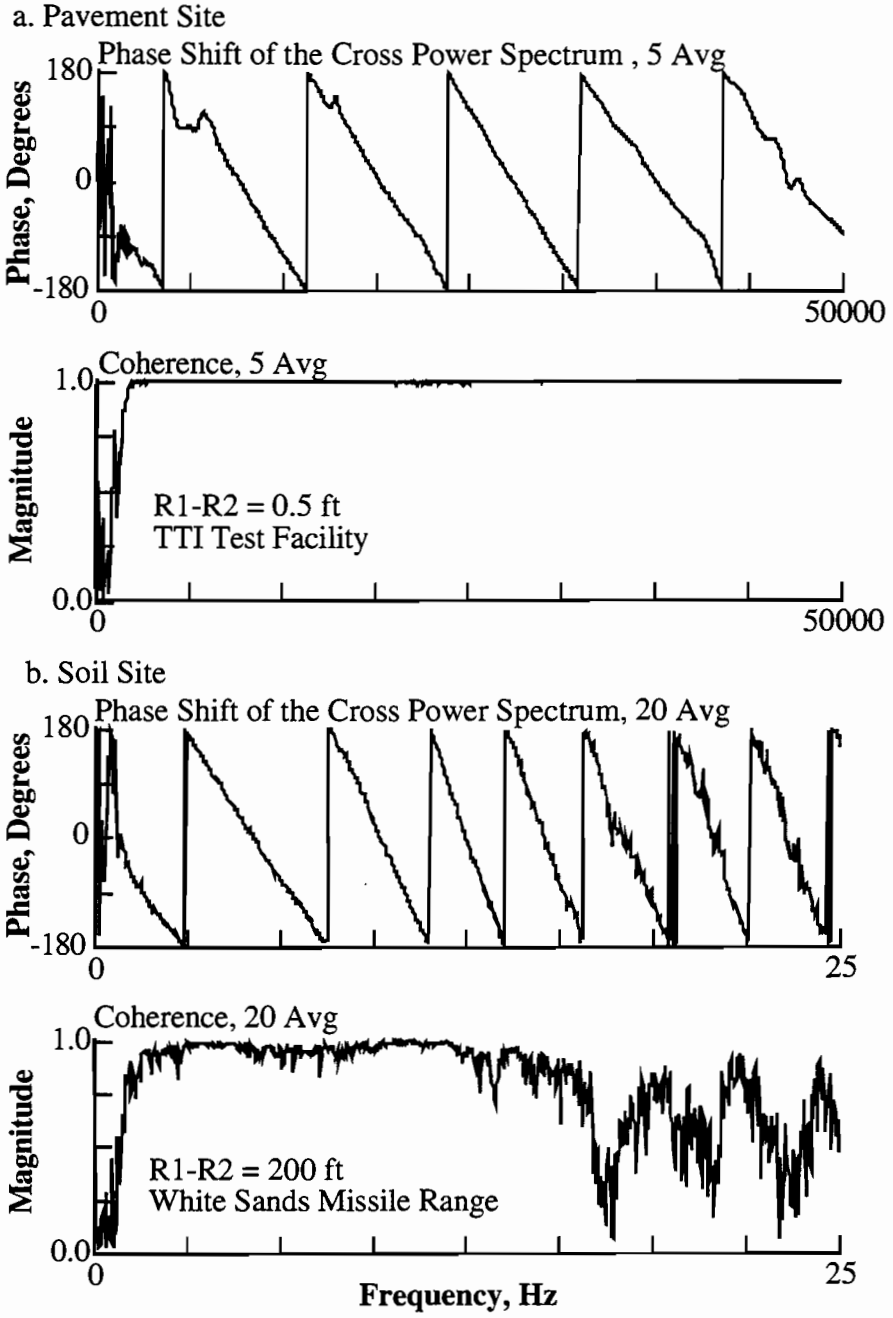

Fig 3.5. Typical Phases of the Cross Power Spectra and Coherence Functions Recorded during SASW Testing (TTI Test Facility and White Sands Missile Range).

and a calibration factor of 1 volt/g. The WR accelerometers have a resonant frequency above 50 kHz when mounted and a calibration factor of 0.1 volt/g.

To generate the high frequencies required to sample shallow layers, high-frequency sources are needed. In the past, small ball-peen hammers (weight ~ 57 gm (2 oz)) were used as high-frequency generators. However, the ball-peen hammers did not perform adequately as high-frequency sources over the entire range of temperatures encountered in asphalt concrete pavements. A V-meter (piezoelectric source with a central output frequency of 54 kHz) and a WR model F-7 piezoelectric shaker were investigated and compared to the ball-peen hammers as high-frequency generators. The performance of the above high-frequency sources is presented in Chapters Four and Five.

Low-Frequency Measurements

Geophones are used in testing pavement systems for R1-R2 distances from 2.44 m (8 ft) to 9.75 m (32 ft) and in testing soil sites/pavement subgrades for R1-R2 distances from 1.22 m (4 ft) to 61 m (200 ft). Mark Products model L-4C geophones were used exclusively at all sites presented in this work. These geophones have a natural frequency of 1 Hz and a calibration constant of approximately 3.9 volts/cm/sec (10 volts/in./sec). The maximum frequency at which the 1-Hz geophones were used is about 400 Hz.

An important element in testing soil sites is the selection of low-frequency generators. The White Sands Missile Range (WSMR) site was selected for illustrating the performance of low-frequency sources. Receiver spacings at WSMR ranged from 1.22 m (4 ft) to 61 m (200 ft). The phase shifts of the cross power spectra and coherence functions for receiver spacings of 1.22 m (4 ft) and 4.88 m (16 ft) using a 45-N (10-lb) sledge hammer as a source are shown in Figs. 3.6a and b and Figs. 3.6c and d, respectively. The sledge hammer was tried as a source for a receiver spacing of 9.75 m (32 ft), but the surface wave energy was insufficient to be captured by the two receivers. A 312-N (70-lb) drop weight

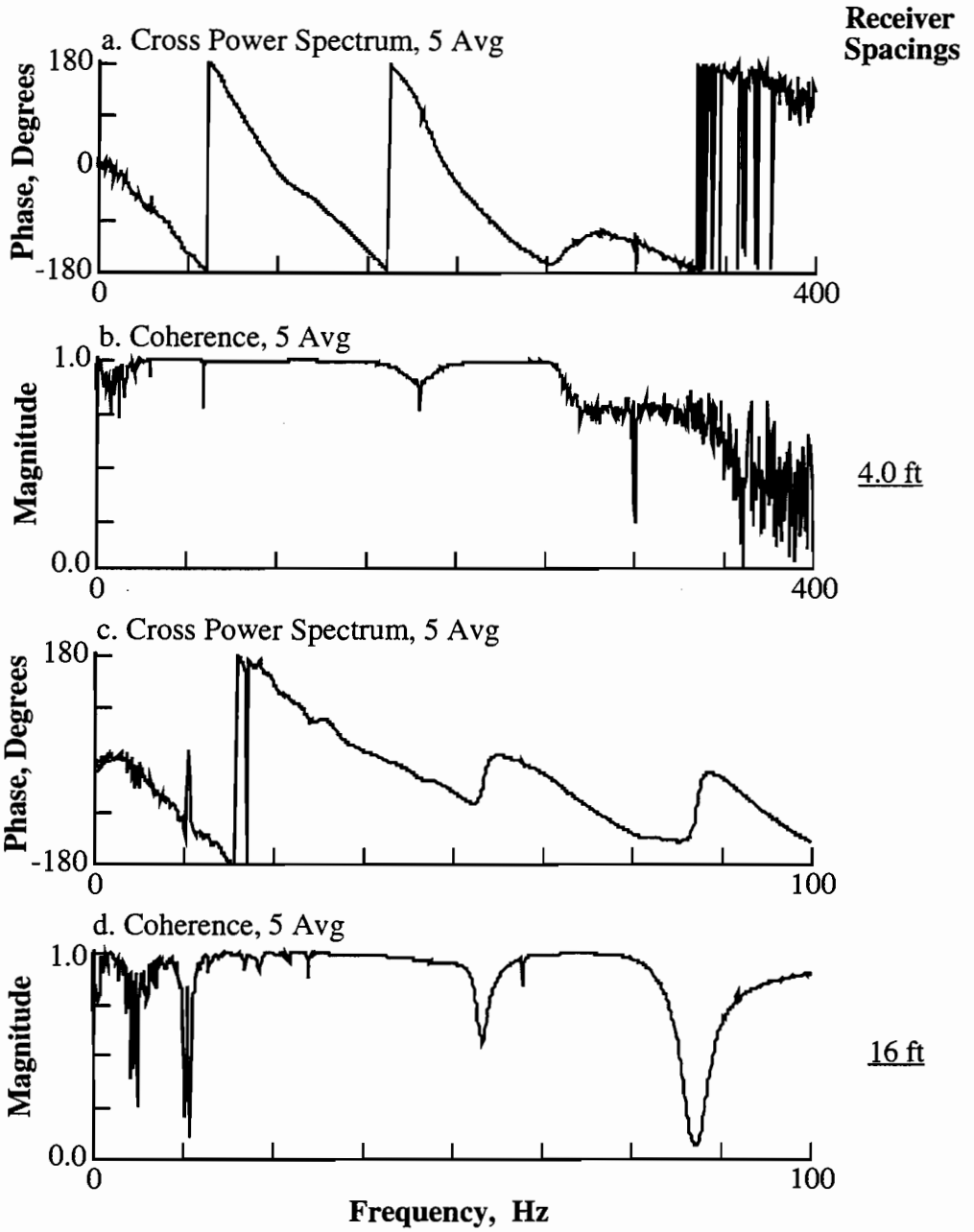

Fig 3.6. Phase Shifts of the Cross Power Spectra and Coherence Functions Using a 10-lb Sledge Hammer as a Source.

generated the frequencies of interest at receiver spacing of 9.75 m (32 ft) as shown in Figs. 3.7a and b. At receiver spacings of 19.5 m (64 ft), 39 m (128 ft) and 61 m (200 ft), the only source which performed adequately over the desired range of frequencies (0 to 40 Hz) was a bulldozer moving back and forth within a small area. The bulldozer approximates random noise and is an excellent generator of very low frequencies. The phase shifts of the cross power spectra and coherence functions for receiver spacings of 19.5 m (64 ft), 39 m (128 ft) and 61 m (200 ft) are shown in Figs. 3.7c and d, 3.8a and b, and 3.8c and d, respectively.

3.2.3 Determination of Dispersion Curves

As discussed earlier, surface waves are dispersive in a horizontally layered system. Dispersion means that the velocity of the surface wave varies with wavelength (or frequency). For a site like the one illustrated in Fig. 1.1 where the stiffness changes with depth, the surface wave velocity will vary as described in the following discussion. A plot of the surface wave velocity versus wavelength (or frequency) is called a dispersion curve. Dispersion curves are presented below in terms of plots of surface wave velocity versus wavelength. The dispersion curves plotted in this fashion are closely related to plots of shear wave velocity versus depth with scaling factors as noted in Section 3.1.

To determine a dispersion curve, the phase shift of the cross power spectrum, $\phi_{XY}(f)$ given in Eq. 3.8, is used in the calculations of the surface wave velocity, V_R, and wavelength, λ, as follows:

$$t(f) = \phi_{XY}(f) / (360 \cdot f) \tag{3.9}$$

$$V_R(f) = d_1 / t(f) \tag{3.10}$$

$$\lambda(f) = V_R(f) / f \tag{3.11}$$

where

$t(f)$ = travel time for a given frequency,
$\phi_{XY}(f)$ = phase shift between the two receivers in degrees,
f = frequency,

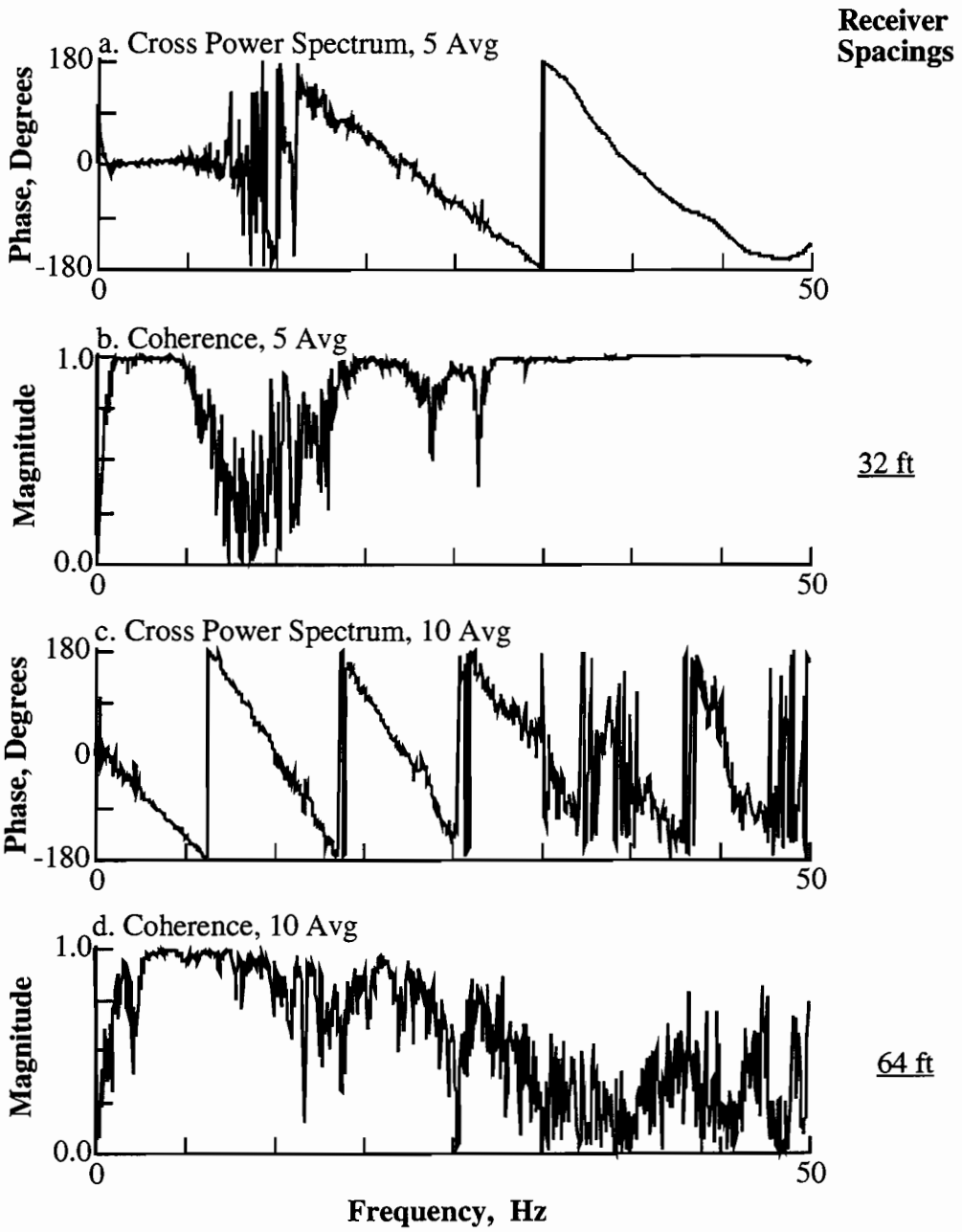

Fig 3.7. Phase Shifts of the Cross Power Spectra and Coherence Functions Using a Drop Weight as a Source at Receiver Spacing of 32 ft and a Bulldozer as a Source at Receiver Spacing of 64 ft.

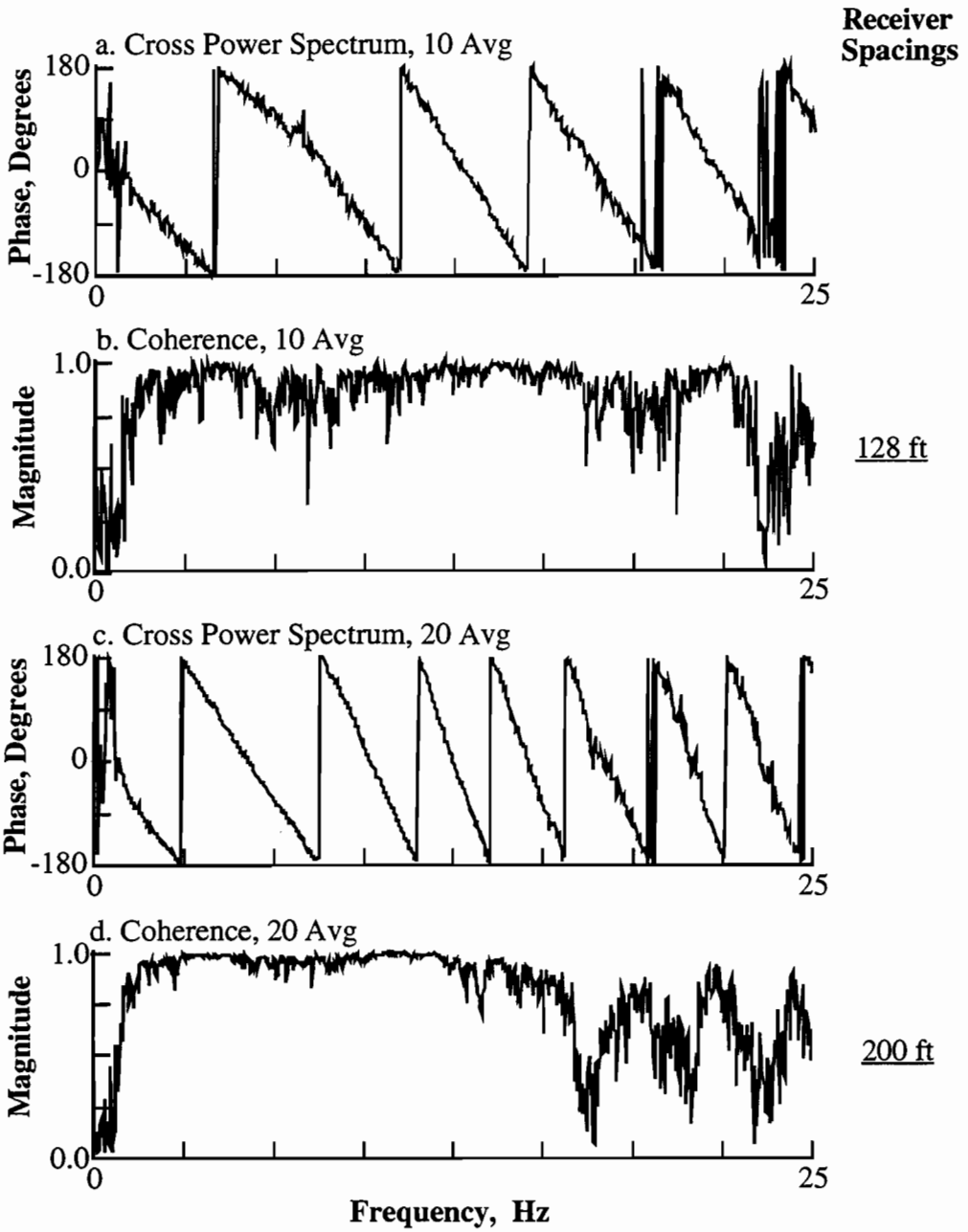

Fig 3.8. Phase Shifts of the Cross Power Spectra and Coherence Functions Using a Bulldozer as a Source.

$V_R(f)$ = surface wave velocity for a given frequency,
d_1 = distance between the two receivers, and
$\lambda(f)$ = wavelength at a given frequency.

To illustrate the calculation of the dispersion curve, consider the phase shift of the cross power spectrum in Fig. 3.6a measured at WSMR for a receiver spacing of 1.22 m (4 ft). This could just as easily represent a measurement directly on an exposed pavement subgrade. Before calculating the dispersion curve, parts of the phase shift plot should be masked. Based on studies at several sites, Heisey et al. (1981) suggested an upper and a lower bound on wavelengths for a specific receiver spacing according to the following equation:

$$d_1/2 < \lambda(f) < 3d_1 \tag{3.12}$$

The upper limit ($3d_1$) was justified on the basis that the wavelengths should be short enough compared to the receiver spacings to allow surface waves to be fully developed (minimize near-field effects). In terms of the phase shift, the upper limit criterion ($3d_1$) corresponds to the following relationship:

$$\phi_{XY}(f) > 120 \text{ degrees} \tag{3.13}$$

All the phase shifts at frequencies smaller than the frequency at which the 120-degree phase shift occurred should be masked, as shown in Fig. 3.9. The lower limit criterion ($d_1/2$) was found to be unnecessary and was not used in the masking process in this work. The lower limit criterion was originally proposed based on the resolution of the earlier equipment which has been improved with newer equipment in this work.

Another criterion as what range of data to use from the phase shift plot is to observe the coherence function. For coherence values less than 0.95 in Fig. 3.9, the phase shifts should be masked. However, in some situations where the coherence values are low, the phase shifts between the two receivers followed the

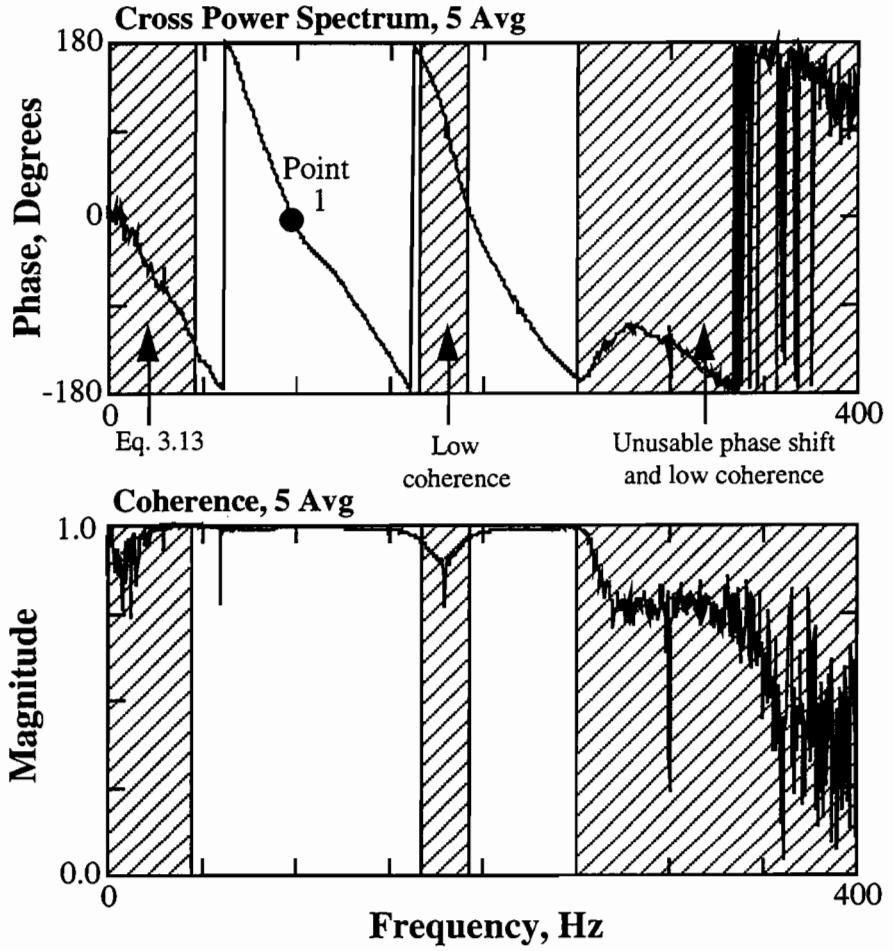

Fig 3.9. Masking Some Phase Shift Information of the Cross Power Spectrum before Calculating a Dispersion Curve; WSMR Site, R1-R2 = 4 ft.

general "seesaw" trend and should only be used cautiously in the development of a dispersion curve.

The dispersion curve determined (using Eqs. 3.9 through 3.11 and 3.13) from the phase shift of the cross power spectrum for a receiver spacing of 1.22 m (4 ft) is shown in Fig. 3.10. Point 1 on the experimental dispersion curve (Fig. 3.10) corresponds to the point on the phase shift plot where the actual (unwrapped) phase shift is equal to 360 degrees. It should be mentioned that the phase shift should be unwrapped and the actual phase shift at each frequency can be obtained by adding the appropriate phase shifts (0, 360, 720, ..., n x 360 degrees), depending on the number of jumps observed in the wrapped phase shift plot (0, 1, 2, ..., n).

The phase shifts of the cross power spectra shown in Figs. 3.6 through 3.8 were used to calculate the dispersion curves for each receiver spacing. These individual dispersion curves were then combined to a single dispersion curve, called the composite dispersion curve, as shown in Fig. 3.11. The increase in the surface wave velocity, V_R, with wavelength, λ, as shown in Fig. 3.11, corresponds to an increasing stiffness with depth for the WSMR site.

It should be noted that during the course of this work, it was felt that Eq. 3.13 should be changed to $\phi_{XY}(f) > 180$ degrees, and the wavelengths lost in the range of phase shifts from 120 to 180 degrees can be obtained from a larger receiver spacing.

3.2.4 Effect of Low Coherence on Experimental Dispersion Curve

The experimental dispersion curve is developed after masking some parts of the phase shift of the cross power spectrum, as shown in Fig. 3.9. Parts of the phase shift where the coherence is below 0.95 are usually masked. However, in a few instances, portions of the phase shift were used in the development of the experimental dispersion curve where the coherence value dropped to about 0.7.

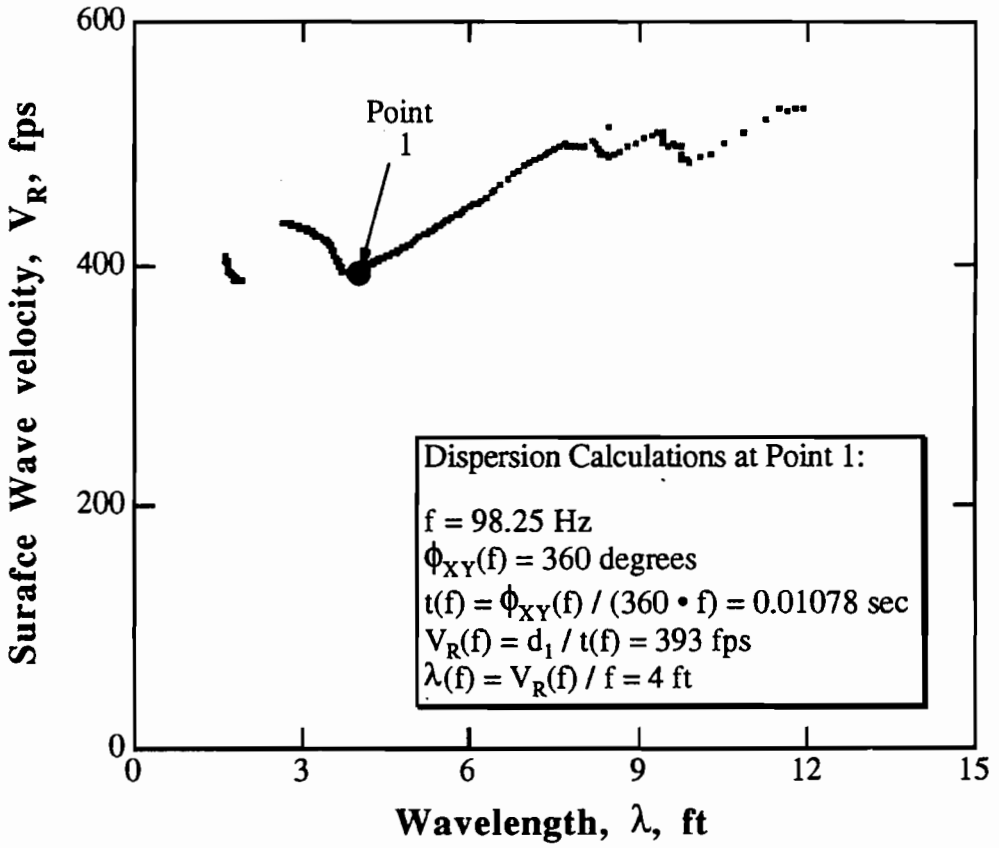

Fig 3.10. Experimental Dispersion Curve Determined from the Masked Phase Shift Shown in Fig. 3.9; WSMR Site, R1-R2 = 4 ft.

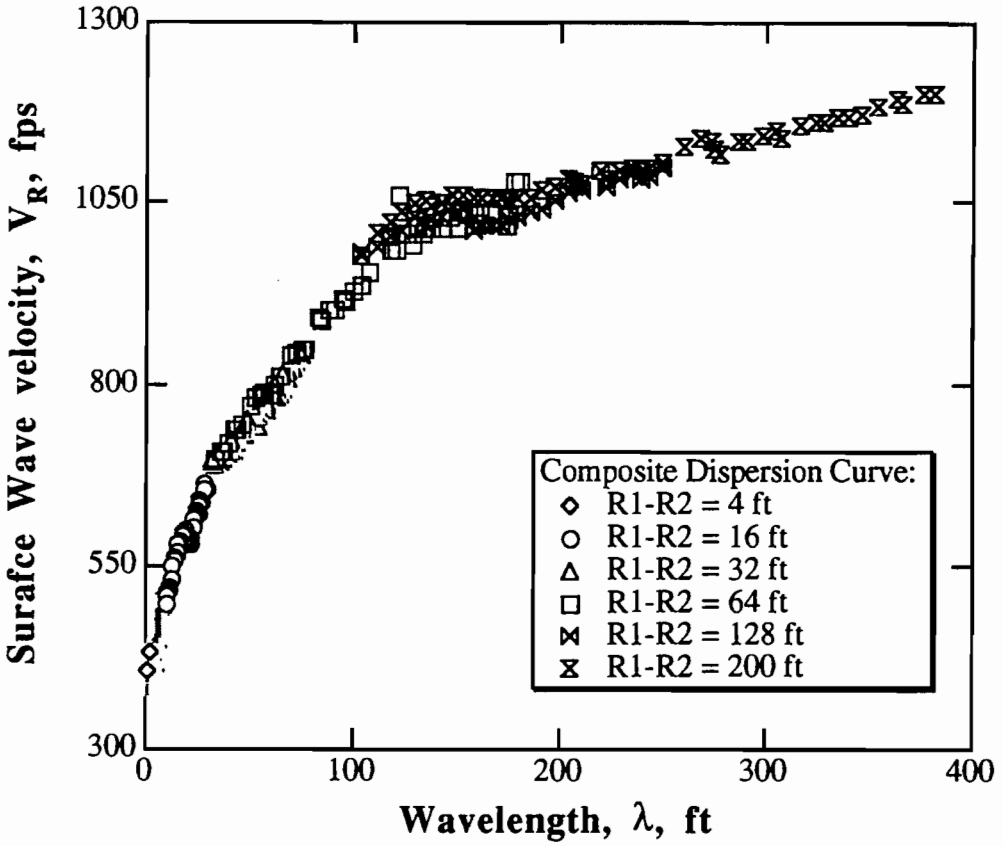

Fig 3.11. Composite Dispersion Curve Determined from SASW Measurements at the WSMR Site.

To understand the effect of low coherence on the experimental dispersion curve, two noise-free signals were created to represent the outputs of the two receivers in SASW measurements as shown in Fig. 3.12a. Then, Gaussian noise was introduced into the two signals as shown in Fig. 3.12b. A comparison of the phase shifts of the cross power spectra and coherence functions obtained from the "clean" (noise-free) and noisy signals is presented in Figs. 3.13a and b, respectively. The noise level that was introduced into the original signals was high enough to produce a coherence function that dropped below the 0.7 value used cautiously in developing a few portions of some dispersion curves used in this research.

The experimental dispersion curves (a receiver spacing of 0.3 m (1 ft) were assumed) obtained from the phase shifts of the cross power spectra of the "clean" and noisy signals are compared in Fig. 3.14. As shown in Fig. 3.14, the two dispersion curves exhibit the same trends, and the velocities compare quite well. There is a maximum difference of about 15% in velocity at low frequencies or long wavelengths and about 8% at high frequencies or short wavelengths. Consequently, the limited use of the phase shift of the cross power spectrum where the coherence dropped below 0.95 seems justified as long as the phase shift followed the general trend ("seesaw" shape in Fig. 3.13) observed in the SASW measurements.

3.2.5 Averaging the Phase Shifts from Forward and Reverse Profiles

SASW tests are normally performed by propagating surface waves in two opposite directions (forward and reverse profiles). One expects that the forward and reverse profiles would be identical. In many instances, the phase shifts of the cross power spectra from the forward and reverse profiles match well over the frequency bandwidth, except maybe over a limited frequency range. Fluctuations in the dispersion curves occur where the phase shifts do not match, and these fluctuations are generally shifted away from each other in opposite directions. Thus, the fluctuations are shifted from an average value that needs to be determined. Instead of averaging the dispersion curves obtained from the forward

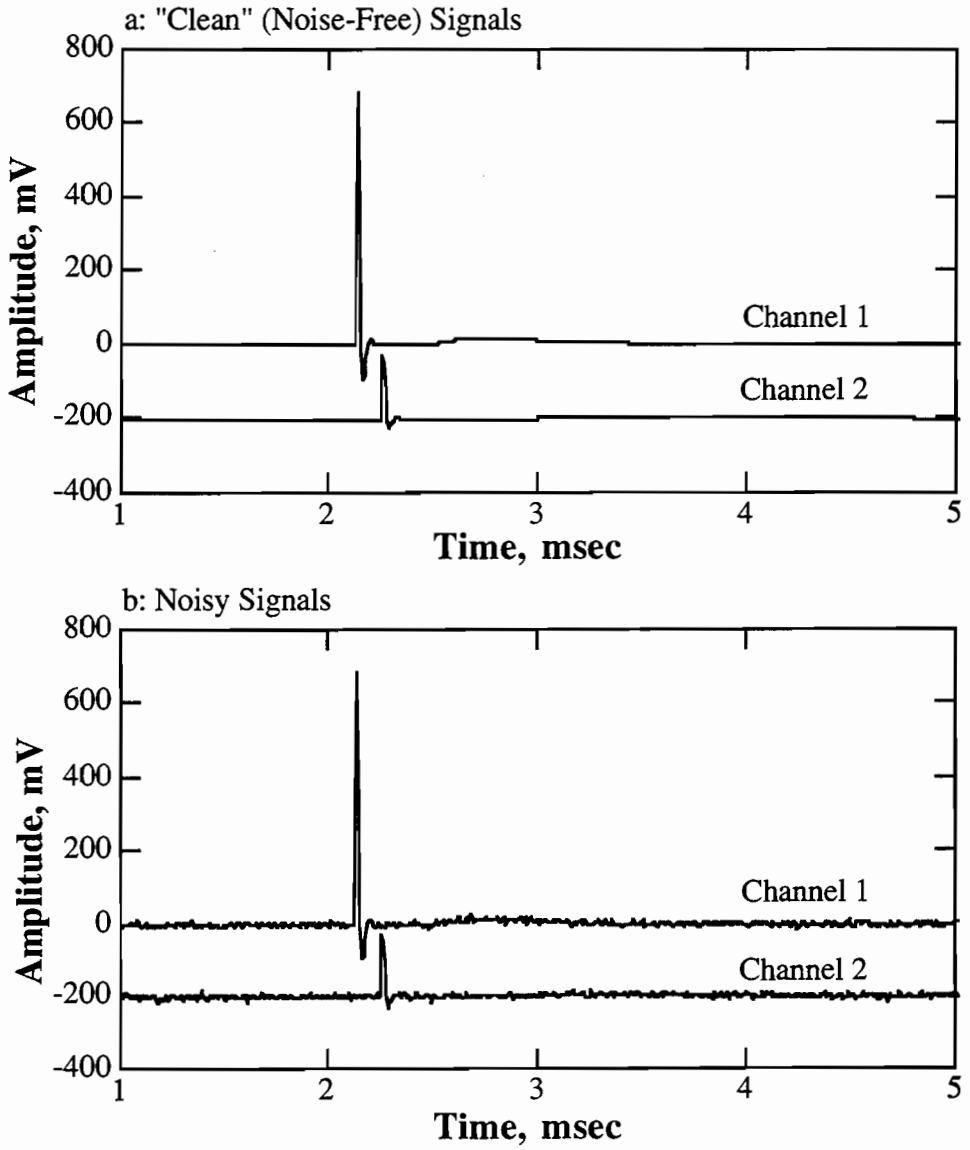

Fig 3.12. Comparison between Time Records of Clean and Noisy Synthetic Signals.

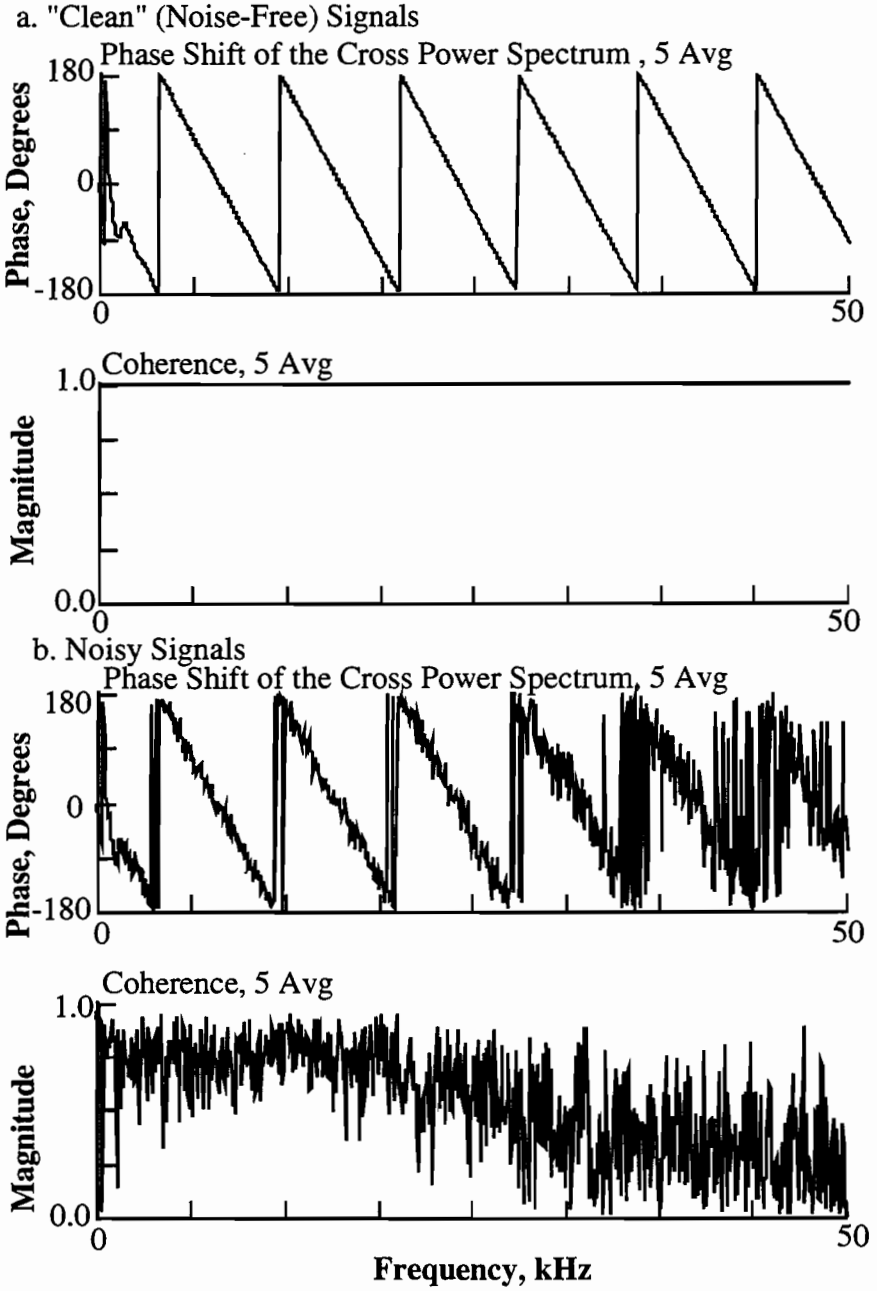

Fig 3.13. Comparison of Phase Shifts of the Cross Power Spectra and Coherence Functions of Clean and Noisy Synthetic Signals.

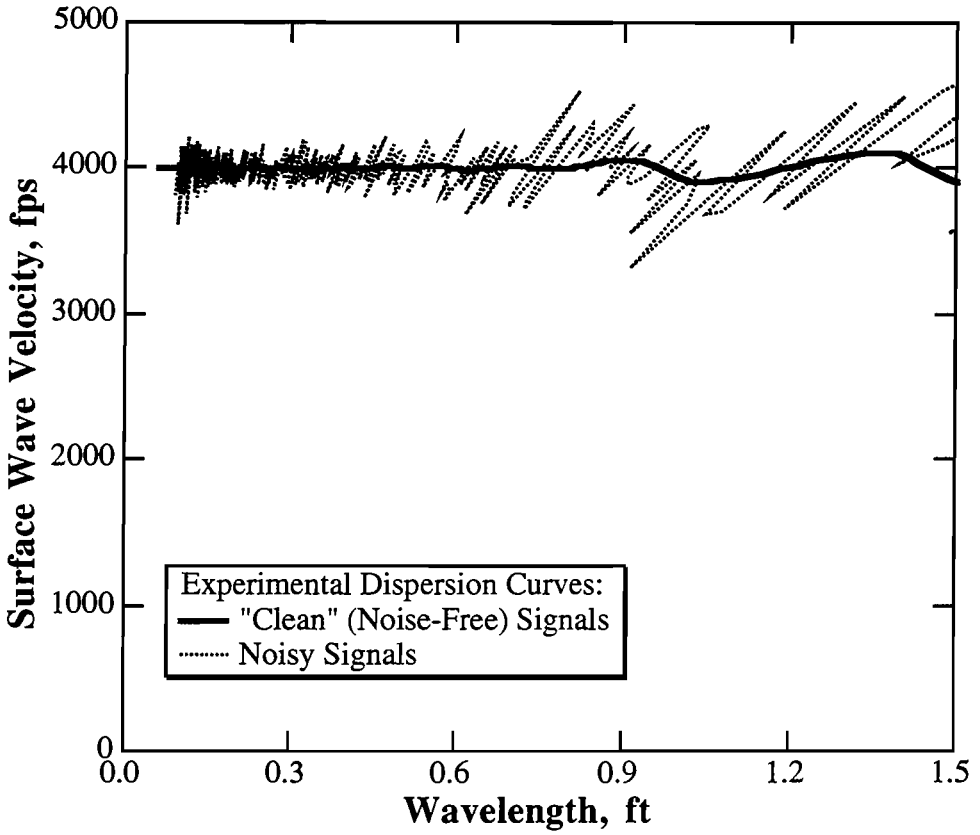

Fig 3.14. Comparison of Experimental Dispersion Curves Determined from the Phase Shifts of the Cross Power Spectra of the Clean and Synthetic Noisy Signals.

and reverse measurements (velocities at the same wavelength do not correspond to the same frequency), it is better to average the phase shifts at each frequency and then calculate a dispersion curve based on the average value of the phase shift.

The cross power spectrum between the two receivers is a vector quantity (phase and magnitude). To ensure that only the phase shifts from the forward and reverse profiles are averaged (not the vectors), two vectors with the same phase shifts as the ones obtained from the forward and reverse profiles and with unit magnitudes were created. The two new vectors were then averaged at each frequency. The creation and averaging of the unit-magnitude vectors were performed by the HP 3562A analyzer through the built-in math functions. Figure 3.15 is a graphical illustration of the averaging process.

One possible reason for the mismatch between the phase shifts of the cross power spectra from the forward and reverse profiles over a limited frequency range can be due to resonances in the coupled receiver-pavement or receiver-ground system. At frequencies below resonance, the phase shifts are due to the propagated waves resulting in a good match between the forward and reverse profiles. At a certain frequency, one of the coupled receivers resonates, introducing an additional phase shift resulting in a mismatch in the phase shifts from the forward and reverse profiles. At a higher frequency, the second coupled receiver resonates, introducing the same phase shift from the first accelerometer resulting again in a good match between the phase shifts from the forward and reverse profiles. Another reason for the mismatch can be due to reflections of body waves from close-by boundaries.

To illustrate the above-mentioned points, the phase shifts of the cross power spectra from the forward and reverse measurements at Site 9 at the TTI test facility in Bryan, Texas, were used. The phase shifts for a receiver spacing of 0.3 m (1 ft) are presented in Fig. 3.16 along with the average phase shift from the forward and

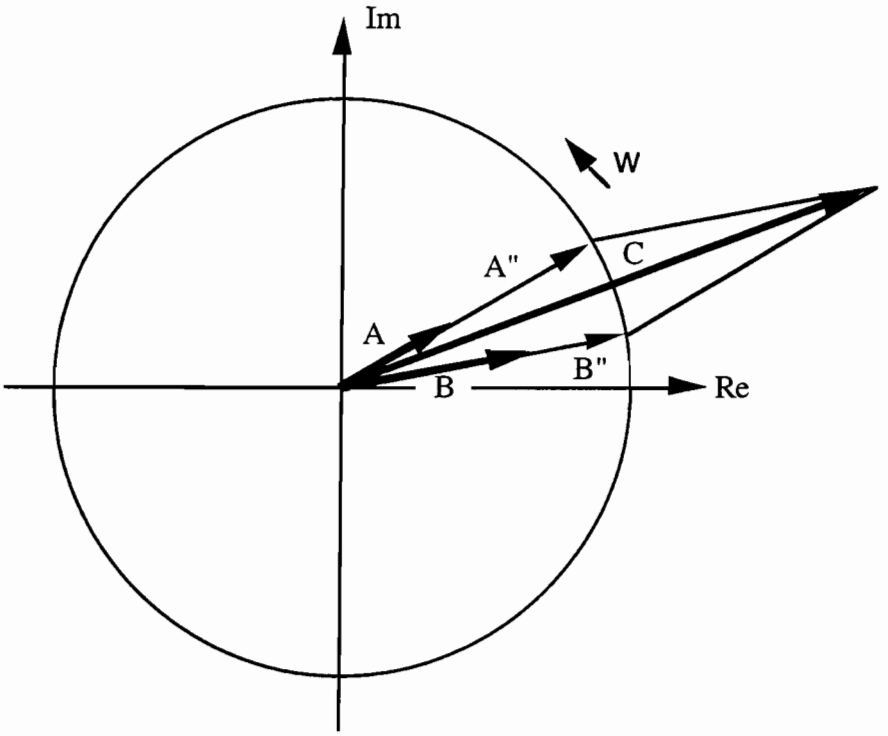

Vector A represents the cross power spectrum from the forward profile
Vector A" is a vector of unit magnitude and phase equal to the phase of vector A
Vector B represents the cross power spectrum from the reverse profile
Vector B" is a vector of unit magnitude and phase equal to the phase of vector B
Vector C has a phase equal to the average phases of vectors A and B (or A" and B")

Fig 3.15. Graphical Illustration of the Averaging of the Phase Shifts of the Cross Power Spectra from Forward and Reverse SASW Measurements.

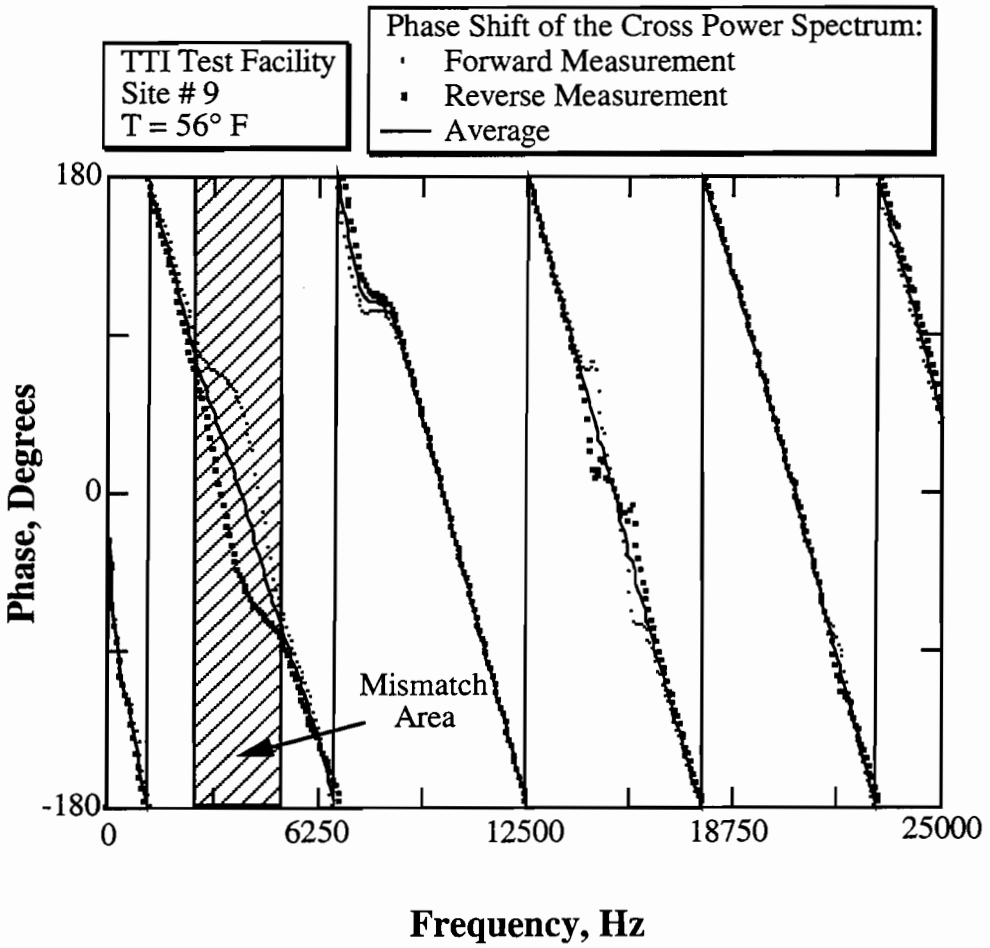

Fig 3.16. Comparison between the Phase Shifts of the Cross Power Spectra from the Forward, Reverse and Average Profiles; R1-R2 = 1 ft.

reverse profiles. As seen in Fig. 3.16, the phase shifts from the forward and reverse profiles compare favorably except in the frequency range from 2,625 to 5,250 Hz. The experimental dispersion curves for the forward, reverse and average profiles are shown in Fig. 3.17. Note the smoothness of the average dispersion curve compared to the forward and reverse dispersion curves. It is recommended that the phase shifts from the forward and reverse profiles be compared before the development of the dispersion curves. In cases similar to that presented in Fig. 3.16, the phase shifts should be averaged to obtain a representative dispersion curve of the site under study.

3.2.6 Forward Modeling Process

The final step in the analysis of the SASW data is called forward modeling or inversion. Forward modeling is defined as the process of predicting the results of measurements based on a given model and assumed model parameters. However, inversion is defined as the process of using the results of measurements and a given model to predict the model parameters. All of the work pertaining to this report is based on the forward modeling process.

The purpose of the forward modeling is to determine a shear wave velocity profile from the measured dispersion curve. This is achieved by assuming a shear wave velocity profile and assigning Poisson's ratios and mass densities of each layer in the profile. A theoretical dispersion curve for the assumed layered profile is calculated and compared to the experimental dispersion curve. If the two curves reasonably match, the assumed shear wave velocity profile is considered to be the actual profile. If the two curves do not match, the shear wave velocity profile is adjusted by changing the thicknesses and/or velocities of the assigned layers (and/or changing the number of layers), and another iteration is performed. The two dispersion curves are compared again. This iterative process is continued until a reasonable match between the experimental and theoretical dispersion curves is achieved.

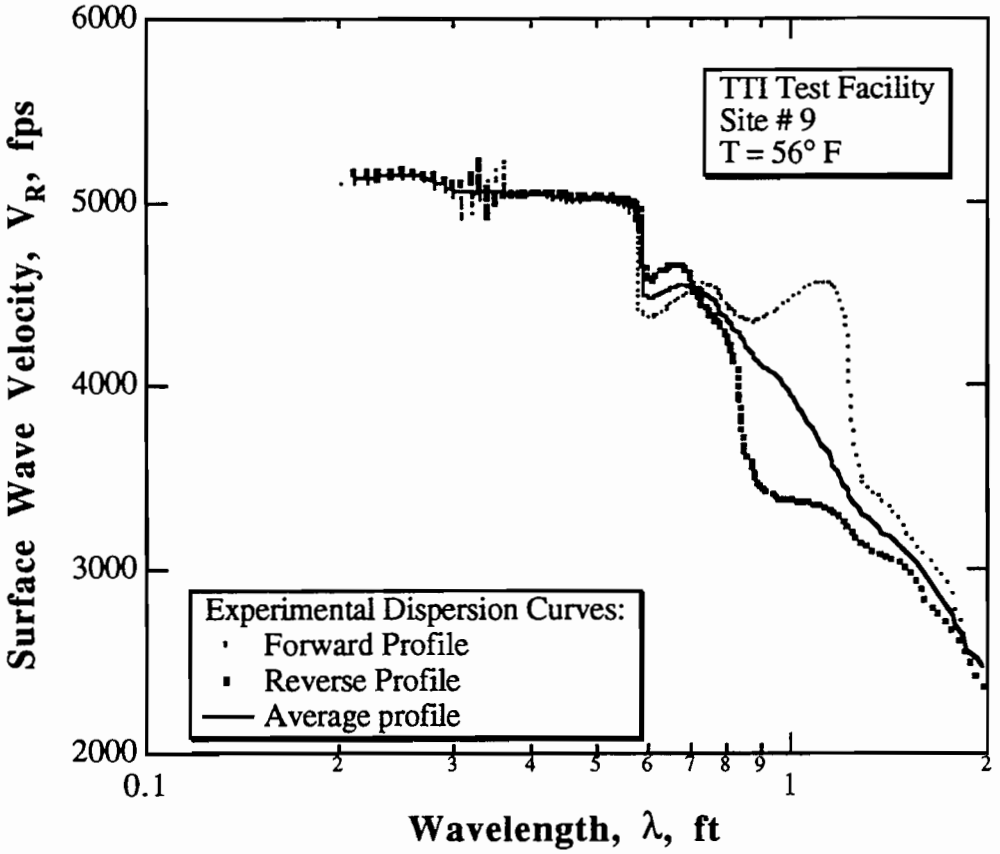

Fig 3.17. Dispersion Curves Determined from the Phase Shifts of the Cross Power Spectra for the Forward, Reverse and Average Profiles Shown in Fig. 3.13; R1-R2 = 1 ft.

The theoretical dispersion curve is calculated from a two-dimensional (2-D) model based on the propagation of plane Rayleigh waves (Nazarian, 1984; Sánchez-Salinero, 1987; and Chang, 1991). A matrix solution (transfer matrix (Thomson, 1950; Haskell, 1953) or dynamic stiffness matrix (Kausel and Roesset, 1981)) is used in the generation of the theoretical dispersion curve. The two-dimensional model works properly if the stiffness of the site increases with depth. In cases where a stiff layer overlying softer layers exists (pavement), problems with the 2-D model were encountered. The theoretical dispersion curve based on the fundamental (first) mode of vibrations does not represent the measured dispersion curve. To model more realistically the SASW test setup, a 3-D model was developed by Roesset and his students (Sánchez-Salinero, 1987; Chang, 1991; Foinquinos, 1991). The 3-D model takes into account all types of seismic waves (Rayleigh interface, and body waves). The theoretical dispersion curve is determined from the complex response of the pavement due to a disk load applied at the surface.

To illustrate the forward modeling process, the WSMR soil site (discussed earlier) and a pavement site located on SH 82 in Paris, Texas (discussed in Chapter Six), are considered herein. The experimental dispersion curves for the two sites are presented in Fig. 3.18.

To calculate the theoretical dispersion curve, one assumes an initial shear wave velocity profile. A good initial estimate for soil sites, where the stiffness increases with depth, is a profile based on the crude inversion process (depth = $\lambda/2$ and $V_S = 1.1\ V_R$). Then, the initial estimate is refined until a match between the experimental and theoretical dispersion curves is achieved. Figure 3.19 shows the initial estimate of the shear wave velocity profile and the refined profile for the WSMR site. The theoretical dispersion curves for the two profiles are compared with the experimental dispersion curve in Fig. 3.20. The theoretical dispersion curves calculated from the 2-D and 3-D models compare well. It is recommended that the 2-D model be used for soil sites due to the lengthy calculations involved with the 3-D model. The SASW results were compared with results from

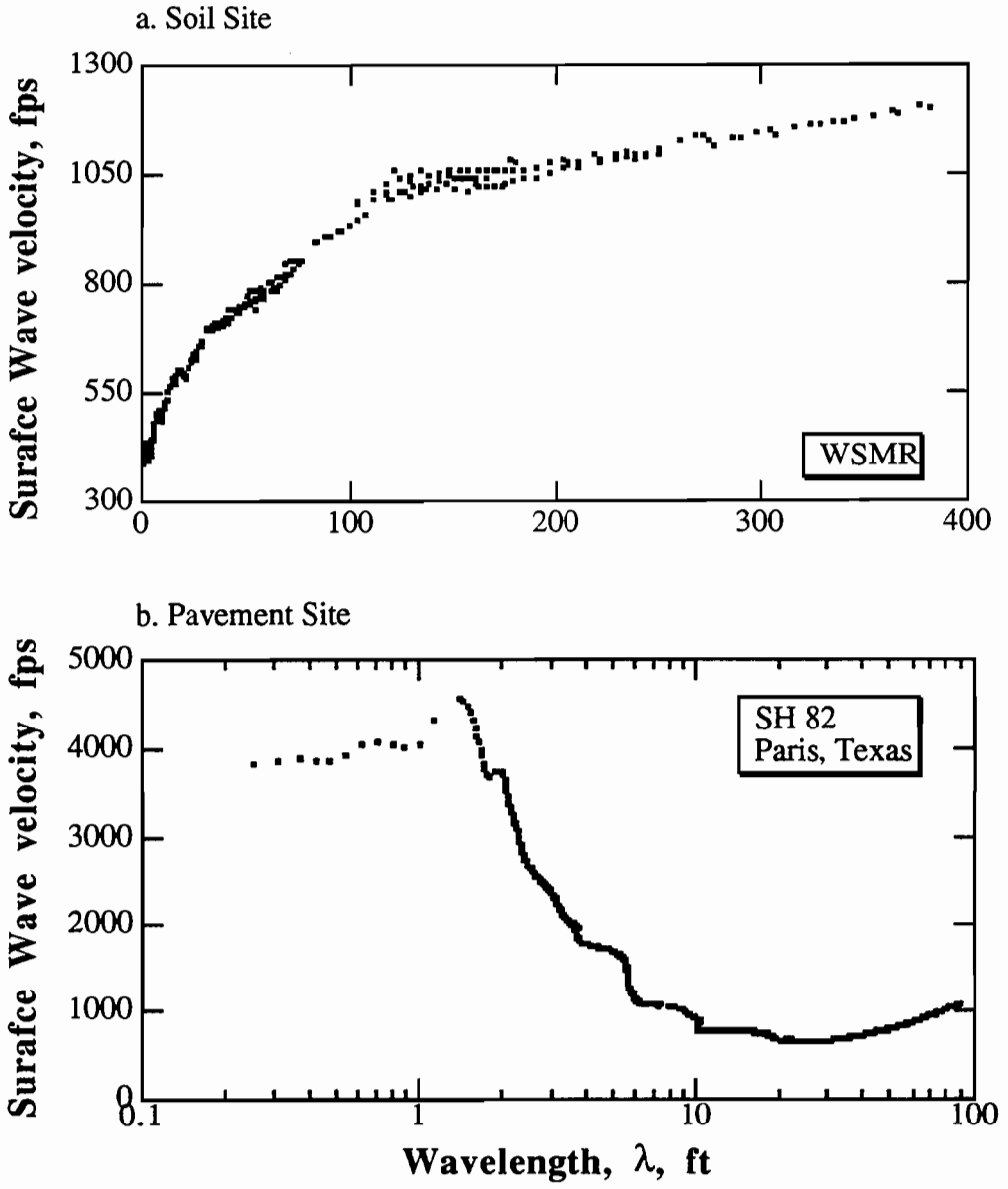

Fig 3.18. Experimental Dispersion Curves Determined at a Soil Site (WSMR) and a Pavement Site (SH 82).

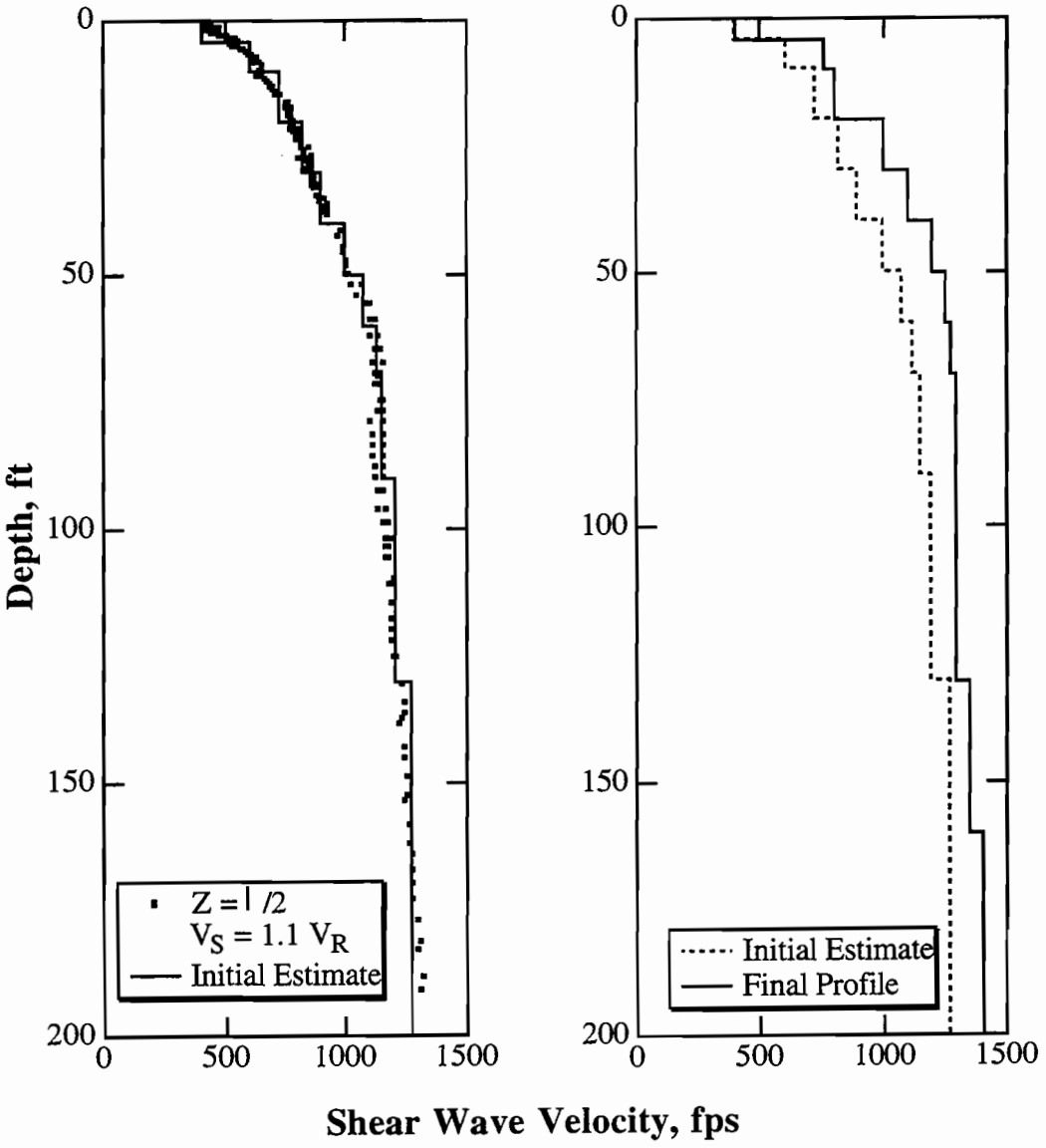

Fig 3.19. Initial Estimate and Final Shear Wave Velocity Profiles for the WSMR Site.

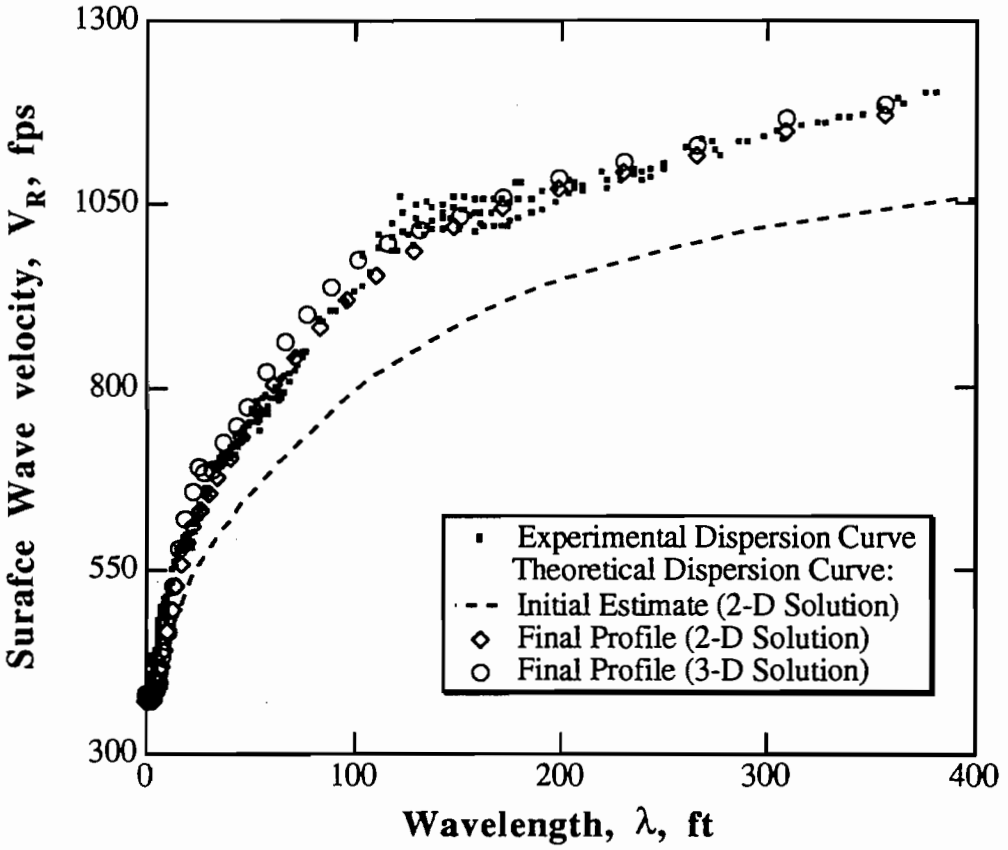

Fig 3.20. Comparison between Experimental and Theoretical Dispersion Curves for WSMR Site.

crosshole tests performed at the same site (Stokoe and Mok, 1988) in Fig. 3.21. The SASW and crosshole results compare well to a depth of approximately 15 m (50 ft). Generally, SASW results showed slower shear wave velocities than those from crosshole tests for depths below 50 ft (15 m). This may be due to the lateral variability encountered at the WSMR site and the larger volume of soil sampled by the SASW test (large receiver spacings are used to sample deep soils) as compared with the volume sampled by the localized crosshole measurements.

For the pavement site (SH 82), the theoretical dispersion curves based on 2-D and 3-D analyses are compared with the experimental dispersion curve in Fig. 3.22. The theoretical dispersion curves were calculated using the shear wave velocity profile also shown in Fig. 3.22. The match between the theoretical dispersion curves from 2-D and 3-D analyses is not good for wavelengths between about 0.3 and 1.5 m (1 and 5 ft). This poor match occurs for two reasons. The first one reason is the approximation in the formulation of the 2-D model where the imaginary part of the determinant is neglected and the real part of the determinant is set equal to zero (Chang, 1991; Foinquinos, 1991). The second (and more important) reason is that wave propagation in the layered system with a strong contrast in stiffness contains significant higher modes. These higher modes have large amplitudes so that their contribution to wave propagation leads to phase velocities that are significantly different from those of plane Rayleigh waves as assumed in 2-D analyses. Therefore, it is recommended that the 3-D analysis be used for inverting pavement sites because it combines all modes participating in waves propagating through the pavement system which models more realistically the field setup used in SASW testing.

3.3 Summary

The Spectral-Analysis-of-Surface-Waves method is a nondestructive technique that is used to evaluate the shear moduli of soil sites and Young's moduli of pavement sites. The method relies on the generation and detection of surface waves. A detailed description of the method is presented in this chapter.

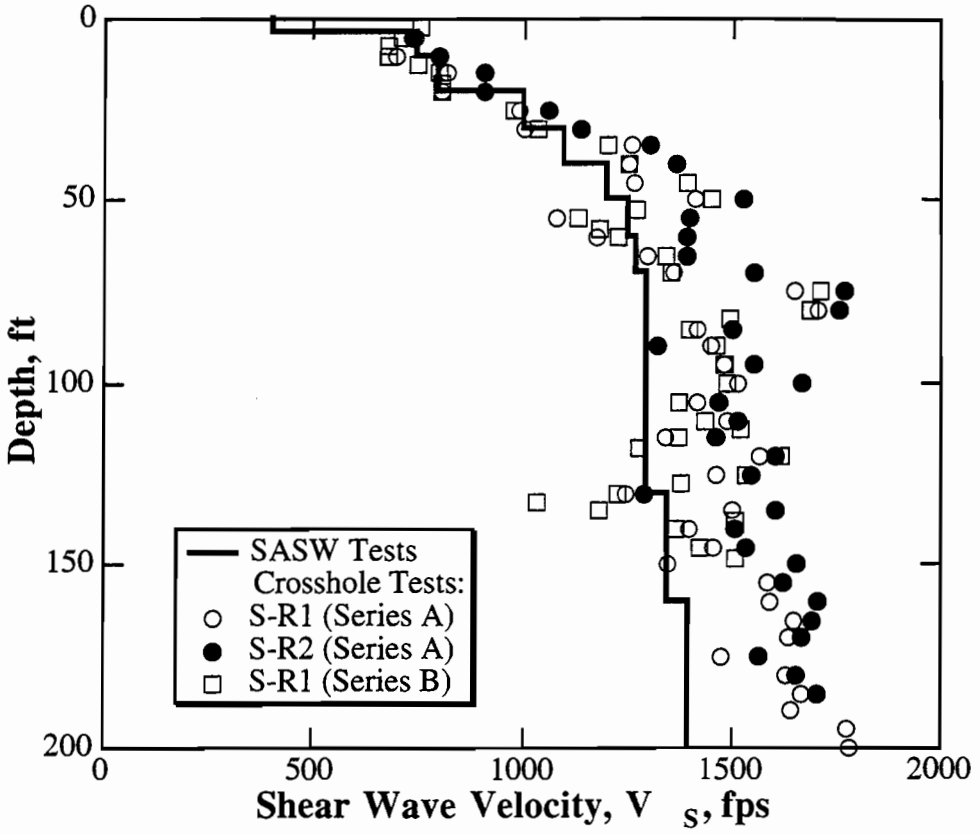

Fig 3.21. Comparison between Shear Wave Velocities from SASW and Crosshole Tests; WSMR Site.

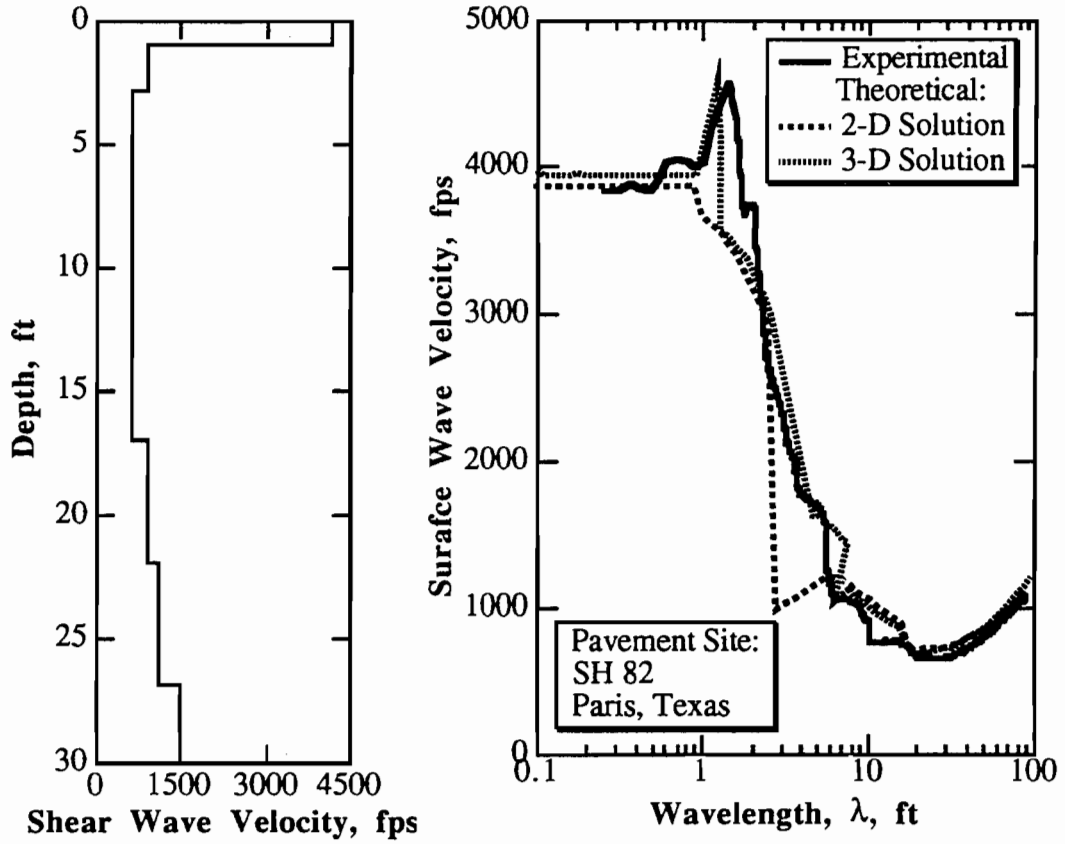

Fig 3.22. Comparison between Experimental and Theoretical Dispersion Curves for the Given Shear Wave Velocity Profile.

The discussion includes field procedures and data reduction techniques. Evaluation of the performance of low- and high-frequency sources and receivers is also presented. At large receiver spacings (say 61m (200 ft)), bulldozers are recommended for use as low-frequency generators. At short receiver spacings (say 0.15 m (0.5 ft)), piezoelectric sources (V-meter and WR F-7 shaker) are recommended as high-frequency generators.

Before obtaining the experimental dispersion curves, the phase shifts of the cross power spectra between the two receivers from the forward and reverse profiles should be compared. If a mismatch between the two phase shifts occurs, averaging the phase shifts in the frequency domain helps to smooth the experimental dispersion curve. For soil sites where the stiffness increases with depth, forward modeling based on a 2-D model can be used. However, if a stiff layer overlying softer layers exists (pavement systems), the 2-D formulation is not a good model due to some numerical approximations as discussed at the end of Section 3.2.6 and by Huerta et al., 1994. Forward modeling based on a 3-D model should be used to obtain shear wave velocity profiles of pavement sites because this model incorporates the higher modes involved in wave propagation at such sites.

CHAPTER FOUR
SASW MEASUREMENTS AT THE TTI ANNEX

4.1 Introduction

In this chapter, use of the SASW method at the Texas Transportation Institute (TTI) Annex in Bryan, Texas, is presented to demonstrate the precision and effectiveness of the method in determining changes in stiffness of the asphalt concrete (AC) surface layer due to solar warming and cooling.

SASW testing was employed at Sites 4, 9 and 12 at the TTI test facility (shown in Fig. 4.1) at two different times. The first time involved measurement of the material stiffness during the last week of July, 1988, when the temperature of the surface layer rose up to 64° C (143° F). The second time involved field measurements during the cold season, in the first week of March, 1989, when the temperature dropped to an unusually low value of –1° C (30° F). Sites 4, 9 and 12 represent pavements with "thick" AC surface layers. Each pavement has an AC layer thickness of 12.7 cm (5 in.). The definition of "thick" as used in these tests refers to the ability to generate surface waves in the AC layer which are shorter than the thickness of the AC layer.

Additional testing was also performed at Sites 10 and 11 at the TTI facility and at a pavement site in Granger, Texas. In this case, the AC surface layer was "thin": The thickness was 2.54 cm (1 in.) or less. However, the word "thin" was used to denote the case where wavelengths in the SASW test could not be generated that were less than the thickness of the layer.

The objective of testing at TTI and Granger was to study the effect of the thickness of the AC layer on the measurement of stiffness, to determine if the SASW method ceases to perform adequately at some thicknesses, and to

recommend when other techniques should be used in conjunction with the SASW method to characterize the structural capacity of the pavement system.

4.2 Site Descriptions at the TTI Facility

This study was performed at the TTI test facility of Texas A&M University. The facility consists of 27 pavement sections which were constructed under well-controlled conditions for research purposes. A plan view of the general layout of the test facility is shown in Fig. 4.1. Testing was performed at Sites 4, 9, 10, 11 and 12, which are marked with thick solid lines and cross-hatching.

The material profiles of the 27 pavement sections as reported by Scrivner and Michalak (1974) are presented in Table 4.1. Site 4 consists of a 5-in. (12.7-cm) asphalt concrete (AC) surface layer, 30.5 cm (12 in.) of cement-stabilized (4% cement) crushed limestone base, and a 30.5-cm (12-in.) crushed limestone subbase. Sites 9 and 12 differ from Site 4 in their base characteristics. Site 9 has a 10.2-cm (4-in.) crushed limestone base and Site 12 has a 30.5-cm (12-in.) crushed limestone base. The selection of the three sites was based on their proximity to each other which reduced the mobilization time so that SASW measurements could be done without a significant change in the temperature of the surface layer. Another motive to select these sites was that they all have a 12.7-cm- (5-in.-) thick surface layer which made performance of SASW tests at high temperatures (lower frequencies needed) possible. The difference in the base material allowed examination of the effectiveness of the SASW method in evaluating the elastic constants of the base material.

Sites 10 and 11 at the TTI facility were selected because of their thin AC surface layer. These two sites consist of a 2.54-cm (1-in.) AC surface layer underlain by crushed limestone base and subbase.

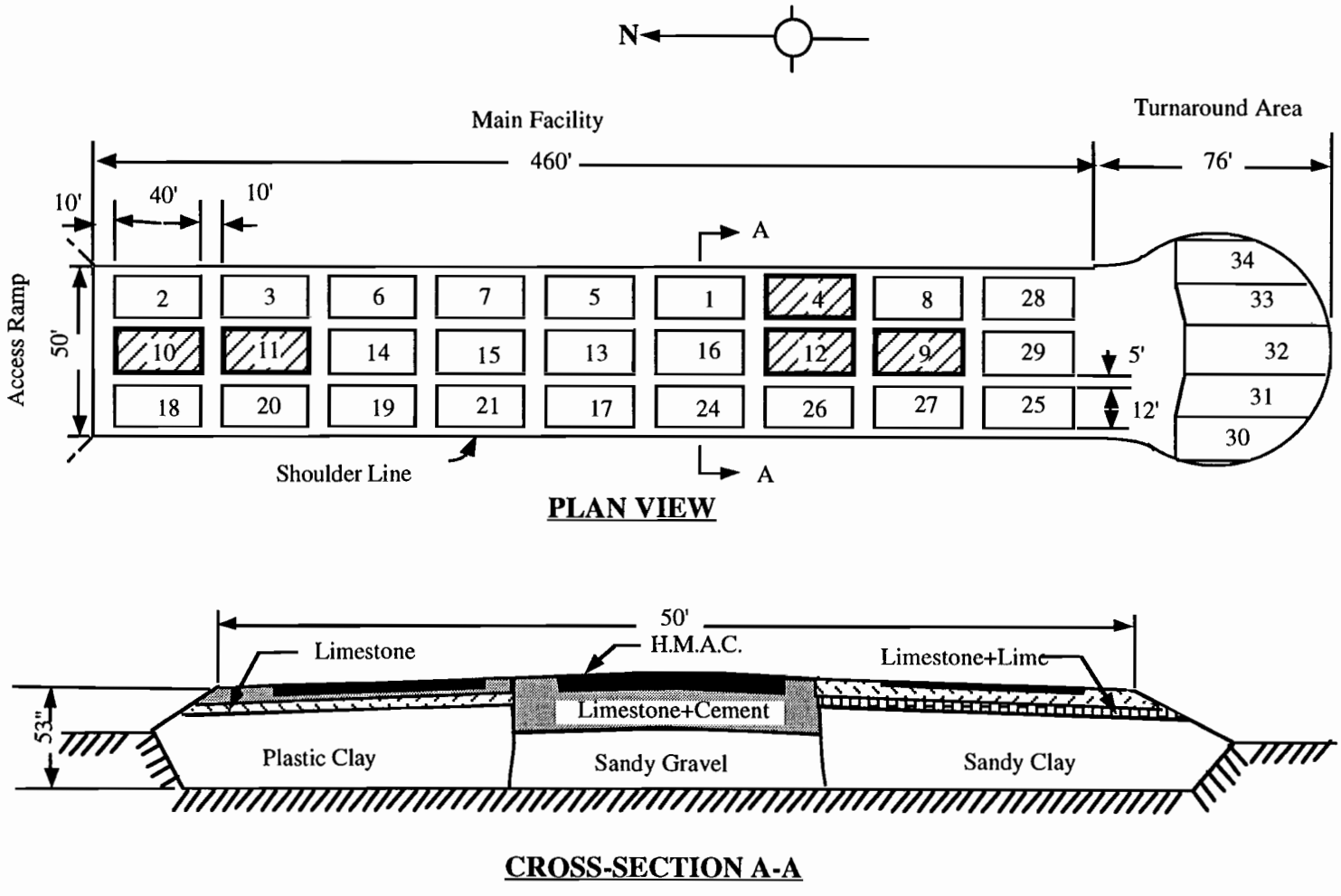

Fig 4.1. General Layout of the Pavement Test Facility at the Texas Transportation Institute Annex, Bryan, Texas (Scrivner and Michalak, 1974).

Table 4.1. Material Profiles of TTI Pavement Test Facility (Scrivner and Michalak, 1974)

	Thickness (in.)				Material Type			
Section	Surface	Base	Subbase	Emb.	Surface	Base	Subbase	Emb.
1	5	4	4	40	AC	LS+C	LS	PC
2	1	12	4	36	AC	LS+C	LS	PC
3	1	4	12	36	AC	LS+C	LS	PC
4	5	12	12	24	AC	LS+C	LS	PC
5	5	4	4	40	AC	LS	LS+C	PC
6	1	12	4	36	AC	LS	LS+C	PC
7	1	4	12	36	AC	LS	LS+C	PC
8	5	12	12	24	AC	LS	LS+C	PC
9	5	4	4	40	AC	LS	LS	GR
10	1	12	4	36	AC	LS	LS	GR
11	1	4	12	36	AC	LS	LS	GR
12	5	12	12	24	AC	LS	LS	GR
13	5	4	4	40	AC	LS+C	LS+C	GR
14	1	12	4	36	AC	LS+C	LS+C	GR
15	1	4	12	36	AC	LS+C	LS+C	GR
16	5	12	12	24	AC	LS+C	LS+C	GR
17	3	8	8	34	AC	LS+L	LS+L	SC
18	1	8	8	36	AC	LS+L	LS+L	SC
19	5	8	8	32	AC	LS+L	LS+L	SC
20	3	4	8	38	AC	LS+L	LS+L	SC
21	3	12	8	30	AC	LS+L	LS+L	SC
24	3	8	8	34	AC	LS	LS+L	SC
25	3	8	8	34	AC	LS+C	LS+L	SC
26	3	8	8	34	AC	LS+L	LS	SC
27	3	8	8	34	AC	LS+L	LS+C	SC
28	3	8	8	34	AC	LS+L	LS+L	PC
29	3	8	8	34	AC	LS+L	LS+L	GR

AC: Hot Mix Asphaltic Concrete
LS+C: Crushed Limestone Mixed with 4% Cement
LS+L: Crushed Limestone Mixed with 2% Lime
LS: Crushed Limestone
GR: Sandy Gravel
SC: Sandy Clay
PC: Plastic Clay

4.3 Temperature Measurements at the TTI Facility

The temperature of the surface layer was measured with a Fluke digital thermometer using a J-type thermocouple as the temperature sensor. The thermocouple was inserted to a depth of approximately 1.27 cm (0.5 in.). The measured temperature is referred to as the surface temperature hereafter. Simultaneously, the surface temperature was recorded using a temperature gun. The readings from the Fluke digital thermometer were consistently higher by about –13° C (8° F) than those from the temperature gun.

To make sure that the recorded surface temperatures from the thermocouple and Fluke recording device were correct, the device was calibrated in the laboratory with a thermometer using a water bath. The recorded temperatures from the thermometer and the thermocouple device are listed in Table 4.2. The thermocouple readings were corrected to the values measured with the thermometer and are the values reported herein.

Table 4.2. Calibration of the Fluke Digital Device with a Thermometer in the Laboratory

Fluke Digital Device		Thermometer	
°C	°F	°C	°F
49.1	120.4	50.0	122.0
40.3	104.5	41.1	106.0
37.1	98.8	37.6	99.7
35.4	95.7	35.9	96.6
31.0	87.8	31.3	88.3
24.2	75.6	24.6	76.3
19.4	66.9	19.6	67.3
11.7	53.1	11.8	53.2
6.8	44.2	7.0	44.6
4.0	39.2	4.1	39.4

4.4 Stiffness Changes of Sites 4, 9 and 12 with Temperature

The asphalt concrete pavement stiffness is dependent on temperature due to the viscous nature of asphalt. The modulus of the pavement can change significantly if evaluated under various temperature conditions.

To evaluate the variation in stiffness of the surface layer in the field as temperatures vary, SASW tests were performed at Sites 4, 9 and 12 at the TTI Annex. Two series of SASW measurements were performed, one during the summer of 1988 and the other during the winter of 1989. These two test series covered a wide range in pavement temperatures.

4.4.1 SASW Measurements during July, 1988

The first series of SASW tests at Sites 4, 9 and 12 was conducted during July, 1988, with surface temperature variations from 27° C (80° F) in the morning (5:30 am) to about 60° C (143° F) in the afternoon (2:15 pm).

Two sources were used to generate wave energy. A small ball-peen hammer and a V-meter were used as sources to generate high frequencies. The generated surface waves were detected by two PCB Model 308B02 accelerometers placed on the ground surface. These accelerometers have a resonant frequency of 25 kHz and a calibration factor of 1 volt/g. The accelerometers were coupled to the asphalt concrete by attaching 10-32 threaded rods to the bottom of the accelerometers which, in turn, were attached to nuts glued to the AC surface.

The performance of the small ball-peen hammer and the V-meter as high-frequency sources was evaluated. As the temperature of the surface layer rose, the surface layer became too soft to allow impact sources such as the small hammer to be used as a high-frequency source. A comparison of the cross power spectra and the coherence functions from SASW measurements at Site 12 using both sources is shown in Fig. 4.2. The V-meter generated significant energy up to 45 kHz, as opposed to the 20-kHz energy level generated by the small hammer. Despite the rather poor coherence at high frequencies due to attenuation and noise interference, the cross power spectrum data using the V-meter as a source could be easily interpreted to obtain the experimental dispersion curve. Based on the comparison of the two sources in terms of their frequency generation, the V-meter was adopted as a better source for the generation of the high frequencies needed to sample the

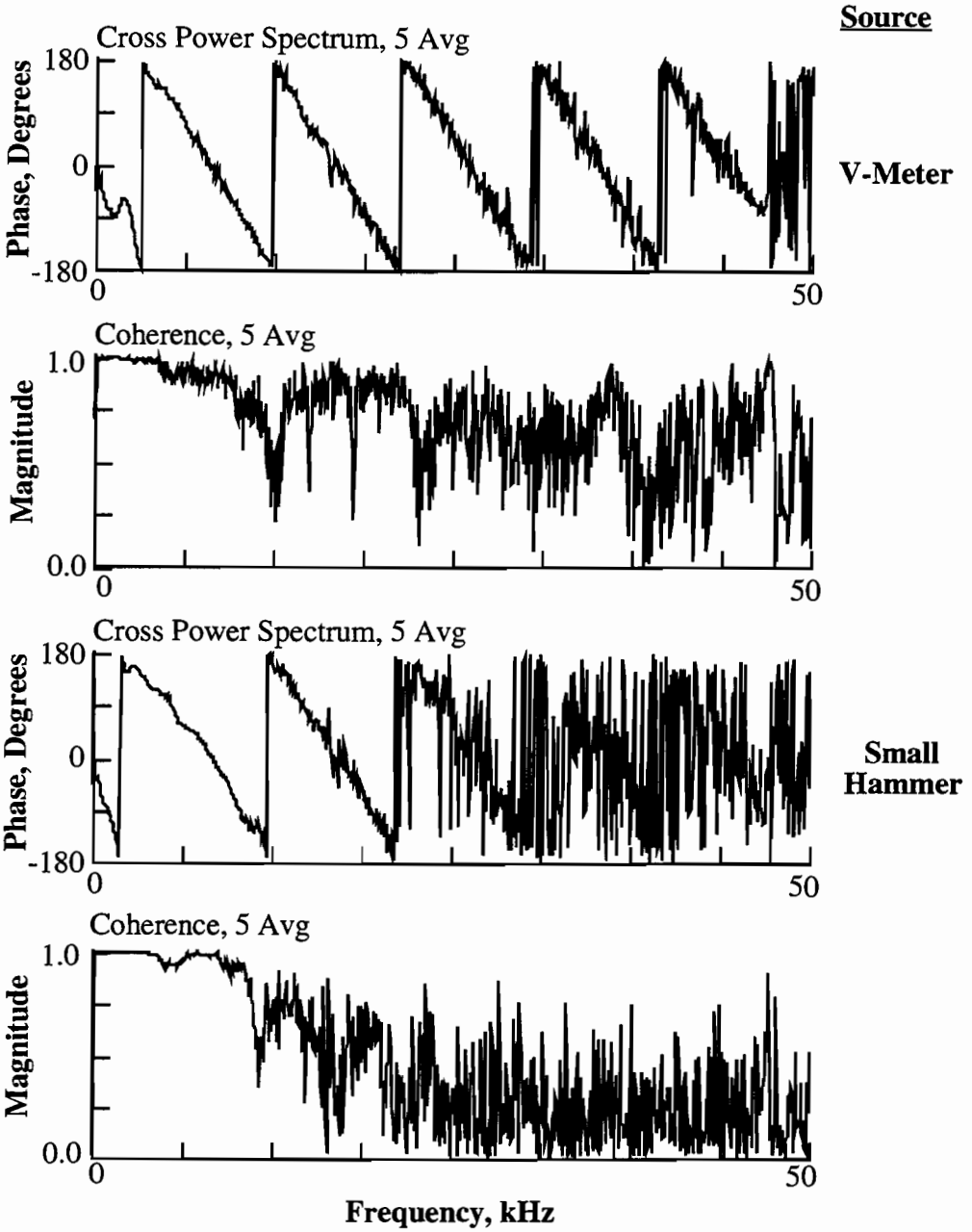

Fig 4.2. Comparison of Phases of the Cross Power Spectra and Coherence Functions Using Two Different Sources; Site 12 at TTI Annex (T = 97° F, R1-R2 = 6 in.).

asphalt concrete layer and was used for the remainder of the SASW measurements in the first series of testing.

A comparison of the phases of the cross power spectra for a temperature range from 32 to 60° C (89 to 143° F) using a receiver spacing of 15.2 cm (6 in.) is presented in Figs. 4.3 through 4.5 for Sites 4, 9 and 12, respectively. Figures 4.3 through 4.5 show the deterioration of the phase shift of the cross power spectrum as the surface layer warms. At a temperature of 27° C (80° F), frequencies up to 45 kHz were generated, as opposed to frequencies of about 15.5 kHz when the temperature rose to 60° C (143° F).

4.4.2 SASW Measurements during March, 1989

The second series of SASW tests at Sites 4, 9 and 12 was conducted during March, 1989, where the surface temperature varied from –1° C (30° F) early in the morning (5:50 am) to 27° C (81° F) in the early afternoon (12:45 pm).

The source used to generate the high frequencies in the second series of tests was a small ball-peen hammer due to its simplicity. The performance of this source was checked against that of the V-meter for low surface temperatures. A comparison of the cross power spectra and coherence functions at Site 12 using both sources is shown in Fig. 4.6. The ball-peen hammer performed adequately over the range of temperatures and frequencies required to sample the surface layer. Both sources generated energy up to 50 kHz. The generated surface waves were detected by two WR Model 736 accelerometers placed on the ground surface. These accelerometers have a resonant frequency above 50 kHz when mounted and a calibration factor of 0.1 volt/g. The accelerometers were coupled to the asphalt concrete by attaching a magnet to a steel plate at the bottom of the accelerometers which, in turn, was attached to a nail driven into the surface layer.

A comparison of the phases of the cross power spectra for a temperature range from –1 to 27° C (30 to 81° F) using a receiver spacing of 15.2 cm (6 in.) is

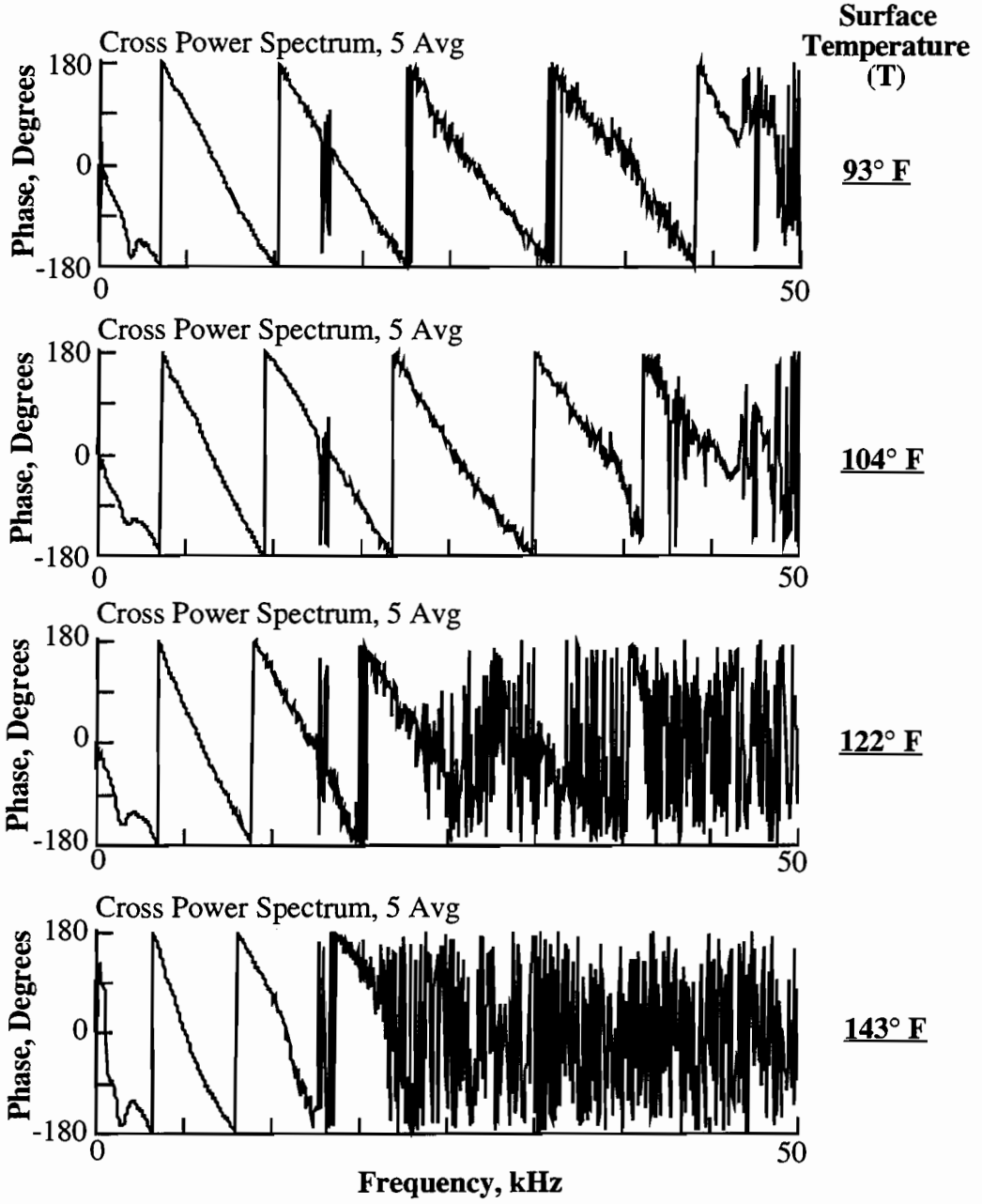

Fig 4.3. Variation in Phase of the Cross Power Spectrum as the Asphalt Concrete Surface Layer Warms from 93 to 143° F; Site 4 at TTI Annex (V-Meter Source, R1-R2 = 6 in.).

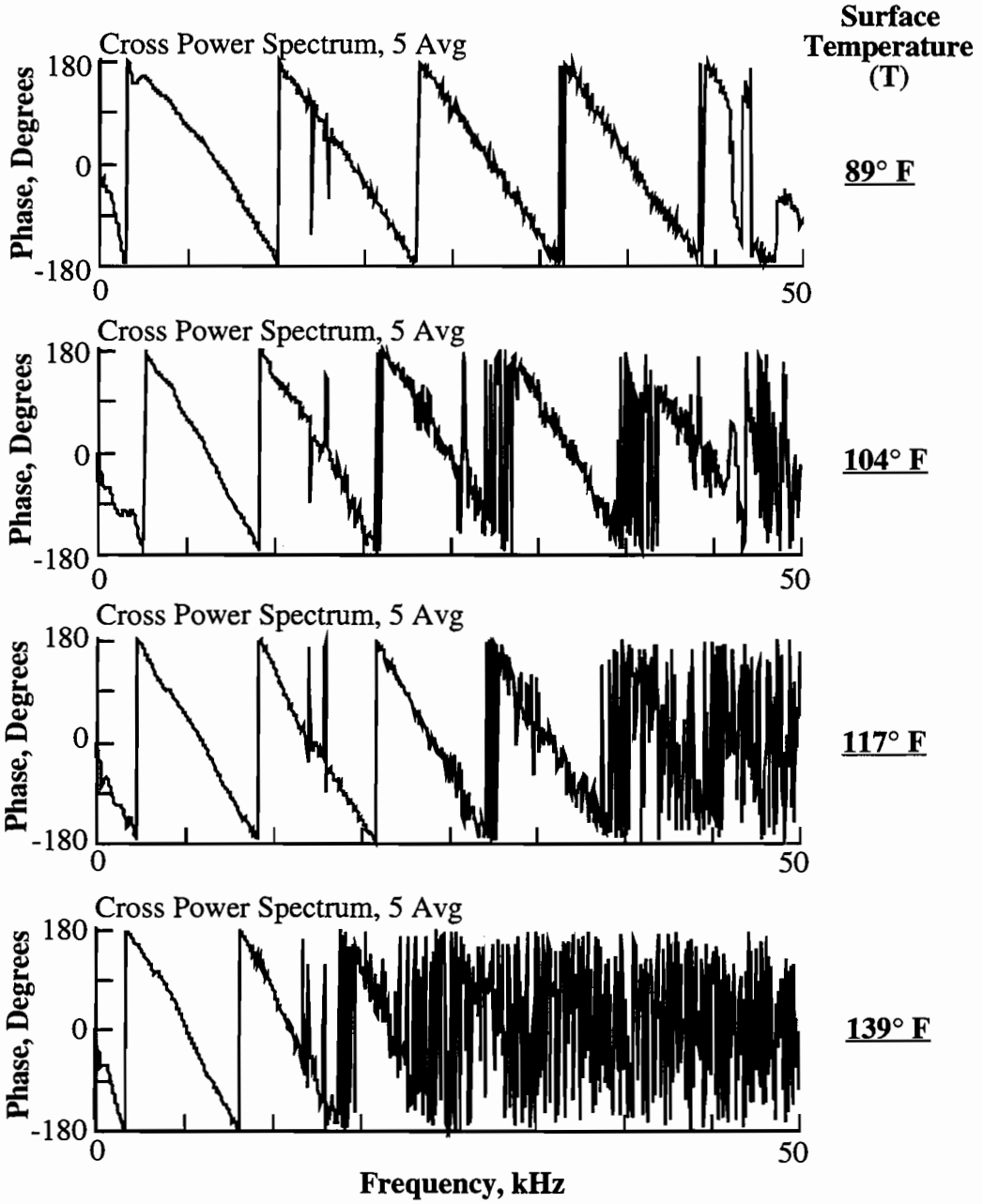

Fig 4.4. Variation in Phase of the Cross Power Spectrum as the Asphalt Concrete Surface Layer Warms from 89 to 139° F; Site 9 at TTI Annex (V-Meter Source, R1-R2 = 6 in.).

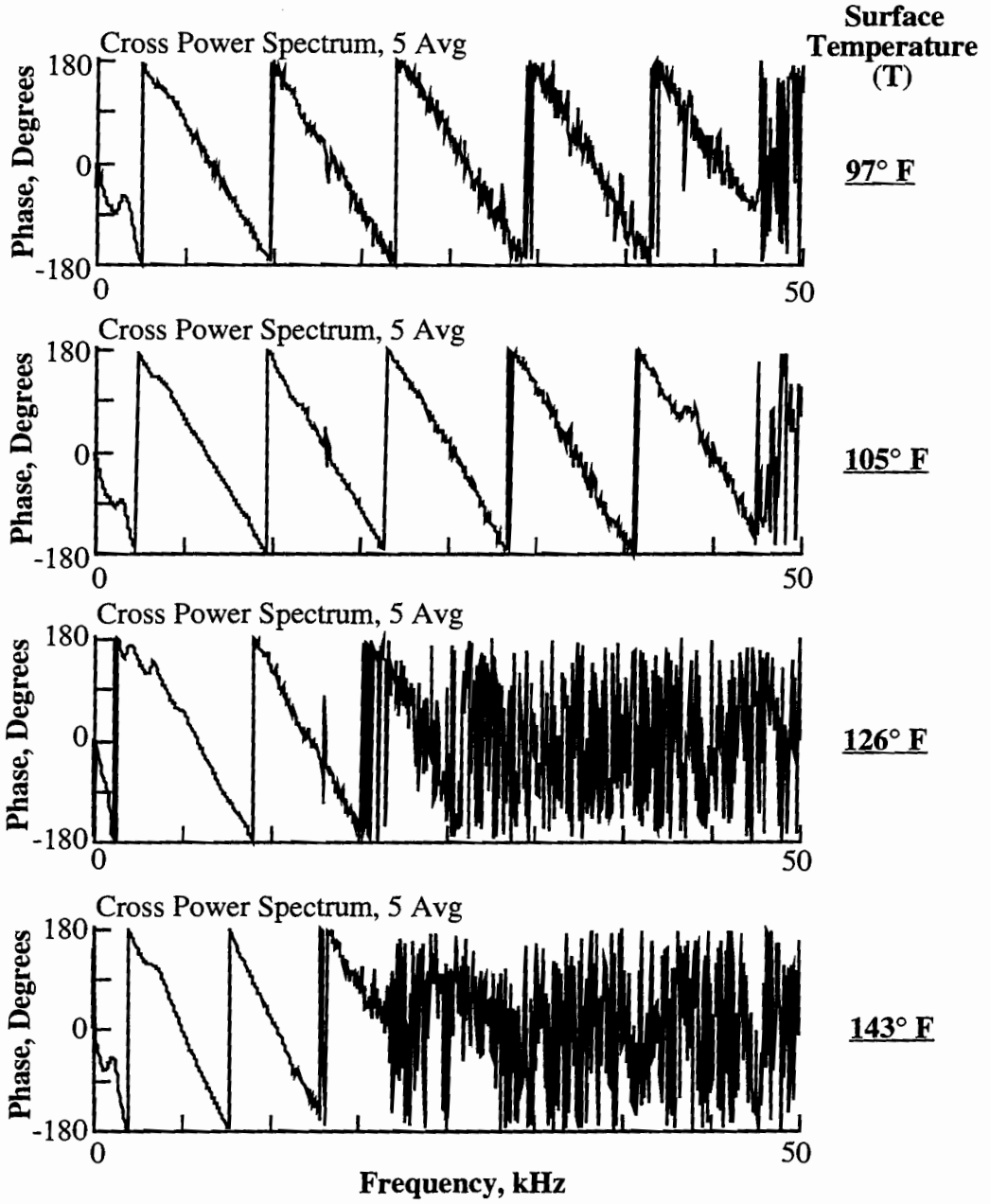

Fig 4.5. Variation in Phase of the Cross Power Spectrum as the Asphalt Concrete Surface Layer Warms from 97 to 143° F; Site 12 at TTI Annex (V-Meter Source, R1-R2 = 6 in.).

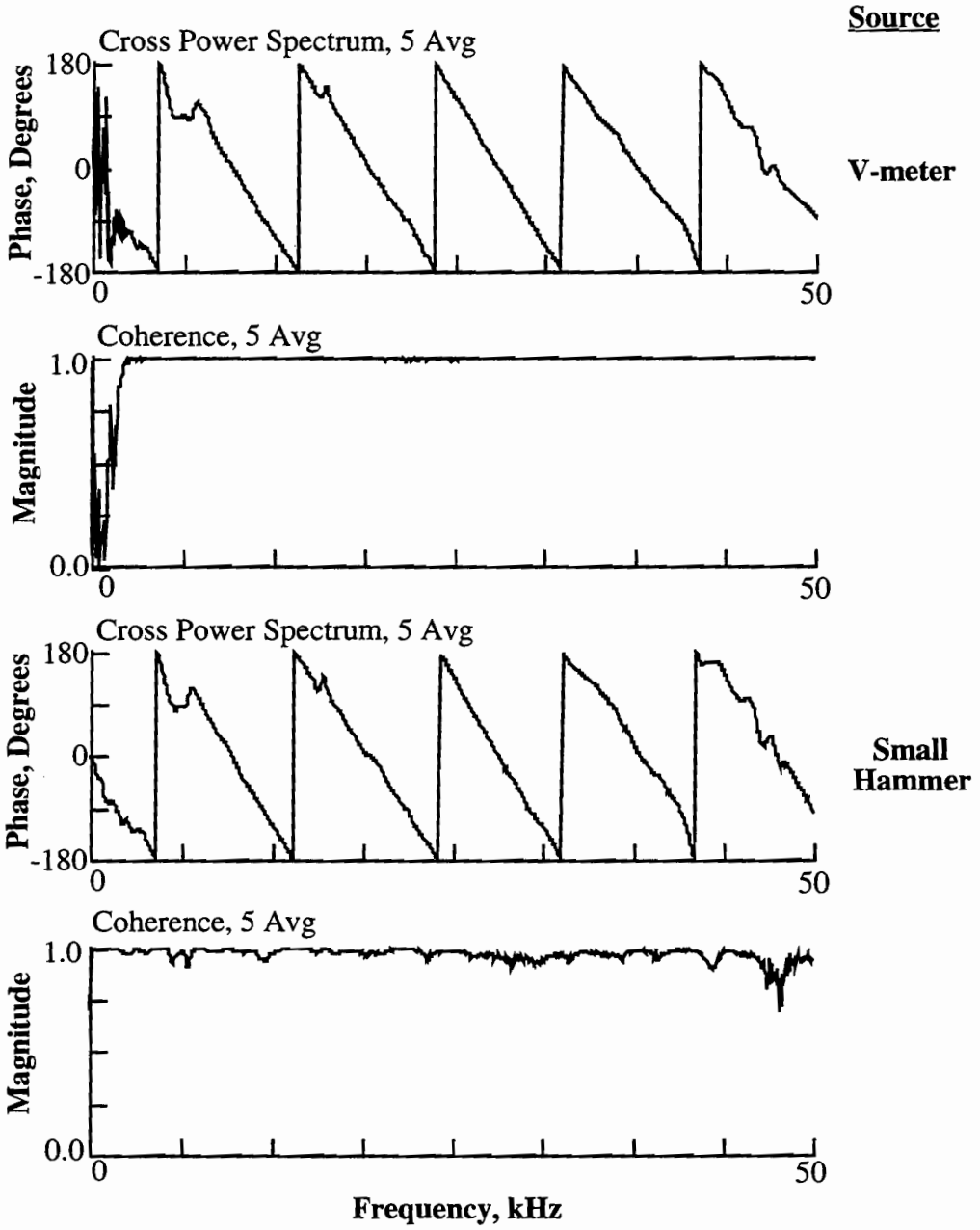

Fig 4.6. Comparison of Phases of the Cross Power Spectra and Coherence Functions Using Two Different Sources; Site 12 at TTI Annex (T = 59° F, R1-R2 = 6 in.).

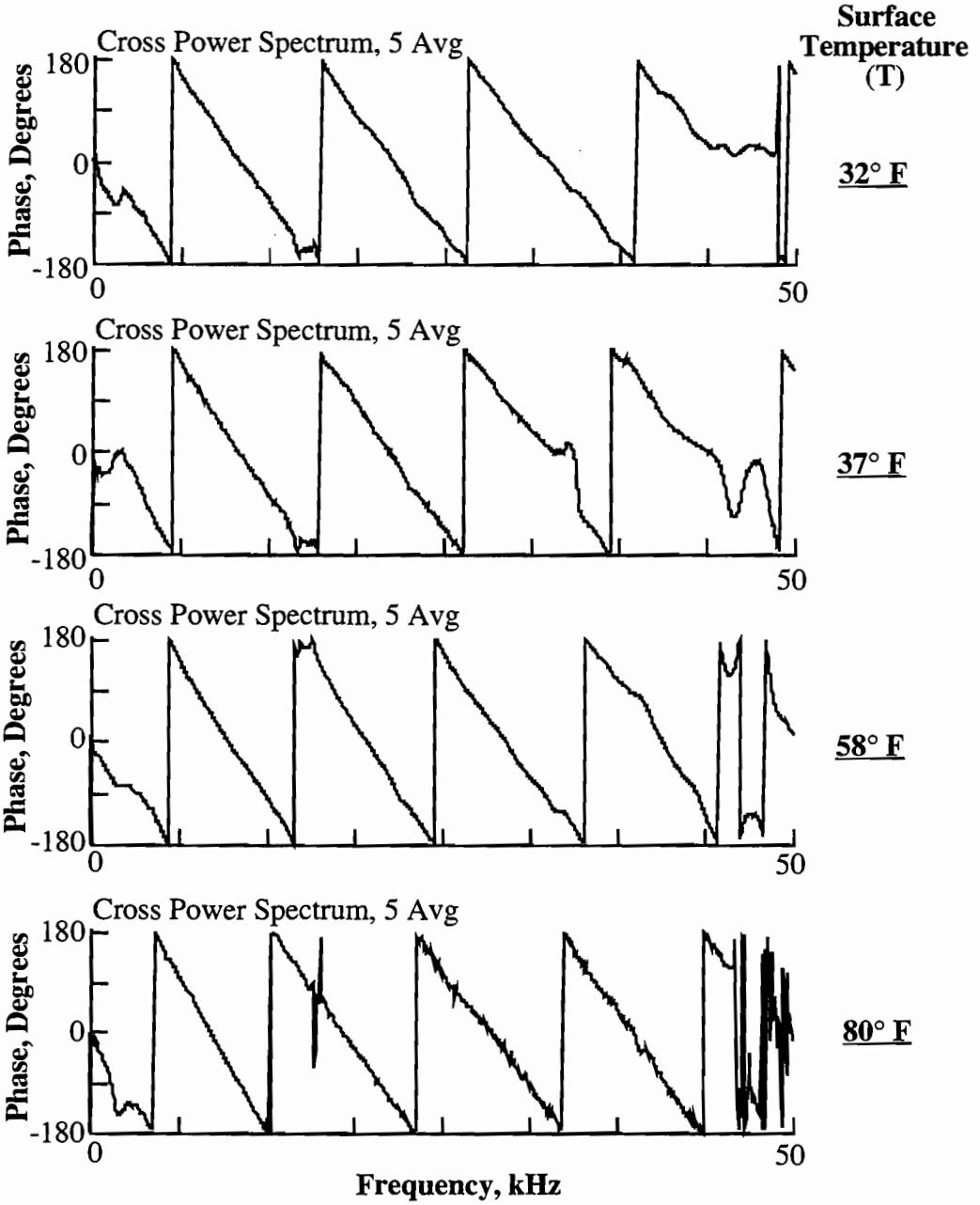

Fig 4.7. Variation in Phase of the Cross Power Spectrum as the Asphalt Concrete Surface Layer Warms from 32 to 80° F; Site 4 at TTI Annex (Hammer Source, R1-R2 = 6 in.).

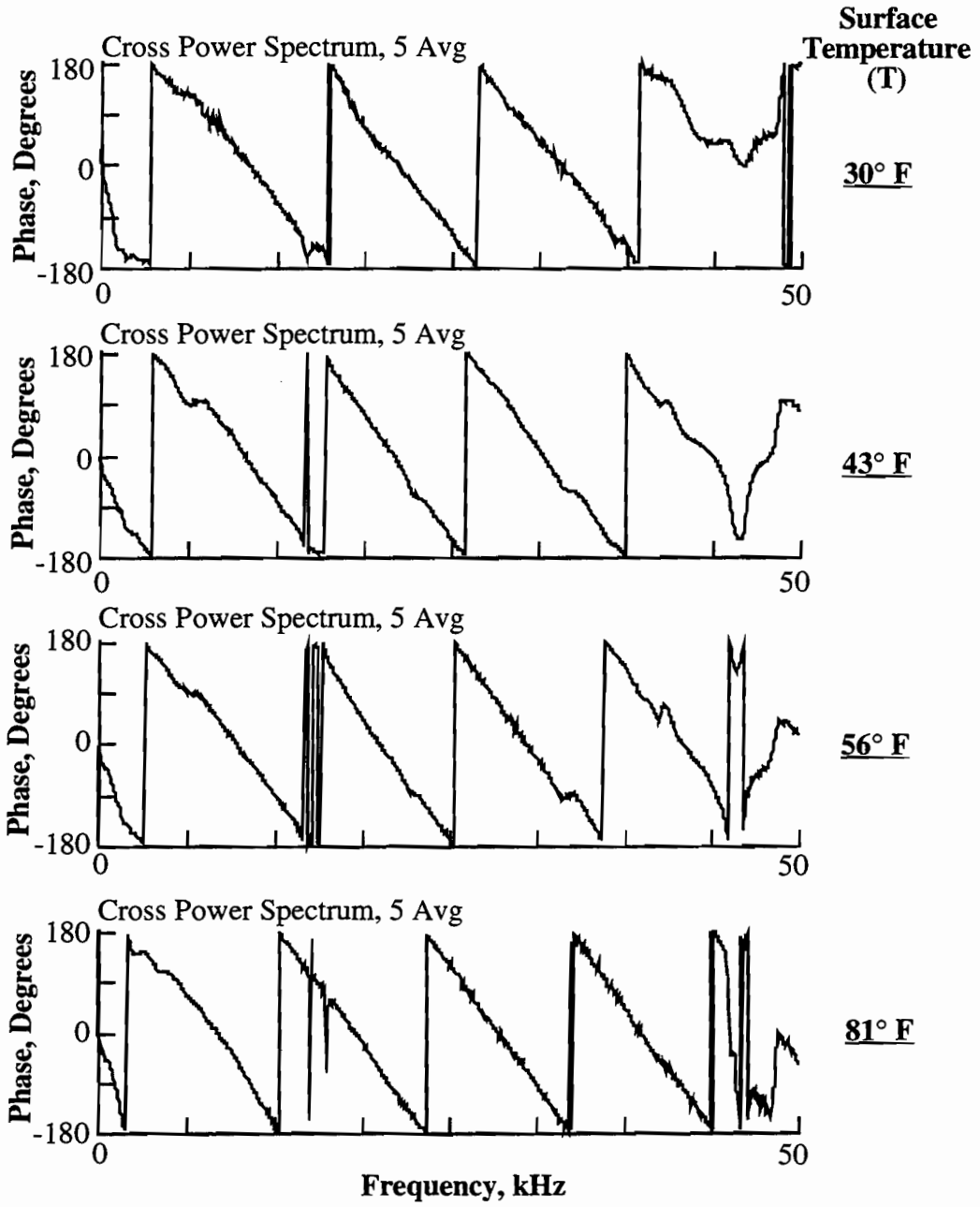

Fig 4.8. Variation in Phase of the Cross Power Spectrum as the Asphalt Concrete Surface Layer Warms from 30 to 81° F; Site 9 at TTI Annex (Hammer Source, R1-R2 = 6 in.).

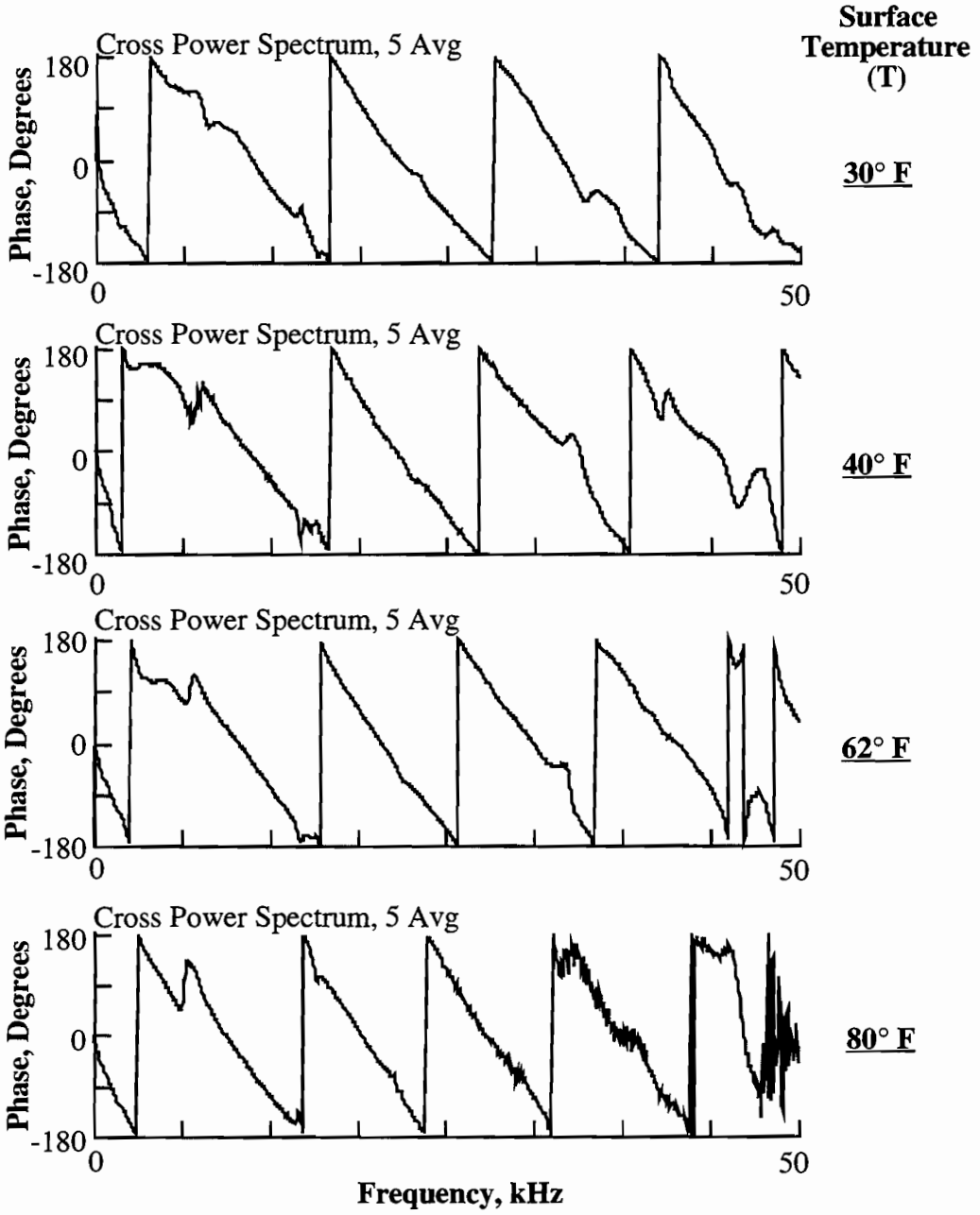

Fig 4.9. Variation in Phase of the Cross Power Spectrum as the Asphalt Concrete Surface Layer Warms from 30 to 80° F; Site 12 at TTI Annex (Hammer Source, R1-R2 = 6 in.).

presented in Figs. 4.7 through 4.9 for Sites 4, 9 and 12, respectively. Figures 4.7 through 4.9 show no deterioration of the phase shift of the cross power spectrum as the surface layer warms. Frequencies up to 50 kHz were generated over the temperature range from –1 to 27° C (30 to 80° F). Thus, if thin pavements were to be tested, high temperatures would cause a problem in attenuating all the high frequencies needed to define the stiffness of the top layer. In such cases, it is recommended that the pavement be tested when it is cool (temperature less than 27° C (80° F)) or that P-wave measurements (see Section 4.5.2) based on the first arrival be performed in conjunction with the SASW measurements to evaluate the stiffness of the top layer at high temperatures. The stiffness of the top layer is a key element in obtaining the stiffnesses of the layers underneath the surface layer in SASW testing.

4.4.3 Experimental Dispersion Curves of Sites 4, 9 and 12

The phase shifts of the cross power spectra shown in Figs. 4.3 through 4.8, in addition to the coherence functions, were used to obtain the experimental dispersion curves shown in Figs. 4.10 through 4.12 for Sites 4, 9 and 12, respectively. The experimental dispersion curves shown are the composite dispersion curves based on receiver spacings of 0.15 and 0.30 m (0.5 and 1 ft). The 0.30-m (1-ft) spacing was used to sample the base layer.

Some important observations can be made by examining Figs. 4.10 through 4.12. First, the stiffness of the surface layer can be determined with great precision as it warms up or cools down. At a temperature of –1° C (30° F), an average value of the surface wave velocity of the asphalt layer was found to be 1,655 m/s (5,430 fps) as opposed to the value of 1,025 m/s (3,370 fps) at a temperature of 60° C (143° F). These values correspond to Young's moduli of 18.8 x 10^3 MPa (2,735 ksi) and 7.3 x 10^3 MPa (1,055 ksi) at –1° C and 60° C (30° F and 143° F) at an average measurement frequency of 15.5 kHz (assuming a Poisson's ratio of 0.27). Second, Figs. 4.10 through 4.12 show a slight decrease in the velocity of the surface layer with an increase in wavelength, suggesting a

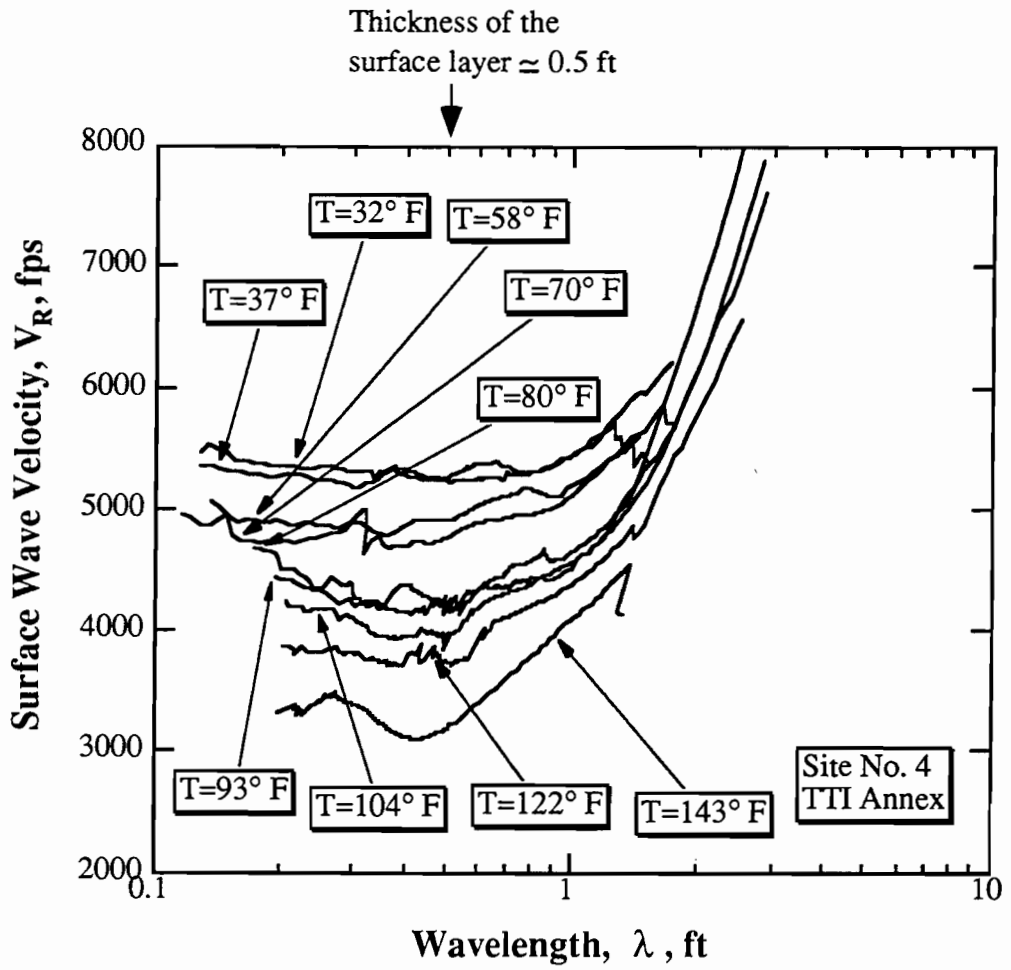

Fig. 4.10. Changes in the Stiffness of the Asphalt Concrete Surface Layer as a Result of Solar Heating at Site 4; TTI Annex, Bryan, Texas.

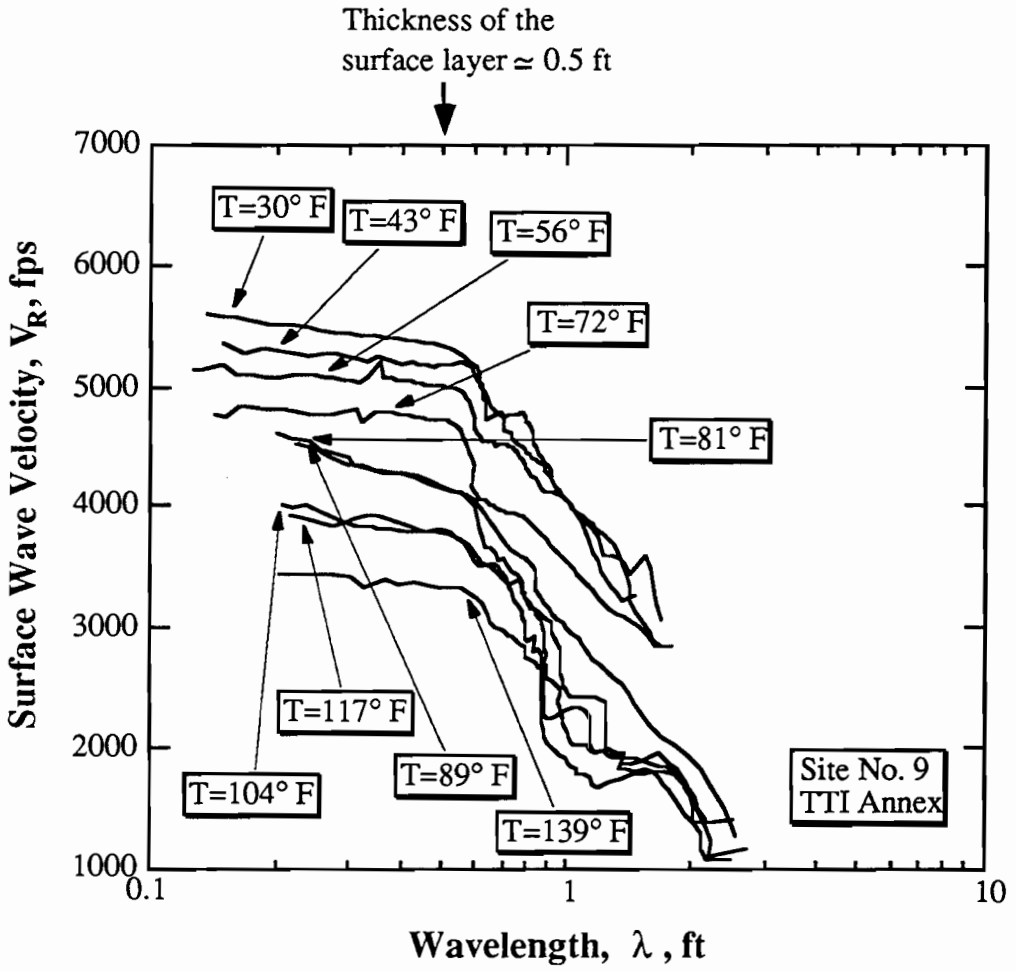

Fig 4.11. Changes in the Stiffness of the Asphalt Concrete Surface Layer as a Result of Solar Heating at Site 9; TTI Annex, Bryan, Texas.

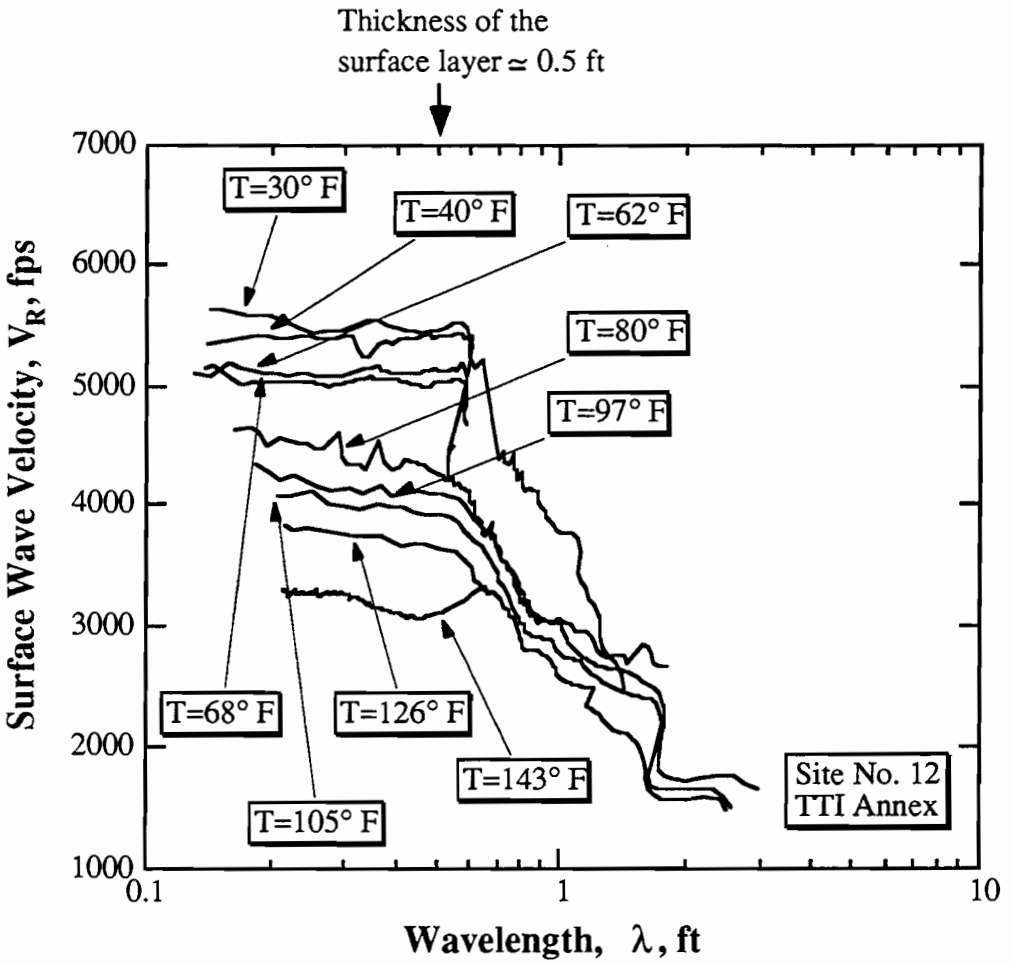

Fig 4.12. Changes in the Stiffness of the Asphalt Concrete Surface Layer as a Result of Solar Heating at Site 12; TTI Annex, Bryan, Texas.

frequency dependency of the surface wave velocity which is discussed in Chapter Five.

Finally, the base material was sampled with SASW measurements using a 0.30-m (1-ft) receiver spacing. Without any further analysis of the data such as performing forward modeling, it is clear that the base material of Site 4, which consists of 4% cement-stabilized crushed limestone is stiffer than the surface layer, as opposed to the lower velocity of the base material of Sites 9 and 12. This is illustrated in Fig. 4.13, which shows a comparison of the dispersion curves of Sites 4 and 12 for measurements at two surface temperatures. From the SASW measurements, the thickness of the surface layer was estimated to be 0.15 m (0.5 ft), which is in reasonable agreement with the construction drawings that show a thickness of 0.13 m (0.42 ft).

4.4.4 Development of an AC Modulus Adjustment Curve

The values of surface wave velocities determined from the SASW measurements were used to calculate Young's moduli of the surface layer. A unit weight of 22 kN/m^3 (140 pcf) and a Poisson's ratio of 0.27 were assumed for the asphalt concrete layer. Table 4.3 lists the values of the surface wave velocities and Young's moduli for wavelengths of 0.08 and 0.13 m (0.25 and 0.42 ft). The wavelength of 0.08 m (0.25 ft) was selected because it was the minimum wavelength measured when the surface temperature rose to 60° C (143° F). The wavelength of 0.13 m (0.42 ft) was selected because it corresponds to the actual thickness of the AC surface layer. Figure 4.14 shows the variation of the surface-layer modulus with temperature. At a wavelength of 0.08 m (0.25 ft), the modulus exhibits a slightly higher value than that at a wavelength of 0.13 m (0.42 ft) due to the frequency effect as discussed in Chapter Five.

To remove the effect of frequency, the moduli of the surface layer was calculated using surface wave velocities at a frequency of 15.5 kHz and was normalized to a modulus at 21° C (70° F) ($E_{70° F}$ = 2,140 ksi). The frequency of 15.5 kHz was selected because it was the highest frequency generated when the

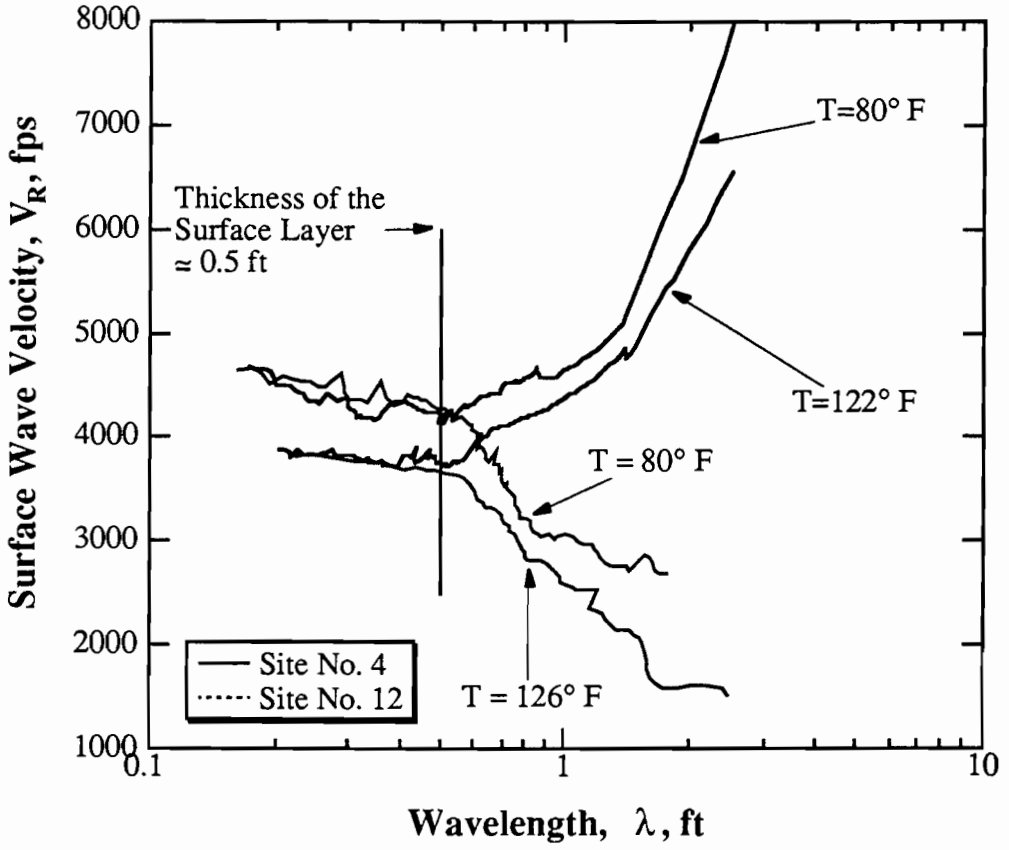

Fig 4.13. Comparison of Experimental Dispersion Curves Determined at Sites 4 and 12 for Two Different Temperatures.

Table 4.3. Surface Wave Velocities and Young's Moduli of the Asphalt Concrete Surface Layer at Wavelengths of 0.25 ft and 0.42 ft Determined from SASW Measurements at Sites 4, 9 and 12

Temp. (° F)	Site 4				Site 9				Site 12			
	l = 0.25 ft		l = 0.42 ft		l = 0.25 ft		l = 0.42 ft		l = 0.25 ft		l = 0.42 ft	
	V_R (fps)	E (ksi)	V_R (fps)	E (ksi)	V_R (fps)	E (ksi)	V_R (fps)	E (ksi)	V_R (fps)	E (ksi)	V_R (fps)	E (ksi)
30	-----	-----	-----	-----	5,482	27,88	5,355	2,661	5,545	2,853	5,471	2,777
32	5,359	2,665	5,249	2,557	-----	-----	-----	-----	-----	-----	-----	-----
37	5,251	2,559	5,190	2,500	-----	-----	-----	-----	-----	-----	-----	-----
40	-----	-----	-----	-----	-----	-----	-----	-----	5,246	2,553	5,195	2,504
43	-----	-----	-----	-----	5,292	2,598	5,190	2,499	-----	-----	-----	-----
56	-----	-----	-----	-----	5,098	2,411	5,010	2,329	-----	-----	-----	-----
58	4,878	2,208	4,920	2,246	-----	-----	-----	-----	-----	-----	-----	-----
62	-----	-----	-----	-----	-----	-----	-----	-----	5,146	2,457	5,142	2,453
68	-----	-----	-----	-----	-----	-----	-----	-----	5,036	2,353	5,034	2,351
70	4,811	2,148	4,737	2,082	-----	-----	-----	-----	-----	-----	-----	-----
72	-----	-----	-----	-----	4,782	2,122	4,736	2,081	-----	-----	-----	-----
80	4,368	1,770	4,216	1,649	-----	-----	-----	-----	4,484	1,865	4,286	1,704
81	-----	-----	-----	-----	4,495	1,874	4,191	1,629	-----	-----	-----	-----
89	-----	-----	-----	-----	4,433	1,823	4,170	1,613	-----	-----	-----	-----
93	4,326	1,736	4,199	1,636	-----	-----	-----	-----	-----	-----	-----	-----
97	-----	-----	-----	-----	-----	-----	-----	-----	4,193	1,631	4,090	1,552
104	4,171	1,614	3,937	1,438	3,984	1,472	3,822	1,355	-----	-----	-----	-----
105	-----	-----	-----	-----	-----	-----	-----	-----	4,120	1,575	3,917	1,423
117	-----	-----	-----	-----	3870	1389	3770	1318	-----	-----	-----	-----
122	3,821	1,354	3,729	1,290	-----	-----	-----	-----	-----	-----	-----	-----
126	-----	-----	-----	-----	-----	-----	-----	-----	3,828	1,359	3,648	1,234
139	-----	-----	-----	-----	3,436	1,095	3,330	1,029	-----	-----	-----	-----
143	3,417	1,083	3,193	946	-----	-----	-----	-----	32,72	993	3,105	894

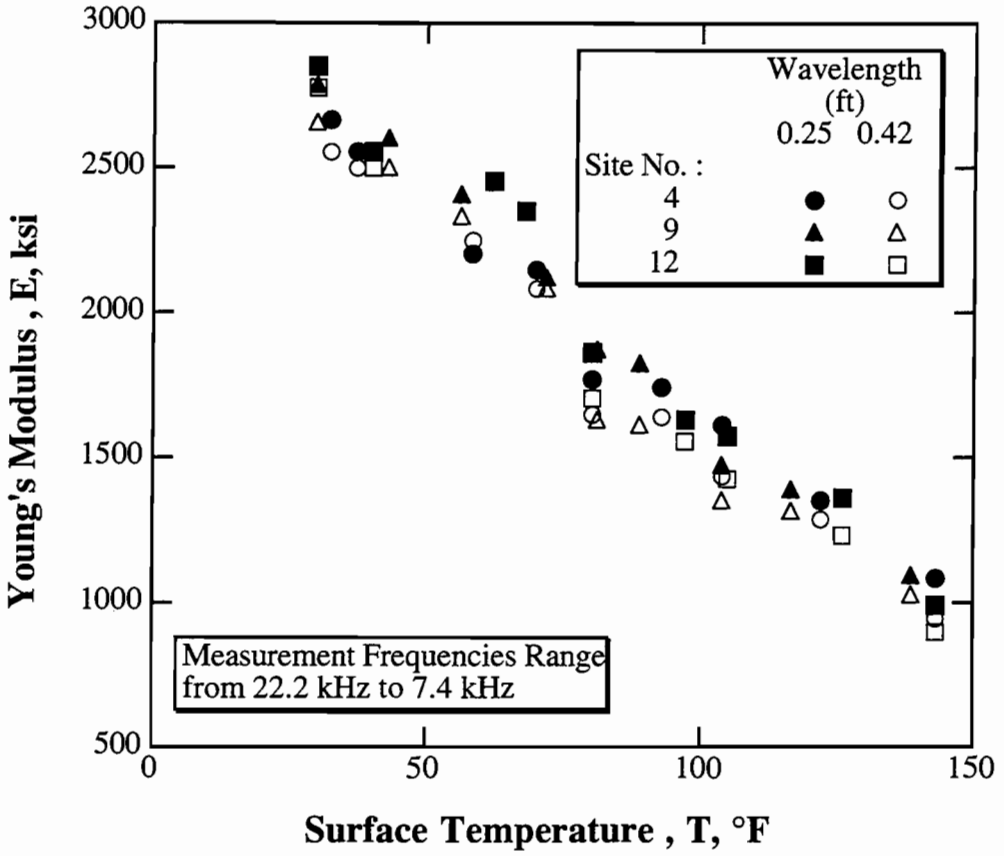

Fig 4.14. Variation in Low-Strain Young's Modulus with Temperature for Wavelengths of 0.25 ft and 0.42 ft at the TTI Annex, Bryan, Texas.

temperature rose up to 60° C (143° F). Table 4.4 lists the surface wave velocities and normalized modulus at a frequency of 15.5 kHz. The variation of normalized modulus with temperature is presented in Fig. 4.15. A change in modulus by a factor of about 2.6 was observed for the change in temperature from –1 to 60° C (30 to 143° F). When such correlation curves become well established, thin pavements could be tested when cool, and values of moduli at higher temperatures could be obtained from correlation curves such as the one shown in Fig. 4.15.

Table 4.4. Surface Wave Velocities and Normalized Young's Moduli of the Asphalt Concrete Surface Layer Determined from SASW Measurements at Sites 4, 9 and 12; Measurement Frequency is ~ 15.5 kHz

Site 4			Site 9			Site 12		
T (° F)	V_R (fps)	$E/E_{70°F}$	T (° F)	V_R (fps)	$E/E_{70°F}$	T (° F)	V_R (fps)	$E/E_{70°F}$
32	5,316	1.2266	30	5,431	1.2802	30	5,545	1.3345
37	5,254	1.1981	43	5,250	1.1963	40	5,246	1.1945
58	4,880	1.0336	56	5,081	1.1205	62	5,146	1.1494
70	4,800	1.0000	72	4,817	1.0071	68	5,063	1.1126
80	4,400	0.8403	81	4,440	0.8556	80	4,474	0.8688
93	4,223	0.7740	89	4,380	0.8327	97	4,160	0.7511
104	4,100	0.7296	104	3,984	0.6889	105	4,050	0.7119
122	3,821	0.6337	117	3,870	0.6500	126	3,800	0.6267
143	3,378	0.4953	139	3,440	0.5136	143	3,291	0.4701

Normalized moduli of the asphalt concrete layer obtained from SASW measurements and corrected to a frequency of 30 Hz using Fig. 5.34 (frequency effect is discussed in Chapter 5) are shown in Fig. 4.16. These values are compared with values suggested by the AASHTO Guide for Design of Pavement Structures (1986) in Fig. 4.17. As seen in Fig. 4.17, the normalized moduli of the surface layer determined by SASW measurements at temperatures less than 38° C (100° F) compare closely with normalized moduli suggested by the AASHTO

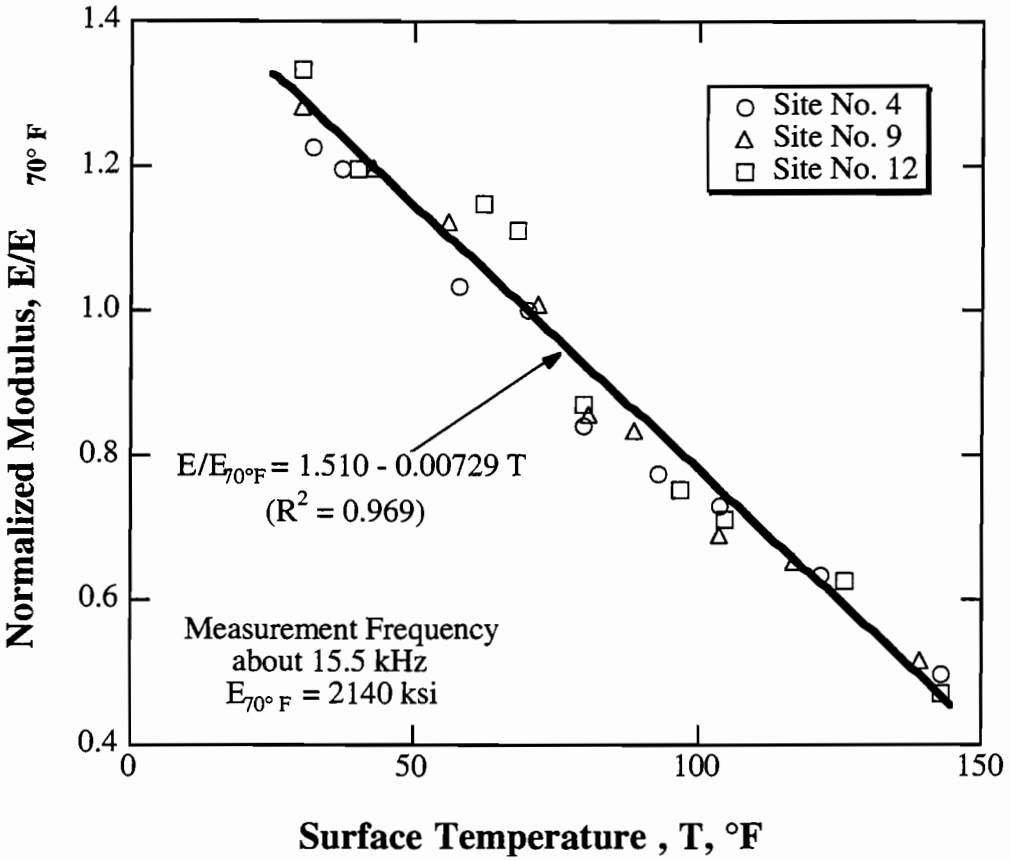

Fig 4.15. Variation in Low-Strain Young's Modulus (Normalized to a Modulus at a Temperature of 70° F) with Temperature for Three Sites at the TTI Annex, Bryan, Texas.

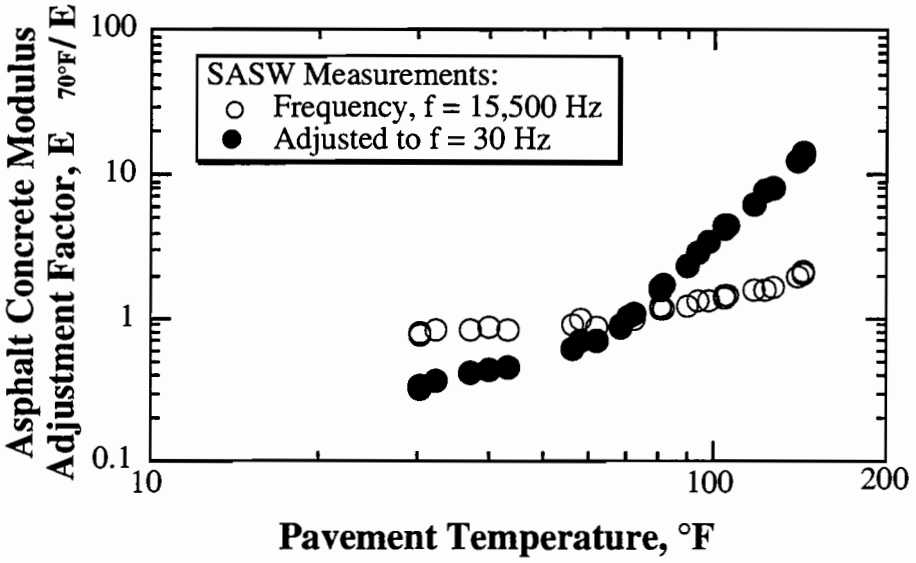

Fig 4.16. Normalized Modulus Determined from SASW Measurements at the TTI Pavement Facility and Adjusted for Frequency Using Fig. 5.34.

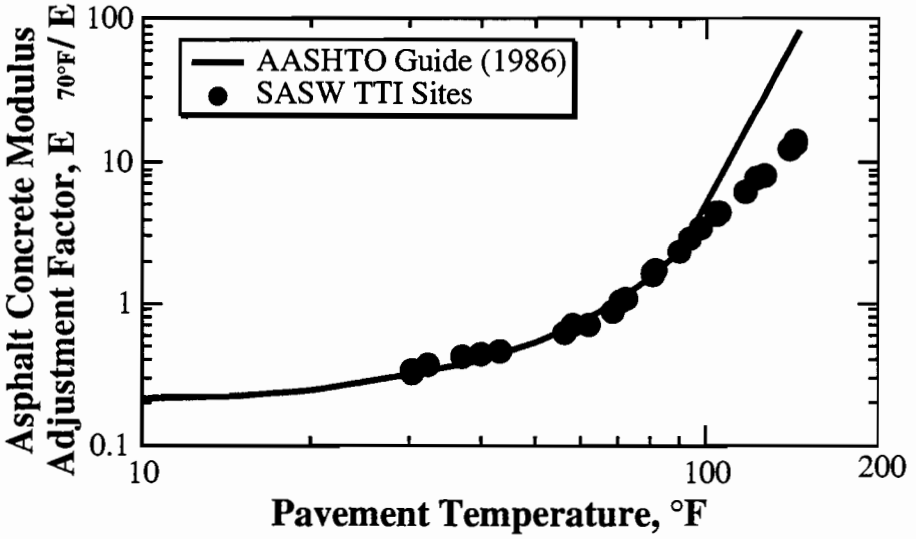

Fig 4.17. Comparison of the Variation of AC Modulus with Temperature from SASW Measurements and That Suggested by the AASHTO Guide for Design of Pavement Structures (1986).

guide. However, at temperatures above 38° C (100° F), the AASHTO guide underestimates the in-situ moduli evaluated by the SASW test. It should be noted that the SASWmeasurements were made at small strains (less than 0.001%). It is assumed that the lower values of moduli determined at high temperatures for the AASHTO guide are due to the higher strains associated with stress-controlled laboratory testing of soft AC specimens which were most likely used to develop the AASHTO guide. In addition, to accommodate the frequency effect in the SASW test, different calibration factors are applied at different surface temperatures, as shown in Fig. 5.34. The factor at high temperatures is quite large, and errors in this factor could also contribute to the differences seen in Fig. 4.17.

4.5 Testing of Thin Pavements (t < 5.08 cm or 2 in.)

4.5.1 SASW Measurements at Sites 10 and 11

Sites 10 and 11 at the TTI Annex were selected as representative sites with thin pavement layers. They consist of a 1-in. (2.54-cm) compacted AC surface layer underlain by crushed limestone base and subbase. SASW measurements were performed at the two sites to evaluate the material profile. Figure 4.18 shows the cross power spectra and the coherence functions for a receiver spacing of 15.2 cm (6 in.) for Sites 10 and 11 using the ball-peen hammer as a source. It is clear from Fig. 4.18 that the minimum wavelength generated is about 7.6 cm (3 in.), which is not less than the thickness of the surface layer. Figure 4.19 shows the composite dispersion curve for Site 10 for receivers spacings of 0.15, 0.30, 0.61 and 1.22 m (0.5, 1, 2 and 4 ft). It is clear in Fig. 4.19 that the stiffness of the surface layer cannot be determined from SASW measurements because wavelengths shorter than the thickness of the surface layer were not generated. A receivers spacing of 7.6 cm (3 in.) was also tried, but wavelengths shorter than the maximum aggregate size (~ 2.54 cm, or 1 in.) were not measured. In this case, P-wave measurements should be performed in conjunction with SASW measurements to determine the material profile as discussed below.

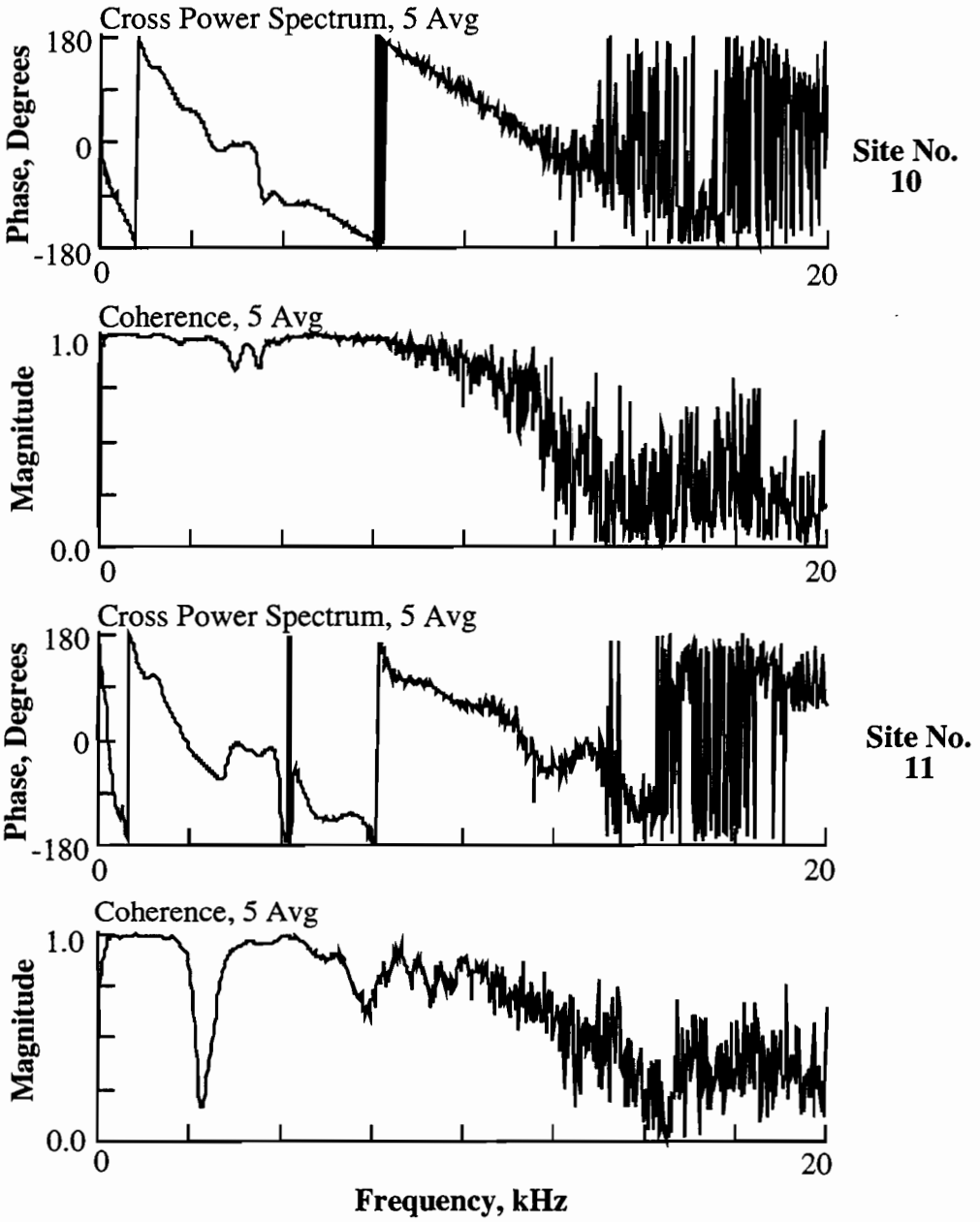

Fig 4.18. Cross Power Spectra and Coherence Functions Determined from SASW Measurements at Sites 10 and 11, TTI Annex, Bryan, Texas (Hammer Source, T = 78° F, R1-R2 = 6 in.).

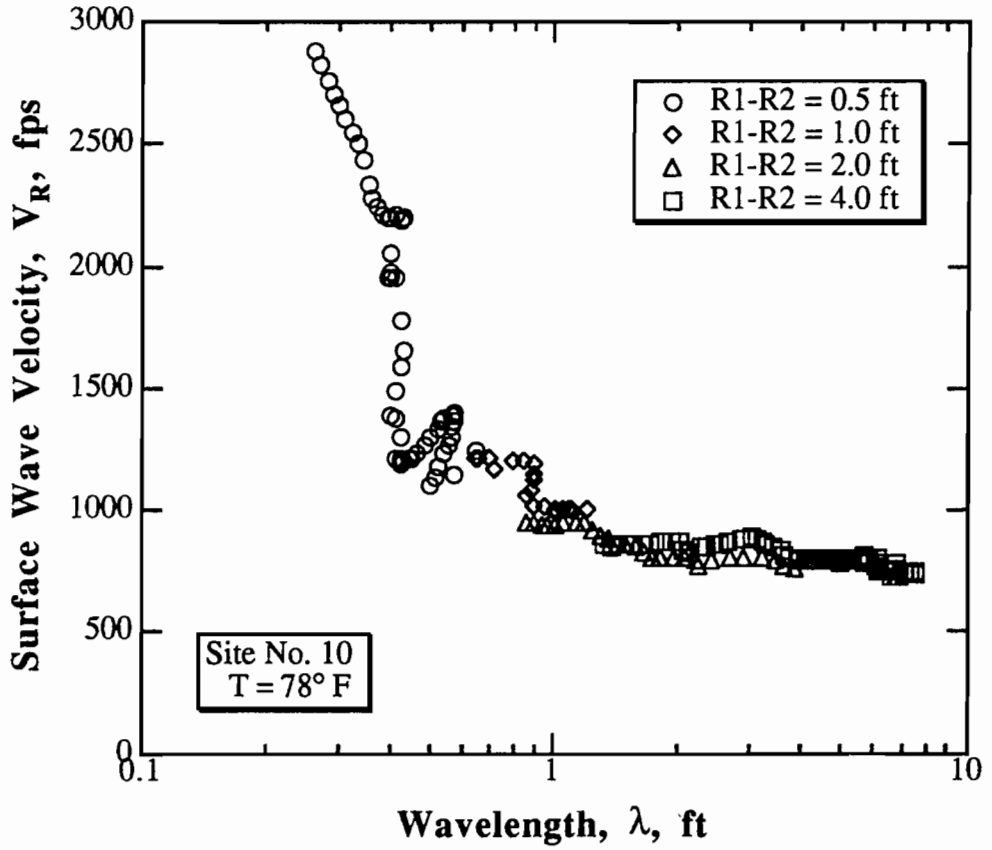

Fig 4.19. Composite Dispersion Curve Determined from SASW Measurements at Site 10; TTI Annex, Bryan, Texas.

4.5.2 SASW and P-Wave Measurements at Granger, Texas

SASW and P-wave measurements were performed at an embankment site in Granger, Texas. The test site is located on FM 971 about 8 km (5 miles) east of Granger. The site consists of a 1.91-cm (0.75-in.) penetration seal, a 27.9-cm (11-in.) crushed limestone base, and approximately 6.1 m (20 ft) of compacted fill subgrade over natural soil. The selection of this site was based on its thin surface layer to demonstrate how SASW and P-wave measurements can be used in conjunction to determine the material profile.

SASW Measurements

The SASW array was located in the middle of the road at about 5.5 m (18 ft) from the sloping side of the embankment to avoid reflections from the boundaries. Receiver spacings of 0.15, 0.30, 0.61, 1.22, 2.44, 4.88 and 9.75 m (0.5, 1, 2, 4, 8, 16 and 32 ft) were used. A WR Model F-7 shaker and WR Model 736 accelerometers were used to generate and capture the wave signals at receiver spacings of 0.15, 0.30 and 0.61 m (0.5, 1 and 2 ft). The signals generated by the F-7 shaker were too small to be received by the accelerometers at the 1.22-m (4-ft) spacing. Therefore, a geology hammer was employed to generate the wave energy at a receiver spacing of 1.22 m (4 ft). Measurements at receiver spacings greater than 2.44 m (8 ft) were made using sledge hammers and 1-Hz geophones as sources and receivers, respectively.

The phase shifts of the cross power spectra between the two receivers for all receiver spacings are shown in Figs. 4.20 and 4.21. The composite dispersion curve is shown in Fig. 4.22. The minimum wavelength is about 0.06 m (0.2 ft). Thus, the surface layer was not sampled in the SASW measurements.

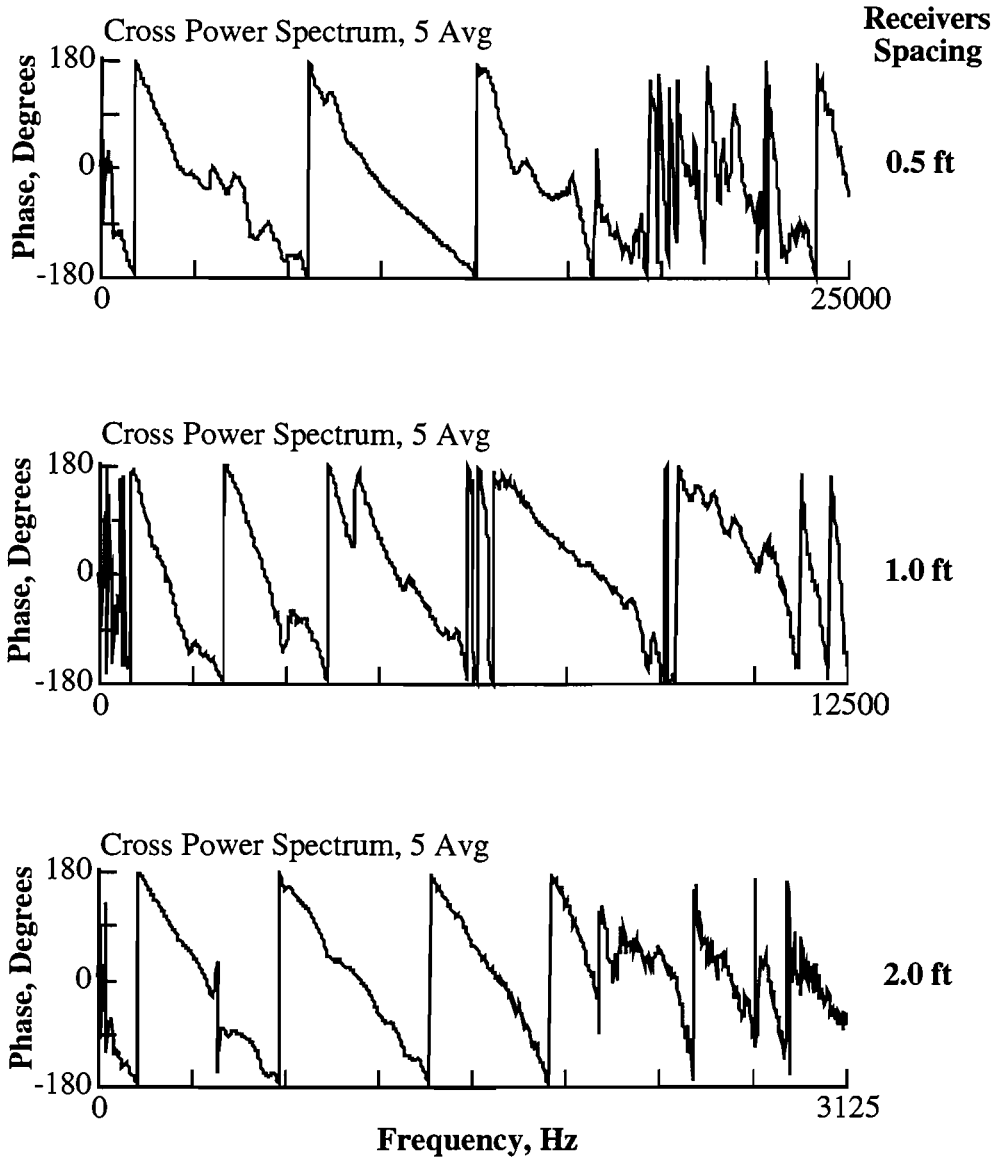

Fig 4.20. Phase Shifts of the Cross Power Spectra between the Two Receivers for Spacings of 0.5, 1 and 2 ft; Granger, Texas.

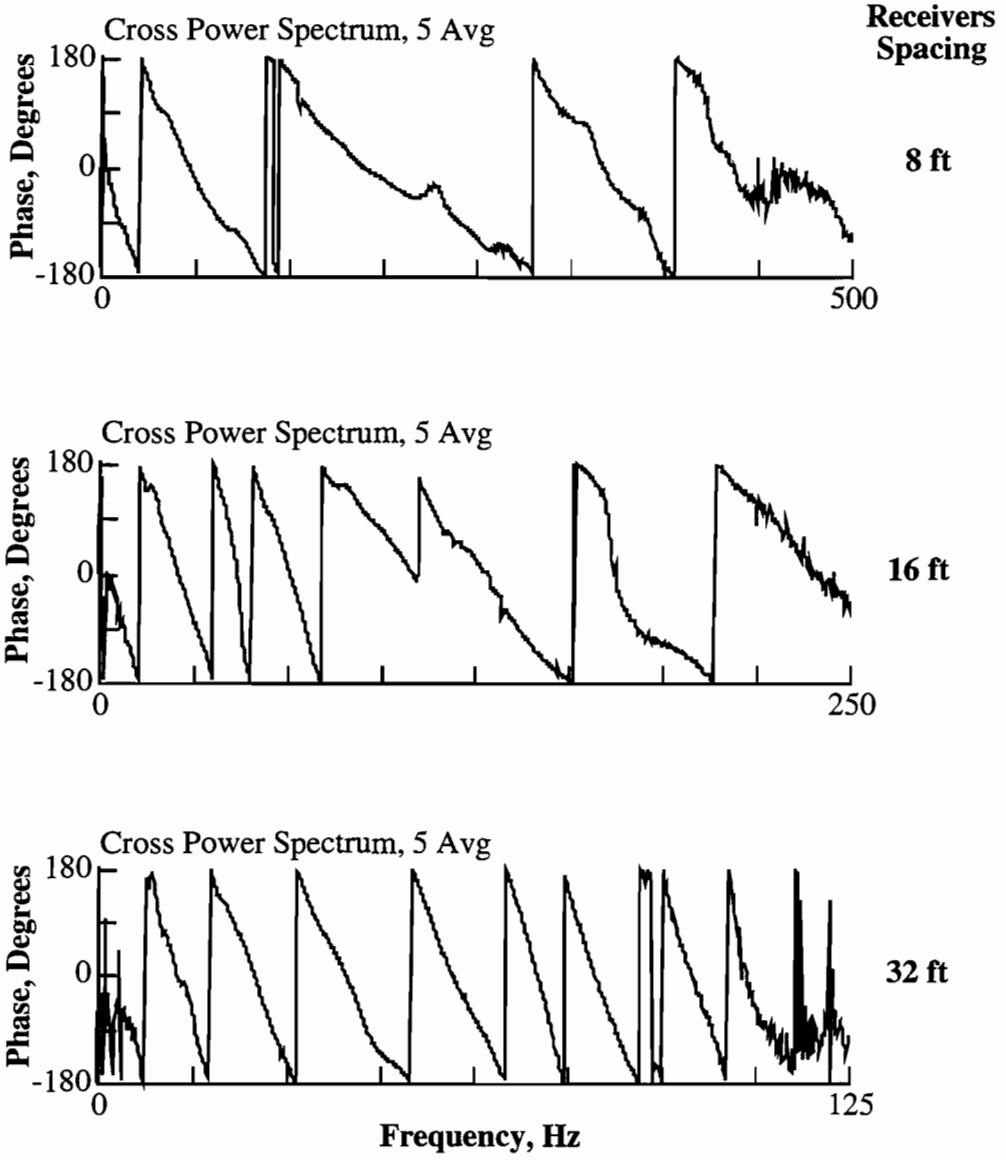

Fig 4.21. Phase Shifts of the Cross Power Spectra between the Two Receivers for Spacings of 8, 16 and 32 ft; Granger, Texas.

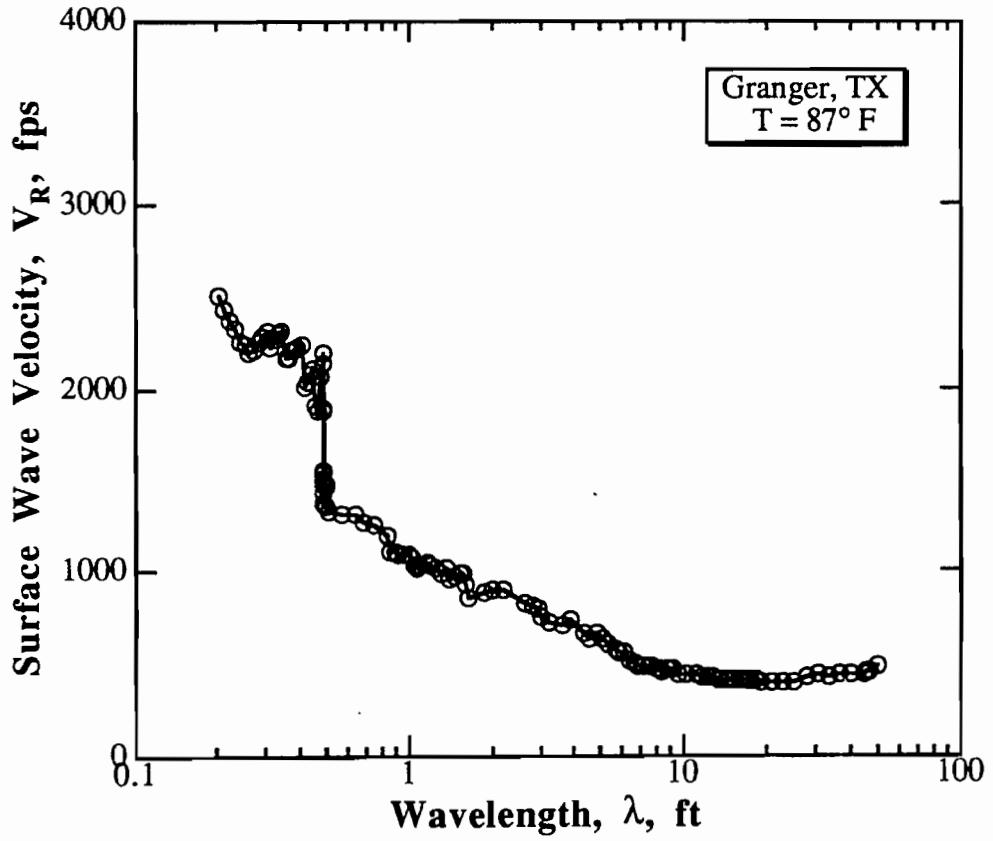

Fig 4.22. Composite Dispersion Curve Determined from SASW Measurements at Granger, Texas.

P-Wave Measurements

A schematic diagram for the general setup used in the P-wave measurements is shown in Fig. 4.23. An accelerometer was placed horizontally on the pavement surface using the same nail-magnet coupling arrangement used in SASW testing. An inclined chisel, hammer and Resistance-Capacitance (RC) trigger were used as the source. The inclined chisel was moved in selected steps away from the receiver. Source-receiver (S-R) distances of 7.6, 15.2, 22.9, 30.5, 45.7 and 61 cm (3, 6, 9, 12, 18 and 24 in.) were used. The inclined chisel was struck by a hammer to generate the wave energy. An RC trigger box was used to define the initiation time of the impulse. Typical time traces for three S-R distances are shown in Fig. 4.24. The times (t) that compression waves required to travel from the source to the receiver are listed in Table 4.5.

Table 4.5. Travel Times from Source to Receiver (Compression Waves)

Distance d (in.)	Travel Time t (μs)
3.0	117
6.0	164
9.0	215
12.0	238
18.0	316
24.0	382

A travel distance versus travel time plot for the propagating compression wave is shown in Fig. 4.25. A compression wave velocity, V_C (unconstrained wave, see Section 5.5), of 1,940 m/s (6,360 fps) was determined from the slope of the line in Fig. 4.25. Note that the x-axis intercept of 79 μs represents the time needed for the wave to travel in the chisel (38.1 cm (15 in.) of steel rod). The rod velocity was calculated to be 4,815 m/s (15,800 fps), which is consistent with wave velocity in steel. Assuming a Poisson's ratio, ν, of 0.27, the shear wave velocity, V_S, of the AC layer of 1,216 m/s (3,990 fps) was calculated using the following equation:

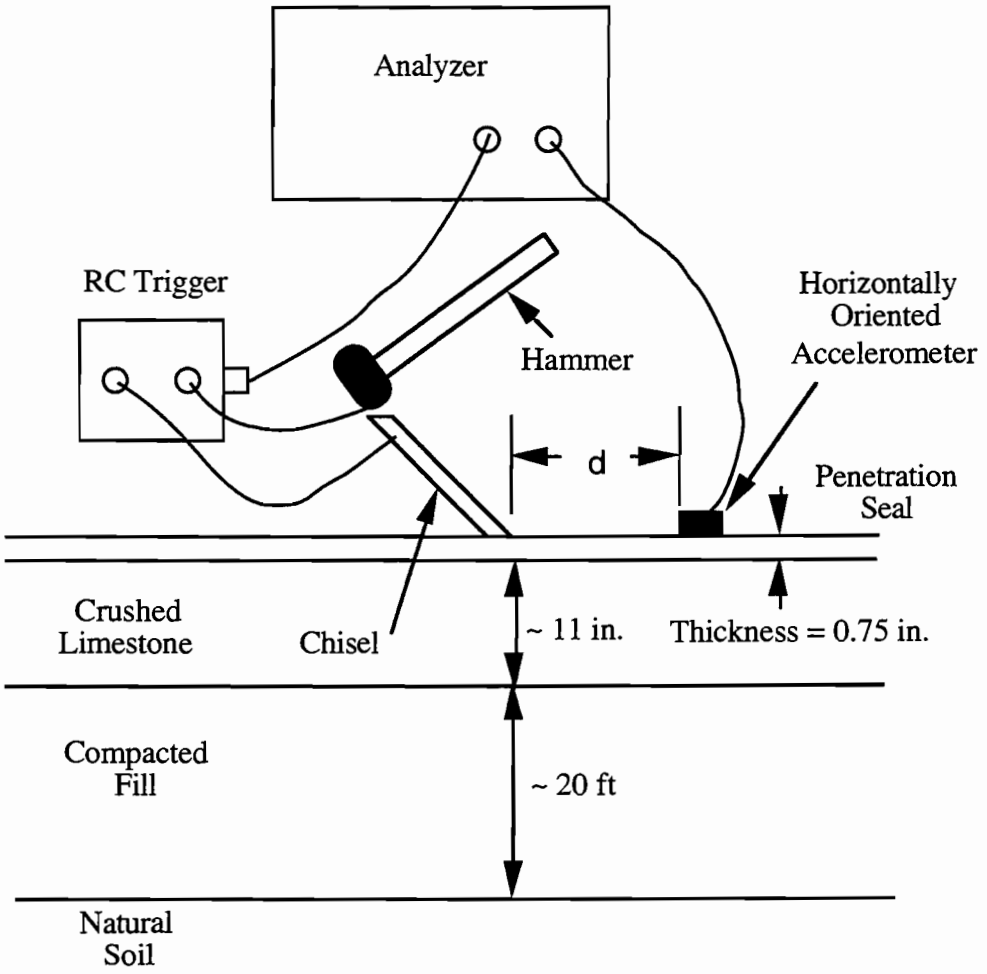

Fig 4.23. Schematic Diagram of Experimental Setup for P-Wave Measurements at Granger Site.

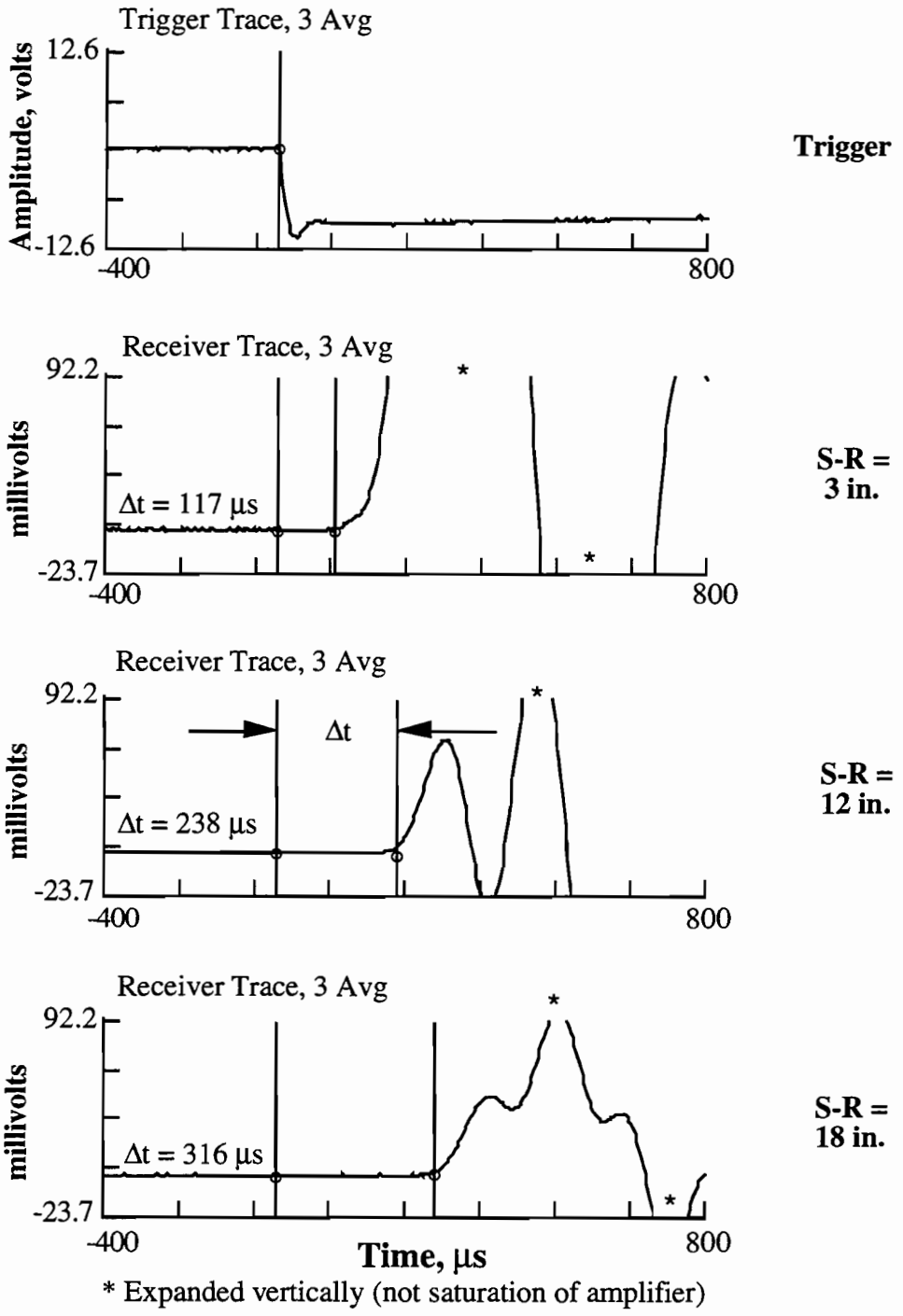

Fig 4.24. Typical Time Records for Propagating Compression Waves, Source-Receiver Distances of 3, 12 and 18 in. at Granger Site.

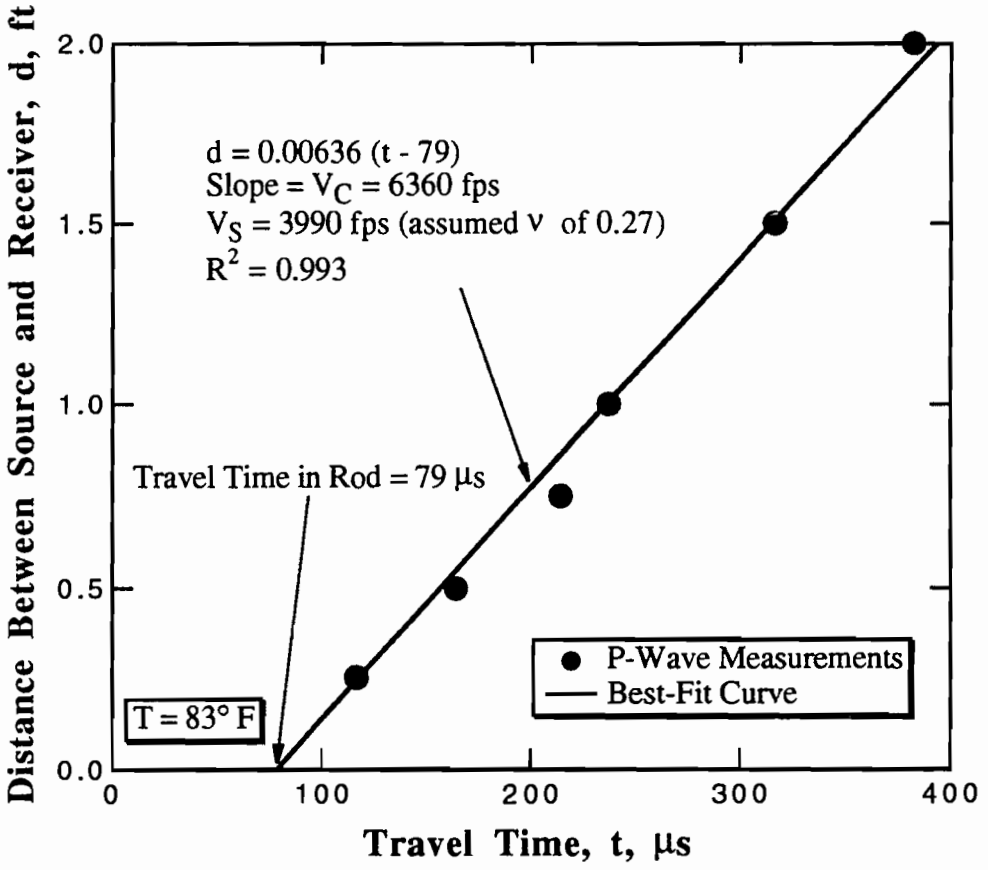

Fig 4.25. Travel Distances Versus Travel Times for P-Waves Measured at Granger Site.

$$V_S = V_C \cdot \sqrt{\frac{1}{2\,(1+\nu)}} \qquad (4.1)$$

Finally, the SASW and P-wave measurements were used to determine the pavement-soil profile at the Granger site. Forward modeling of the SASW data using a 3-D inversion procedure was performed assuming that the stiffness of the surface layer was 1,215 m/s (3,990 fps) as determined from the P-wave measurements. The final material profile from the forward modeling process is listed in Table 4.6.

Table 4.6. Shear Wave Velocities Determined from SASW and P-Wave Measurements; Granger, Texas

Thickness (ft)	Shear Wave Velocity (fps)
0.063	3,990
0.150	2,000
0.100	850
0.667	700
20.00	450
Half-Space	800

Figure 4.26 shows a comparison between the experimental and theoretical dispersion curves for two different surface layer velocities. If P-wave measurements were not made (unknown surface layer velocity) and a velocity of 1,525 m/s (5,000 fps) was assumed with no variations in the stiffnesses or the thicknesses of the underlain layers, the experimental and theoretical dispersion curves could not be matched unless the base material assumed a lower velocity value, which seems unrealistic. Thus, in the case of thin pavements, it is important to determine the velocity of the surface layer in order to correctly characterize the material stiffness of the base layer. For wavelengths greater than 0.3 m (1 ft), the theoretical dispersion curves for the two surface layer wave velocities match the experimental dispersion curve. Therefore, the influence of the AC surface layer on the subgrade stiffness is not pronounced.

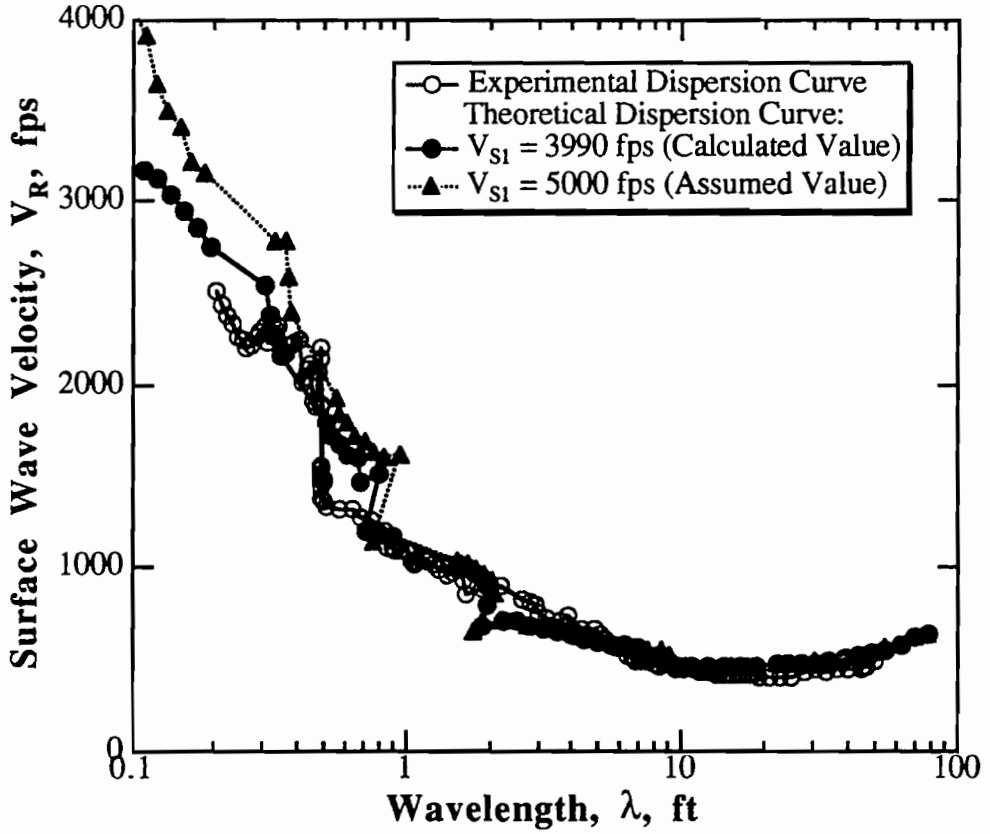

Fig 4.26. Comparison between the Experimental and Theoretical Dispersion Curves Using Two Different Surface Layer Velocities for Granger Site.

The SASW results were compared to results from crosshole tests performed at the Granger site as shown in Fig. 4.27. The SASW and crosshole results compare well except at depths of 4.3 and 4.9 m (14 and 16 ft). At these two depths, the crosshole measurement showed a stiffer layer as compared to the rest of the subgrade layer. This layer was not detected by the SASW measurements due to its small thickness.

4.6 Summary

The SASW method was employed at the TTI test facility in Bryan, Texas, to evaluate the stiffness of the AC surface layer under different temperatures. The method proved to be effective in determining the stiffness over a wide range of temperatures ranging from –1 to 60° C (30 to 143° F). The method was employed at those sites where the thickness of the surface layer was equal to 12.7 cm (5 in.). This surface layer is considered to be a "thick" AC layer because wavelengths can be generated in SASW testing which are considerably shorter than the layer thickness. As a result, direct measurement of only the AC layer can be performed in the SASW test. This aspect is very important because no forward modeling is required to evaluate the modulus of the AC layer. The modulus can simply be calculated from the measured wave velocity and assumed values of mass density and Poisson's ratio using Eqs 2.3 and 3.2.

Two sources were used to generate the high frequencies required to sample thick AC surface layers. The sources were a piezoelectric source, the V-meter, and a small ball-peen hammer. The V-meter performed better than the small hammer as a high-frequency source, especially for temperatures higher than 27° C (80° F). However, the small hammer was very effective at temperatures below 27° C (80° F).

The SASW method was also used to determine the material stiffness of pavement sites where a thin AC surface layer was encountered (Sites 10 and 11 at the TTI test facility with 2.54 cm (1 in.) of AC and one site in Granger, Texas, with

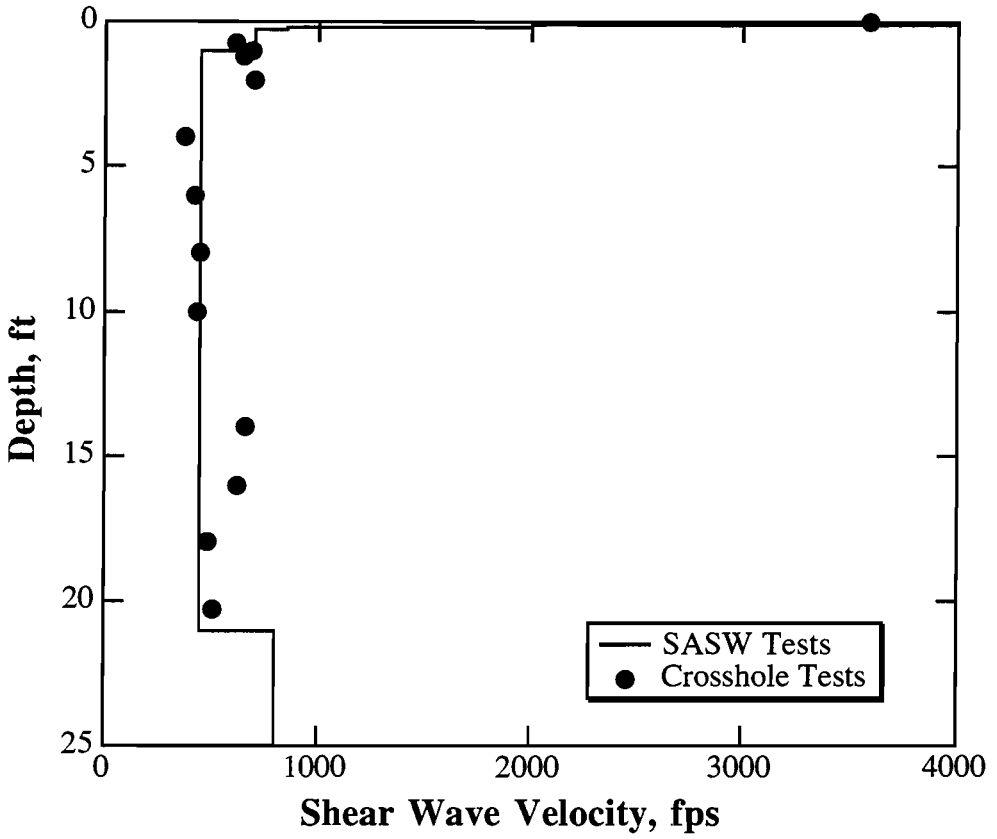

Fig 4.27. Comparison between Shear Wave Velocities from SASW and Crosshole Tests at Granger Site.

1.91 cm (0.75 in.)) of AC. The high frequencies needed to sample the surface layer were not generated because the sampling wavelengths were on the order of the maximum aggregate size in the AC layer. As a result, SASW testing could not be used to evaluate the thin AC layer. In such cases, P-wave measurements were used to characterize the stiffness of the surface layer.

CHAPTER FIVE
FIELD MEASUREMENTS ON LOOP 1, AUSTIN, TEXAS

5.1 Introduction

A newly constructed site at the intersection of Loop 1 and US 183 in Austin, Texas, was investigated. The goal of this study was to determine the material properties of the site through the implementation of seismic (SASW and crosshole) and deflection basin (FWD) methods. In addition, laboratory tests, including the resonant column torsional shear and resilient modulus tests, were performed on extracted samples to evaluate the dynamic moduli of the surface layer, base and subgrade.

A comprehensive testing program was conducted following the construction stages. Field seismic measurements were performed after the compacted fill was placed (Stage 1). Stages 2 and 3 involved field measurements after the placement of first and second asphalt concrete surface layers, respectively. The AC layers had nominal thicknesses of 10.2 and 7.6 cm (4 and 3 in.), respectively.

Results from the different field and laboratory measurements are presented in this chapter. The parameters studied included: the changes of AC moduli with temperature, the effect of frequency on the AC moduli, and the effect of depth to bedrock on the FWD results.

5.2 Site Description

Field measurements were conducted on the southwest (SW) overpass embankment of the interchange between Loop 1 and US 183 (referred to as Embankment SW hereafter). The site consists of a compacted fill of varying thickness placed over natural soil underlain by limestone bedrock. The sloping embankment provides a varying depth to bedrock at the test locations. The

compacted fill was placed between December, 1988, and February, 1989, with a 15.2-cm- (6-in.-) thick crushed limestone placed in March, 1989. Two layers of asphalt concrete (AC) were then placed to achieve a total thickness of 17.8 cm (7 in.) for the surface layer. The first lift of Type-A AC was 10.2 cm (4 in.) thick, and the second lift of Type-C AC was 7.62 cm (3 in.) thick. Tests were performed in the middle of the approximately 15.2-m (50-ft) wide embankment along a length of 91.5 m (300 ft), stretching from Station 275+50 to Station 278+50. Station coordinates are given in ft, per conventional U.S. practice. An approximate longitudinal cross-section of the embankment is shown in Fig. 5.1. The stations where crosshole, SASW and FWD tests were performed are also shown in Fig. 5.1.

5.3 Tests after Placement of the Fill

5.3.1 Crosshole Seismic Tests

Crosshole seismic tests were performed at Stations 275+50, 276+50 and 278+50. Two boreholes were drilled at each test station, one for the source and one for the receiver. The receiver borehole was drilled to its full depth, which ranged from 1.5 to 3.7 m (5 to 12 ft) deep. The source borehole was drilled in steps to the depths at which the measurements were made. Drilling of the source borehole continued until measurements along the full depth of interest were made. Two sources were used to generate the wave energy. A solid-bottom steel cylinder attached to steel rods was used to generate compression wave energy, and a Shelby tube was used in the generation of shear wave energy. An RC trigger box defined the initiation time of the propagated wave. A three-component geophone was used to capture the wave arrivals at the receiver borehole. The radial component was used to measure the arrival of compression waves and the vertical component was used to measure the arrival of shear waves.

Crosshole measurements were made from a depth of 0.3 m (1 ft) to depths of 1.4 m (4.5 ft), 3.4 m (11 ft), and 1.2 m (4 ft) at Stations 275+50, 276+50 and

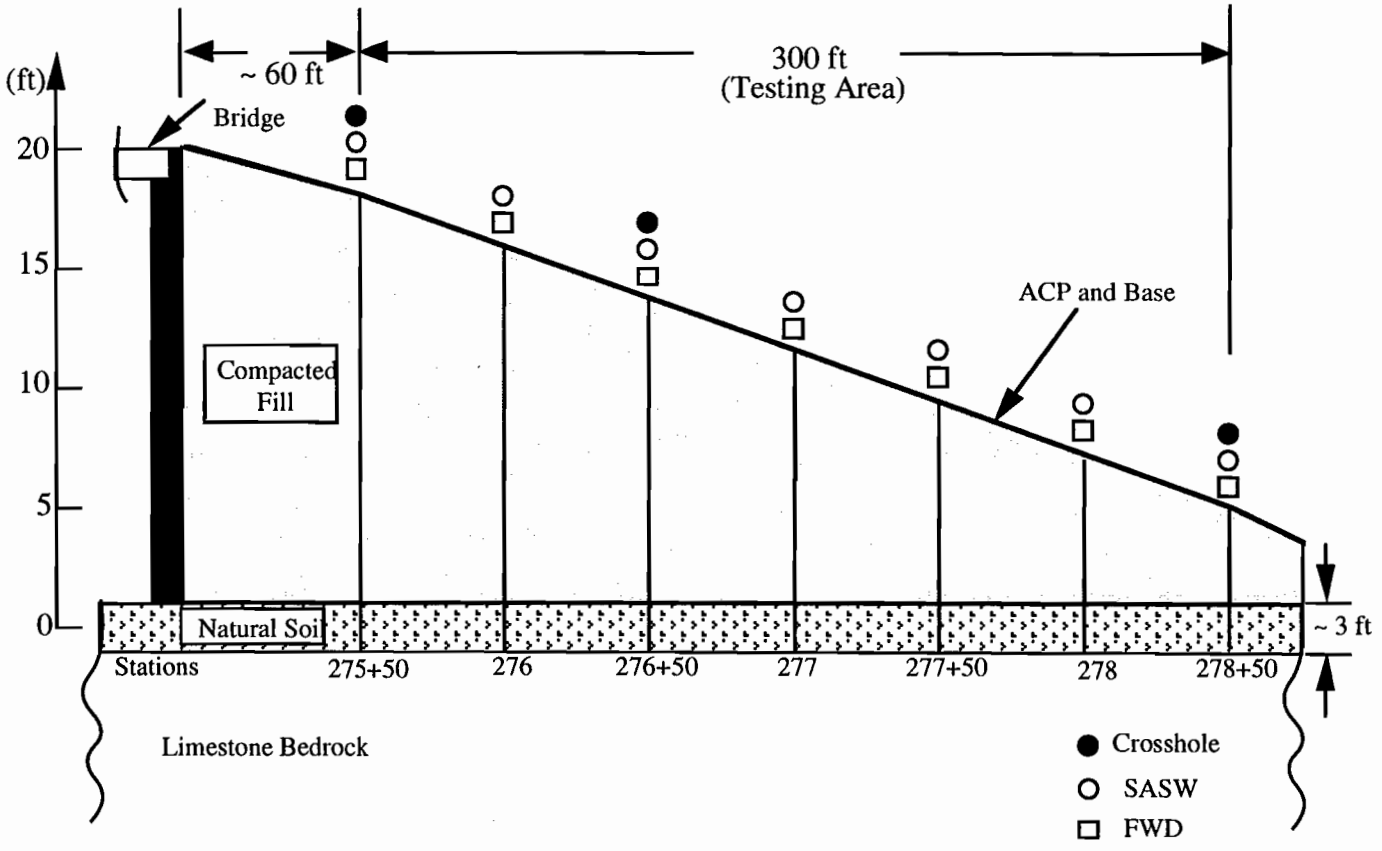

Fig 5.1. Approximate Longitudinal Cross-Section of Embankment SW

278+50, respectively. The drilling operation was stopped at a depth of 3.7 m (12 ft) at Station 276+50 and at a depth of 1.5 m (5 ft) at Station 278+50 because bedrock was encountered. However, SASW and FWD results showed that the rigid bedrock was deeper than that encountered by the drilling operator. It appears that a layer of weathered rock with a stiffness close to that of the compacted fill exists on top of the limestone. Typical time records for compression and shear waves are shown in Fig. 5.2. The compression and shear wave velocities were calculated as follows:

$$V_P = D / T_{P\text{-}COR} \tag{5.1}$$

$$T_{P\text{-}COR} = T_P - T_{rod} \tag{5.2}$$

$$T_{rod} = \text{Length of rod} / V_{rod} \tag{5.3}$$

$$V_S = D / T_{S\text{-}COR} \tag{5.4}$$

$$T_{S\text{-}COR} = T_S - T_{rod} \tag{5.5}$$

where

V_P = constrained compression wave velocity,

D = distance from source to receiver (D = 4.75 ft, 5 ft and 4.83 ft at Stations 275+50, 276+50 and 278+50, respectively),

$T_{P\text{-}COR}$ = corrected travel time of compression waves,

T_P = total travel time of compression waves,

T_{rod} = compression wave travel time in rod,

V_{rod} = measured rod velocity of 16,500 fps (5,029 m/s),

V_S = shear wave velocity,

$T_{S\text{-}COR}$ = corrected travel time of shear waves, and

T_S = total travel time of shear waves.

The compression and shear wave velocities determined at the three stations are listed in Table 5.1. The total unit weight of the fill was equal to 20.47 kN/m^3 (130 pcf). The constrained modulus, M, shear modulus, G, and Poisson's ratio, ν, of the compacted fill were calculated using Eqs. 2.1, 2.3 and 2.4, respectively. Then, Young's modulus, E, was calculated from the following equation:

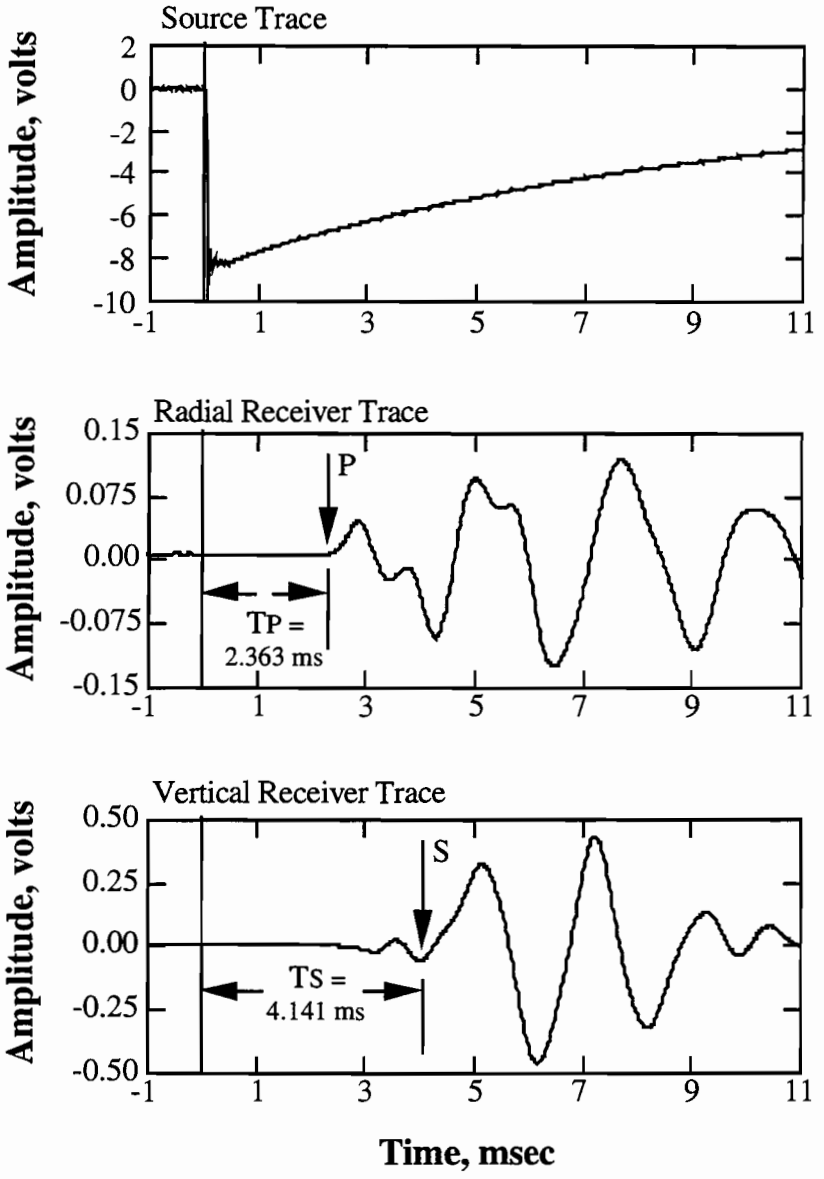

Fig 5.2. Typical Time Records for Compression and Shear Waves Measured in Crosshole Testing; Station 276+50, Depth = 7 ft.

Table 5.1. Crosshole Seismic Wave Velocities Determined at Stations 275+50, 276+50 and 278+50; Loop 1 and US 183, Austin, Texas

Depth (ft)	Shear Waves				Compression Waves			
	T_S (msec)	Rod length (ft)	Trod (msec)	V_S (fps)	T_P (msec)	Rod length (ft)	Trod (msec)	V_P (fps)
Station 275+50								
1.5	4.246	6.3	0.384	1230	2.307	6.6	0.399	2490
2.5	4.066	6.3	0.384	1290	2.492	6.6	0.399	2270
3.5	4.154	6.3	0.384	1260	2.420	6.6	0.399	2350
4.5	4.184	6.3	0.384	1250	2.420	6.6	0.399	2350
Avg				1258				2365
Station 276+50								
2.0	4.648	5.5	0.333	1160	2.461	6.6	0.399	2425
3.4	4.355	9.0	0.546	1310	2.520	9.0	0.546	2530
5.0	5.098	9.0	0.546	1100	2.969	9.0	0.546	2065
7.0	4.141	12.4	0.753	1480	2.363	11.6	0.702	3010
9.0	4.609	12.4	0.753	1295	2.637	11.6	0.702	2585
10.0	4.805	12.4	0.753	1235	3.066	11.6	0.702	2115
11.0	5.801	16.3	0.985	1035	3.437	17.8	1.081	2120
Avg				1230				2407
Station 278+50								
1.0	5.117	6.3	0.384	1020	3.047	6.6	0.399	1825
2.0	4.863	6.3	0.384	1080	3.008	6.6	0.399	1855
4.0	5.293	6.3	0.384	990	2.480	6.6	0.399	2320
Avg				1030				2000

$$E = 2 \bullet G (1+\nu) \tag{5.6}$$

The average values of moduli and Poisson's ratios over depths of 1.4, 3.4 and 1.2 m (4.5, 11 and 4 ft) for Stations 275+50, 276+50 and 278+50, respectively, are listed in Table 5.2.

Table 5.2. Average Values of Constrained, Shear and Young's Moduli and Poisson's Ratios of the Compacted Fill Determined from Crosshole Tests at Stations 275+50, 276+50 and 278+50; Loop 1 and US 183, Austin, Texas

Station	Constrained Modulus (ksi)	Shear Modulus (ksi)	Poisson's Ratio	Young's Modulus (ksi)
275+50	156.8	44.4	0.303	115.7
276+50	162.4	42.4	0.323	112.2
278+50	112.1	29.7	0.320	78.4

5.3.2 SASW Tests

SASW tests were performed at Stations 275+50, 276+50 and 278+50. Receiver spacings from 0.3 m (1 ft) to 9.75 m (32 ft) were used. Two sources were used to generate the wave energy. A 223 N (50-lb) electromagnetic vibrator was used for receiver spacings up to 2.44 m (8 ft). Sledge hammers were used for receiver spacings of 4.88 m (16 ft) and 9.75 m (32 ft). The phase shifts of the cross power spectra obtained from SASW measurements at Station 275+50 are shown in Fig. 5.3. A swept sine mode was employed to optimize the measurement at each frequency of interest. Similar phase shifts were determined at Stations 276+50 and 278+50. The composite dispersion curves for the three stations are shown in Fig. 5.4.

The rigid bedrock layer at Station 275+50 was not sampled because receiver spacings of 4.88 m (16 ft) and 9.75 m (32 ft) were not used. As shown in Fig. 5.4, the rigid bedrock layer was deeper at Station 276+50 than at Station 278+50 due to the varying thickness of the compacted fill. The measured SASW data were

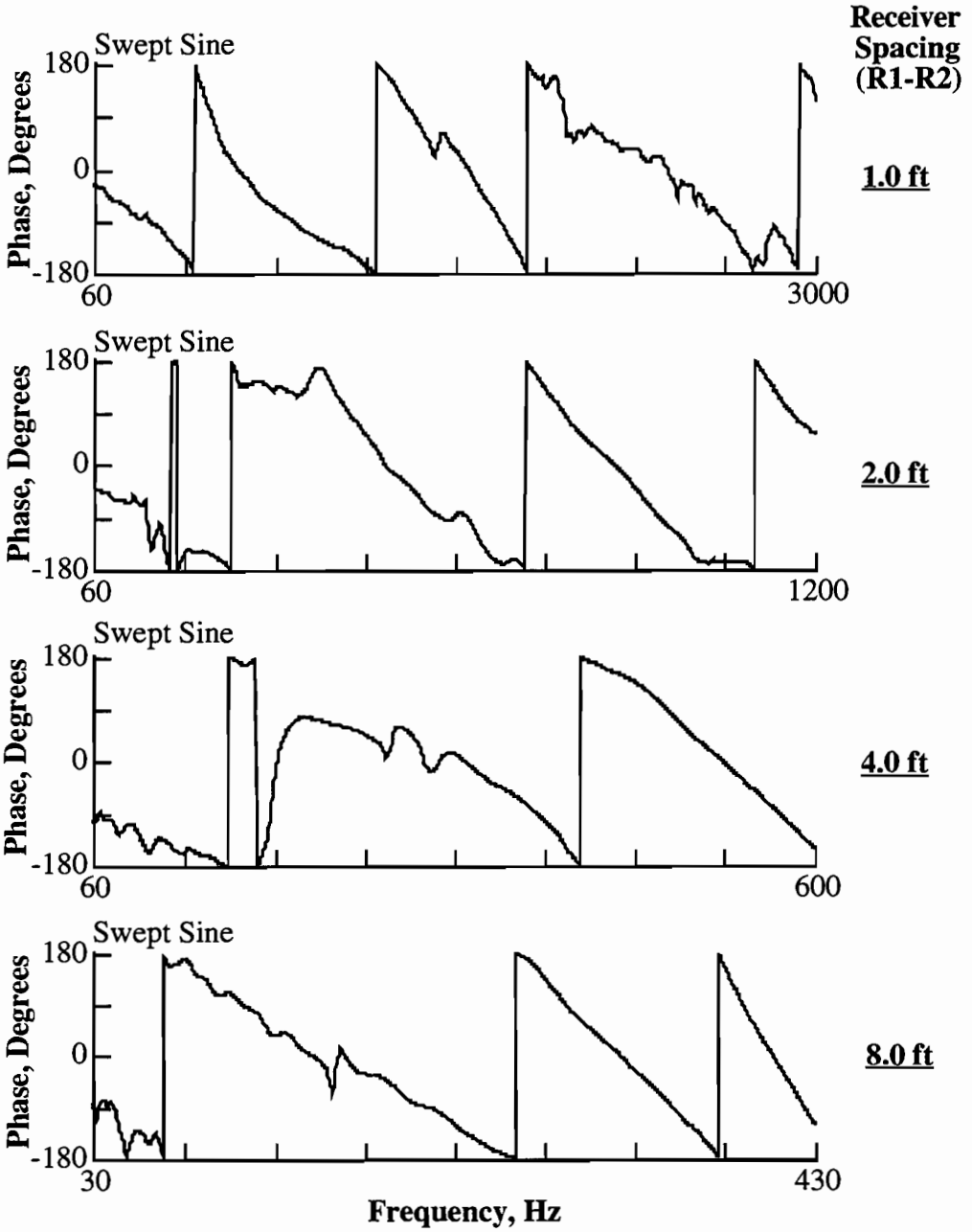

Fig 5.3. Phase Shifts of the Cross Power Spectra between the Two Receivers for Spacings of 1, 2, 4 and 8 ft; Station 275+50, Loop 1 and US 183, Austin, Texas.

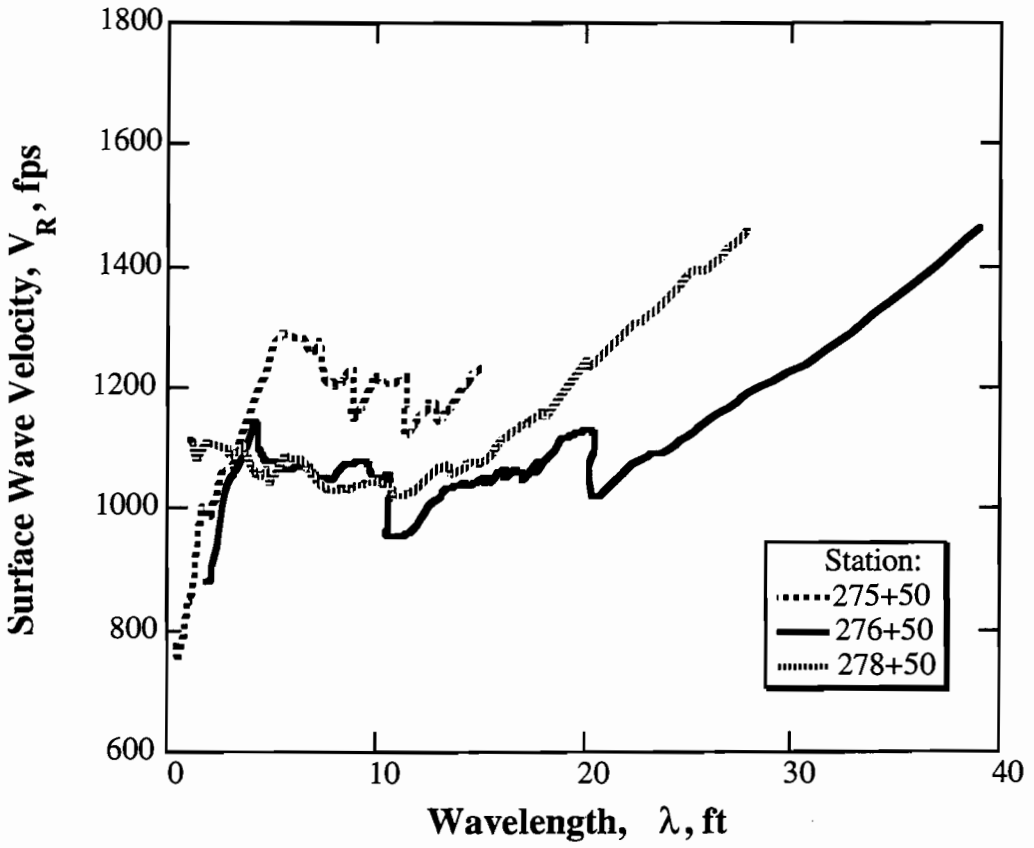

Fig 5.4. Experimental Dispersion Curves Determined from SASW Measurements before Placing Base and AC Surface Layer at Stations 275+50, 276+50 and 278+50; Loop 1 and US 183.

then analyzed to obtain the shear wave velocity profiles at Stations 276+50 and 278+50. Figure 5.5 shows a comparison between the experimental and theoretical dispersion curves determined at Stations 276+50 and 278+50. The theoretical dispersion curves correspond to the shear wave velocity profiles shown in Fig. 5.6 (crosshole data are also shown). The depth to bedrock was determined to be equal to 4.6 m (15 ft) at Station 276+50 and 2.9 m (9.5 ft) at Station 278+50. The inclination of the ramp resulted in a 0.21-m (0.7-ft) difference in elevation of the two receivers at the maximum receiver spacing of 9.8 m (32 ft) used in SASW tests. However, the inclination of the ramp was neglected in modeling of the SASW data (horizontal layers were assumed). Numerical values of the shear wave velocities and Young's moduli (Poisson's ratio, $\nu = 0.32$, determined from crosshole tests) obtained from SASW measurements at the two stations are listed in Table 5.3. Note that these values represent Young's moduli at small strains. It should be mentioned that the SASW data at Station 275+50 were not analyzed (forward modeling) because the depth of bedrock cannot be determined due to the absence of long wavelengths.

Table 5.3. Shear Wave Velocities and Young's Moduli of Compacted Fill Determined from SASW Tests at Stations 276+50 and 278+50; Loop 1 and US 183, Austin, Texas

Station 276+50			Station 278+50		
Layer Thickness (ft)	Shear Wave Velocity (fps)	Young's Modulus (ksi)	Layer Thickness (ft)	Shear Wave Velocity (fps)	Young's Modulus (ksi)
1	950	66.8	4	1150	97.9
2	1250	115.7	5.5	1050	81.6
5	1150	97.9			
7	1100	89.6			
Bedrock	5000	.....	Bedrock	5000	.....
Avg. Values (Fill only)	1125	93.7	Avg. Values (Fill only)	1090	87.9

In addition, laboratory tests were performed on an intact sample taken from a depth of 7 ft (2.13 m) at Station 276+50. The sample was taken by pushing a 7.6-cm (3-in.) OD Shelby tube about 0.3 m (1 ft). Torsional resonant column (RC) and resilient modulus tests were performed by Dong-Soo Kim at The University of

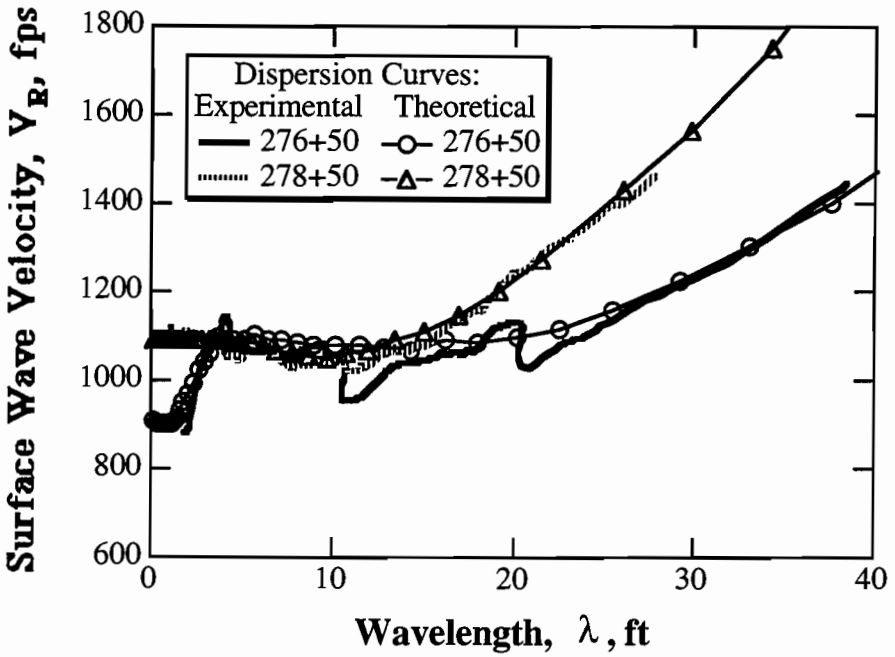

Fig 5.5. Comparison between Experimental and Theoretical Dispersion Curves Determined at Stations 276+50 and 278+50; Loop 1 and US 183, Austin, Texas.

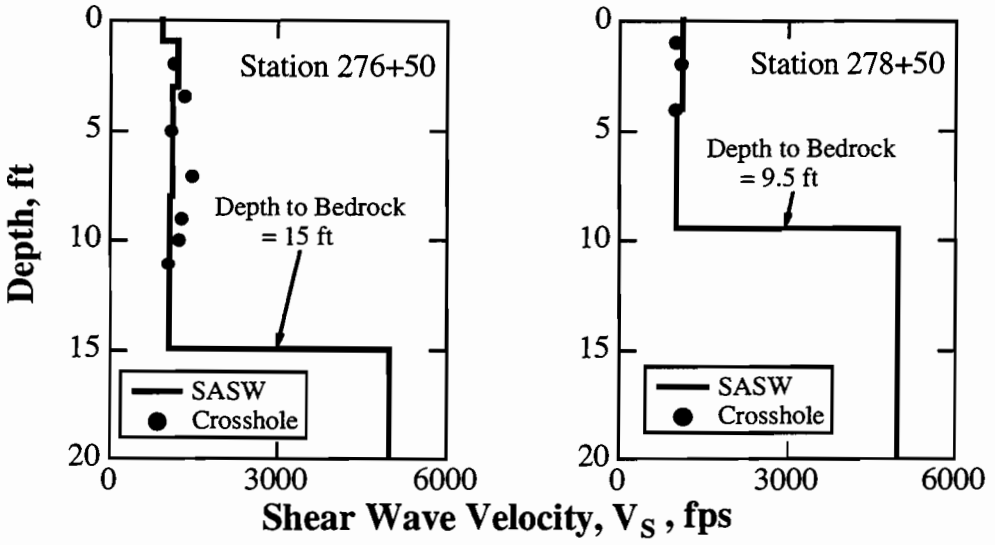

Fig 5.6. Shear Wave Velocities Determined from Forward Modeling of SASW Measurements and Crosshole Tests at Stations 276+50 and 278+50; Loop 1 and US 183, Austin, Texas.

Texas at Austin. RC tests were conducted at confining pressures ranging from 19.4 kPa (2.8 psi) to 168.6 kPa (24.4 psi). Young's moduli determined from RC tests are presented in Table 5.4 assuming a Poisson's ratio of 0.32 determined from crosshole tests. At a depth of 2.13 m (7 ft), the total confining pressure is approximately equal to 41.5 kPa (6 psi) if $K_O = 1$. For comparison purposes with field tests, Young's modulus determined at the 37.3 kPa (5.4 psi) confining pressure in the RC test was used. The moduli values reported in Table 5.4 are at 0.0002% strain. Young's modulus determined from the resilient modulus test was equal to 360 MPa (52 ksi) at an axial strain of 0.007% and a confining pressure of 41.4 kPa (6 psi). The low value of Young's modulus determined from the resilient modulus test is due to the strain dependency of the subgrade material (Stokoe et al., 1991).

Table 5.4. Young's Moduli of Compacted fill Determined from a Torsional Resonant Column Test, Sample Extracted from Station 276+50, Depth = 7 ft; Loop 1 and US 183, Austin, Texas

Confining Pressure (psi)	Shear Wave Velocity (fps)	Young's Modulus (ksi)
2.8	1125	94
5.4	1180	103
11.5	1275	120
24.4	1350	135

5.4 Tests after Placement of Limestone Base

Before placing the first AC surface layer, a 15.2-cm- (6-in.-) thick crushed limestone base was placed. One crosshole measurement was made at a depth of 7.6 cm (3 in.) at Station 276+50 to determine the stiffness of the base material. The time records of the propagating compression waves, V_P, are shown in Fig. 5.7. A compression wave velocity of 823 m/s (2,723 fps) was measured from which a shear wave velocity of 427 m/s (1,400 fps) was calculated assuming Poisson's ratio of 0.32 (same as average ν of compacted fill). The unit weight of the base was equal to 21.3 kN/m^3 (135 pcf). The calculated values of constrained modulus, M, shear modulus, G, and Young's modulus, E, for the base material were 1,492 MPa (216 ksi), 395 MPa (57 ksi) and 1,041 MPa (151 ksi), respectively.

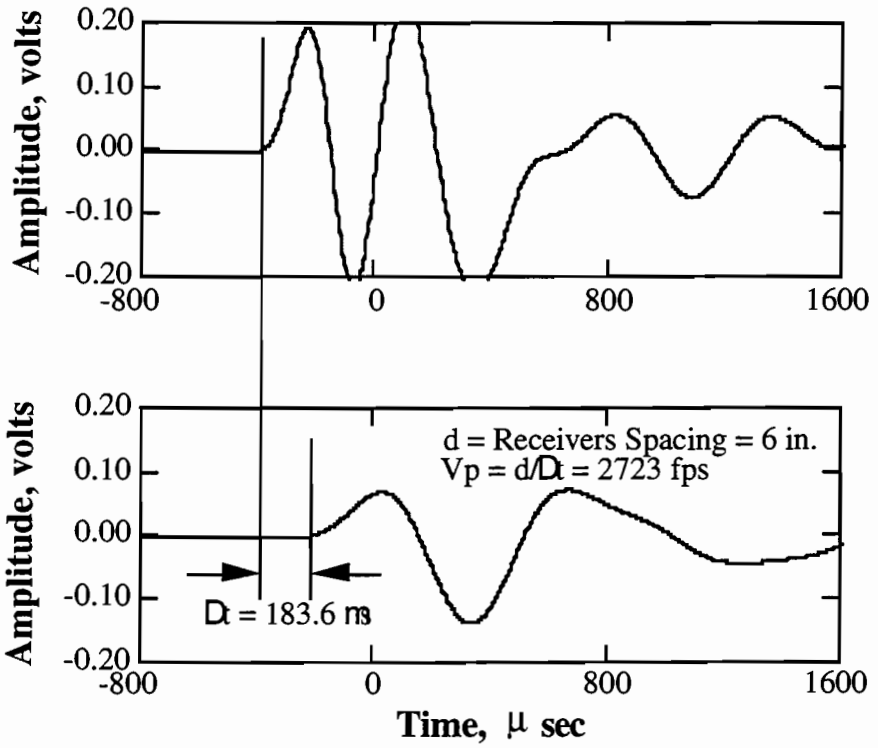

Fig 5.7. Time Records for Compression Waves in Base Material Measured at Two Receivers Spaced 6 in. Apart; Station 276+50, Depth = 3 in.

5.5 Tests after Placement of the First AC Surface Layer

The first AC surface layer was placed on May 25, 1989. The nominal thickness of this surface layer was 10.2 cm (4 in.). Field testing was performed at different times after placement of the asphalt concrete layer.

5.5.1 Testing on May 26, 1989

On May 26, 1989, only SASW measurements were performed at Stations 275+50, 276+50 and 278+50. The objective was to determine the stiffness of the surface layer immediately after placement of AC layer. However, wavelengths shorter than the thickness of the surface layer were not generated, as shown in Figs.

5.8 and 5.9. As a result, the stiffness of the surface layer could not be determined. In this series of tests, only small hammers were used as generators of high frequencies. Figures 5.8 and 5.9 show the effect of the surface layer and limestone base on the dispersion curves determined at Stations 275+50 and 276+50. Similar results were obtained at Station 278+50.

To sample the subgrade after placing the base and the AC layers, wavelengths of approximately 1.5 to 3.1 m (5 to 7 ft) were needed at the three stations. These wavelengths were generated from receiver spacings of at least 1.2 m (4 ft) and are 15 to 21 times the thickness of the AC surface layer. The base had little effect on these measurements because the velocity of the base was slightly higher than the velocity of the subgrade. As the thickness of the AC surface layer increased, larger receiver spacings have to be used if the objective of the test is to determine the stiffness of the subgrade.

5.5.2 Testing on May 29, 1989

On May 29, 1989, SASW and FWD measurements were performed on Embankment SW, four days after placing the first layer of asphalt concrete. The test locations stretched from Station 275+50 to Station 278+50. Testing was performed every 15.2 m (50 ft). The objective was to determine the stiffness of the pavement layers and to study the effect of depth-to-bedrock on the FWD measurements.

SASW Measurements

SASW tests were conducted at seven stations on Embankment SW where the depth-to-bedrock was varying due to the sloping embankment. In this series of SASW tests, a piezoelectric source was used because the small hammer did not perform adequately in generating the high frequencies required to sample the surface layer as discussed in Section 5.5.1. The WR Model F-7 piezoelectric shaker generates dynamic forces on the order of 892 N (200 lbs) up to frequencies

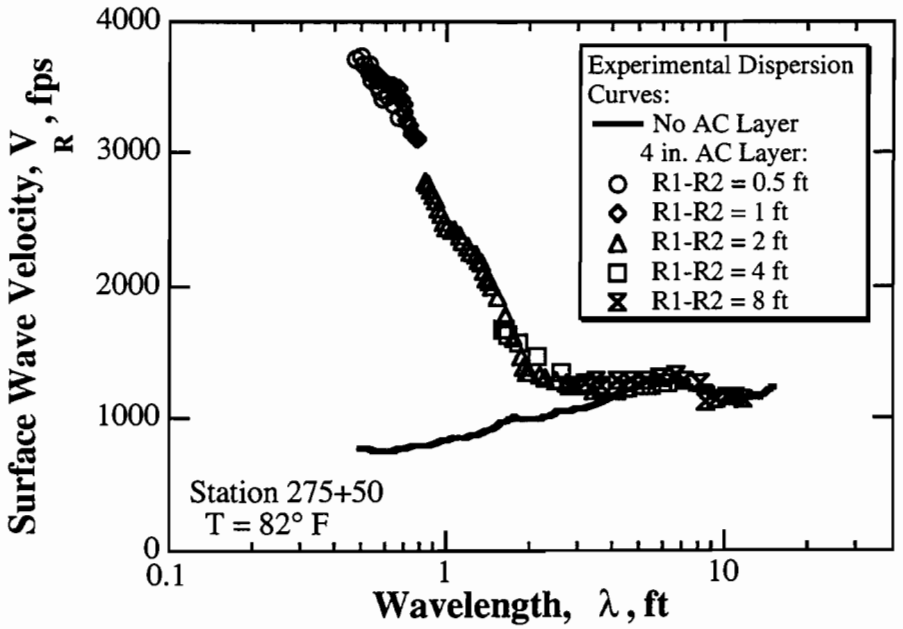

Fig 5.8. Comparison between Experimental Dispersion Curves Determined at Station 275+50 before and after Placement of the Base and the First AC Layer.

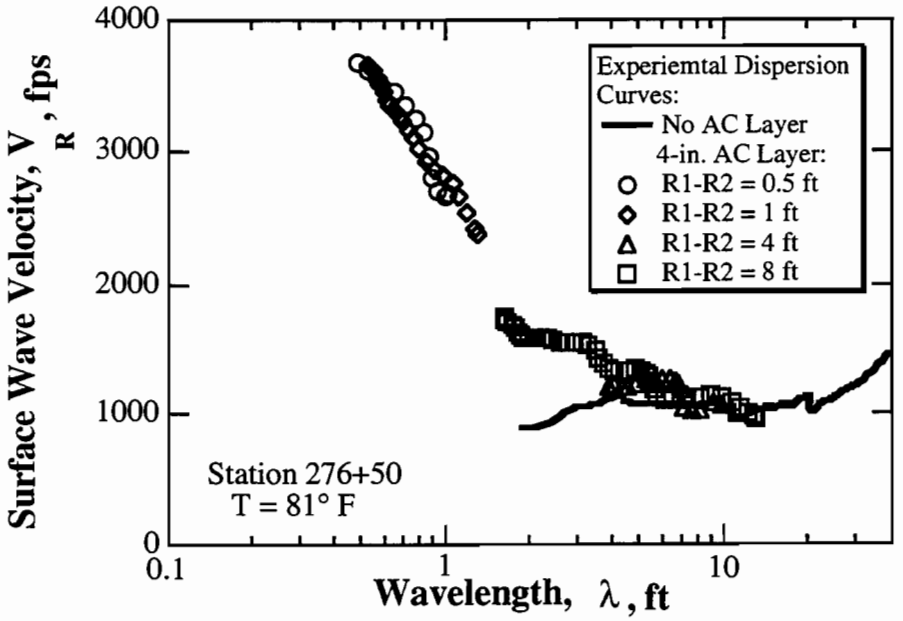

Fig 5.9. Comparison between Experimental Dispersion Curves Determined at Station 276+50 before and after Placement of the Base and the First AC Layer.

of about 30 kHz. A comparison of the phase shifts of the cross power spectra using the small hammer and F-7 shaker as high-frequency generators is presented in Fig. 5.10. The F-7 shaker generated frequencies up to 25 kHz needed to sample the surface layer and was adopted as the appropriate source for the remainder of the SASW tests.

Composite dispersion curves determined from SASW measurements at the seven stations were similar. Only the dispersion curves at stations 275+50, 276+50 and 278+50 are shown in Figs. 5.11 through 5.13, respectively. These figures show that the stiffness of the asphalt layer is frequency dependent. Values of frequencies and surface wave velocities at a wavelength of 0.102 m (0.334 ft), which is equal to the thickness of the surface layer, and at the minimum wavelength generated are also shown in Figs. 5.11 through 5.13. The surface wave velocities at a frequency of 15.5 kHz were used to calculate Young's moduli of the surface layer. In calculating Young's moduli, a Poisson's ratio of 0.27 and a total unit weight of 22 kN/m^3 (140 pcf) measured in the laboratory were used. The surface wave velocities and Young's moduli determined at the seven stations are listed in Table 5.5. In SASW tests, the values of Young's moduli of the surface layer were not affected by the presence of bedrock because short wavelengths were used in sampling the surface layer; these wavelengths were very short in comparison to the depth of bedrock.

Table 5.5. SASW Results for the Asphalt Concrete for Testing Four Days after Placement, AC Thickness = 4 in.; Embankment SW, Loop 1 and US 183, Austin, Texas

Station	Surface Temperature (°F)	Frequency Range (kHz)	V_R Range (fps)	V_R at f = 15.5 kHz (fps)	Young's Modulus (ksi)
275+50	76	12.3-21.3	4100-4640	4415	1809
276+00	76	12.4-21.6	4110-4945	4525	1900
276+50	77	11.9-25.9	3970-5050	4460	1846
277+00	77	12.7-23.8	4185-5230	4585	1951
277+50	78	11.6-22.1	3890-4965	4410	1805
278+00	77	12.1-19.2	3600-4300	4050	1522
278+50	82	13.8-23.6	4595-5155	4680	2032
Average	77			4445	1838
		Standard Deviation		185	149

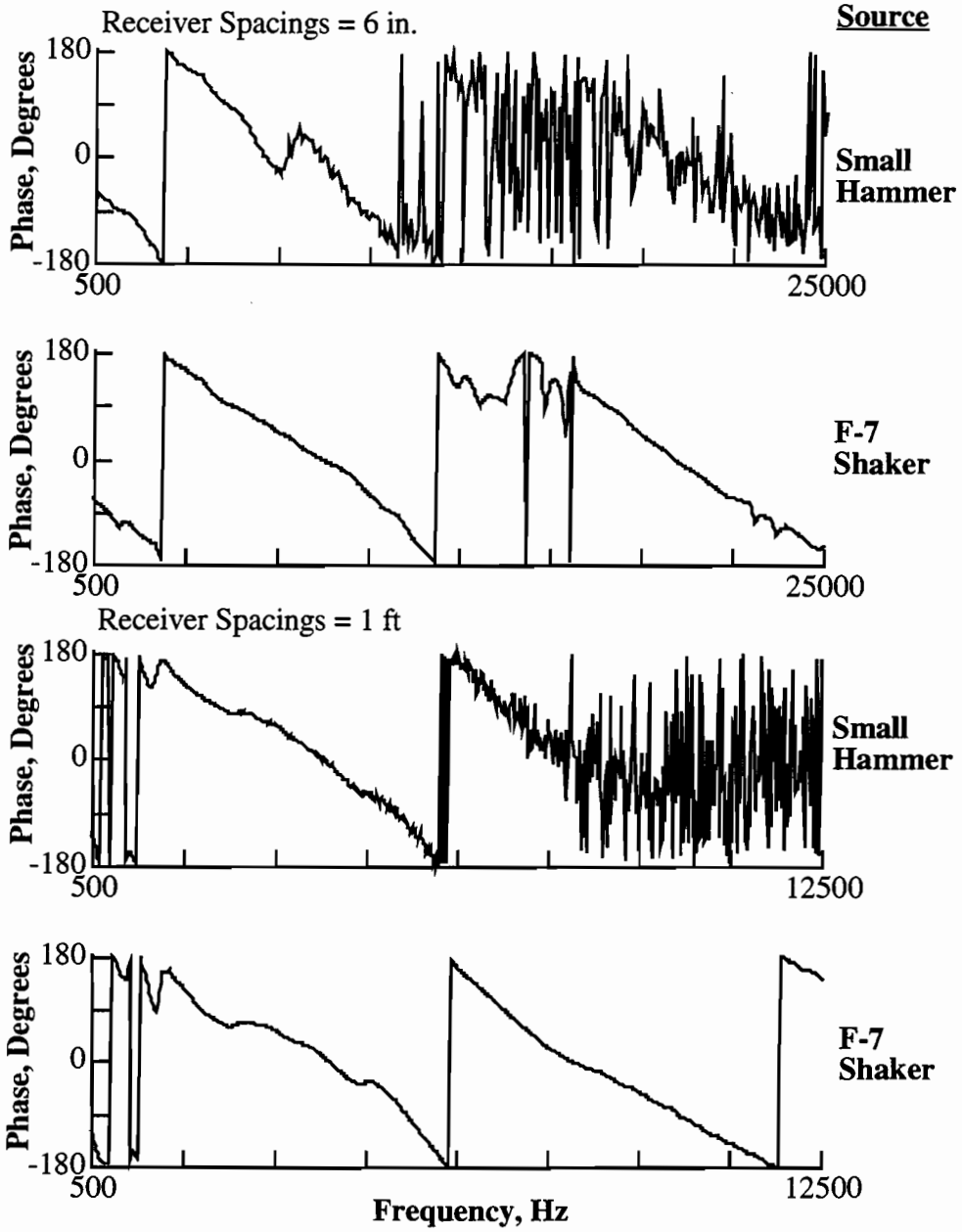

Fig 5.10. Comparison of Phase Shifts of the Cross Power Spectra between the Two Receivers Using Two Different Sources; Station 278+50, Loop 1 and US 183, Austin, Texas.

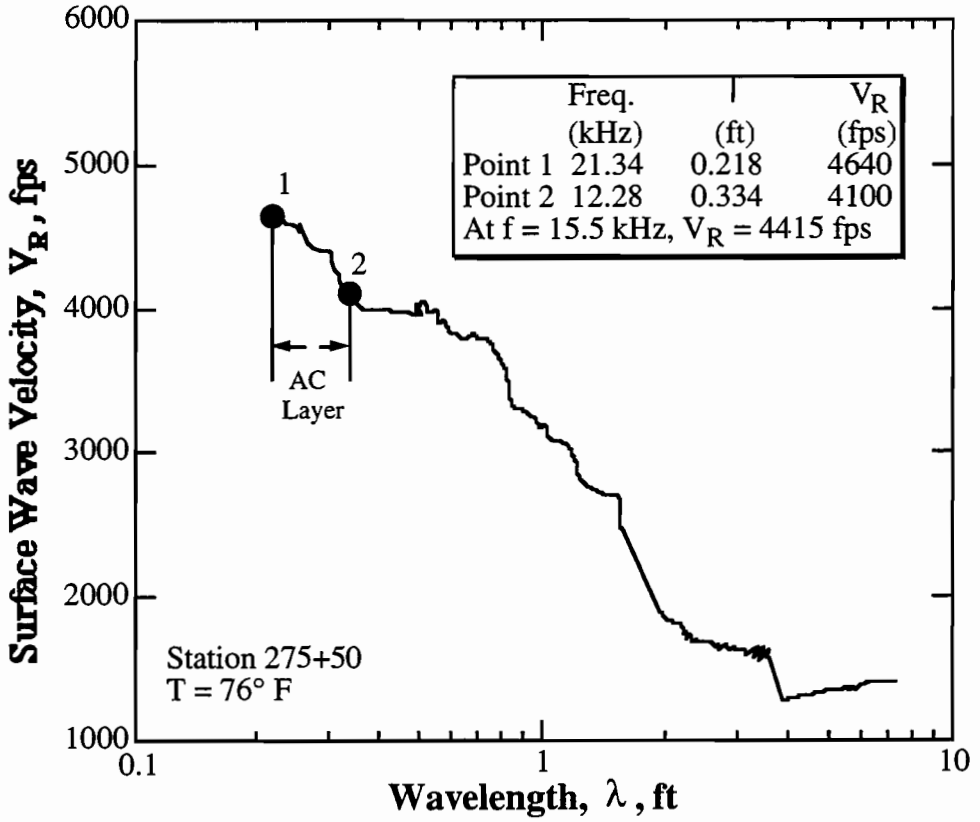

Fig 5.11. Experimental Dispersion Curve Determined from SASW Measurements after Placing 4 In. of Asphalt Concrete at Station 275+50; Loop 1 and US 183.

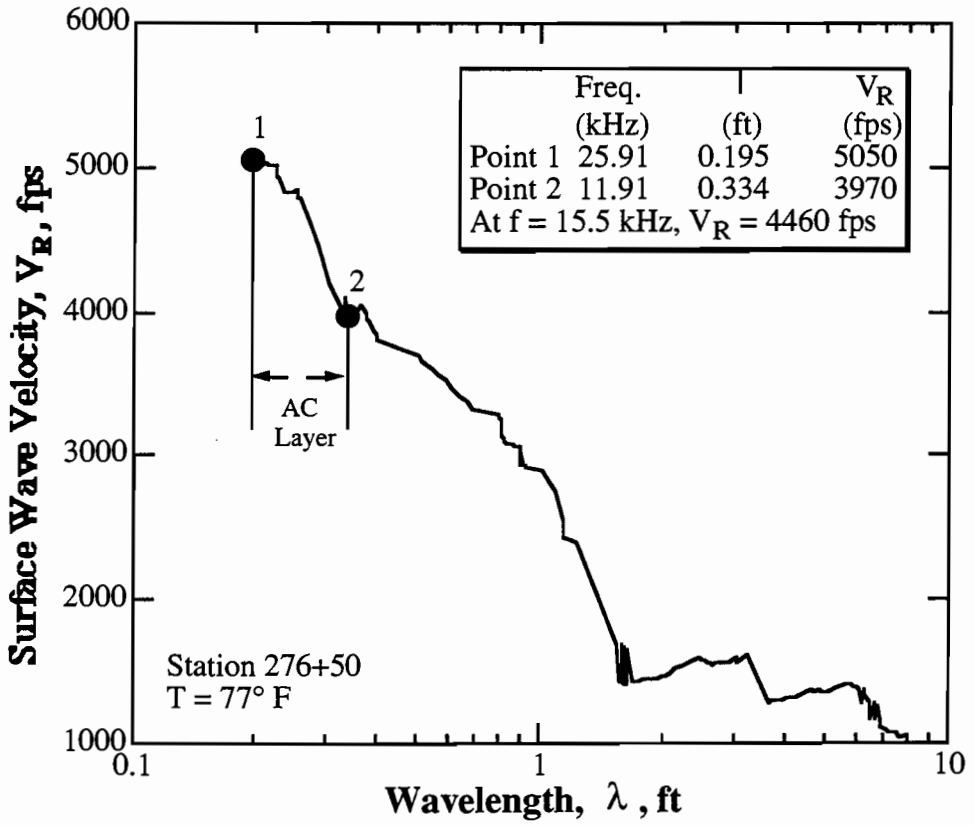

Fig 5.12. Experimental Dispersion Curve Determined from SASW Measurements after Placing 4 In. of Asphalt Concrete at Station 276+50; Loop 1 and US 183.

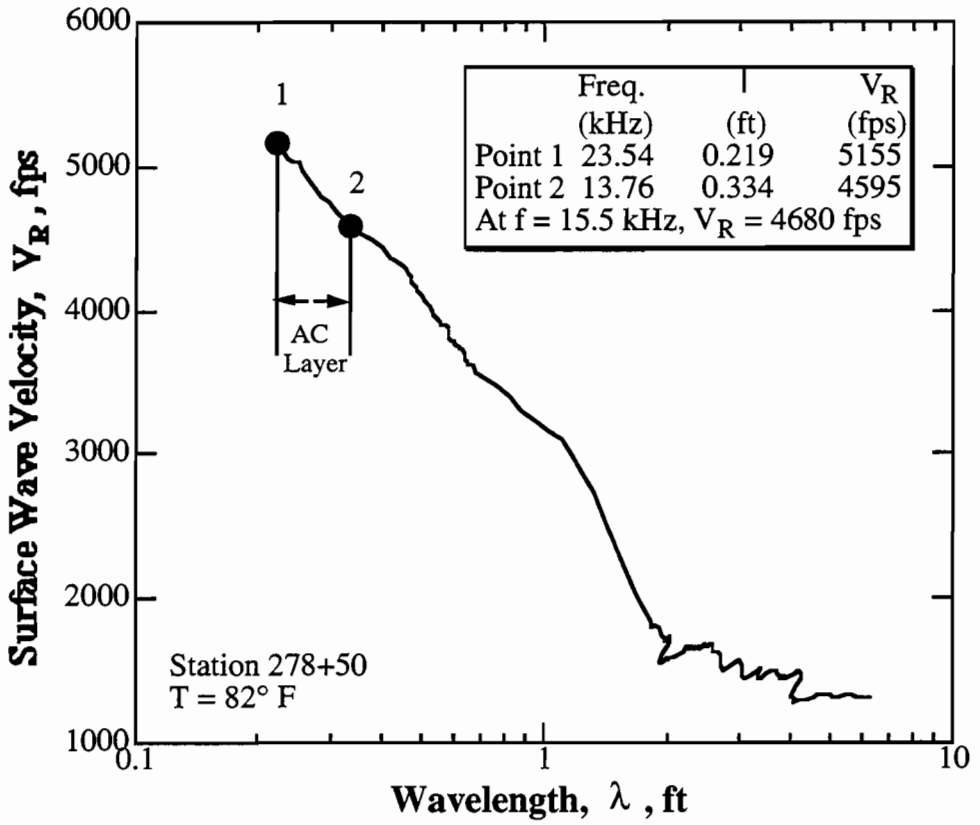

Fig 5.13. Experimental Dispersion Curve Determined from SASW Measurements after Placing 4 In. of Asphalt Concrete at Station 278+50; Loop 1 and US 183.

FWD Measurements

FWD measurements were made at the same time SASW measurements were conducted. The FWD data were collected by Robert Miner at The University of Texas at Austin (Miner, 1991). Fitting of the measured deflection basins after placing the 10.2-cm- (4-in.-) thick AC surface layer involved only static analysis using program MODULUS (Uzan et al., 1988). Static and dynamic analyses of the FWD data were performed when the surface layer was brought to its total thickness of 17.8 cm (7 in.) as discussed in Section 5.5.3. For a complete analysis of the FWD data, the reader is advised to consult Research Report 1123-7F, a publication of the Center for Transportation Research at The University of Texas at Austin (Stokoe et al., 1991).

The Young's moduli of the surface layer, base and subgrade determined from FWD measurements are presented in Table 5.6. These values represent the backcalculated moduli using program MODULUS (static analysis).

Table 5.6 Young's Moduli Backcalculated from FWD Data Using Program MODULUS (Static Analysis) for Testing Four Days after Placement of a 4-In.-Thick Asphalt Concrete Layer

	Young's Moduli of AC Surface Layer, Base and Subgrade (ksi)						
Station No.	275+50	276+00	276+50	277+00	277+50	278+00	278+50
Surface Layer	556	375	381	412	380	441	936
Base	103	120	80	52	105	139	176
Subgrade	79	62	58	54	46	43	39

5.5.3 Testing on June 3, 1989

On June 3, 1989, SASW and FWD measurements were performed on Embankment SW, four days after placing the second layer of asphalt concrete. The total thickness of the AC layer was now equal to 17.8 cm (7 in.).

SASW Measurements

SASW tests were conducted at the seven stations in the same locations where tests were performed on May 29, 1989. The F-7 shaker was used as the source of high-frequency energy. Composite dispersion curves determined from SASW measurements at the seven stations were similar. Only the dispersion curves at stations 275+50, 276+50 and 278+50 are shown in Figs. 5.14 through 5.17, respectively. These figures show that the stiffness of the asphalt layer is frequency dependent. Values of frequencies and surface wave velocities at a wavelength of 0.178 m (0.583 ft), which is equal to the thickness of the surface layer, and at the minimum wavelength generated are also shown in Figs. 5.14 through 5.17. The surface wave velocities at a frequency of 15.5 kHz were used to calculate Young's moduli of the surface layer. The surface wave velocities and Young's moduli determined at the seven stations are listed in Table 5.7.

Table 5.7. SASW Results for the Asphalt Concrete for Testing Four Days after Placement of the Top 3 in., AC Thickness = 7 in.; Embankment SW, Loop 1 and US 183, Austin, Texas

Station	Surface Temperature (°F)	Frequency Range (kHz)	V_R Range (fps)	V_R at f = 15.5 kHz (fps)	Young's Modulus (ksi)
275+50	85	6.4-23.0	3740-4650	4435	1825
276+00	85	6.6-27.0	3890-4805	4435	1825
276+50	83	6.7-28.2	3890-4870	4620	1981
277+00	83	9.5-25.8	4290-4910	4605	1968
277+50	84	7.1-29.1	4130-4860	4680	2032
278+00	84	7.1-20.0	4130-4620	4450	1838
278+50	88	6.7-25.0	3880-4750	4555	1925
Average	85			4540	1913
		Standard Deviation		93	78

SASW tests were performed at station 276+50 to monitor the changes in stiffness of the AC layer as the temperature increased. Figure 5.17 shows the experimental dispersion curves determined at Station 276+50 for surface temperatures of 28° C (83° F), 35° C (94° F), 44° C (110° F), and 56° C (133° F). The maximum frequency generated when the surface temperature rose to 56° C (133° F) was equal to 6 kHz.

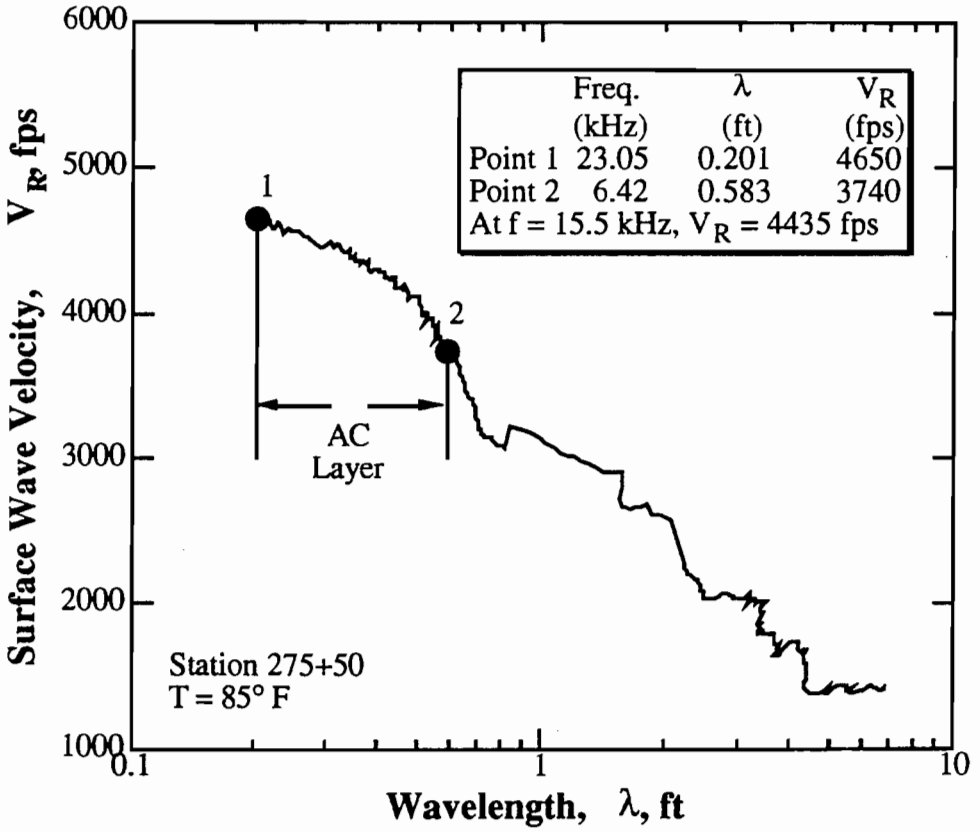

Fig 5.14. Experimental Dispersion Curve Determined from SASW Measurements after Placing 7 In. of Asphalt Concrete at Station 275+50; Loop 1 and US 183.

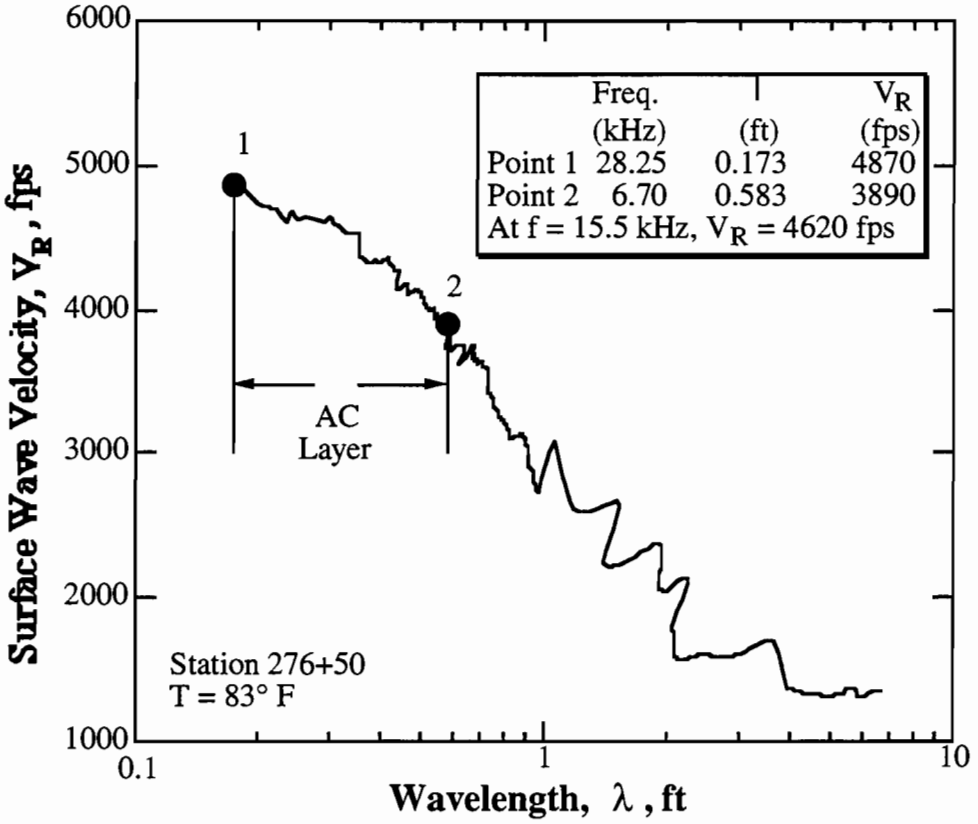

Fig 5.15. Experimental Dispersion Curve Determined from SASW Measurements after Placing 7 In. of Asphalt Concrete at Station 276+50; Loop 1 and US 183.

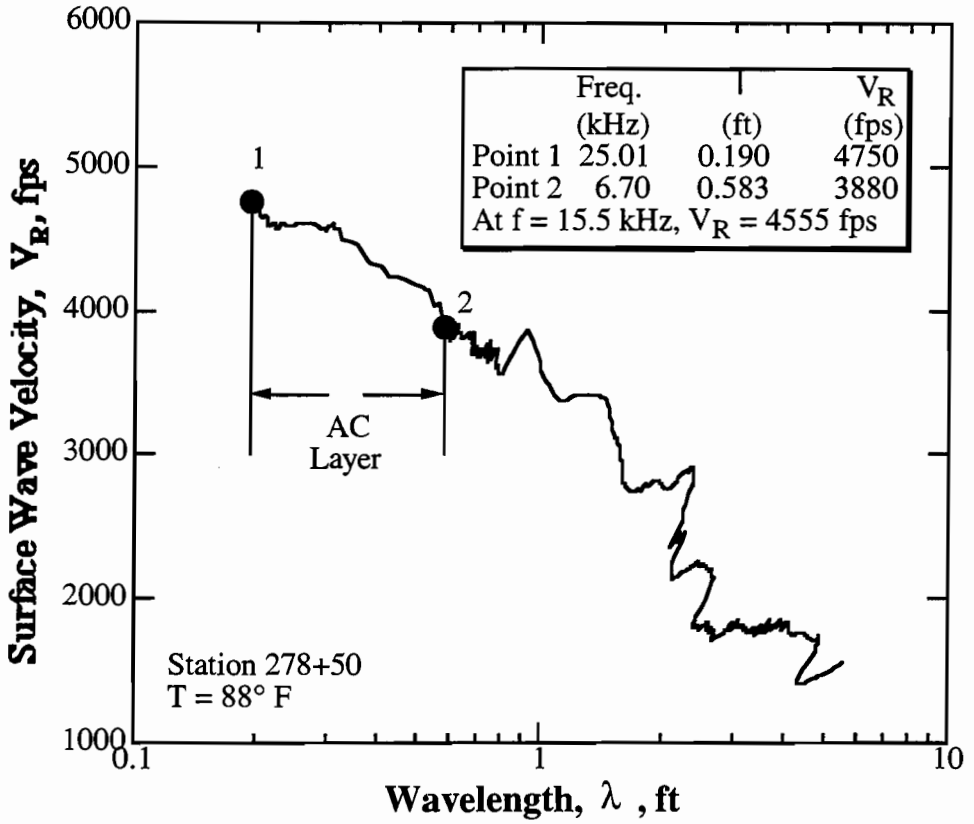

Fig 5.16. Experimental Dispersion Curve Determined from SASW Measurements after Placing 7 In. of Asphalt Concrete at Station 278+50; Loop 1 and US 183.

Therefore, this frequency was selected to compare wave velocities because the stiffness of asphalt is frequency dependent. Surface wave velocities and Young's moduli determined at a frequency of 6 kHz are listed in Table 5.8. Poisson's ratios of 0.28, 0.29, 0.31 and 0.34 were used in the calculation of Young's moduli at temperatures of 28° C, 35° C, 44° C, and 56° C (83° F, 94° F, 110° F and 133° F), respectively. These Poisson's ratios were obtained from laboratory tests on asphalt cylinders as discussed in Section 5.9. Frequencies of 15.5 kHz were generated when the surface temperature was equal to 28° C and 35° C (83° F and 94° F). The surface wave velocities determined at a frequency of 15.5 kHz were equal to 1,408 m/s (4,620 fps) and 1,240 m/s (4,070 fps) for temperatures of 28° C and 35° C (83° F and 94° F), respectively. The corresponding Young's moduli determined at a frequency of 15.5 kHz were equal to 13.7 x 10^3 MPa (1,981 ksi) and 10.8 x 10^3 MPa (1,561 ksi) for temperatures of 28° C and 35° C (83° F and 94° F), respectively.

Table 5.8 Surface Wave Velocities and Young's Moduli of the Asphalt Concrete at Four Different Temperatures; AC Thickness = 7 in., f = 6 kHz, Station 276+50, Embankment SW, Loop 1 and US 183, Austin, Texas

Surface Temperature (°F)	Surface Wave Velocity (fps)	Young's Modulus (ksi)
83	3720	1294
94	3255	999
110	2635	675
133	1800	317

FWD Measurements

FWD measurements were made at the same time SASW measurements were taken. The FWD data were collected by Robert Miner at The University of Texas at Austin. Miner fitted the measured deflection basins using two approaches. First, the measured deflection basins were fitted statically using program MODULUS. The second approach involved dynamic analysis to incorporate the effect of depth to bedrock on the measured deflection basins using program UTPV. Program UTPV is a slight modification of the program described by Roesset and Shao, 1985. Young's moduli of the surface layer, base and

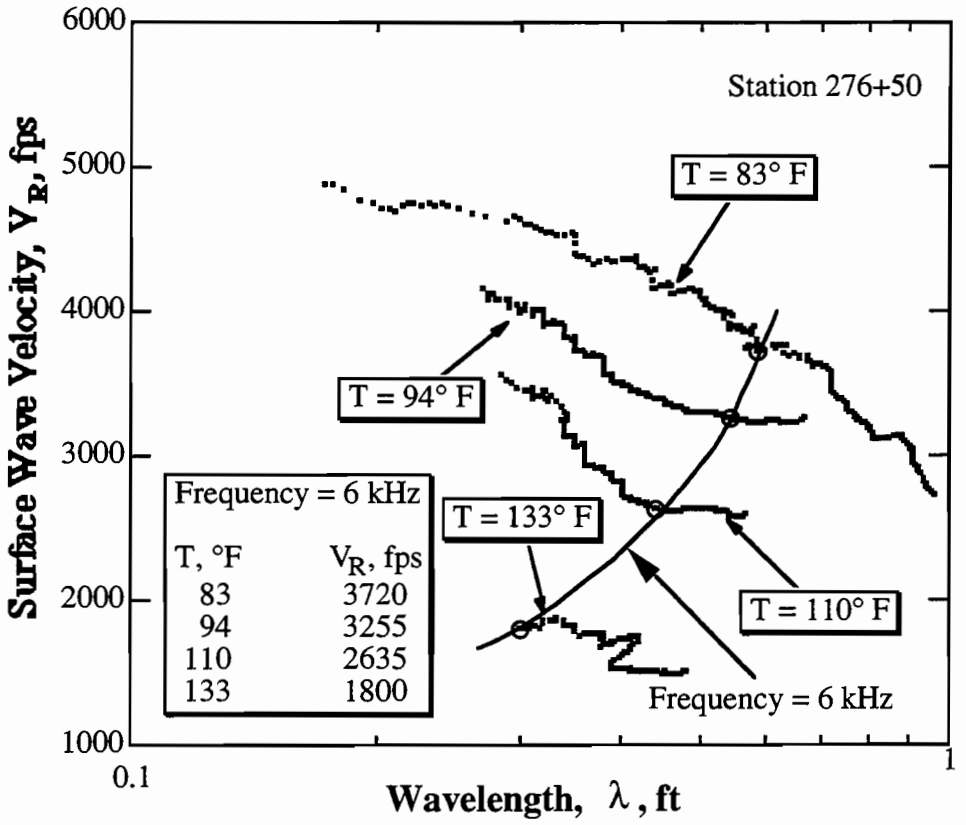

Fig 5.17. Experimental Dispersion Curves Determined from SASW Measurements at Four Different Temperatures; 7 In. of Asphalt Concrete, Station 276+50, Loop 1 and US 183.

subgrade determined from FWD measurements are presented in Tables 5.9 and 5.10 for static and dynamic analyses. These values represent the backcalculated moduli using program MODULUS (static analysis) and program UTPV (dynamic analysis).

Table 5.9. Young's Moduli Backcalculated from FWD Data with 7 In. of Asphalt Concrete Using Program MODULUS (Static Analysis)

	Young's Moduli of AC Surface Layer, Base and Subgrade* (ksi)						
Station No.	275+50	276+00	276+50	277+00	277+50	278+00	278+50
Surface Layer	274	263	251	218	275	280	409
Base	161	221	120	106	201	308	318
Subgrade	76	65	59	57	49	46	40

* Average surface temperature of 85° F

Table 5.10. Young's Moduli Backcalculated from FWD Data with 7 In. of Asphalt Concrete Using Program UTPV (Dynamic Analysis)

	Young's Moduli of AC Surface Layer, Base and Subgrade (ksi)						
Station No.	275+50	276+00	276+50	277+00	277+50	278+00	278+50
Surface Layer	313	282	282	226	268	297	361
Base	73	68	73	79	73	76	76
Subgrade	93	88	73	79	68	65	55

In the analysis of the FWD data, the depth to bedrock had to be known to include the dynamic effects. Chang et al. (1992) developed a procedure to determine the depth to bedrock based on the damped natural period of the free vibrations provided the shear wave velocity of the subgrade is known. Seng (1992) performed a parametric study on a large number of pavement profiles by varying the stiffness and thickness of each layer in the pavement profile in order to predict the depth to bedrock from the time histories of the deflections calculated at the receivers in the FWD test. For flexible pavements and unsaturated subgrade conditions, Seng suggested the following equation to determine the depth to bedrock:

$$D_b = \frac{T_d^{1.08}\, V_S^{1.13}}{(6.33 - 5.04\nu)} \tag{5.7}$$

where

D_b is the depth to bedrock in feet,

T_d is the damped natural period in seconds,

V_S is the shear wave velocity of the subgrade in feet per second, and

ν is Poisson's ratio of the subgrade.

The deflection-time histories measured at receivers 5 and 6 during FWD measurements at Stations 276+50 and 278+50 are shown in Fig. 5.18. The FWD measurements were recorded in a time window 0.06 second long, and only half a cycle of the free vibrations curve was captured. For future applications, the time window in FWD measurements should be increased to about 0.2 second to adequately record the free vibrations which result from a shallow depth to bedrock.

As shown in Fig. 5.18, the damped natural period of free vibrations was equal to 33 ms and 22.4 ms at Stations 276+50 and 278+50, respectively (average from receivers 5 and 6). The shear wave velocities and Poisson's ratios determined from crosshole measurements were equal to 375 m/s (1,230 fps), 0.323, 314 m/s (1,030 fps) and 0.32 at Stations 276+50 and 278+50, respectively. Using Eq. 5.7, the depths to bedrock were calculated to be 5.1 m (16.6 ft) and 2.7 m (8.9 ft) at Stations 276+50 and 278+50, respectively. These depths to bedrock compare reasonably well with the depths determined from SASW measurements shown in Fig. 5.6, 4.6 m(15 ft) and 2.9 m (9.5 ft) at Stations 276+50 and 278+50, respectively.

Effect of Frequency on Stiffness of Asphalt Concrete

Resonant column tests and cyclic torsional shear tests (Kim, 1991) were performed in the lab on a 5.1-cm- (2-inch-) diameter sample of asphalt concrete cored from Station 276+50. The specimen was taken from the first 10.2-cm-

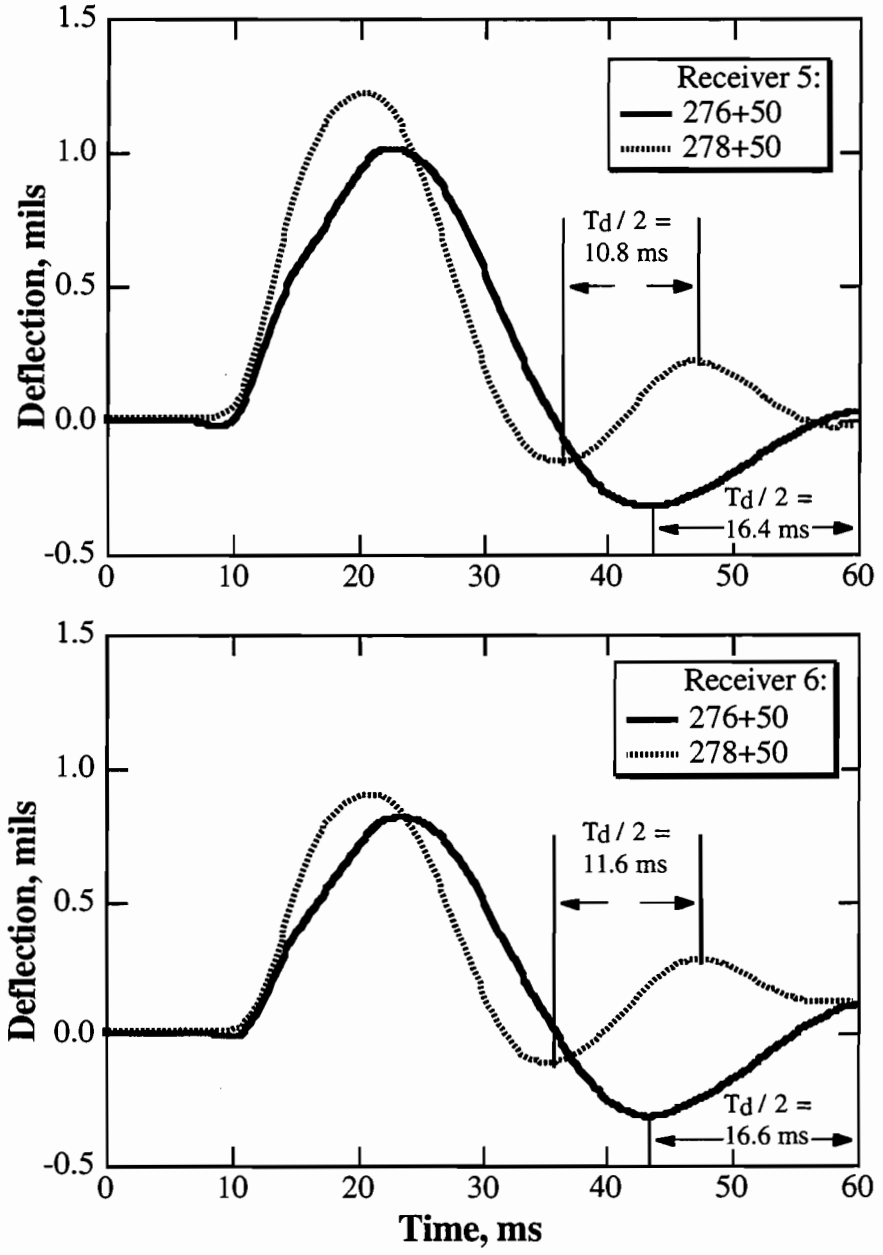

Fig 5.18. Deflection-Time Histories from FWD Measurements Recorded at Receivers 5 and 6; Stations 276+50 and 278+50, Loop 1 and US 183, Austin, Texas.

(4-in.-) thick lift. The excitation frequency in the cyclic torsional shear tests varied from 0.01 Hz to 10 Hz. The resonant frequency in the RC tests was controlled by the stiffness and the length of the specimen. Figure 5.19 shows the variation of Young's modulus with frequency for temperatures of 23°, 30°, and 38° C (73°, 85° and 101° F). Moduli obtained from SASW measurements at Station 276+50 at frequencies of 28 kHz and 6.7 kHz are also shown in Fig. 5.19. A log-log scale shows a nearly linear relationship between Young's modulus and the frequency of excitation.

5.6 Comparison of Moduli of Pavement Layers from Different Tests

5.6.1 Young's Moduli of the Subgrade

Station 276+50 was considered as the main station where extensive testing was performed. For the subgrade modulus, values determined at Station 276+50 were compared for the various types of tests. Results from all tests before adjusting for the effect of strain amplitude are presented in Fig. 5.20. Young's moduli determined from crosshole, SASW and RC tests (small strain) yielded higher values than those determined from FWD and resilient modulus tests. Fitting the deflection basins in FWD tests dynamically provided higher values of moduli than those determined from statically fitting the deflection basins. This is due to the presence of shallow bedrock where dynamic amplification occurred (Chang, 1991).

For a better comparison, values of moduli were adjusted to an axial strain of 0.007% associated with FWD tests (Stokoe et al., 1991). The adjustment was based on RC and resilient modulus tests performed on the subgrade material over a wide range of shearing strains as shown in Fig. 5.21. Table 5.11 lists the modulus adjustment factors based on the strains associated with each test. The adjusted moduli at an axial strain of 0.007% are presented in Fig. 5.22.

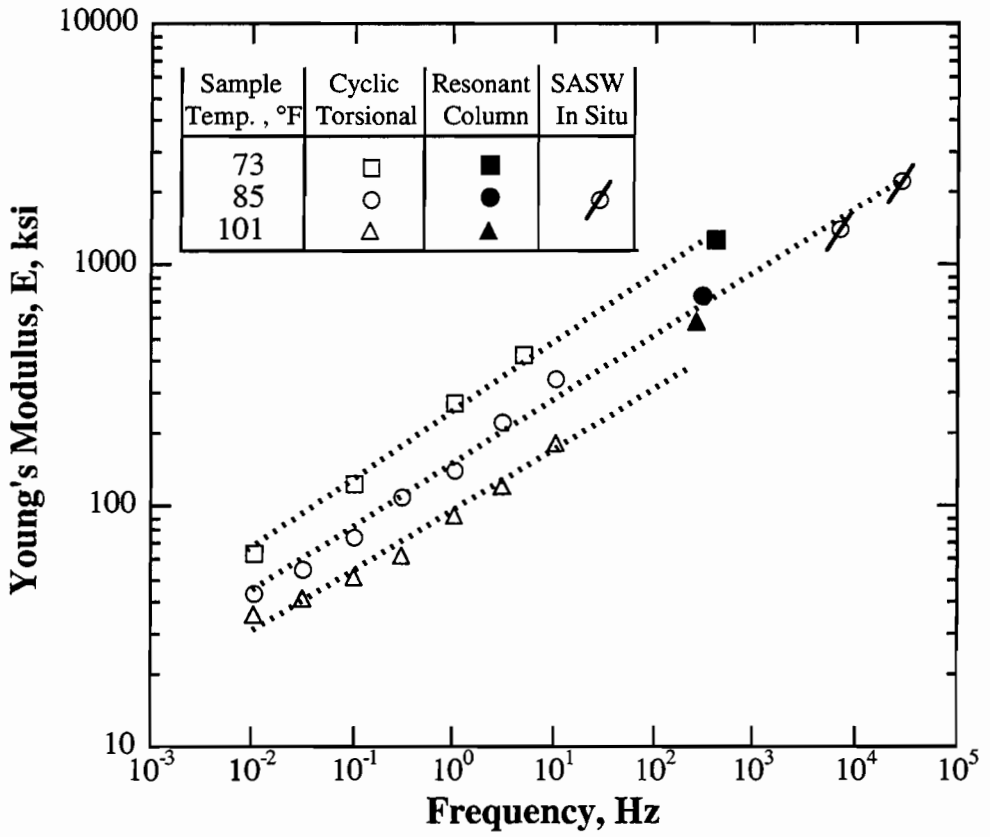

Fig 5.19. Variation of Young's Modulus of Asphalt Concrete with Loading Frequency at Different Temperatures; Specimen Taken from Station 276+50, Loop 1 and US 183, Austin, Texas.

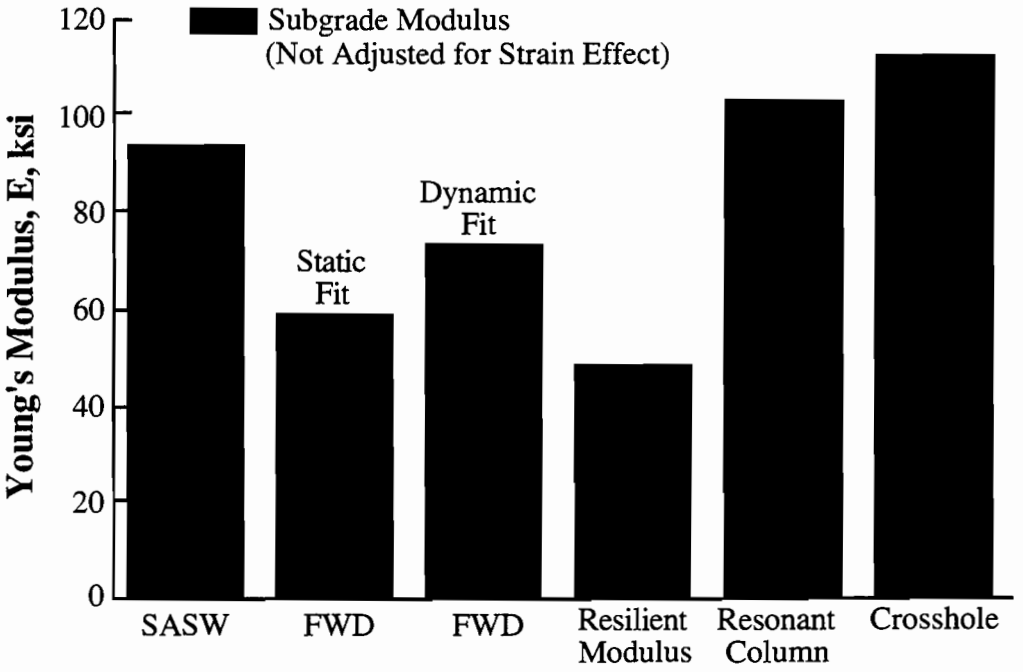

Fig 5.20. Values of Subgrade Modulus before Adjusting for the Effect of Strain Amplitude; Station 276+50, Loop 1 and US 183, Austin, Texas.

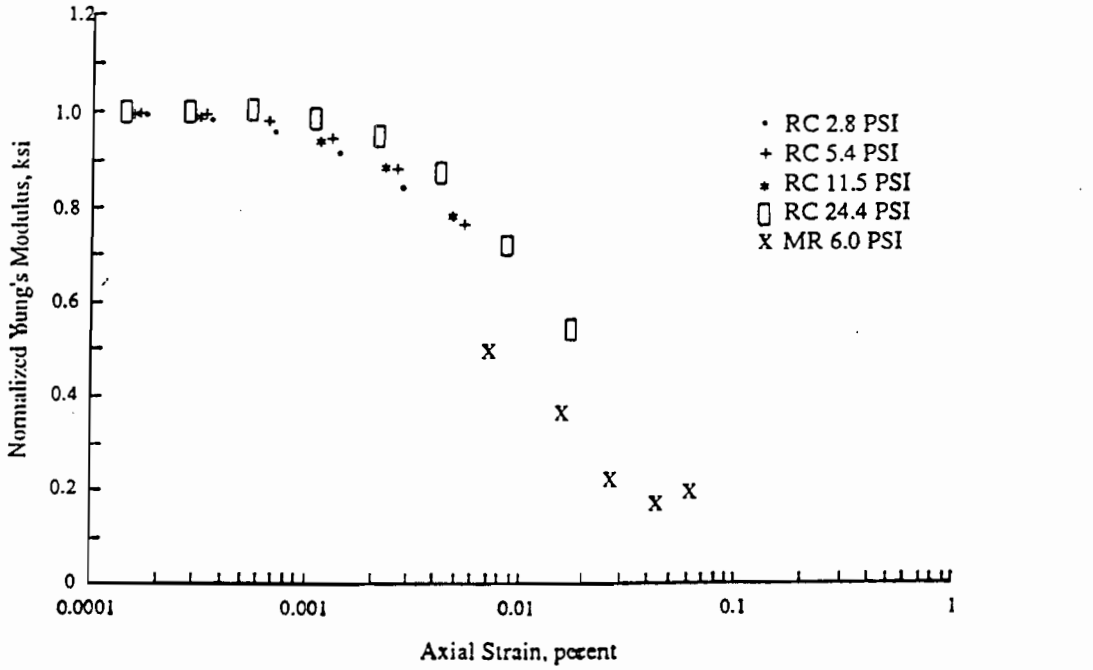

Fig 5.21. Normalized Young's Modulus versus Axial Strain; Station 276+50, Loop 1 and US 183, Austin, Texas (Miner, 1991).

Table 5.11. Correction Factors for Young's Moduli of the subgrade to Adjust to a Strain of 0.007%; Station 276+50, Loop 1 and US 183, Austin, Texas

Test	Effective Test Strain (%)	Modulus Correction Factor
SASW	< 0.0001	0.75
FWD, Static Fit	0.007	1.00
FWD, Dynamic Fit	0.007	1.00
Resilient Modulus	0.007	1.00
Resonant Column	0.0002	0.80
Crosshole	< 0.0001	0.75

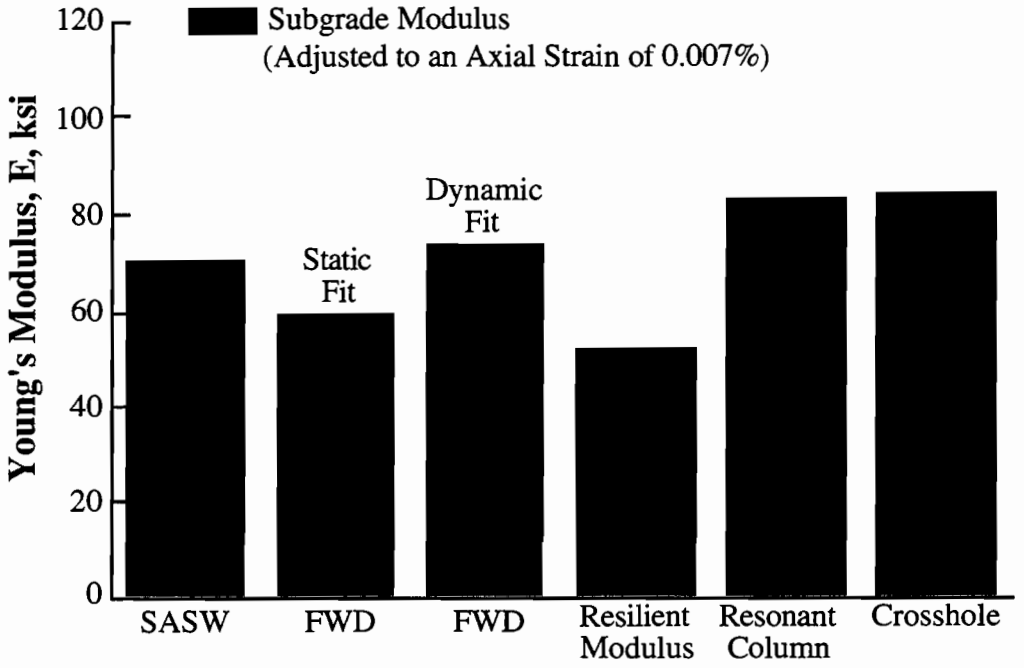

Fig 5.22. Values of Subgrade Modulus Adjusted for 0.007% Axial Strain; Station 276+50, Loop 1 and US 183, Austin, Texas.

5.6.2 Young's Moduli of the Base

Young's moduli of the base material obtained from the forward modeling of the SASW measurements at Stations 275+50, 276+50 and 278+50 were equal to 1,041, 965, and 1,075 MPa (151, 140 and 156 ksi), respectively. The backcalculated Young's moduli of the base material from the FWD data averaged 1,412 and 510 MPa (205 and 74 ksi) for static and dynamic analyses, respectively. The moduli values ranged from 730 to 2,191 MPa (106 to 318 ksi) for the static analysis and from 469 to 544 MPa (68 to 79 ksi) for the dynamic analysis of the FWD data. The scatter in the moduli values from the static analysis shows the insensitivity of the FWD test to characterize the stiffness of the base material. Young's modulus of the base material from crosshole tests was equal to 1,041 MPa (151 ksi) determined only at Station 276+50. The moduli values could not be compared in any meaningful manner because of the large scatter in the base moduli values from the FWD tests.

5.6.3 Young's Moduli of the Asphalt Concrete

Young's moduli of the asphalt concrete determined from SASW, FWD and RC tests at a temperature of 35° C (85° F) are presented by the solid histograms in Fig. 5.23. It is clear from Fig. 5.23 that the higher the frequency of the measurement, the higher the value of Young's modulus. In the SASW tests, frequencies in the order of 15.5 kHz were used as opposed to the frequency of 30 Hz in the FWD tests (between 0 and 60 Hz). In the RC tests, the excitation frequency was equal to 310 Hz. In the SASW tests, Young's modulus averaged 13.22×10^3 MPa (1,913 ksi). From the FWD tests, the backcalculated Young's moduli averaged 1,942 and 2,004 MPa (281 and 290 ksi) for static and dynamic analyses, respectively. Young's modulus determined from the RC tests was equal to 5,141 MPa (744 ksi). Figure 5.19 was used to adjust Young's moduli to a frequency of 30 Hz. The SASW-determined modulus was divided by a factor of 5.3 and the RC-determined modulus was divided by a factor of 2.1. A comparison of Young's moduli adjusted to a frequency of 30 Hz is presented by the hatched histograms in Fig. 5.23. Resonant column tests on AC samples showed that

moduli are only slightly affected by the strain level (less than 0.0002% for the strains involved). Thus, adjustment for strain level was neglected.

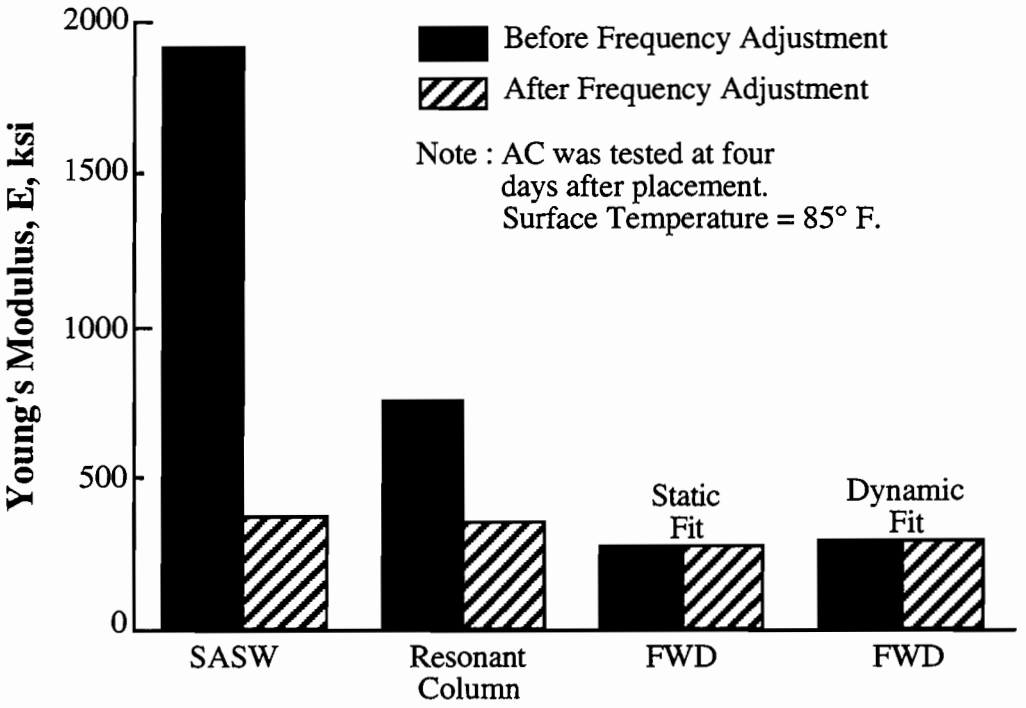

Fig 5.23. Values of the Asphalt Concrete Modulus before and after Adjusting for the Effect of Frequency; Station 276+50, Loop 1 and US 183, Austin, Texas.

5.7 Testing of Older Asphalt at Embankment SW (t > 1.5 Years)

In the previous sections, results from SASW measurements were obtained immediately after placing the asphalt layer. Embankment SW (Station 276+50) was tested again approximately 1.5 years after placing the AC layer. SASW and compression wave tests were conducted to determine the variation in stiffness of the AC layer with time. In addition, compressional and torsional resonant tests were conducted in the laboratory on an AC cylindrical specimen. The specimen was taken from Station 276+50 in the same day SASW and P-wave measurements were performed and was tested in the laboratory (resonance tests) at The University of Texas at Austin.

5.7.1 SASW Tests

SASW tests were performed on February 9, 1991. The surface temperature varied from 6° C to 21° C (43° F to 71° F). During this series of SASW tests, an exponential window was employed to minimize the effect of reflected waves from the pavement boundaries. Extreme care should be exercised when using exponential windows. The objective of exponential windowing is to eliminate the unwanted reflections without altering the signal produced by the propagated direct waves. It is recommended that a test using a uniform window be performed in conjunction with exponential windowing to identify the general trend of the phase shifts of the cross power spectrum between the two receivers. Figure 5.24 shows a comparison of the phase shifts of the cross power spectra between the two receivers using uniform and exponential windows.

The experimental dispersion curves determined at temperatures of 6°, 17°, and 21° C (43°, 63° and 71° F) are shown in Fig. 5.25. A comparison of experimental dispersion curves determined immediately (after 4 days) and 1.5 years after placement of the AC layer is shown in Fig. 5.26. It is clear from Fig. 5.26 that the asphalt concrete is more frequency dependent when it is newly placed.

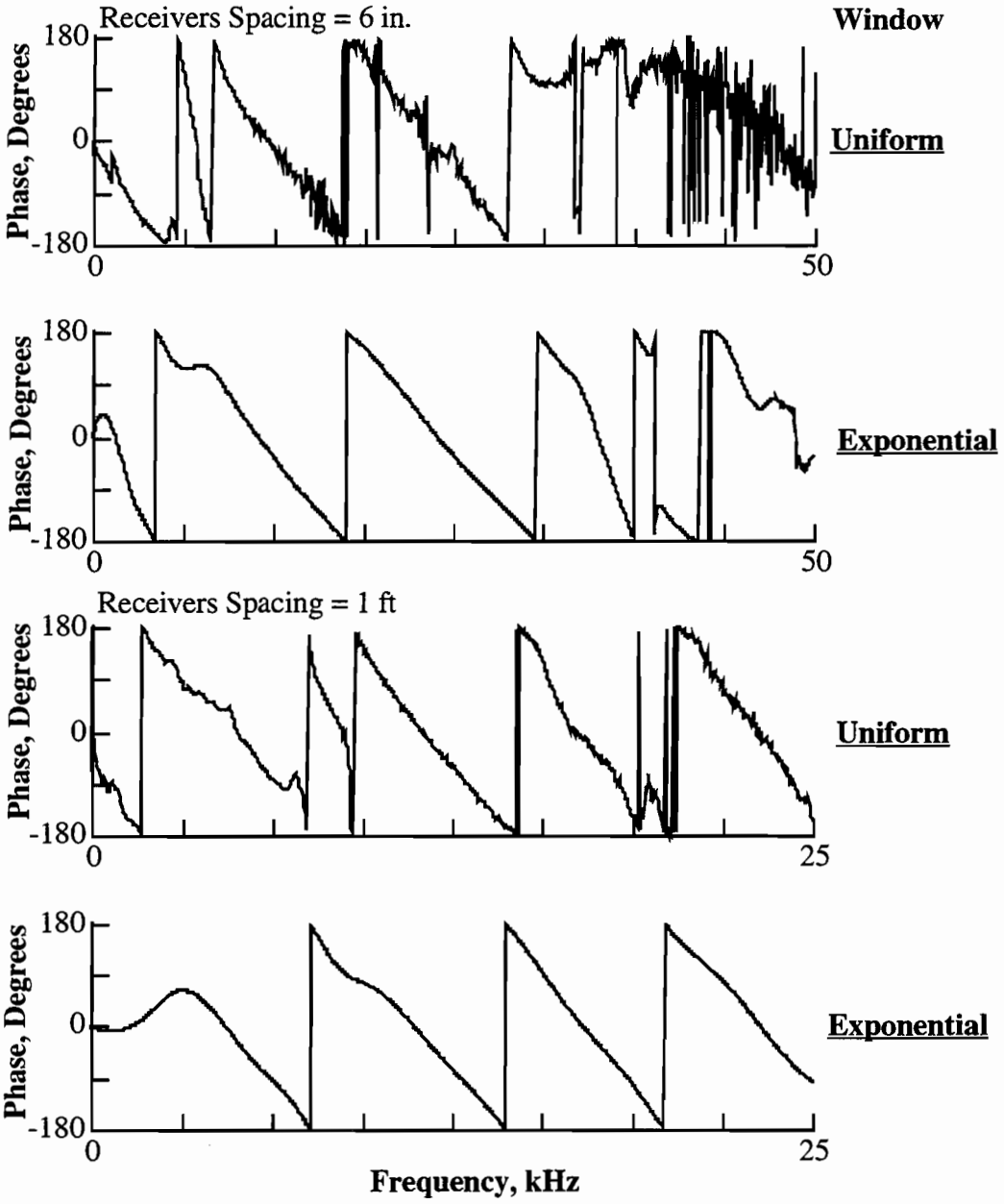

Fig 5.24. Comparison of Phase Shifts of the Cross Power Spectra between the Two Receivers Using Uniform and Exponential Windows at a Surface Temperature of 43° F; T Station 276+50.

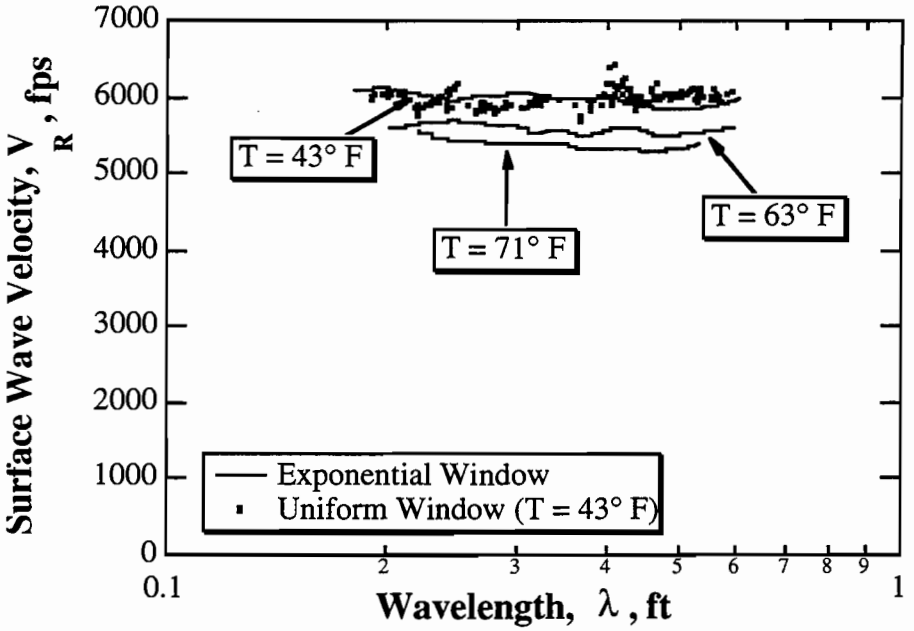

Fig 5.25. Experimental Dispersion Curves Determined at Station 276+50 Approximately 1.5 Years after Placement of the 7-in. Thick AC Layer.

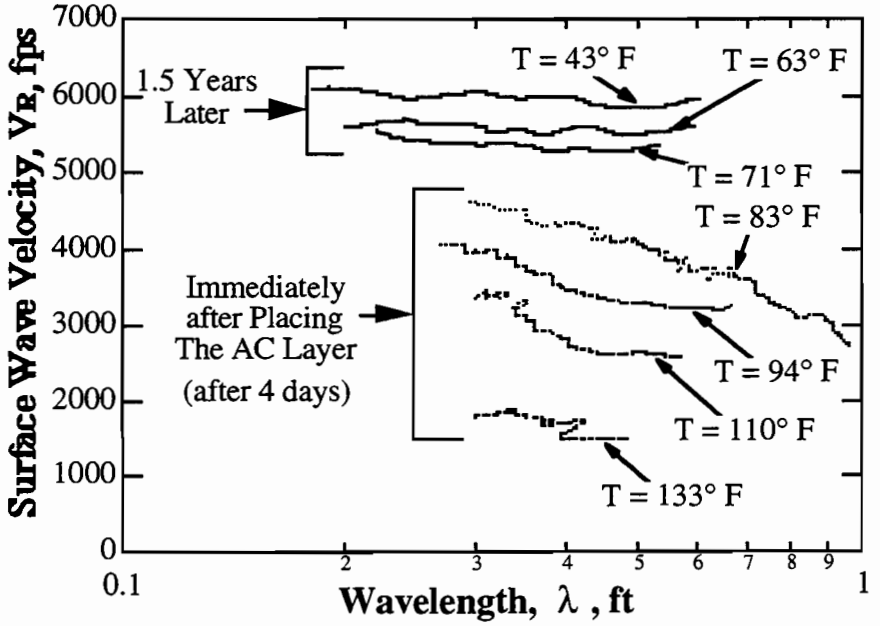

Fig 5.26. Experimental Dispersion Curves Determined at Station 276+50 Immediately and 1.5 Years after Placement of the 7-in. Thick AC Layer.

Young's Moduli

The experimental dispersion curves shown in Fig. 5.25 were used to calculate Young's moduli of the 17.8-cm (7-in.) AC layer. At a frequency of 15.5 kHz, the surface wave velocities were equal to 1,826, 1,684 and 1,637 m/s (5,990, 5,525 and 5,370 fps) at surface temperatures of 6° C, 17° C, and 21° C (43°, 63° and 71° F), respectively. The corresponding Young's moduli were equal to 22.2 x 10^3, 19.4 x 10^3 and 18.4 x 10^3 MPa (3,206, 2,799 and 2,659 ksi) at temperatures of 6° C, 17° C, and 21° C (43°, 63° and 71° F), respectively. Poisson's ratios of 0.223, 0.255 and 0.262 (discussed in Section 5.9) were used in the calculation of Young's moduli at temperatures of 6° C, 17° C, and 21° C (43°, 63° and 71° F), respectively. Unfortunately, the surface layer could not be tested over a wide range of temperatures 1.5 years after placing the AC layer. SASW tests performed on the TTI test facility in Bryan, Texas, covered a wider range of temperatures, and the following relationship was established (Fig. 4.15):

$$E / E_{70° F} = 1.510 - 0.00729\ T \qquad (5.8)$$

where

E is the modulus at any temperature,
$E_{70° F}$ is the modulus at 70° F, and
T is the temperature in °F.

Equation 5.8 was used to calculate Young's moduli at temperatures ranging from 32° F to 136° F for comparison purposes (see Table 5.13).

5.7.2 Compression Wave Measurements

The compression wave test setup described in Section 4.5.2 was used at Embankment SW to determine the stiffness of the AC layer. Compression wave measurements were conducted in conjunction with the SASW measurements at temperatures of 6° C, 17° C, and 21° C (43°, 63° and 71° F). Source-receiver (S-

R) distances of 7.6, 15.2, 22.8, 30.5, 45.7 and 61 cm (3, 6, 9, 12, 18 and 24 in.) were used.

Typical time records for S-R distances of 15.2 and 61 cm (6 and 24 in.) at a surface temperature of 6° C (43° F) are shown in Fig. 5.27. A travel distance versus travel time plot for the propagating compression wave at a temperature of 6° C (43° F) is shown in Fig. 5.28. A compression wave velocity (V_C) of 3,124 m/s (10,250 fps) was determined from the slope of the line in Fig. 5.28. This curve fitting approach reduces much scatter which otherwise arises in the direct P-wave measurements. A Young's modulus of 21.9 x 10^3 MPa (3,172 ksi) was calculated using Eq. 2.2. At temperatures of 17° C and 21° C (63° and 71° F), the compression wave velocities were equal to 2,920 and 2,871 m/s (9,580 and 9,420 fps), respectively. These wave velocities correspond to Young's moduli of 19.1 x 10^3 and 18.5 x 10^3 MPa (2,771 and 2,679 ksi). A comparison of Young's moduli determined from SASW tests and compression wave tests is presented in Fig. 5.29. The comparison of moduli from the SASW and compression wave tests shows that reasonable values for the unconstrained compression wave were measured under these conditions, and use of Eq. 2.2 is appropriate. Of course, the value of Poisson's ratio used with the SASW results has a significant effect. However, values from cylinder tests presented in Section 5.9 were used.

5.7.3 Resonance Tests on Cylindrical Specimen

Resonance tests were conducted on an asphalt concrete cylinder cored from the 17.8-cm- (7-in.-) thick AC layer at Embankment SW. The AC cylinder was placed in a water bath under controlled temperatures so that testing could be performed with the AC specimen at different temperatures. Temperatures were varied from 0° C to 58° C (32° F to 136° F). At each temperature, a compressional resonance test and a torsional resonance test were performed on the AC cylinder.

In the compressional resonance test, an accelerometer was placed on one end of the cylinder and the cylinder was excited in the longitudinal direction as shown in Fig. 5.30a. The cylinder resonates due to the reflected waves off the ends. For free-free end conditions, the resonance wavelengths can be calculated as:

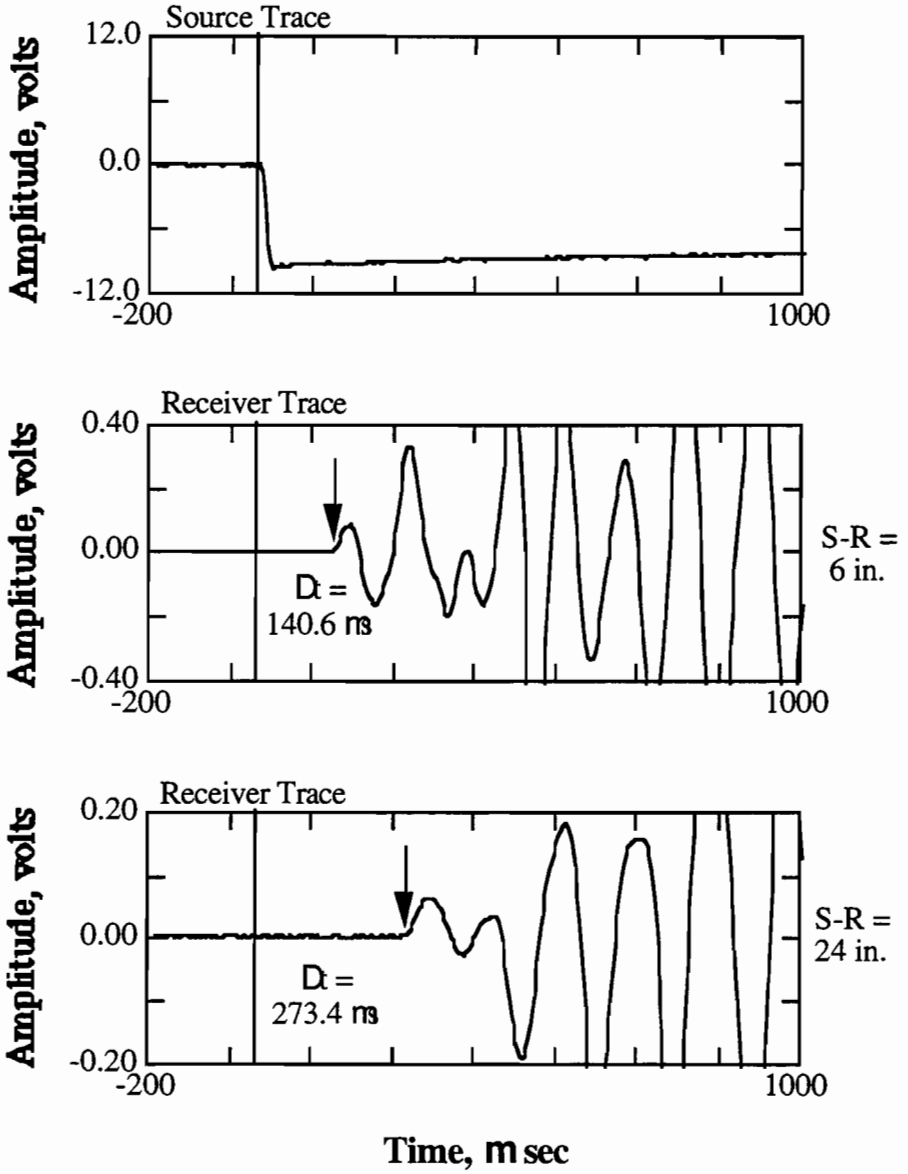

Fig 5.27. Typical Time Records for Compression Waves Propagating in the AC Layer, T = 43° F; Testing on February 9, 1991, Station 276+50, Loop 1 and US 183, Austin, Texas.

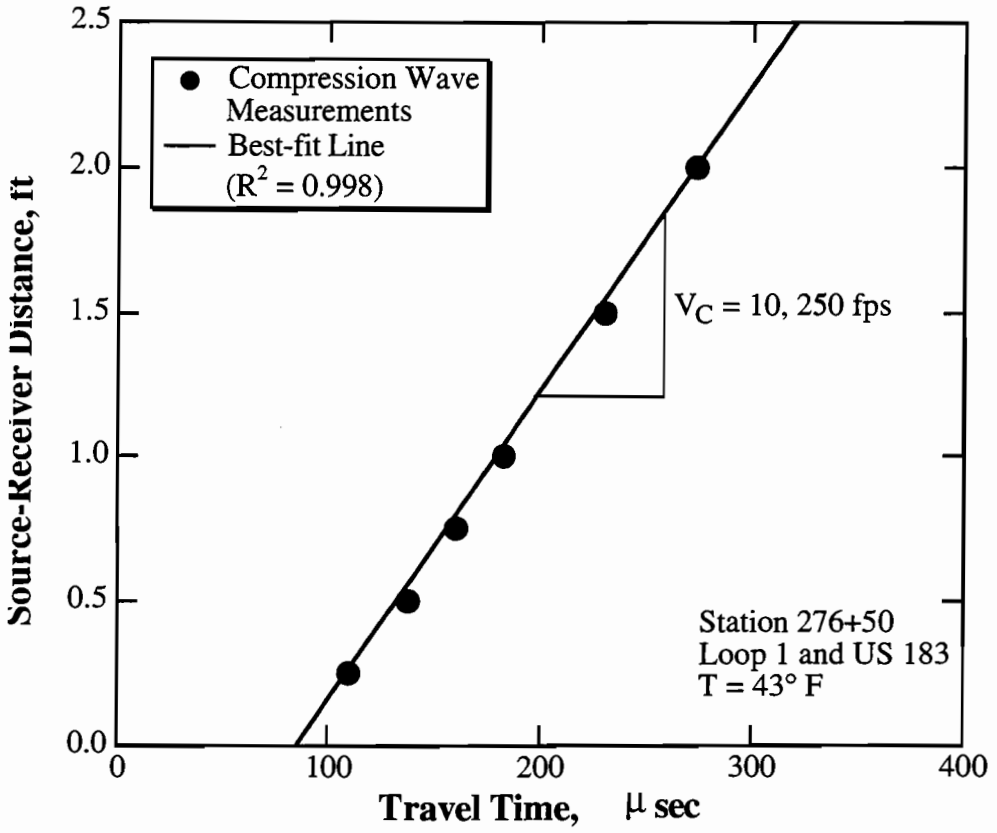

Fig 5.28. Travel Distance Versus Travel Time for Compression Wave Measurements, T = 43° F; Station 276+50, Loop 1 and US 183, Austin, Texas.

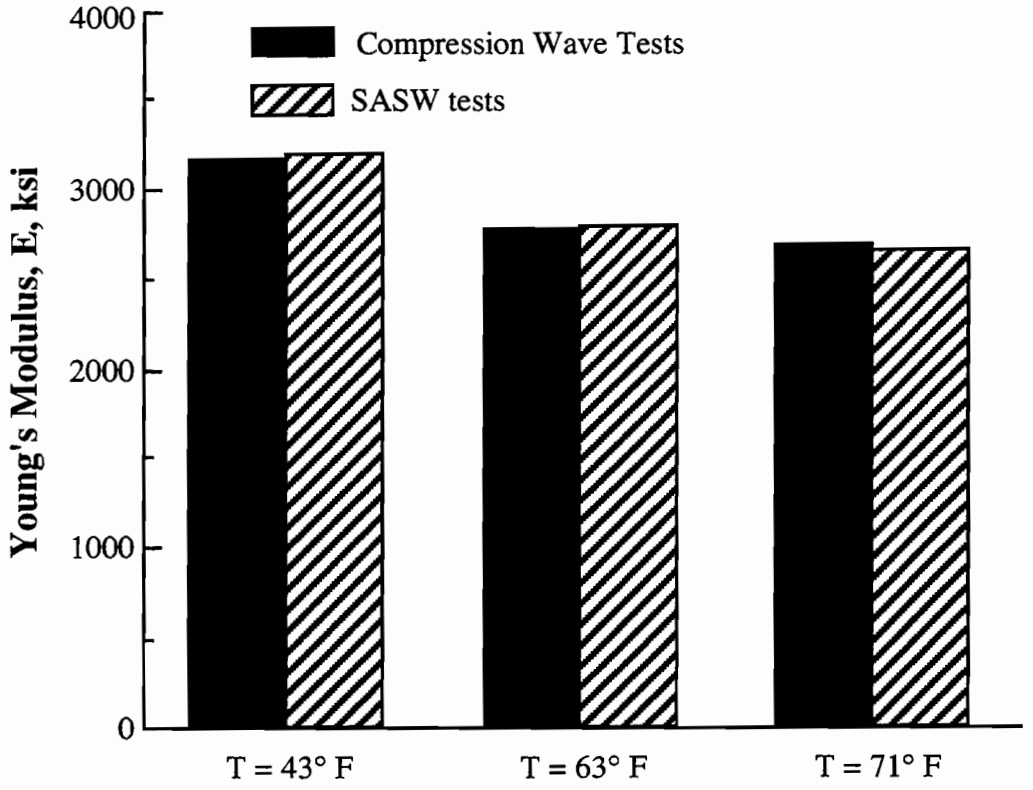

Fig 5.29. Comparison of Young's Modulus of the AC Layer Determined from SASW and Compression Wave Tests; Station 276+50, Loop 1 and US 183, Austin, Texas.

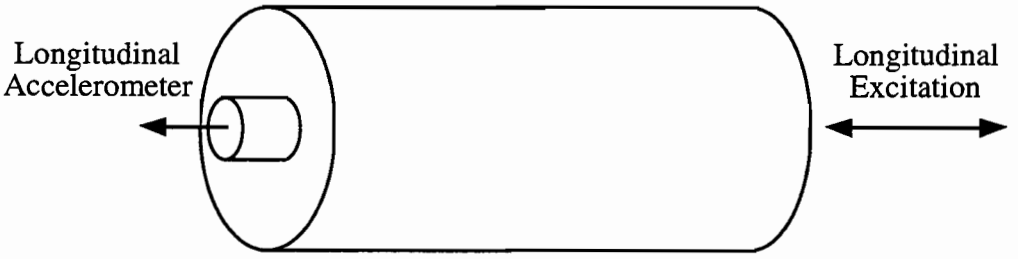

(a) Compressional Resonance Test

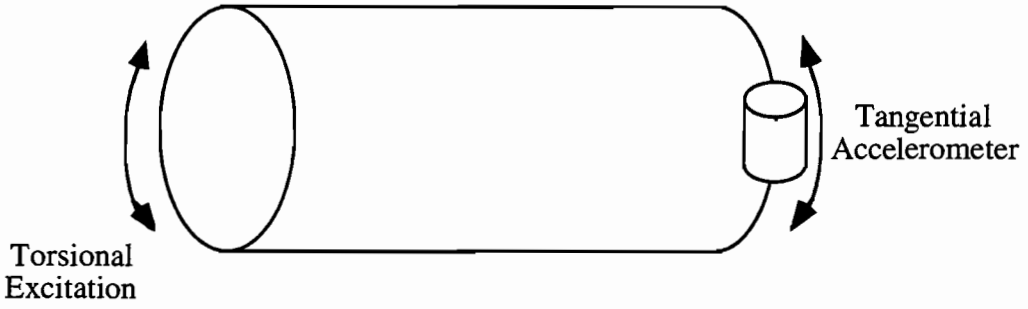

(b) Torsional Resonance Test

Fig 5.30. Configuration of Compressional and Torsional Resonance Tests on Cylindrical Specimens (Bay et al., 1992).

$$\lambda_n = 2L / n \text{ , } n = 1, 2, 3, ..., \text{etc.} \quad (5.9)$$

where

λ_n is the wavelength of the n^{th} mode,

L is the length of the cylinder,

and n is the mode number.

Figure 5.31a shows typical accelerometer spectra from compressional resonance tests at temperatures of 0, 21°, 38°, and 58° C (32°, 70°, 100° and 136° F). It is clear from the response spectra shown in Fig. 5.31a that only the first mode is measured (one peak). Thus, the velocity is calculated as:

$$V = f_1 \bullet \lambda_1 = 2 \bullet L \bullet f_1 \quad (5.10)$$

where

V is the wave velocity, and

f_1 is the frequency of the first mode.

It should be mentioned that compression waves are moving up and down the specimen without any constraints on lateral movement. Thus, the unconstrained compression wave velocity, V_C, is measured.

In the torsional resonance test, two tangentially oriented accelerometers were placed on one end of the cylinder as shown in Fig. 5.30b. The cylinder was excited in torsion by applying a torque on the other end. Response spectra at temperatures of 0°, 21°, 38°, and 58° C (32°, 70°, 100° and 136° F) are shown in Fig. 5.31b. The shear wave velocity is calculated using Eq. 5.10 with f_1 being the resonance frequency in shear of the first mode as shown in Fig. 5.31b.

The resonant frequencies in compression and shear were used to calculate the unconstrained compression and shear wave velocities using Eq. 5.10. Then, Young's and shear moduli were determined from the known velocities to determine

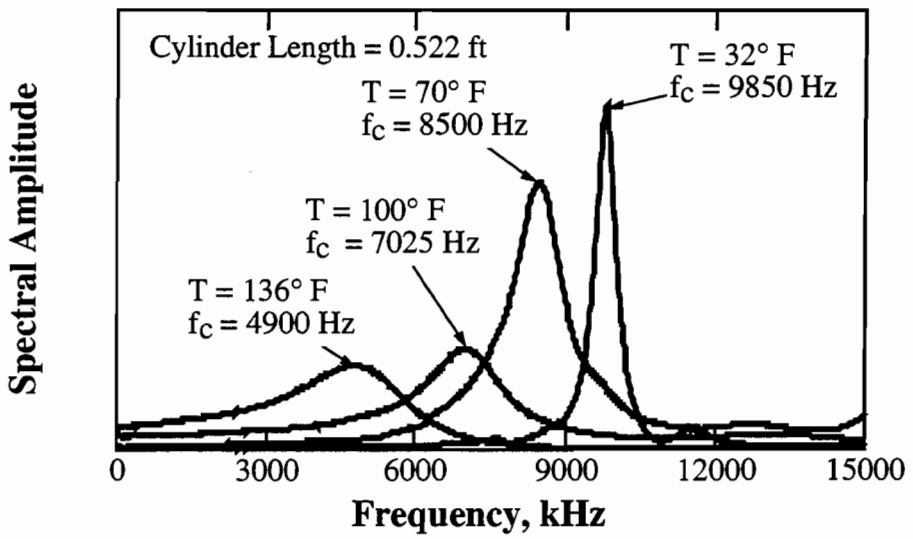

a. Compressional Resonance Tests

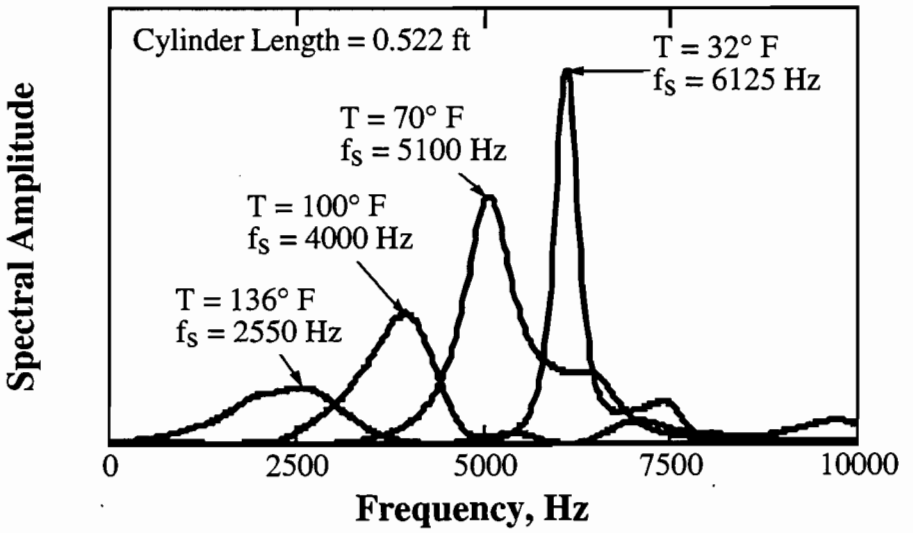

b. Torsional Resonance Test

Fig 5.31. Response Spectra from Resonance Tests on AC Cylinder at Four Different Temperatures.

their variation with temperature. Table 5.12 lists the values of velocities, moduli and Poisson's ratios determined from Eq. 5.6 for the asphalt concrete without regard to frequency. Note that the frequency associated with each modulus value is listed in the table. Figure 5.32 shows the variation of Young's moduli and shear moduli with temperature. The variation of Poisson's ratio with temperature is also shown in Fig. 5.32. The high values of Poisson's ratios are due to the fact that the shear moduli were determined at lower frequencies than Young's moduli were. For a proper determination of the variation of Poisson's ratio with temperature, the shear moduli need to be adjusted to the same frequency used in the determination of Young's moduli, as discussed in the next section. These results illustrate the importance of frequency in testing asphalt concrete.

Table 5.12. Unconstrained Compression Wave Velocities, Young's Moduli, Shear Wave Velocities, Shear Moduli and Poisson's Ratios Determined from Resonance Tests on AC Cylindrical Specimen

Temp. (°F)	Compression Resonant Frequency (Hz)	V_C (fps)	E (ksi)	Shear Resonant Frequency (Hz)	V_S (fps)	G (ksi)	Poisson's Ratio (n)
32	9850	10277	3189	6125	6390	1233	0.293
51	9225	9625	2797	5650	5895	1049	0.333
60	8900	9286	2603	5400	5634	958	0.359
70	8500	8868	2375	5100	5321	855	0.389
80	8000	8347	2103	4700	4904	726	0.448
90	7525	7851	1861	4350	4539	622	0.496
100	7025	7329	1622	4000	4173	526	0.542
110	6450	6730	1367	3575	3730	420	0.627
120	5875	6130	1134	3175	3313	331	0.713
130	5250	5478	906	2800	2921	258	0.756
136	4900	5112	789	2550	2661	214	0.844

5.8 Frequency Adjustment Factor for AC Material

The moduli determined from SASW measurements on the pavement and resonance tests on the cylindrical specimen were used to calculate moduli at a frequency of 30 Hz. The SASW moduli were determined at a frequency of 15.5

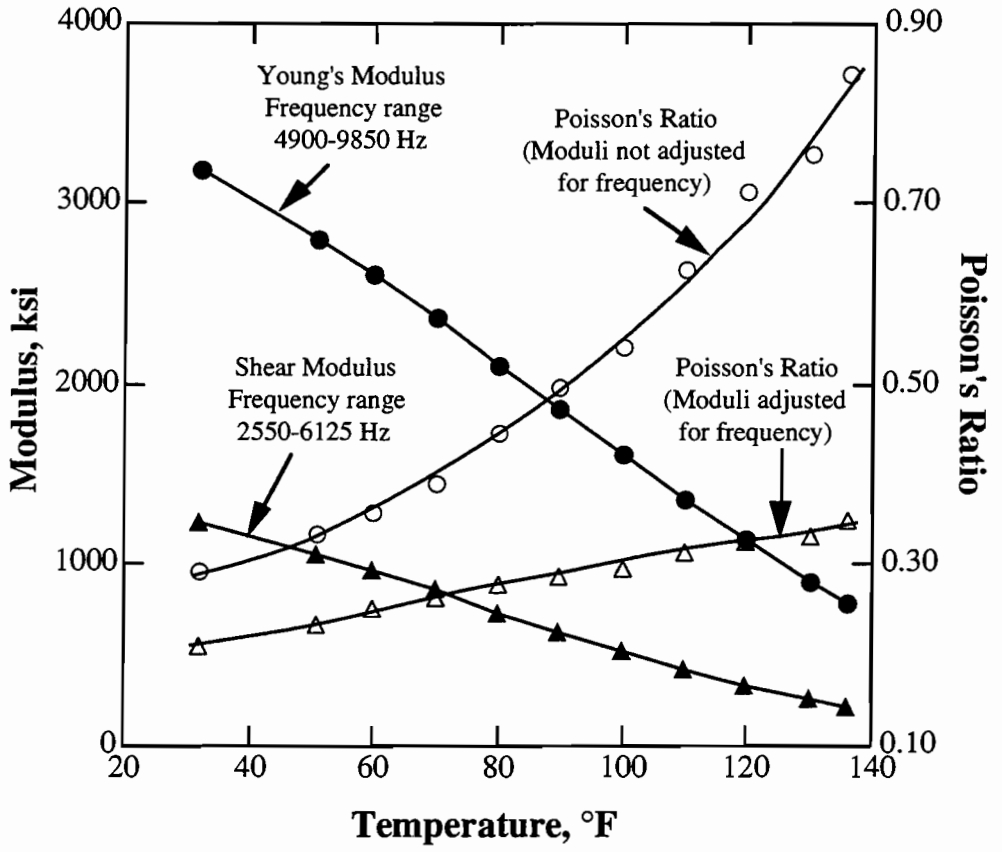

Fig 5.32. Variation of Moduli and Poisson's Ratio of Asphalt Concrete with Temperature as Determined from Resonance Tests.

kHz. The frequency involved in resonance tests varied from 4,900 to 9,850 Hz. In FWD measurements, frequencies ranged from 0 to 60 Hz, with an average frequency of 30 Hz.

In the calculation of Young's moduli at a frequency of 30 Hz, it was assumed that the relationship between modulus and frequency is linear on a log-log scale. Figures 1.2 and 5.19 support this approach as a reasonable first approximation. The variation of Young's moduli with frequency is shown in Fig. 5.33. The values of moduli at frequencies of 15.5 kHz and 30 Hz are listed in Table 5.13 along with the modulus adjustment factor, $E_{15.5kHz} / E_{30Hz}$. The variation of the modulus adjustment factor with temperature is shown in Fig. 5.34. The solid symbols shown in Fig. 5.34 represent extrapolated values from curves obtained by Sousa and Monismith (1988) which agree well with the values determined herein.

Table 5.13. Young's Moduli at Frequencies of 15.5 kHz and 30 Hz and Modulus Adjustment Factors as a Function of Temperature

Temperature (°F)	Young's Modulus at f = 15.5 kHz (ksi)	Young's Modulus at f = 30 Hz (ksi)	Modulus Adjustment Factor $E_{15.5kHz}/E_{30Hz}$
32	3395	1432	2.37
51	3026	1168	2.59
60	2852	1019	2.80
70	2659	821	3.24
80	2464	552	4.46
90	2271	407	5.58
100	2076	296	7.01
110	1883	193	9.78
120	1689	130	13.00
130	1495	83	18.01
136	1379	67	20.64

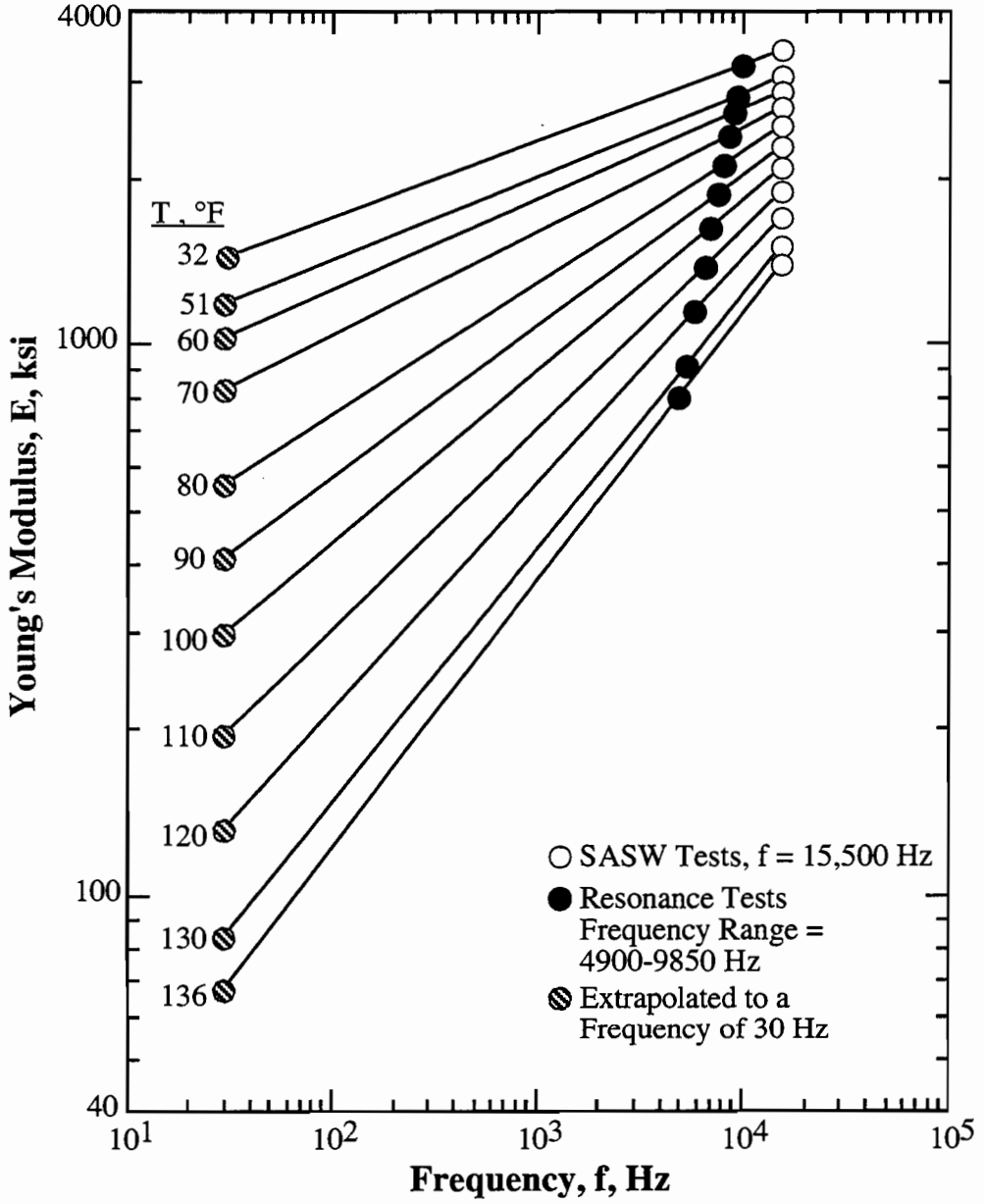

Fig 5.33. Variation of Moduli of Asphalt Concrete with Frequency as Determined from Field SASW and Laboratory Resonance Tests; Approximately 1.5 Years Old Asphalt Concrete.

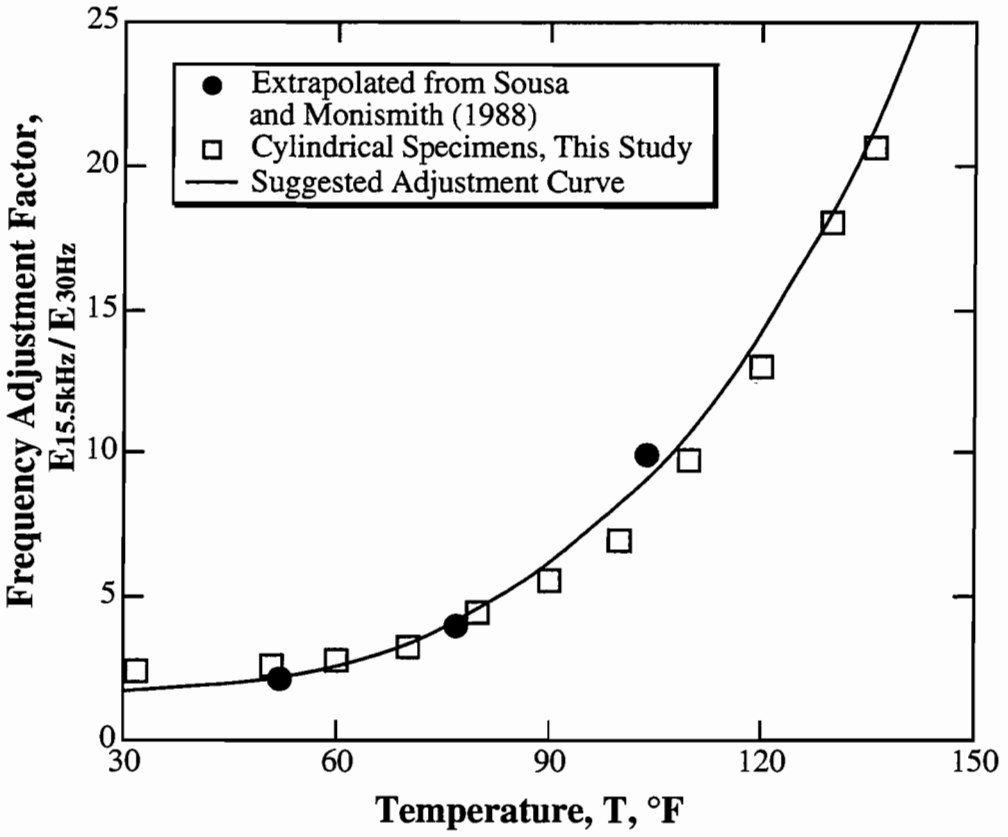

Fig 5.34. Variation of Frequency Adjustment Factor with Temperature for Asphalt Concrete.

5.9 Poisson's Ratios of Asphalt Concrete

Resonance tests on cylindrical specimens provided shear and Young's moduli of the asphalt concrete. Young's moduli were determined from the compressional resonance frequencies which ranged from 4,900 to 9,850 Hz for a temperature change from 58° C to 0° C (136° F to 32° F). The shear moduli were determined at frequencies ranging from 2,550 to 6,125 Hz for the same change in temperature. Poisson's ratios determined from these moduli values ranged from 0.293 to 0.844 as temperature ranged from 0° C to 58° C (32° F to 136° F), respectively. The high values of Poisson's ratios are due to the determination of Young's and shear moduli at different frequencies.

Figure 5.34, along with the assumption of the log-log linear relationship between modulus and frequency (for both G and E), was used to adjust the determined moduli to a frequency of 15.5 kHz. Then, Poisson's ratios were determined from the adjusted moduli using Eq. 5.6. Table 5.14 lists the adjusted moduli values and Poisson's ratios at a frequency of 15.5 kHz. Poisson's ratios after adjustment of the moduli are shown in Fig. 5.32 and should be used in the calculations of Young's moduli of the asphalt concrete from the surface wave velocities determined by the SASW tests.

5.10 Variation of Young's Moduli with Time

SASW measurements were made immediately after placing the AC layer. In addition, SASW and resonance tests were performed approximately 1.5 years later. A comparison of Young's moduli determined at different times is presented in Fig. 5.35. Immediately after placing the AC layer, the moduli values were calculated at a frequency of 6 kHz, because it was the highest frequency generated when the surface temperature rose to 56° C (133° F), as shown in Fig. 5.17. For comparison purposes, the moduli values determined from SASW and resonance tests 1.5 years later were adjusted to a frequency of 6 kHz using Fig. 5.33. At a frequency of 6 kHz, Young's moduli determined from SASW measurements immediately after

Table 5.14. Young's and Shear Moduli at Frequencies of 15.5 kHz and Calculated Poisson's Ratios as a Function of Temperature

Temperature (°F)	Young's Modulus at f = 15.5 kHz (ksi)	Shear Modulus at f = 15.5 kHz (ksi)	Poisson's* Ratio (ν)
32	3395	1404	0.209
51	3026	1226	0.234
60	2852	1139	0.252
70	2659	1053	0.262
80	2464	965	0.277
90	2271	882	0.287
100	2076	802	0.295
110	1883	717	0.313
120	1689	637	0.326
130	1495	562	0.330
136	1379	511	0.349

* Values are frequency independent as long as G and E are at the same frequency.

placing the AC layer were lower than those determined 1.5 years later, showing the increase of Young's modulus with time.

5.11 Summary

A comprehensive testing program was employed at the site of a newly constructed ramp in Austin, Texas. Results from field and laboratory tests to determine Young's modulus of the AC surface layer, base and subgrade are presented in this chapter.

Results from the SASW and resonance tests showed the frequency and time dependencies of the asphalt concrete. The depth to bedrock, which is a key element in the analysis of the FWD, was determined from SASW measurements. In the SASW measurement, the selection of high-frequency sources is very important. An WR Model F-7 shaker performed very well in generating the high frequencies desired to sample the asphalt layer. Results from SASW measurement also showed

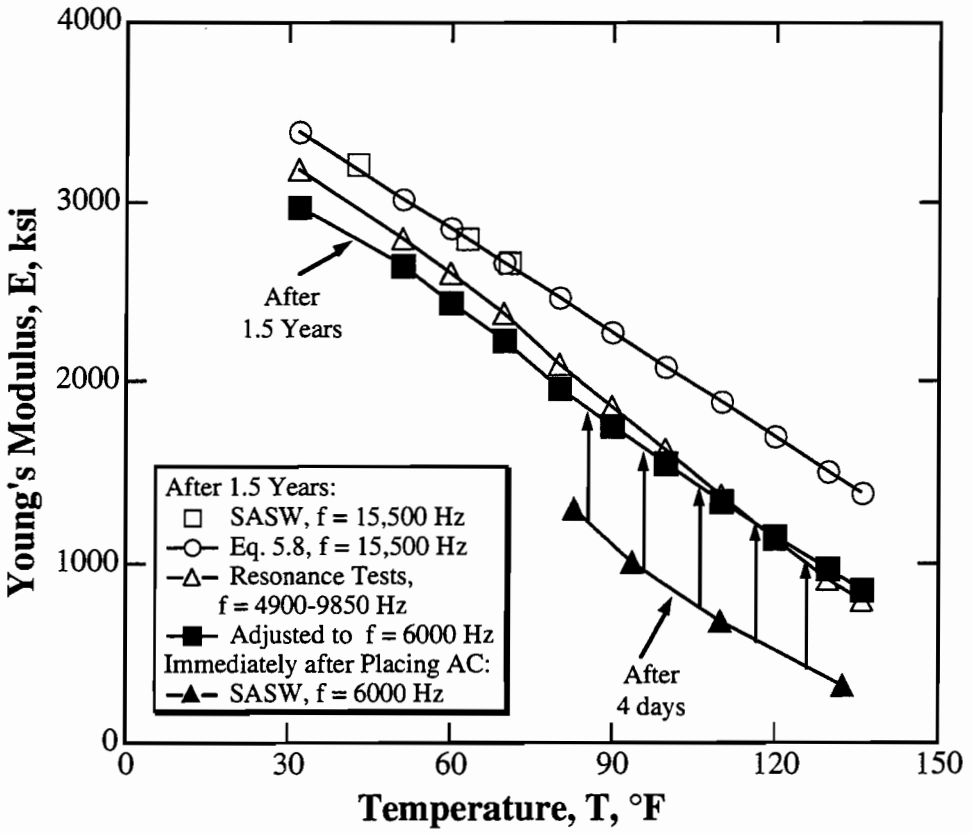

Fig 5.35. Changes in Young's Moduli of Asphalt Concrete with Time at Station 276+50; Loop 1 and US 183, Austin, Texas.

the increase in stiffness (by about 4,134 MPa [600 ksi] at a frequency of 6,000 Hz) of the asphalt concrete with time (from 4 days after the placement of the AC layer to about 1.5 years).

Results from FWD and SASW measurements showed a good agreement in subgrade Young's modulus after correction for the effect of strain and in the AC Young's modulus after correction for frequency effect. The analysis of the FWD data was performed taking into account the dynamic effect produced by the presence of shallow bedrock at the testing site.

CHAPTER SIX
CASE STUDIES: TESTS ON TWENTY-FOUR PAVEMENT SITES IN TEXAS

6.1 Introduction

Twenty-four sites located in four districts in Texas were selected by the Texas Department of Transportation (TxDOT) to be tested nondestructively to evaluate the material profiles. P-wave, SASW and FWD tests were performed at these sites. The P-wave and SASW tests were performed as part of the 1175 study. In conjunction with the 1175 study, FWD tests were performed and the data were analyzed by personnel from Texas A&M University. Results from the P-wave, SASW and FWD tests are presented herein.

Selection of the 24 sites in the four districts was based on various factors. The thicknesses of the surface layer varied from 2.54 cm (1 in.) to 30.5 cm (12 in.) to cover a wide range in thicknesses encountered at pavement sites. The base and subgrade materials included different types such as treated and untreated limestone bases and sandy/clayey subgrades. Tables 6.1 through 6.4 list the locations and material profiles for the test sites in District 1 (Paris), District 8 (Abilene), District 11 (Nacogdoches) and District 21 (Raymondville), respectively.

6.2 Tests in District 1, Texas

6.2.1 P-Wave Measurements

P-wave tests were performed at all five sites in District 1. The P-wave measurements were made according to the procedure described in Section 4.5.2 with a minor modification. A hammer and an inclined chisel were used as the source, and the travel time between two receivers placed horizontally on the pavement surface was measured. At Sites 1 and 2, receiver spacings ranging from

Table 6.1. Site Locations and Material Profiles of Monitored Pavement Sections in District 1, Texas

Site No.	Site Location	Surface* Layer	Base*	Subbase*	Subgrade
1	FM 79 (0.7 Miles East of Pine Creek)	2 in. HMAC (Thin)	6 in. Limestone	8 in. Salvage Black Base	Sand
2	FM 137 (Loop 271 to MP 2.8)	2 in. HMAC (Thin)	10 in. Crushed Limestone	.....	Clay
3	SH 82 (East of Loop 271)	12 in. HMAC (Thick)	22 in. sand	.....	Sandy Clay
4	FM 195 (East of Loop 271)	4 in. HMAC (Medium)	6 in. Oklahoma Gravel	.....	Sandy Clay
5	SH 19 (Paris, Texas to Sulphur River)	9 in. HMAC (Thick)	7 in. Sandstone	8 in. lime Treated Clay	Clay

* Layer thicknesses are from construction drawings

Table 6.2. Site Locations and Material Profiles of Monitored Pavement Sections in District 8, Texas

Site No.	Site Location	Surface* Layer	Base*	Subbase*	Subgrade
1	FM 1983 South (MP 1.0)	1 in. HMAC (Thin)	8 in. Limestone	.....	Sand
2	SH 471 South (MP 0.7)	3 in. HMAC (Medium)	5 in. Pit Run	.....	Sand
3	IH 20 (MP 216)	5 in. HMAC (Medium)	18 in. Limestone	.....	Sand
4	IH 20 (MP 293)	10 in. HMAC (Thick)	4 in. Crushed Limestone	7 in. Crushed Limestone	Clay
5	IH 20 West (MP 273.6)	8 in. HMAC (Thick)	11 in. Red Limestone	.....	Clay
6	FM 1235 East (MP 21)	1 in. Seal Coat (Thin)	8 in. Limestone	.....	Clay

* Layer thicknesses are from construction drawings

Table 6.3. Site Locations and Material Profiles of Monitored Pavement Sections in District 11, Texas

Site No.	Site Location	Surface* Layer	Base*	Subbase*	Subgrade
1	US 59 (MP 13.7)	8.5 in. HMAC (Thick)	Asphalt Treated Sand	Sand	Sandy Clay
2	US 59 (MP 19.5)	8 in. HMAC (Thick)	12 in. Iron Ore Gravel	.....	Sand
3	US 59 (MP 23.2)	2 in. HMAC (Thin)	7 in. Crushed Limestone	6 in. Iron Ore Gravel	Sandy Clay
4	FM 2864 (MP 6.45)	1 in. Seal Coat (Thin)	9.5 in. Iron Ore Gravel	.....	Sandy Clay
5	SH 7 (MP 7.8)	1 in. Surface Treatment (Thin)	10 in. Iron Ore Gravel	.....	Silty Sand
6	No Tests				
7	FM 2259 (Southwest of Nacogdoches)	2 in. Surface Treatment (Thin)	8 in. 4% Cement Treated Ore	.....	.....
8	FM 355 (South of Groveton, Trinity County)	1.5 in. Surface Treatment (Thin)	8 in. 6-7% Cement Treated Sand	.....	.....

* Layer thicknesses are from construction drawings

Table 6.4. Site Locations and Material Profiles of Monitored Pavement Sections in District 21, Texas

Site No.	Site Location	Surface* Layer	Base*	Subbase*	Subgrade
1	SH 186 (MP 33.2)	1.25 in. HMAC (Thin)	4.3 in. Calacie	4.4 in. Lime Treated	Sand
2	FM 491 (MP 6.1)	1 in. HMAC (Thin)	5.5 in. Calacie	.....	Clay
3	US 77 (MP 4.1)	6.5 in. HMAC (Thick)	6 in. Lime Treated	15 in. Lime Treated Sand	Sand
4	FM 1425 (MP 5)	4 in. HMAC (Medium)	5 in. Lime Treated Calacie	.....	Clay
5	FM 1425 (MP 3)	6 in. HMAC (Thick)	6 in. Calacie	.....	Sandy Clay
6	FM 88 (MP 2)	3 in. HMAC (Medium)	7 in. Calacie	.....	Sandy Clay

* Layer thicknesses are from construction drawings

15.2 cm (6 in.) to 121.9 cm (48 in.) were used. At Sites 3, 4 and 5, a receiver spacing of 30.5 cm (12 in.) was the only spacing used. Sites 1 and 2 represent a thin pavement surface where SASW tests are not capable of sampling the surface layer. Thus, different receivers spacings were used at Sites 1 and 2 to better determine the compression wave velocity (assumed to be the unconstrained compression wave for ease in analysis) from which the shear wave velocity was calculated for the forward modeling process. Typical time records of the compression waves measured at Site 1 for receiver spacings of 15.2, 22.9, 38.1, 60.1, 91.4 and 121.9 cm (6, 9, 15, 24, 36 and 48 in.) are shown in Figs. 6.1a and b, 6.2a and b, and 6.3a and b, respectively (the approximate frequency in these records is about 3.5 kHz as shown in Fig. 6.3b) . A plot of the distance between receivers versus the travel times of propagating compression waves for Sites 1 through 5 is shown in Fig. 6.4. The compression wave velocities for the five sites were calculated from the slopes of the lines and are shown in the insert in Fig. 6.4. Equation 2.2 was used in the calculations of Young's moduli of the AC layer assuming a unit weight of 22 kN/m^3 (140 pcf). The calculated moduli of the AC layers are presented in Table 6.5.

Table 6.5. Young's Moduli of the AC Layer Determined from P-wave Measurements; Sites 1 through 5, District 1, Texas

Site No.	Surface Temperature (° F)	Compression Wave Velocity (fps)	Young's * Modulus (ksi)
1	100	6,230	1,172
2	125	5,150	801
3	93	6,920	1,446
4	85	7,830	1,851
5	118	6,095	1,121

* Measurement frequency with hammer-chisel is approximately 3.5 kHz

It should be mentioned that the calculated moduli from the unconstrained compression wave velocity ($E = \rho V_C^2$) are about 4 to 13% (for Poisson's ratios ranging from 0.2 to 0.34) higher than those determined from the wave velocity in a plate ($E = \rho V_{plate}^2 (1-\nu^2)$) (Roesset (1993)) which is actually measured in the field.

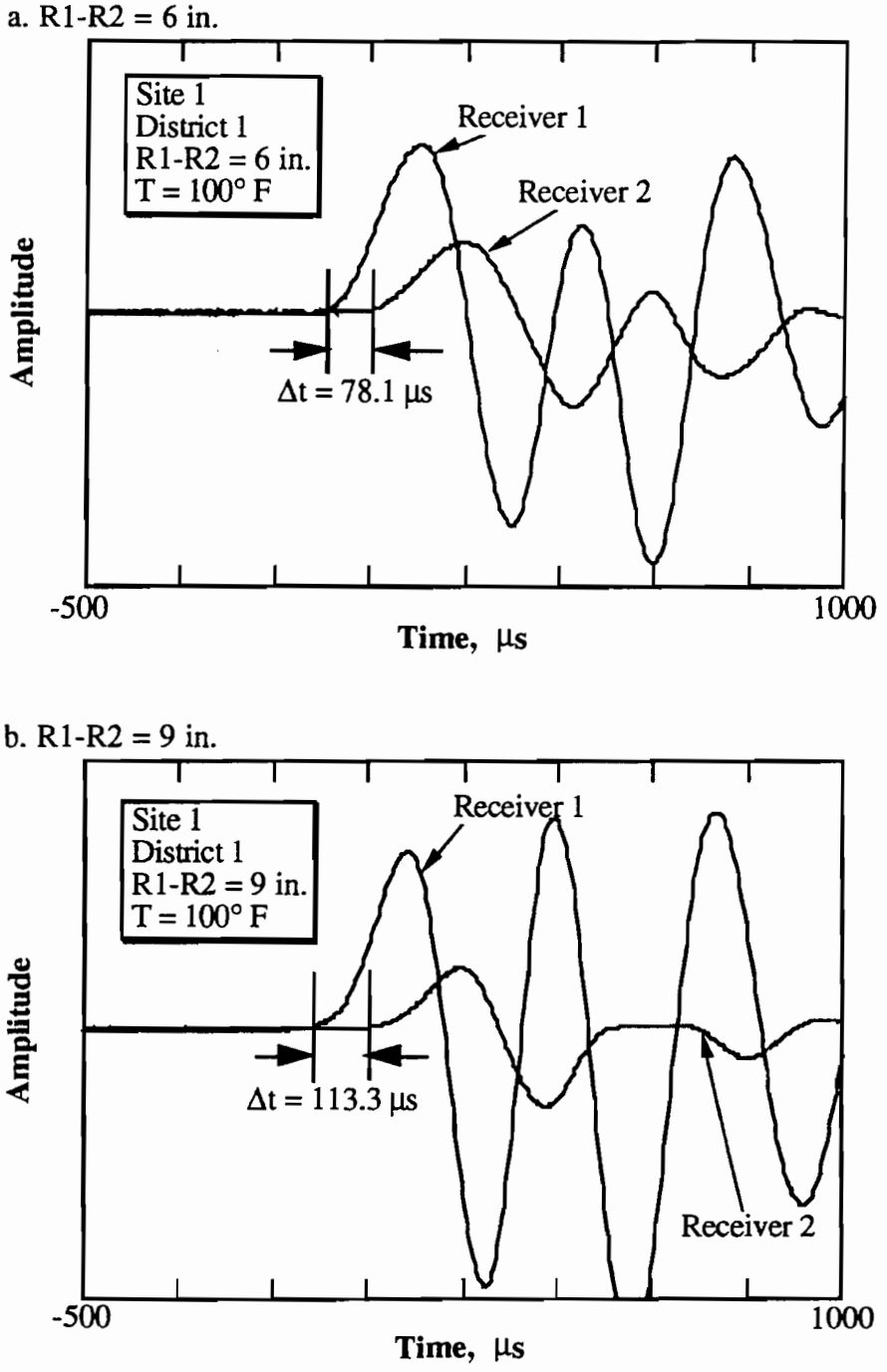

Fig 6.1. Time Records for Propagating Compression Waves, R1-R2 = 6 in. and 9 in.; Site 1, District 1, Texas.

a. R1-R2 = 15 in.

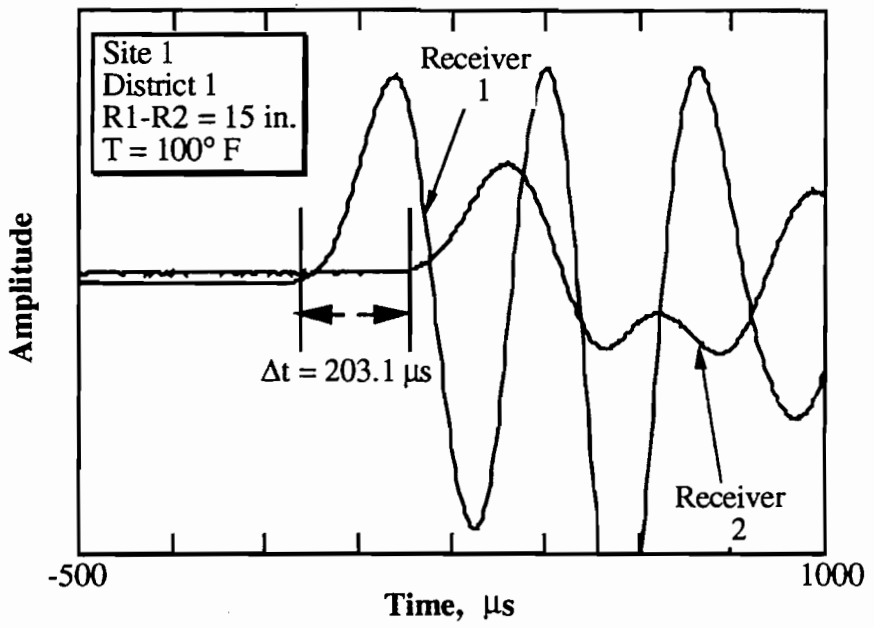

b. R1-R2 = 24 in.

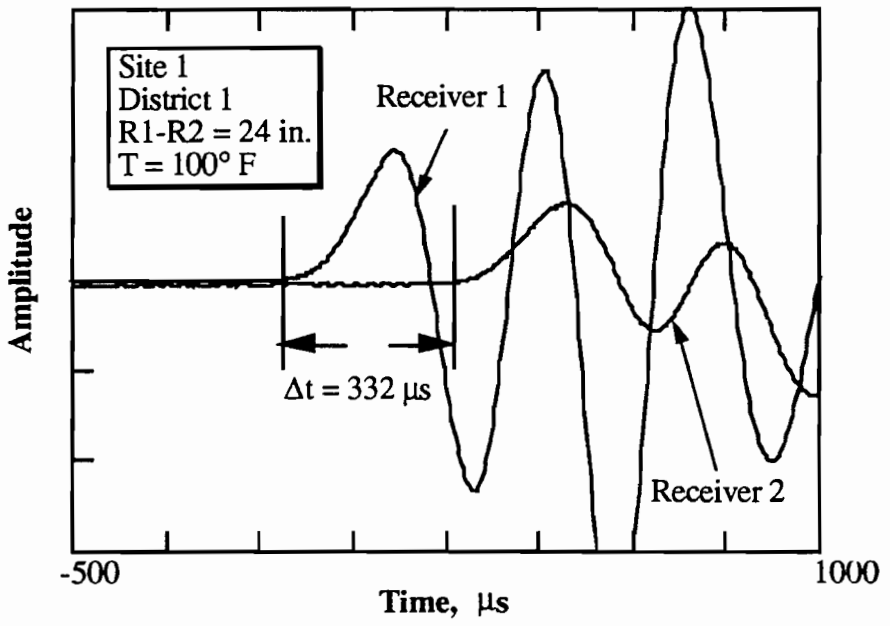

Fig 6.2. Time Records for Propagating Compression Waves, R1-R2 = 15 in. and 24 in.; Site 1, District 1, Texas.

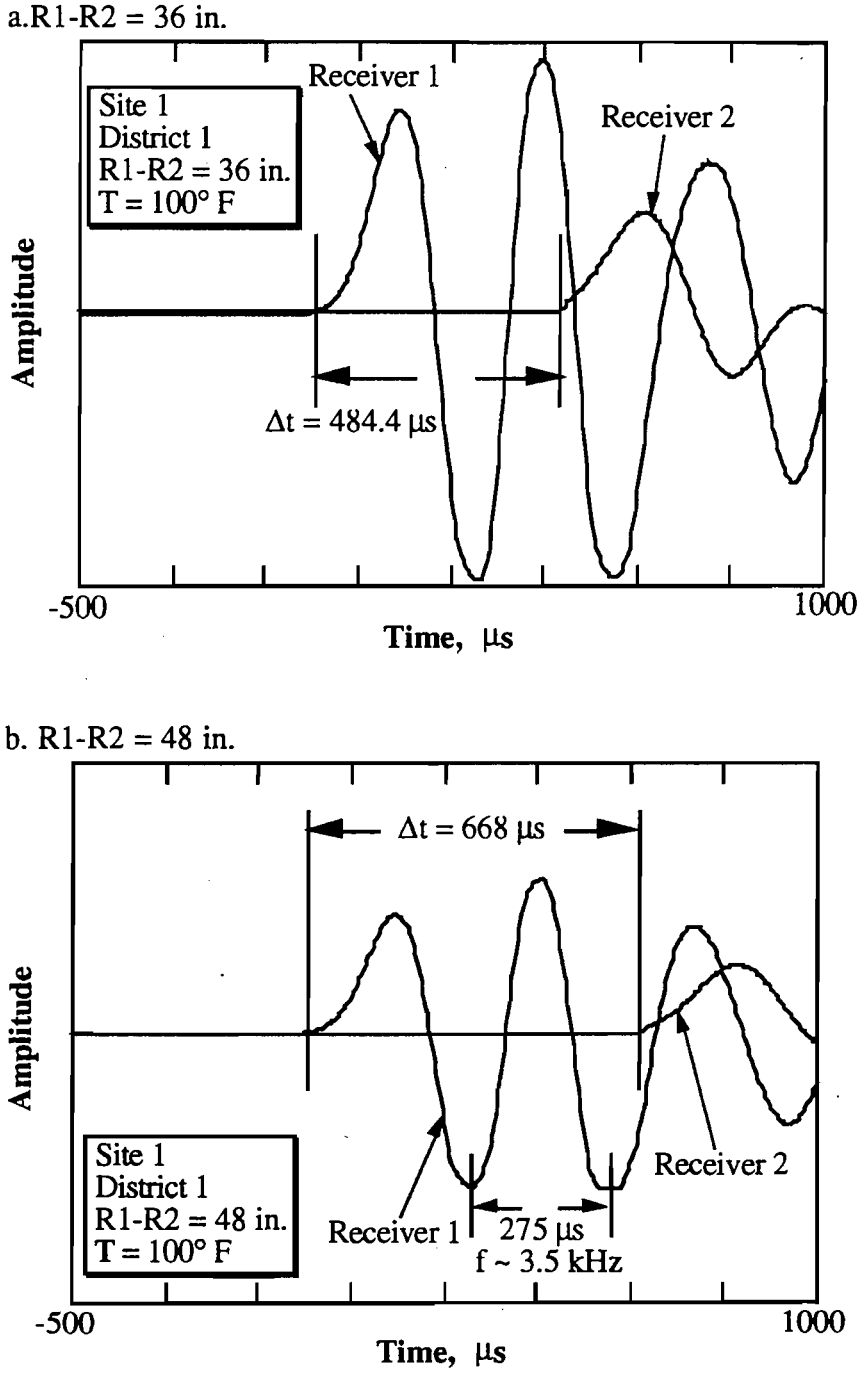

Fig 6.3. Time Records for Propagating Compression Waves, R1-R2 = 36 in. and 48 in.; Site 1, District 1, Texas.

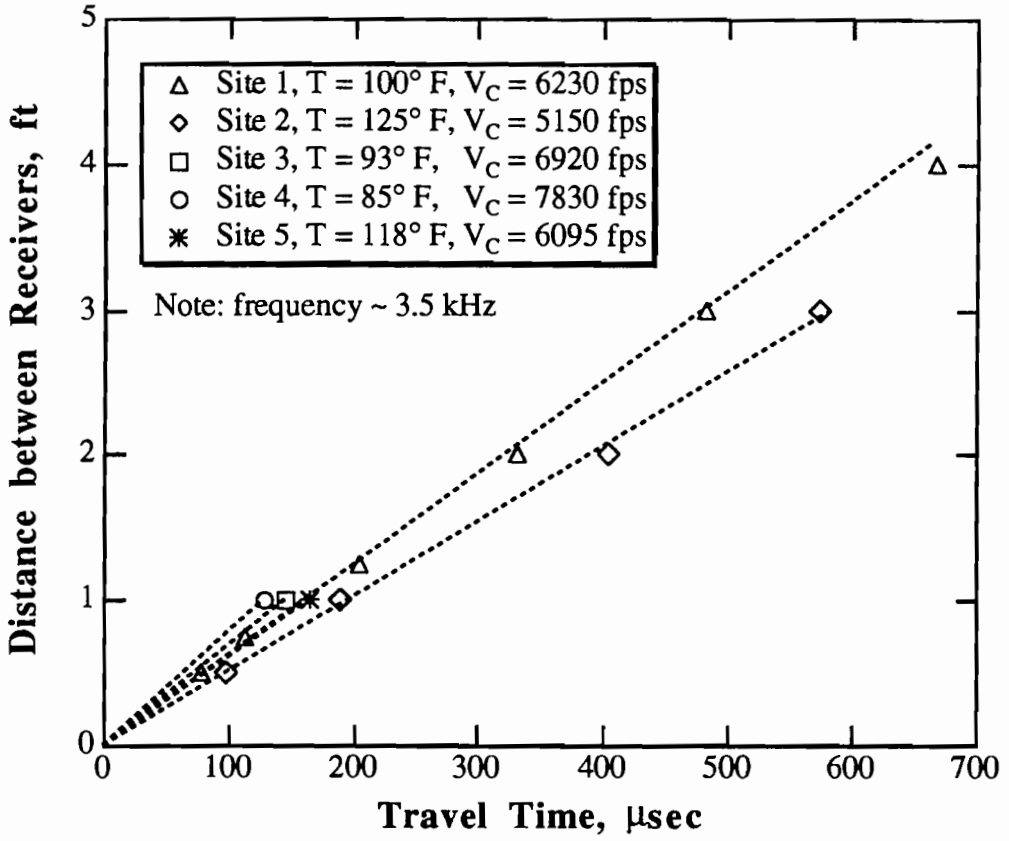

Fig 6.4. Travel Distances Versus Travel Times for P-Waves Measured at Sites 1 through 5; District 1, Texas.

6.2.2 SASW Measurements

SASW tests were performed at the five sites in District 1 using receiver spacings of 0.15, 0.31, 0.61, 1.2, 3.0, 6.1 and 9.1 m (0.5, 1, 2, 4, 10, 20 and 30 ft). The experimental dispersion curves determined at Sites 1 through 5 are shown in Fig. 6.5. As shown in Fig. 6.5, the surface layers at Sites 1 and 2 were not sampled by the SASW measurements. Also, the surface layer at Site 4 was barely tested because the surface temperature was above 27° C (80° F). If Site 4 was tested when cool (say at a temperature of 16° C (60° F)), then the surface layer could be easily sampled.

The SASW measurements were then analyzed using the 3-D model (described in Chapter 3) to determine the variation of shear wave velocity with depth. Figures 6.6 through 6.10 show a comparison between the experimental and theoretical dispersion curves for Sites 1 through 5, respectively. It should be noted that the layer thicknesses from the construction drawings were used in these analyses. However, if these thicknesses were not reasonable, a good fit between the experimental and theoretical dispersion curves could not have been achieved.

The shear wave velocity profiles corresponding to the theoretical dispersion curves shown in Figs. 6.6 through 6.10 are presented in Tables 6.6 through 6.10, respectively. The shear wave velocity profiles determined at Sites 1 through 5 showed a uniform subgrade ranging in thickness from 3 m (10 ft) to 5.5 m (18 ft), followed by layers of increasing stiffnesses with depth. Bedrock was not encountered at any of the test sites. Young's moduli were determined from the shear wave velocities assuming total unit weights of 22, 20.4 and 18.9 kN/m^3 (140, 130 and 120 pcf) for the surface layer, base and subgrade, respectively. Poisson's ratios used in the calculations of Young's moduli of the surface layers (at a frequency of approximately 15 kHz) were interpolated values from those shown in Table 5.13. Young's moduli of the different layers for Sites 1 through 5 in District 1 are also shown in Tables 6.6 through 6.10, respectively.

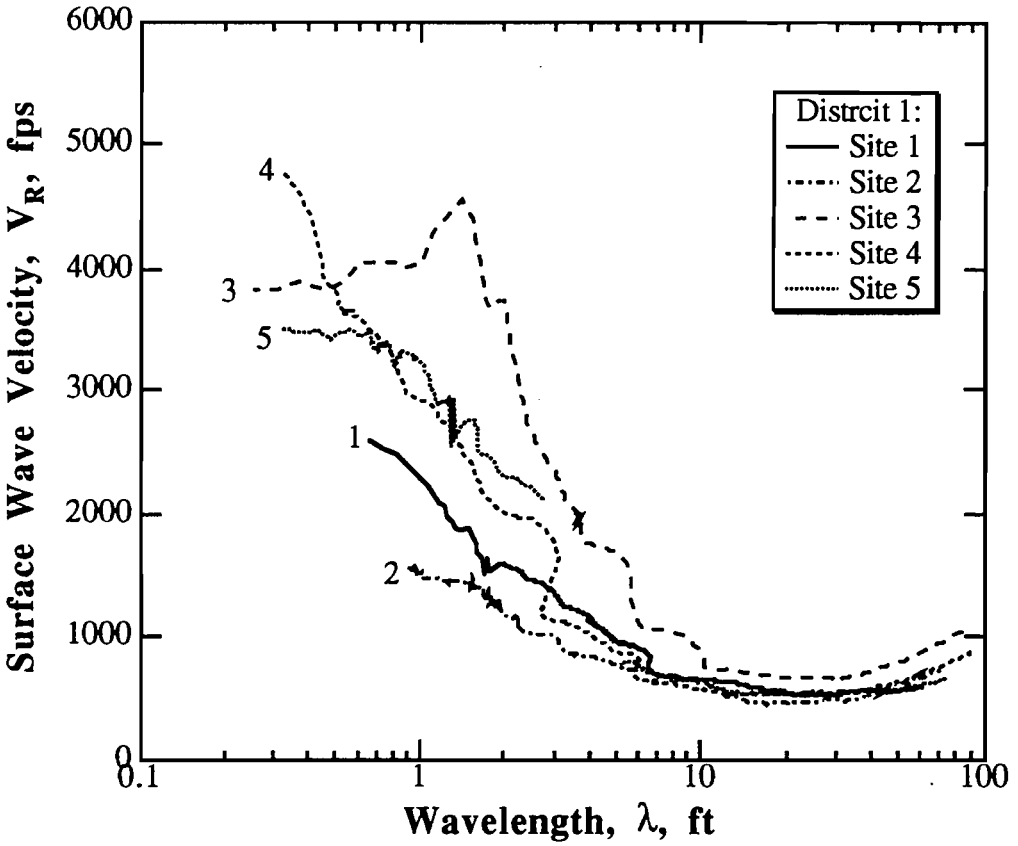

Fig 6.5. Experimental Dispersion Curves Determined from SASW Measurements at Sites 1 through 5; District 1, Texas.

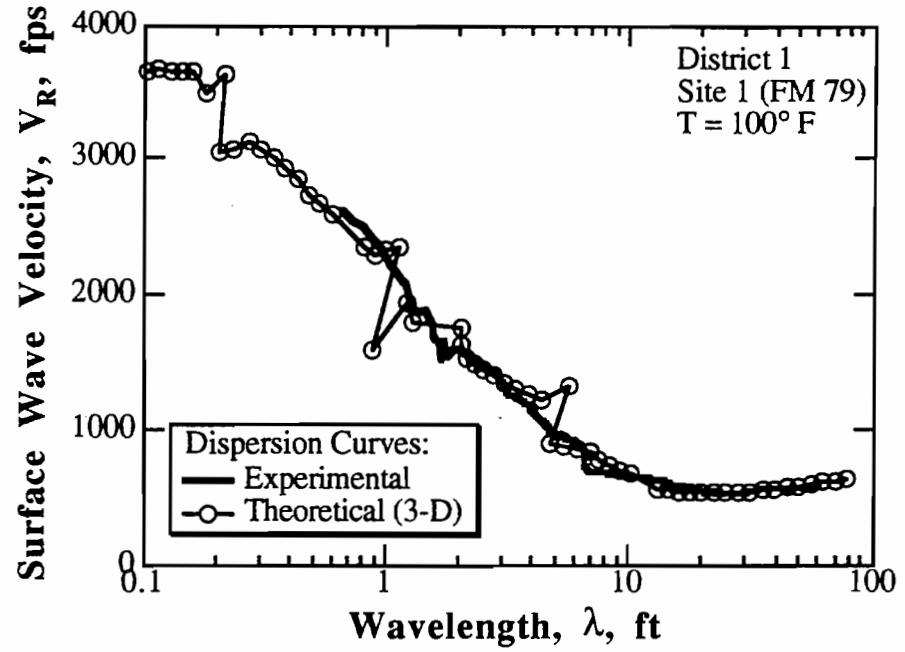

Fig 6.6. Comparison between the Experimental and Theoretical Dispersion Curves Determined at Site 1; District 1, Texas.

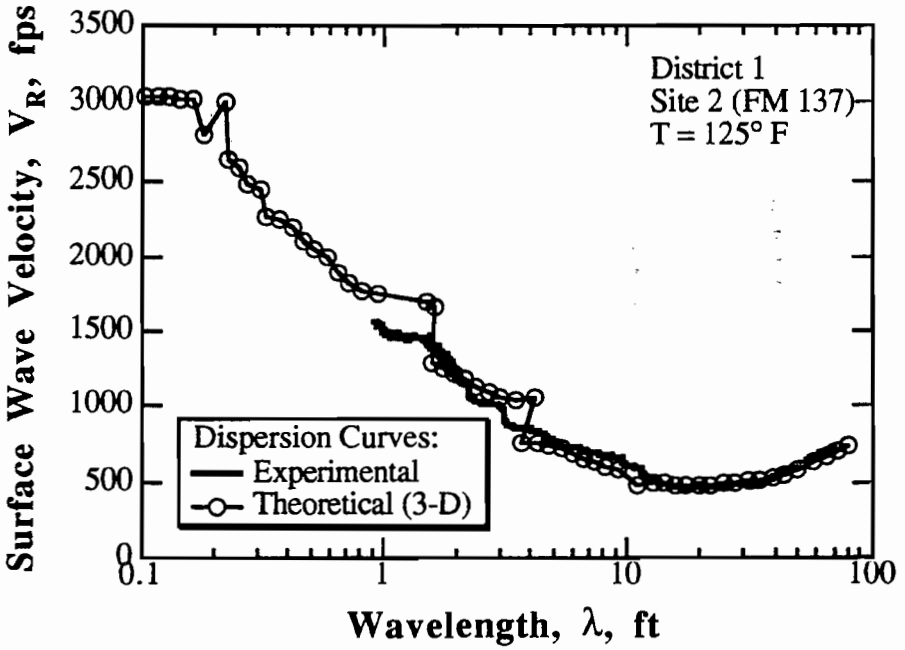

Fig 6.7. Comparison between the Experimental and Theoretical Dispersion Curves Determined at Site 2; District 1, Texas.

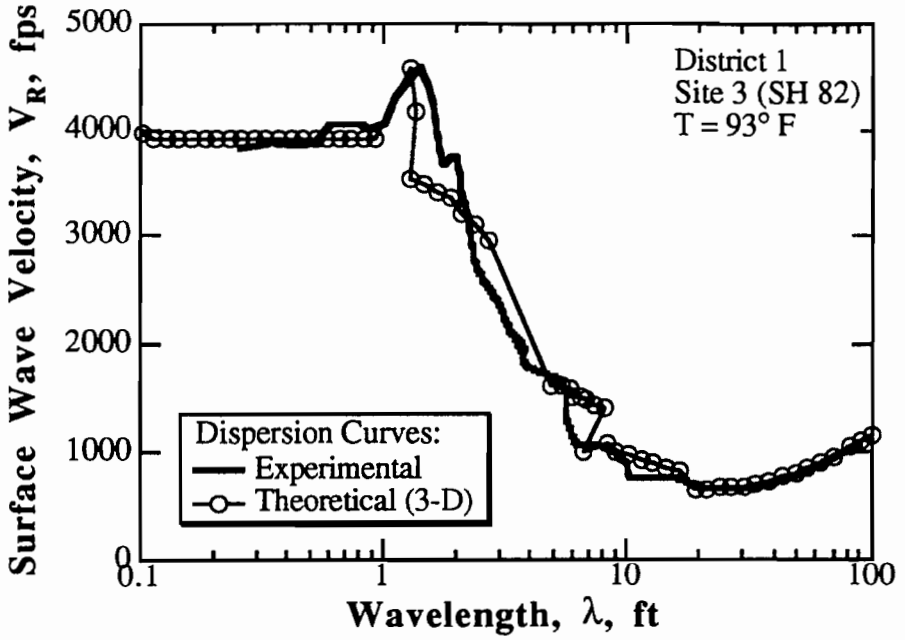

Fig 6.8. Comparison between the Experimental and Theoretical Dispersion Curves Determined at Site 3; District 1, Texas.

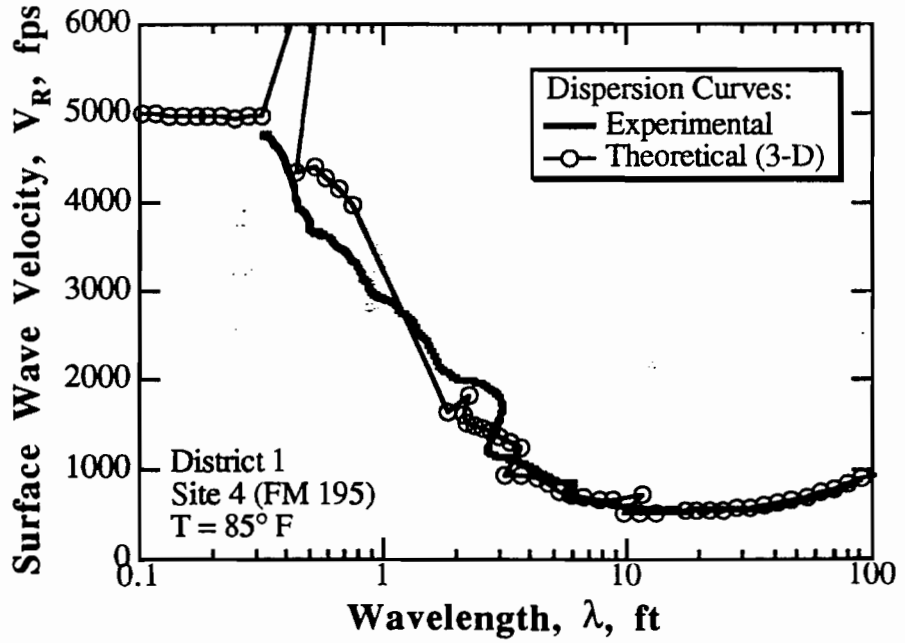

Fig 6.9. Comparison between the Experimental and Theoretical Dispersion Curves Determined at Site 4; District 1, Texas.

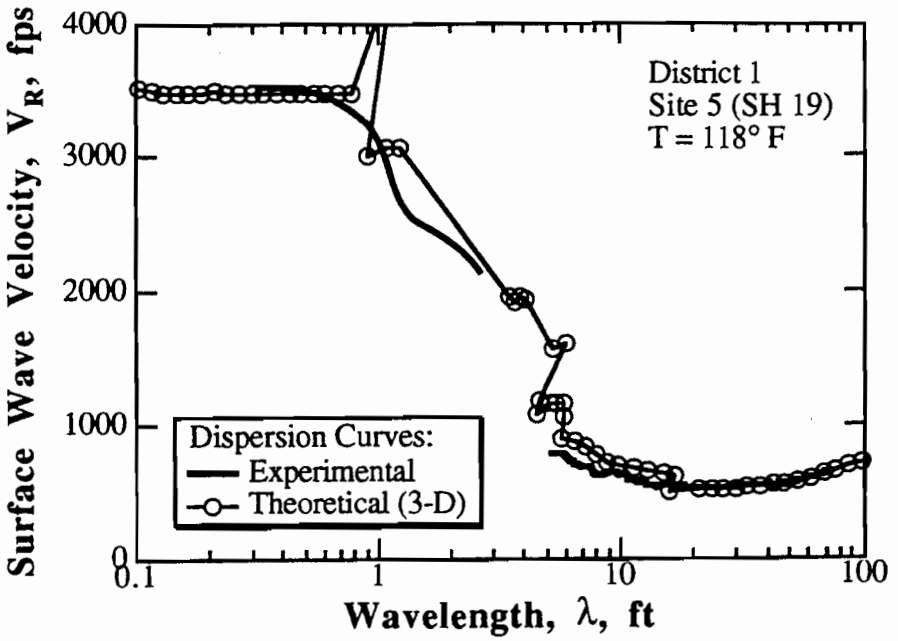

Fig 6.10. Comparison between the Experimental and Theoretical Dispersion Curves Determined at Site 5; District 1, Texas.

Table 6.6. Shear Wave Velocities and Young's Moduli Determined from SASW Measurements at Site 1 (FM 79); District 1, Texas

Layer Thickness (ft)	Shear Wave Velocity (fps)	Poisson's Ratio	Mass Density (Slugs)	Unit Weight (pcf)	Young's Modulus (ksi)
0.167	3,870*	0.295**	4.35	140	1,172
0.500	1,200	0.330	4.03	130	107
0.667	1,100	0.330	4.03	130	90
10.00	500	0.330	3.73	120	17
10.00	550	0.330	3.73	120	21
Half-Space	700	0.330	3.73	120	34

* Determined from the compression wave velocity measured at Site 1

** Assumed from resonance tests on asphalt cylinders presented in Fig. 5.32

Table 6.7. Shear Wave Velocities and Young's Moduli Determined from SASW Measurements at Site 2 (FM 137); District 1, Texas

Layer Thickness (ft)	Shear Wave Velocity (fps)	Poisson's Ratio	Mass Density (Slugs)	Unit Weight (pcf)	Young's Modulus (ksi)
0.167	3,160*	0.328**	4.35	140	801
0.833	1,300	0.330	4.03	130	126
10.00	450	0.330	3.73	120	14
10.00	500	0.330	3.73	120	17
Half-Space	900	0.330	3.73	120	56

* Determined from the compression wave velocity measured at Site 2
** Assumed from resonance tests on asphalt cylinders presented in Fig. 5.32

Table 6.8. Shear Wave Velocities and Young's Moduli Determined from SASW Measurements at Site 3 (SH 82); District 1, Texas

Layer Thickness (ft)	Shear Wave Velocity (fps)	Poisson's Ratio	Mass Density (Slugs)	Unit Weight (pcf)	Young's Modulus (ksi)
1.000	4,150	0.289*	4.35	140	1,341
1.833	800	0.330	4.03	130	48
14.00	630	0.330	3.73	120	27
5.00	900	0.330	3.73	120	56
5.00	1,100	0.330	3.73	120	83
Half-Space	1,500	0.330	3.73	120	155

* Assumed from resonance tests on asphalt cylinders presented in Fig. 5.32

Table 6.9. Shear Wave Velocities and Young's Moduli Determined from SASW Measurements at Site 4 (FM 195); District 1, Texas

Layer Thickness (ft)	Shear Wave Velocity (fps)	Poisson's Ratio	Mass Density (Slugs)	Unit Weight (pcf)	Young's Modulus (ksi)
0.334	5,200	0.282*	4.35	140	2,093
0.500	750	0.330	4.03	130	42
15.00	520	0.330	3.73	120	19
5.00	700	0.330	3.73	120	34
5.00	900	0.330	3.73	120	56
Half-Space	1,100	0.330	3.73	120	83

* Assumed from resonance tests on asphalt cylinders presented in Fig. 5.32

Table 6.10. Shear Wave Velocities and Young's Moduli Determined from SASW Measurements at Site 5 (SH 19); District 1, Texas

Layer Thickness (ft)	Shear Wave Velocity (fps)	Poisson's Ratio	Mass Density (Slugs)	Unit Weight (pcf)	Young's Modulus (ksi)
0.750	3,650	0.323*	4.35	140	1,164
0.583	600	0.330	4.03	130	27
0.667	550	0.330	4.03	130	23
18.00	500	0.330	3.73	120	17
5.00	600	0.330	3.73	120	25
5.00	700	0.330	3.73	120	34
Half-Space	900	0.330	3.73	120	56

* Assumed from resonance tests on asphalt cylinders presented in Fig. 5.32

Young's moduli of the AC surface layer determined from P-wave and SASW measurements are compared in Fig. 6.11. At Sites 1 and 2, Young's moduli were determined only from P-wave tests. At Sites 3, 4 and 5, Young's moduli from both tests compare reasonably well (average within 8%). This confirms again that the assumption of measurement of the unconstrained compression wave is reasonable and is within the measurement accuracy. Note that Young's moduli of the AC layers represent values at high frequencies (3.5 kHz for P-wave tests and 15 kHz for SASW tests). Frequency-adjusted values are presented and discussed in Section 6.7.3.

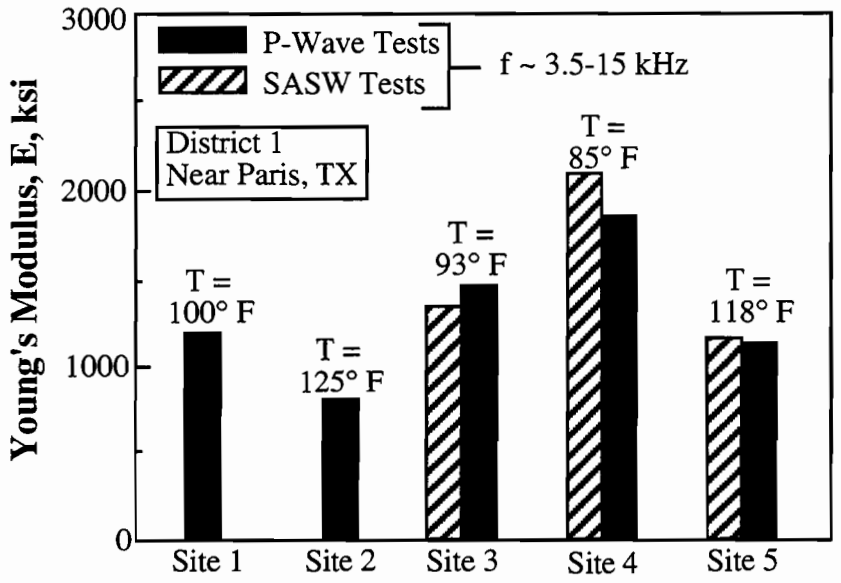

Fig 6.11. Comparison of Young's Moduli of the AC Layer As Determined from P-Wave and SASW Measurements; District 1, Texas.

Young's moduli of the upper subgrade (depth range from approximately 0.3 m (1 ft) to 5.5 m (18 ft)) for the five sites in District 1 are presented in Fig. 6.12. Young's moduli of the base and subbase layers for Sites 1 through 5 are shown in Fig. 6.13.

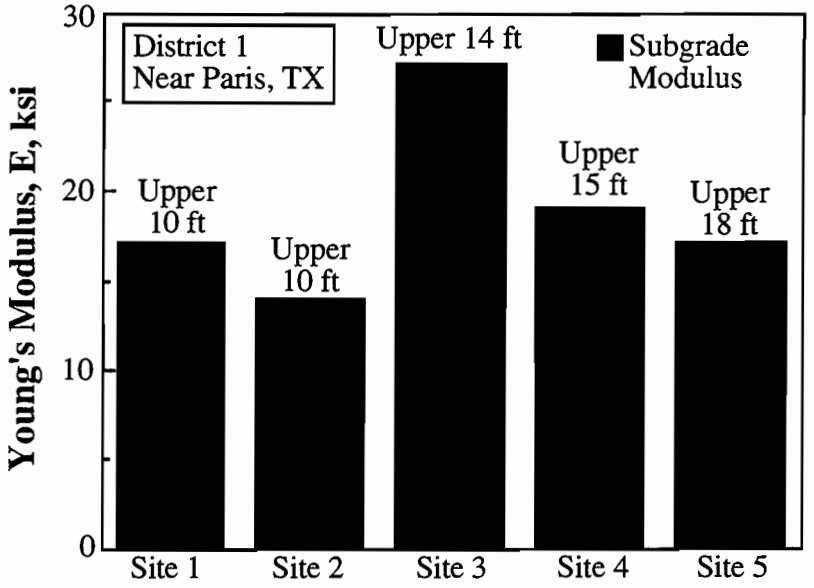

Fig 6.12. Young's Moduli of the Subgrade As Determined from SASW Measurements; District 1, Texas.

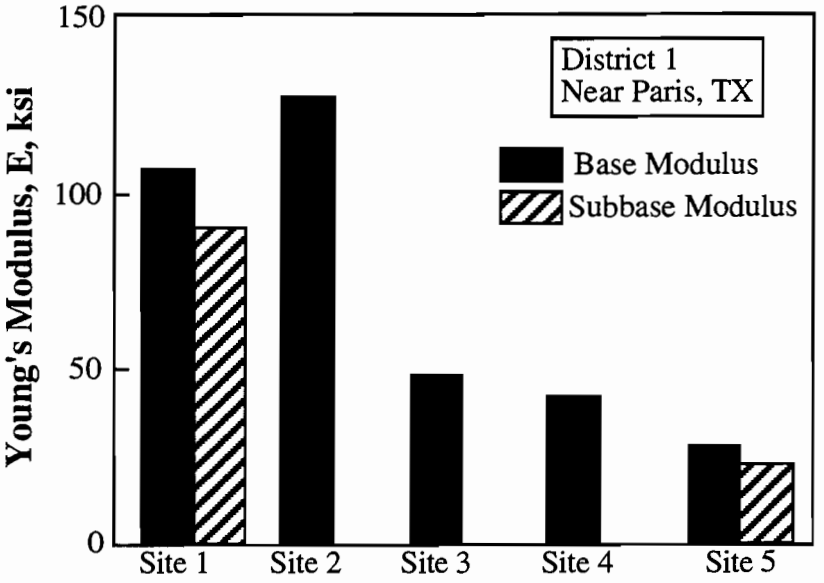

Fig 6.13. Young's Moduli of the Base and Subbase As Determined from SASW Measurements; District 1, Texas.

6.3 Tests in District 8, Texas

6.3.1 P-Wave Measurements

P-wave measurements were performed at Sites 1 through 6 in District 8 using source-receiver spacings of 0.15 m (0.5 ft), 0.3 m (1.0 ft) and 0.46 m (1.5 ft). The WR Model F-7 shaker was used as the source and a WR Model 736 accelerometer was used as a receiver. The source and receiver were calibrated in the field to determine the initiation time for each component. Time records for the source and receiver placed next to each other on the pavement surface are shown in Fig. 6.14 (the approximate frequency in these records is about 7 kHz). The measured time delay of 23.4 μs was subtracted from all direct travel times measured in the source-to-receiver tests.

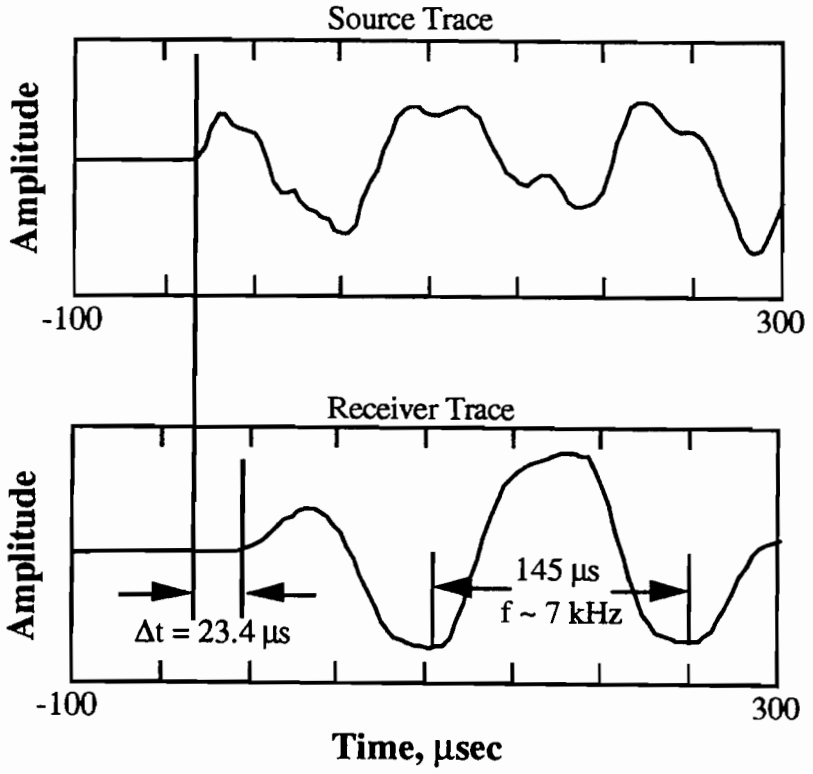

Fig 6.14. Time Records Measured from the F-7 Shaker and WR Model 736 Accelerometer during Calibration on the Pavement.

A plot of the source-receiver distances versus the travel times (calibration factor of 23.4 μs is already subtracted) of propagating compression waves for Sites 1 through 6 is shown in Fig. 6.15. The compression wave velocities for the six sites in District 8 were calculated from the slopes of the lines shown in Fig. 6.15. Equation 2.2 was used in the calculations of Young's moduli of the AC layer assuming a unit weight of 22 kN/m^3 (140 pcf). The calculated moduli of the AC layers at the six sites are presented in Table 6.11. It should be mentioned that a function generator was used to generate a wave with a frequency equal to 15 kHz for the P-wave measurements. As a result, Young's moduli of the AC layer represent values at a frequency of about 15 kHz.

Table 6.11. Young's Moduli of the AC Layer Determined from P-wave Measurements; Sites 1 through 6, District 8, Texas

Site No.	Surface Temperature (° F)	Compression Wave Velocity (fps)	Young's * Modulus (ksi)
1	103	6,130	1,134
2	124	5,995	1,086
3	93	7,410	1,658
4	98	7,640	1,762
5	103	6,730	1,368
6	116	5,360	867

* Measurement frequency is approximately 15 kHz

6.3.2 SASW Measurements

SASW tests were performed at the six sites in District 8 using receiver spacings of 0.15, 0.31, 0.61, 1.2, 3.0, 6.1 and 9.1 m (0.5, 1, 2, 4, 10, 20 and 30 ft). The experimental dispersion curves determined at Sites 1 through 6 are shown in Fig. 6.16. As shown in Fig. 6.16, the surface layers at Sites 1, 2 and 6 were not sampled by the SASW measurements. Note that a log scale was used for the wavelength in Fig. 6.16 to emphasize measurements of the AC surface layer. The experimental dispersion curves determined at Sites 1 through 6 were then plotted using a linear scale for wavelength to emphasize measurements of the subgrade

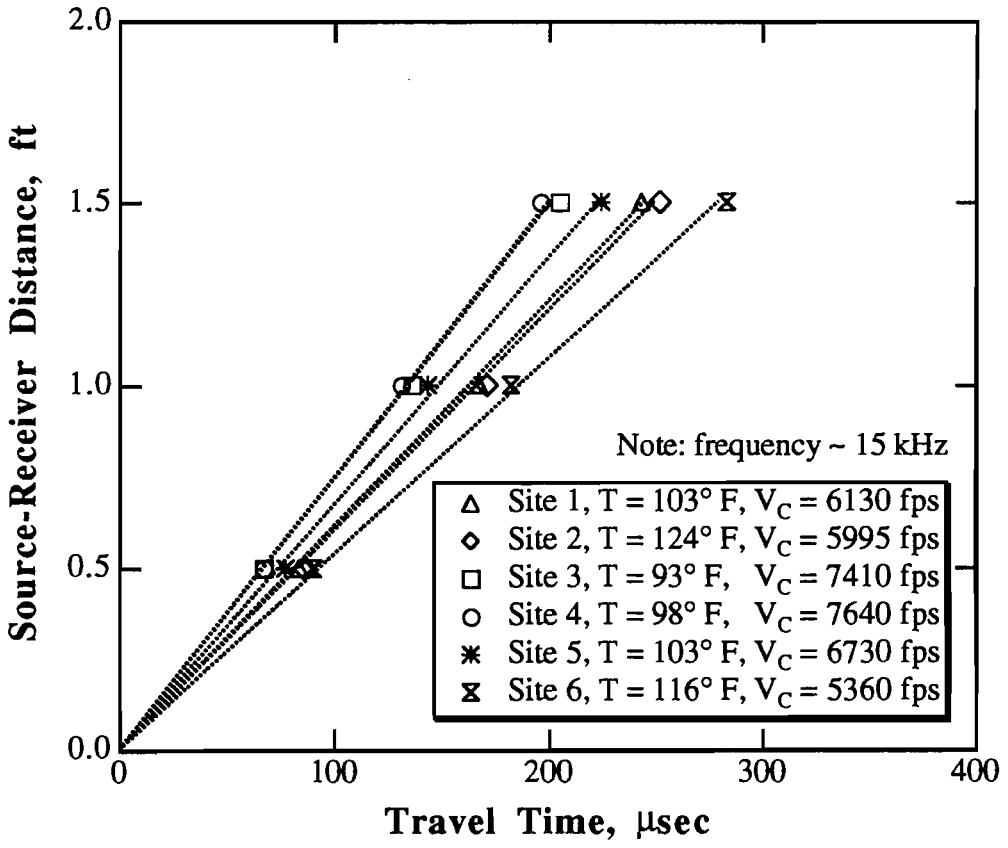

Fig 6.15. Travel Distances Versus Travel Times for P-Waves Measured at Sites 1 through 6; District 8, Texas.

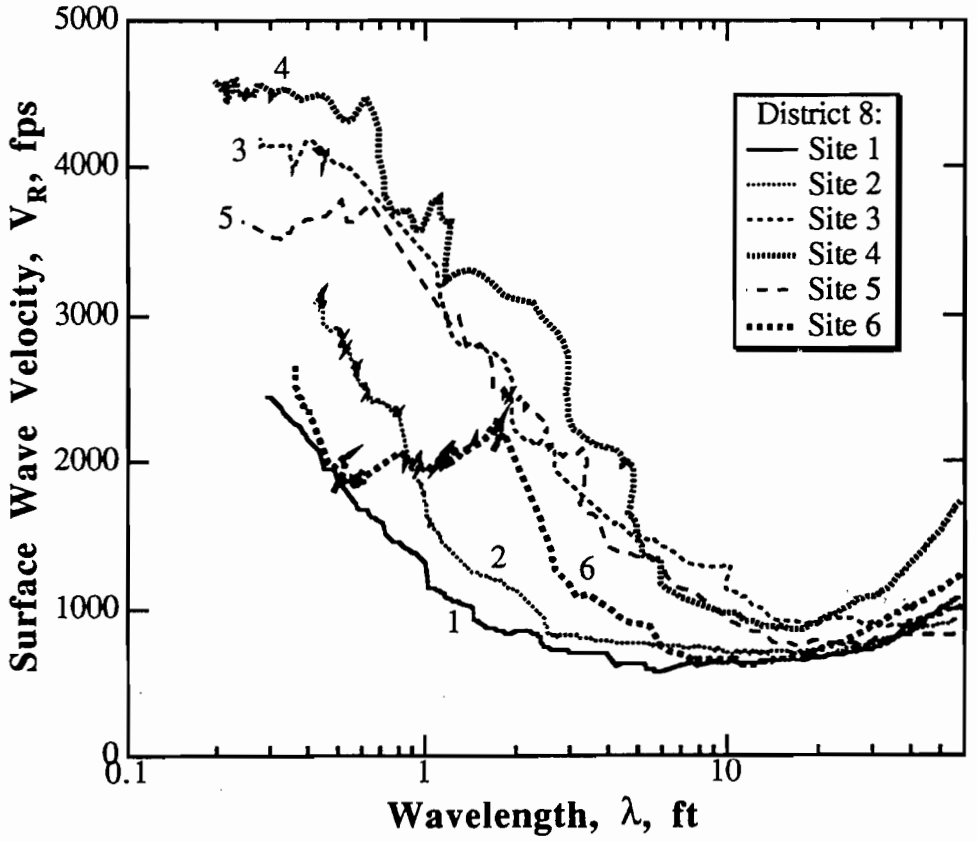

Fig 6.16. Experimental Dispersion Curves Determined from SASW Measurements at Sites 1 through 6, District 8, Texas; Log Scale for Wavelength.

layer as shown in Fig. 6.17. A sudden increase in the surface wave velocity at wavelengths of 5.5 m (18 ft) and 3.7 m (12 ft) was observed for Sites 4 and 6, respectively, suggesting the presence of shallow bedrock at these sites. Site 1 also exhibits an obvious increase in velocity with wavelength for wavelengths greater than about 10.7 m (35 ft). However, this increase is not as abrupt as those at Sites 4 and 6 and is not representative of bedrock as shown in the forward modeling.

The SASW measurements were analyzed to determine the shear wave velocity profiles at the six sites in District 8. As with the SASW tests in District 1, the thicknesses of the layers at each site were taken from the construction drawings, but would have been changed to achieve the proper fit between the experimental and theoretical dispersion curves if necessary. Figures 6.18 through 6.23 show a comparison between the experimental and theoretical dispersion curves for Sites 1 through 6, respectively. The shear wave velocity profiles corresponding to the theoretical dispersion curves shown in Figs. 6.18 through 6.23 are presented in Tables 6.12 through 6.17, respectively. Young's moduli of the various layers calculated from the shear wave velocities are also shown in the tables.

Forward modeling of the SASW data confirmed that bedrock exists at depths of 2.5 and 3 m (8.3 and 9.8 ft) at Sites 4 and 6, respectively.

Young's moduli of the AC layer determined from P-wave and SASW measurements are compared in Fig. 6.24. At Sites 1, 2 and 6, Young's moduli were determined only from P-wave measurements. At Sites 3, 4 and 5, Young's moduli from both tests compare reasonably well (average within 9%). Note that Young's moduli of the AC layer represent values at high frequencies (on the order of 15 kHz for both tests). Frequency-adjusted values are presented and discussed in Section 6.7.3.

Young's moduli of the subgrade and base layers are presented in Figs. 6.25 and 6.26, respectively. The SASW tests showed that the subgrade changes stiffness with depth within the top 3 to 4.6 m (10 to 15 ft). Therefore, the stiffnesses of the upper and lower subgrade layers are presented in Fig. 6.25.

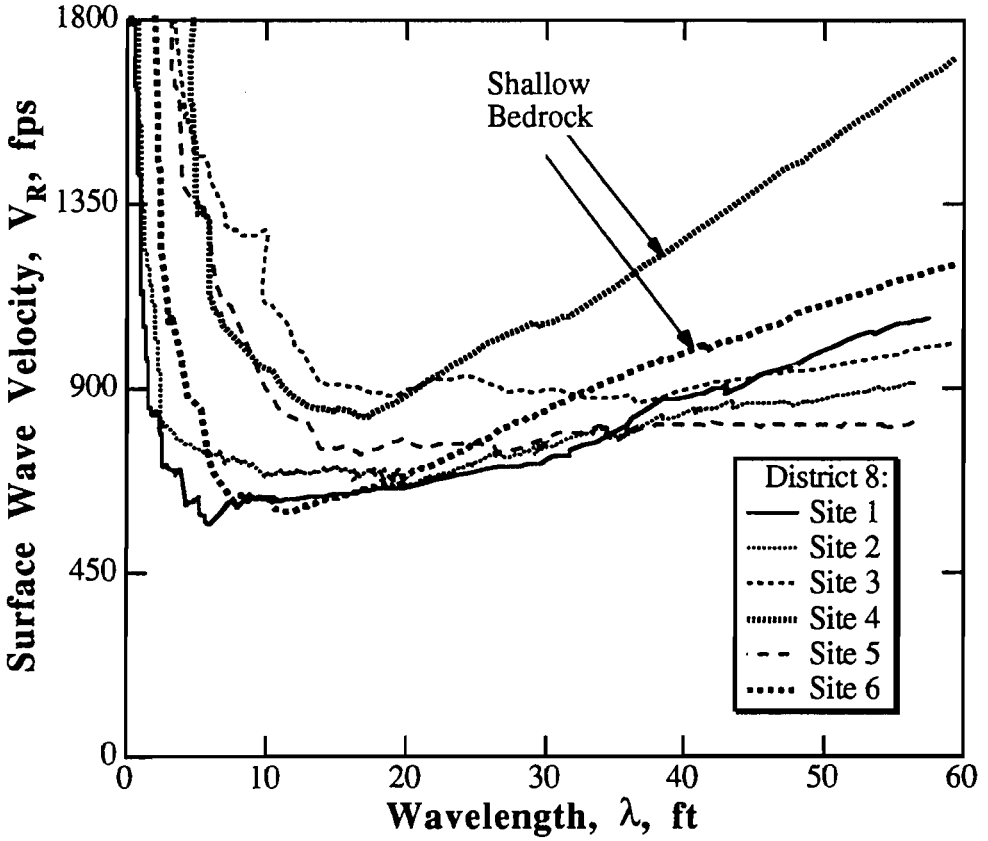

Fig 6.17. Experimental Dispersion Curves Determined from SASW Measurements at Sites 1 through 6, District 8, Texas; Linear Scale for Wavelength.

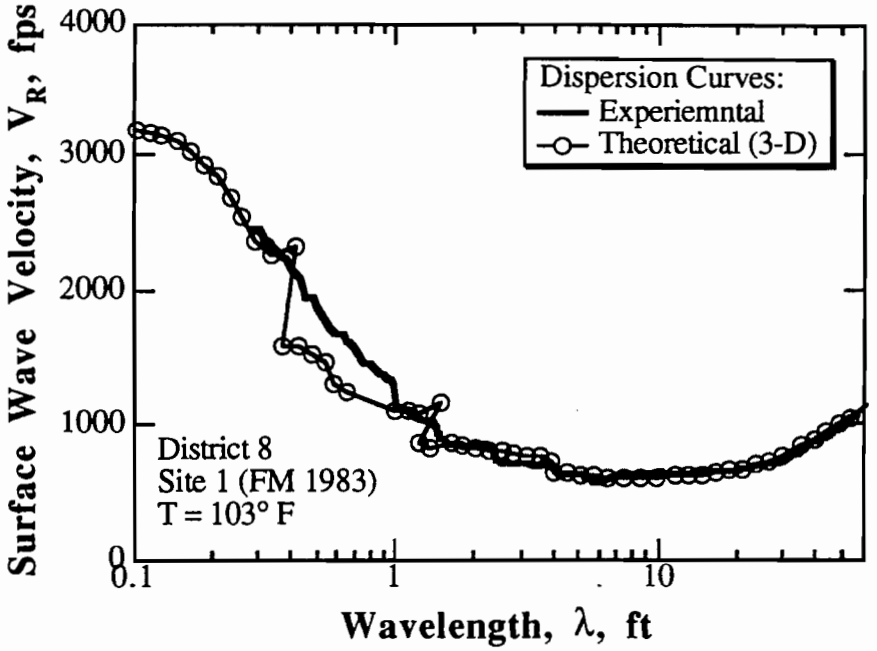

Fig 6.18. Comparison between the Experimental and Theoretical Dispersion Curves Determined at Site 1; District 8, Texas.

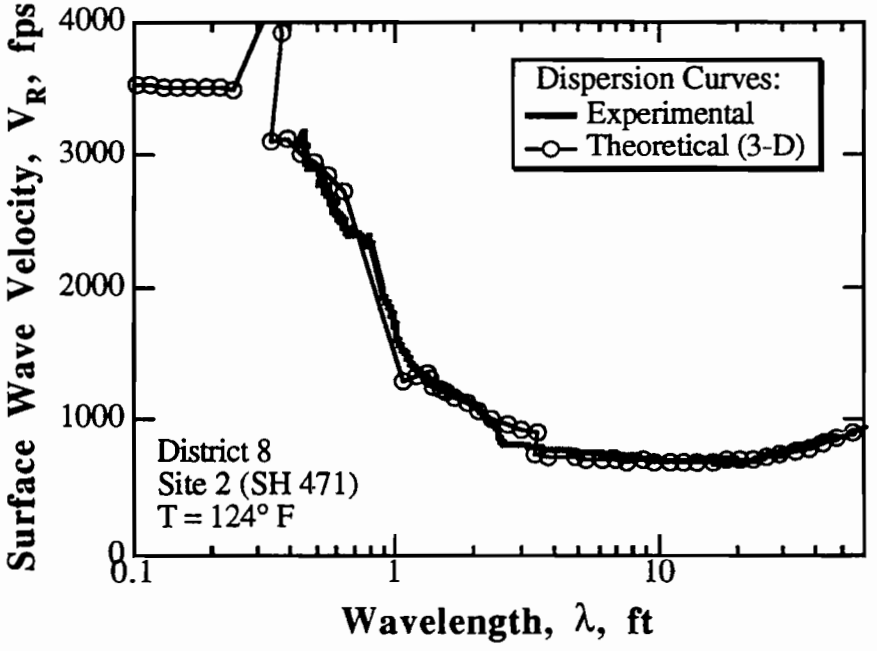

Fig 6.19. Comparison between the Experimental and Theoretical Dispersion Curves Determined at Site 2; District 8, Texas.

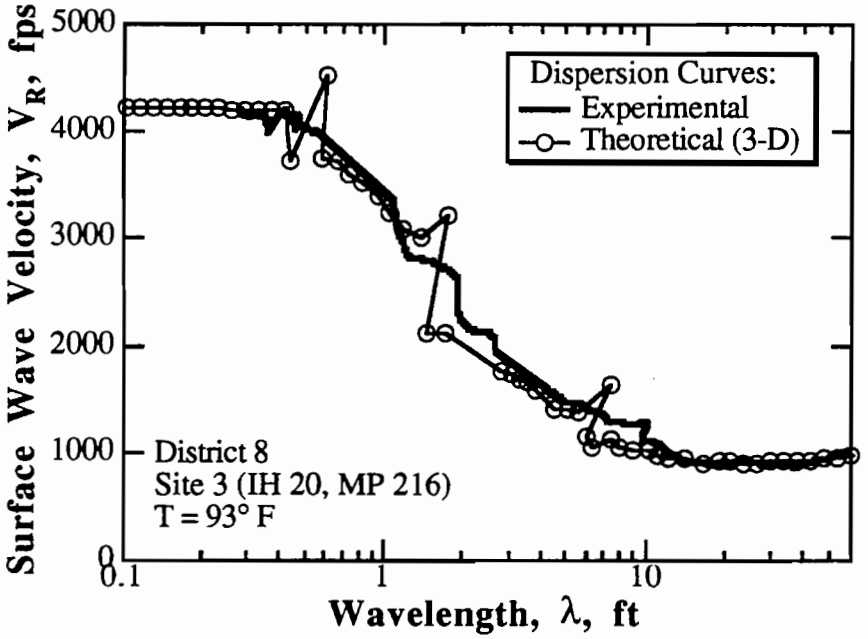

Fig 6.20. Comparison between the Experimental and Theoretical Dispersion Curves Determined at Site 3; District 8, Texas.

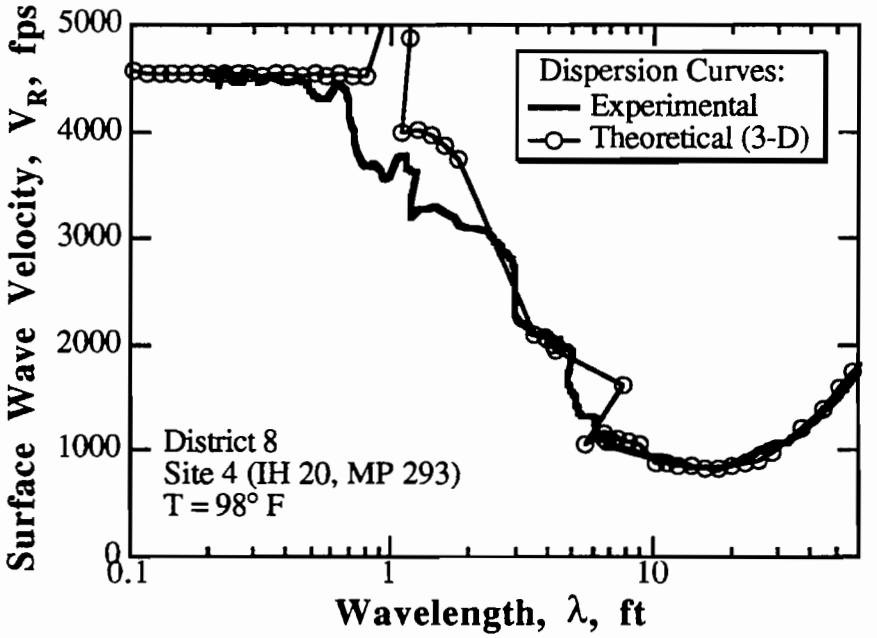

Fig 6.21. Comparison between the Experimental and Theoretical Dispersion Curves Determined at Site 4; District 8, Texas.

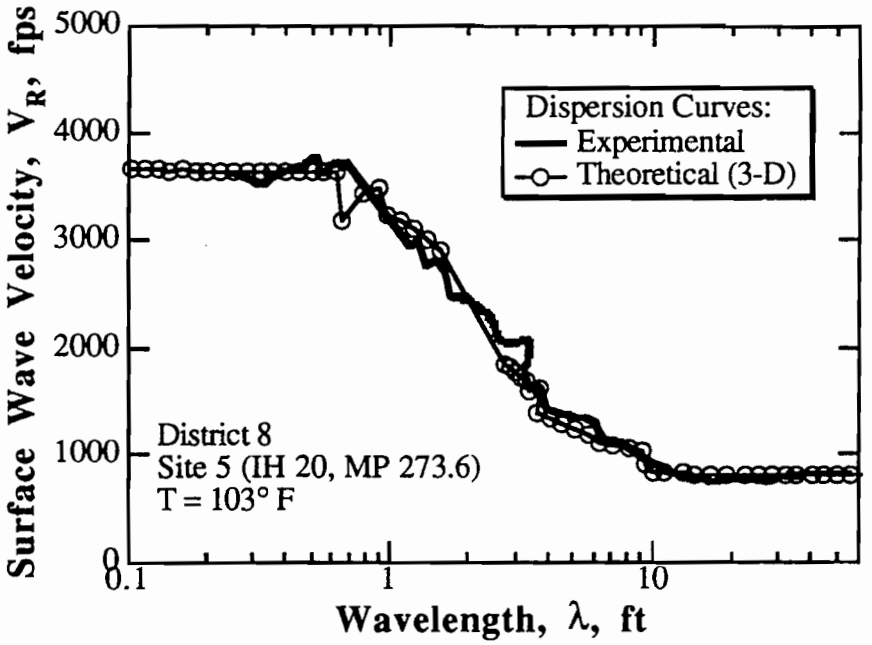

Fig 6.22. Comparison between the Experimental and Theoretical Dispersion Curves Determined at Site 5; District 8, Texas.

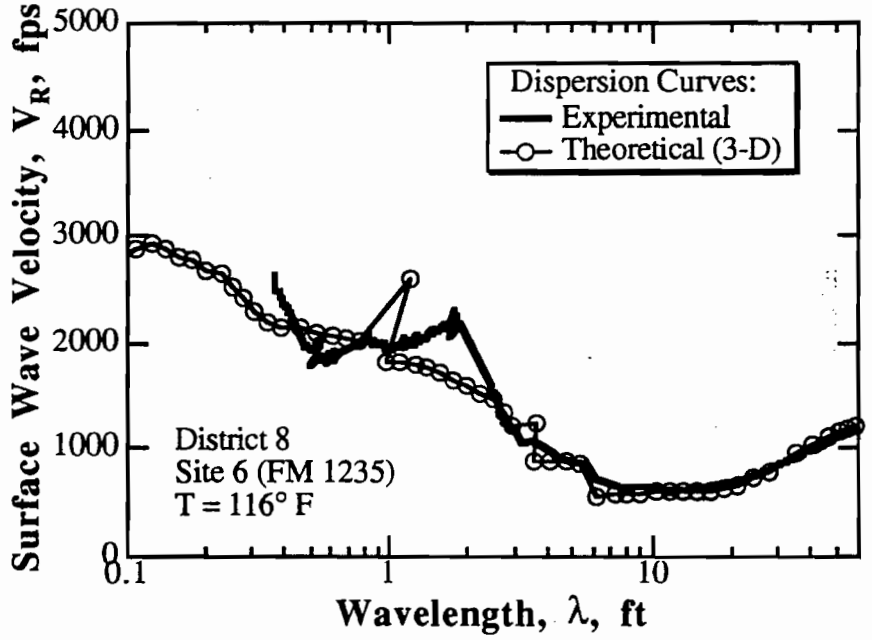

Fig 6.23. Comparison between the Experimental and Theoretical Dispersion Curves Determined at Site 6; District 8, Texas.

Table 6.12. Shear Wave Velocities and Young's Moduli Determined from SASW Measurements at Site 1 (FM 1983); District 8, Texas

Layer Thickness (ft)	Shear Wave Velocity (fps)	Poisson's Ratio	Mass Density (Slugs)	Unit Weight (pcf)	Young's Modulus (ksi)
0.083	3,800*	0.300**	4.35	140	1,134
0.667	900	0.330	4.03	130	60
10.00	600	0.330	3.73	120	25
5.00	1,100	0.330	3.73	120	83
Half-Space	1,400	0.330	3.73	120	135

* Determined from the compression wave velocity measured at Site 1
** Assumed from resonance tests on asphalt cylinders presented in Fig. 5.32

Table 6.13. Shear Wave Velocities and Young's Moduli Determined from SASW Measurements at Site 2 (SH 471); District 8, Texas

Layer Thickness (ft)	Shear Wave Velocity (fps)	Poisson's Ratio	Mass Density (Slugs)	Unit Weight (pcf)	Young's Modulus (ksi)
0.25	3,680*	0.328**	4.35	140	1,086
0.42	750	0.330	4.03	130	42
4.00	700	0.330	3.73	120	34
10.00	660	0.330	3.73	120	30
10.00	1,000	0.330	3.73	120	69
Half-Space	1,300	0.330	3.73	120	116

* Determined from the compression wave velocity measured at Site 2
** Assumed from resonance tests on asphalt cylinders presented in Fig. 5.32

Table 6.14. Shear Wave Velocities and Young's Moduli Determined from SASW Measurements at Site 3 (IH 20, MP 216); District 8, Texas

Layer Thickness (ft)	Shear Wave Velocity (fps)	Poisson's Ratio	Mass Density (Slugs)	Unit Weight (pcf)	Young's Modulus (ksi)
0.417	4,450	0.289*	4.35	140	1,541
1.50	1,200	0.330	4.03	130	107
1.50	1,050	0.330	3.73	120	76
13.0	850	0.330	3.73	120	50
10.0	1,000	0.330	3.73	120	69
Half-Space	1,100	0.330	3.73	120	83

* Assumed from resonance tests on asphalt cylinders presented in Fig. 5.32

Table 6.15. Shear Wave Velocities and Young's Moduli Determined from SASW Measurements at Site 4 (IH 20, MP 293); District 8, Texas

Layer Thickness (ft)	Shear Wave Velocity (fps)	Poisson's Ratio	Mass Density (Slugs)	Unit Weight (pcf)	Young's Modulus (ksi)
0.833	4,800	0.293*	4.35	140	1,799
0.916	1,100	0.330	4.03	130	90
1.50	600	0.330	3.73	120	25
5.00	650	0.330	3.73	120	29
5.00	2,500	0.330	3.73	120	430
10.0	3,000	0.330	3.73	120	620
Half-Space	3,000	0.330	3.73	120	620

* Assumed from resonance tests on asphalt cylinders presented in Fig. 5.32

Table 6.16. Shear Wave Velocities and Young's Moduli Determined from SASW Measurements at Site 5 (IH 20, MP 273.6); District 8, Texas

Layer Thickness (ft)	Shear Wave Velocity (fps)	Poisson's Ratio	Mass Density (Slugs)	Unit Weight (pcf)	Young's Modulus (ksi)
0.667	3,850	0.300*	4.35	140	1,164
0.916	1,000	0.330	4.03	130	75
20.0	770	0.330	3.73	120	41
Half-Space	770	0.330	3.73	120	41

* Assumed from resonance tests on asphalt cylinders presented in Fig. 5.32

Table 6.17. Shear Wave Velocities and Young's Moduli Determined from SASW Measurements at Site 6 (FM 1235); District 8, Texas

Layer Thickness (ft)	Shear Wave Velocity (fps)	Poisson's Ratio	Mass Density (Slugs)	Unit Weight (pcf)	Young's Modulus (ksi)
0.083	3,300*	0.321**	4.35	140	867
0.667	2,000	0.330	4.03	130	298
5.00	500	0.330	3.73	120	17
4.00	600	0.330	3.73	120	25
20.00	2,000	0.330	3.73	120	275
Half-Space	2,000	0.330	3.73	120	275

* Determined from the compression wave velocity measured at Site 6

** Assumed from resonance tests on asphalt cylinders presented in Fig. 5.32

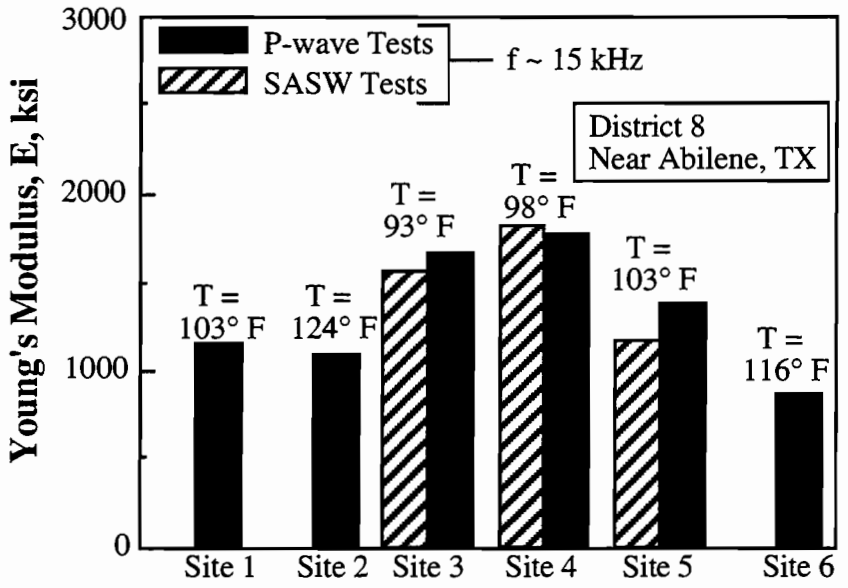

Fig 6.24. Comparison of Young's Moduli of the AC Layer As Determined from P-Wave and SASW Measurements; District 8, Texas.

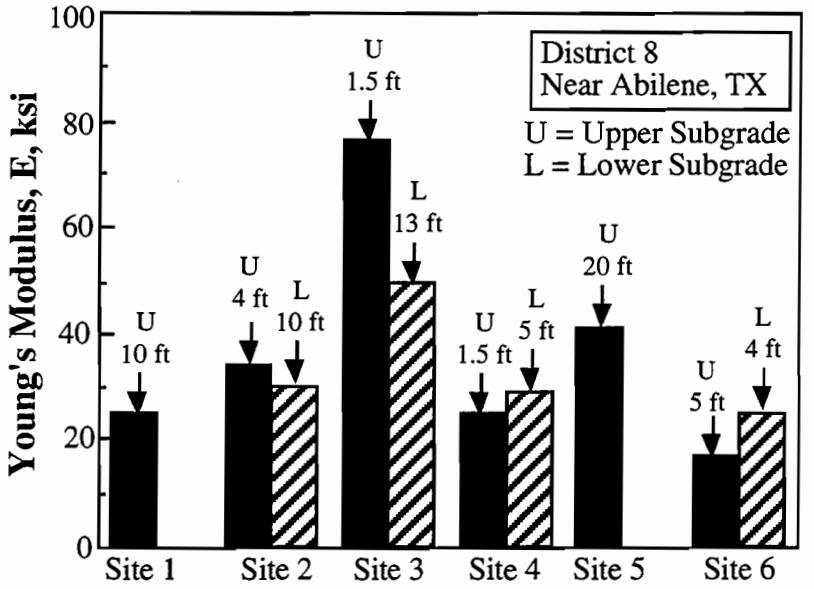

Fig 6.25. Young's Moduli of the Subgrade As Determined from SASW Measurements; District 8, Texas.

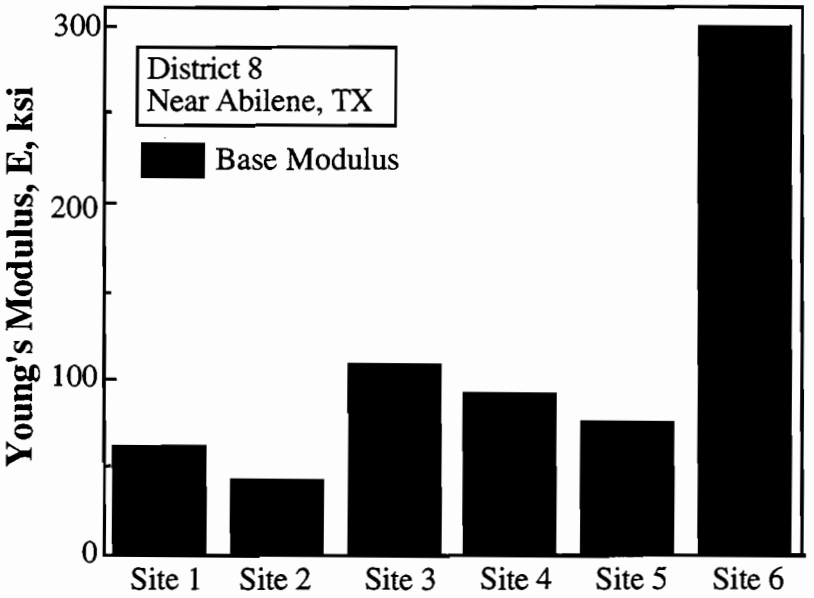

Fig 6.26. Young's Moduli of the Base As Determined from SASW Measurements; District 8, Texas.

6.4 Tests in District 11, Texas

P-wave measurements were not performed in District 11. SASW measurements were performed at seven sites using receiver spacings ranging from 0.15 to 9.1 m (0.5 to 30 ft). A comparison between the experimental and theoretical dispersion curves determined from these SASW measurements is presented in Figs. 6.27 through 6.33 (no SASW tests were performed at Site 6 because of time limitations) for Sites 1 through 8, respectively. Layer thicknesses used in the forward modeling were taken from the construction drawings and agreed well with the modeling results. The shear wave velocity profiles corresponding to the theoretical dispersion curves shown in Figs. 6.27 through 6.33 are presented in Tables 6.18 through 6.24, respectively. It should be mentioned that the shear wave velocity of the AC layer (at sites where the AC layer was not sampled) was assumed based on the initial part (short wavelengths) of the experimental dispersion curve.

Forward modeling of the SASW data showed that bedrock was not encountered at any of the test sites in District 11.

Young's moduli (measurement f ~ 15 kHz) of the AC surface layer determined from SASW measurements are presented in Fig. 6.34. At Sites 3, 4, 5, 7 and 8, the shear wave velocity of the AC surface layer was assumed based on the initial part (short wavelengths) of the experimental dispersion curve. Young's moduli of the subgrade are presented in Fig. 6.35. The SASW tests showed that the subgrade changes stiffness with depth within the top 3 to 4.6 m (10 to 15 ft). Therefore, the stiffnesses of the upper and lower sublayers of the subgrade are presented in Fig. 6.35. Young's moduli of the base layers are presented in Fig. 6.36.

It should be noted that the cement-treated bases at Sites 7 and 8 (as noted in the construction drawings) did not behave as cement-treated materials. They have stiffnesses of untreated materials. A cement-treated base behaves similarly to that at Site 4 at the TTI test facility in Bryan, Texas (Fig. 4.13).

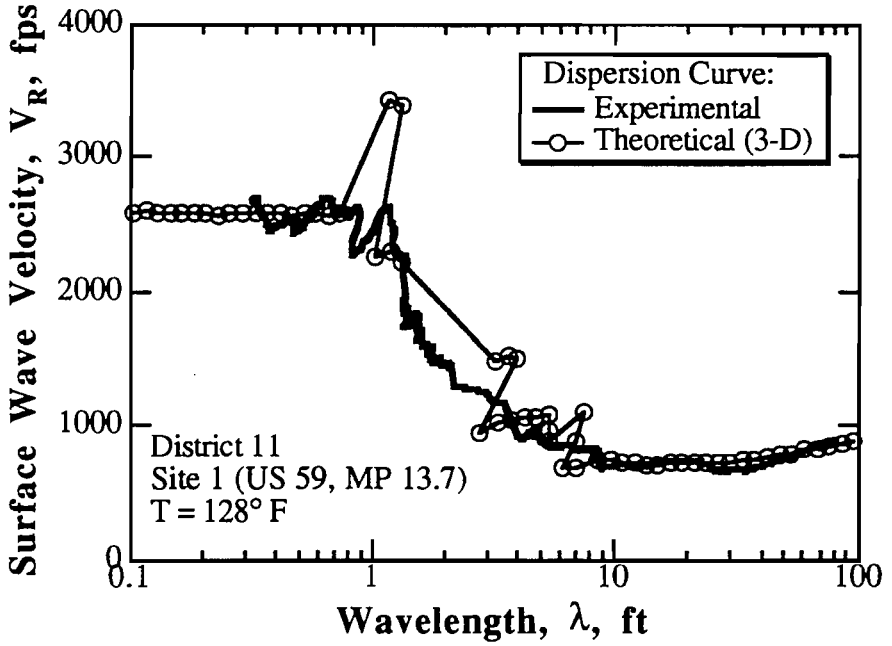

Fig 6.27. Comparison between the Experimental and Theoretical Dispersion Curves Determined at Site 1; District 11, Texas.

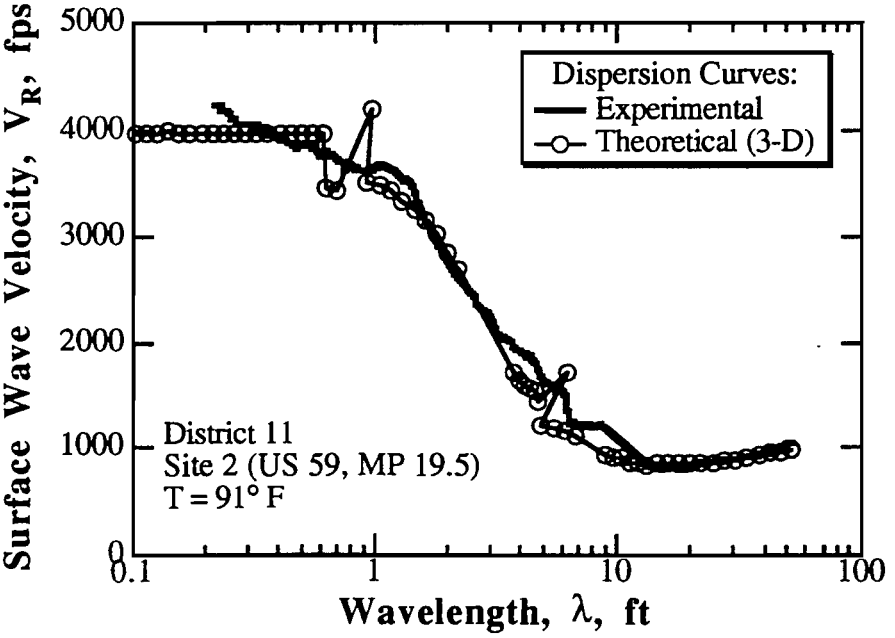

Fig 6.28. Comparison between the Experimental and Theoretical Dispersion Curves Determined at Site 2; District 11, Texas.

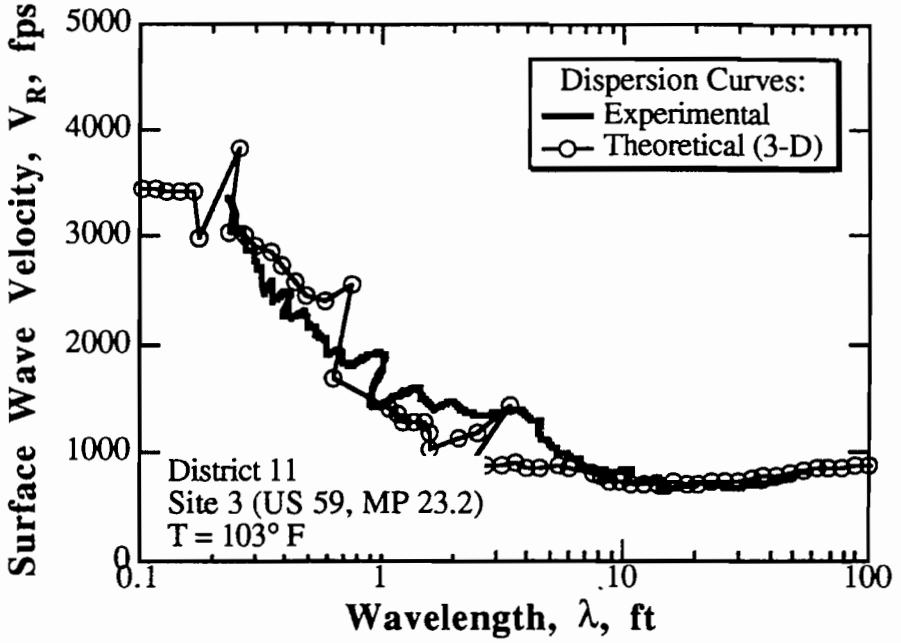

Fig 6.29. Comparison between the Experimental and Theoretical Dispersion Curves Determined at Site 3; District 11, Texas.

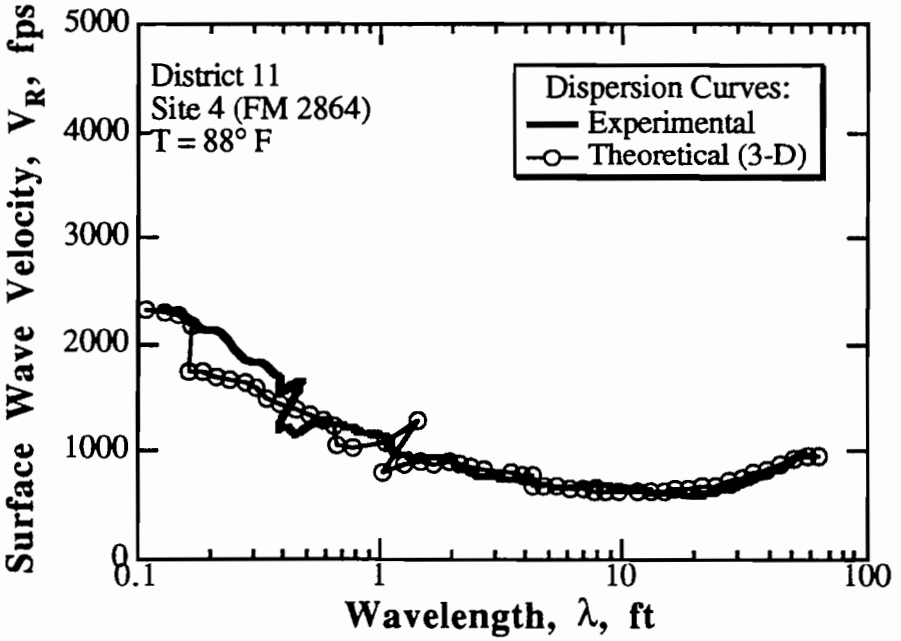

Fig 6.30. Comparison between the Experimental and Theoretical Dispersion Curves Determined at Site 4; District 11, Texas.

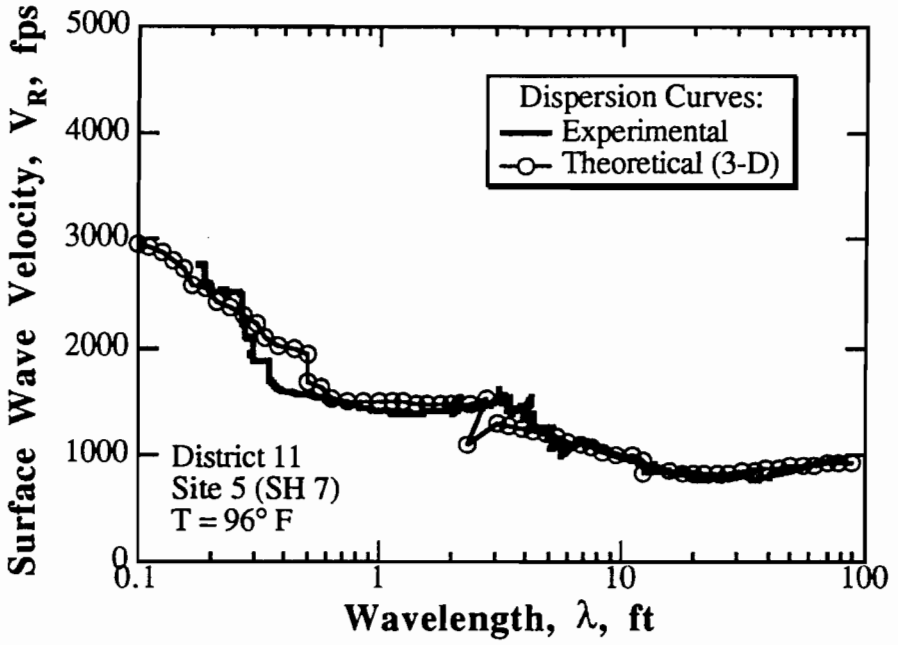

Fig 6.31. Comparison between the Experimental and Theoretical Dispersion Curves Determined at Site 5; District 11, Texas.

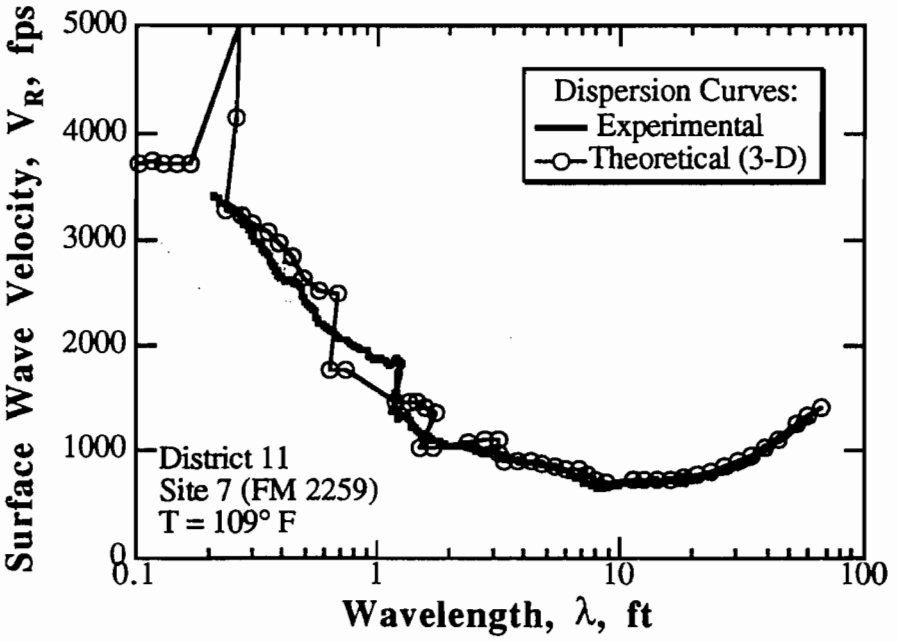

Fig 6.32. Comparison between the Experimental and Theoretical Dispersion Curves Determined at Site 7; District 11, Texas.

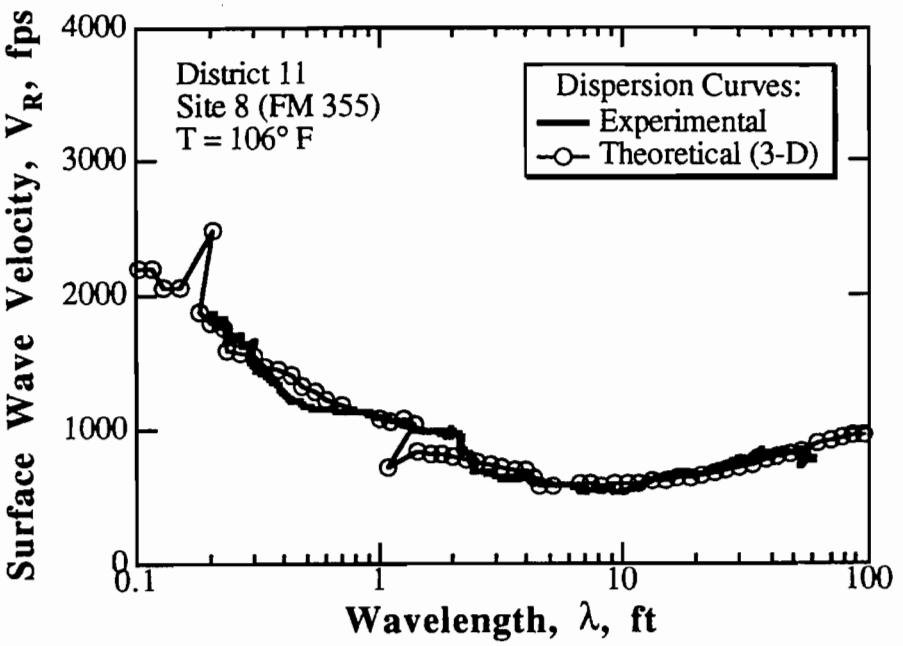

Fig 6.33. Comparison between the Experimental and Theoretical Dispersion Curves Determined at Site 8; District 11, Texas.

Table 6.18. Shear Wave Velocities and Young's Moduli Determined from SASW Measurements at Site 1 (US 59, MP 13.7); District 11, Texas

Layer Thickness (ft)	Shear Wave Velocity (fps)	Poisson's Ratio	Mass Density (Slugs)	Unit Weight (pcf)	Young's Modulus (ksi)
0.740	2,700	0.329*	4.35	140	585
0.667	450	0.330	4.03	130	15
5.00	750	0.330	3.73	120	39
10.00	700	0.330	3.73	120	34
10.00	800	0.330	3.73	120	44
Half-Space	1,000	0.330	3.73	120	69

* Assumed from resonance tests on asphalt cylinders presented in Fig. 5.32

Table 6.19. Shear Wave Velocities and Young's Moduli Determined from SASW Measurements at Site 2 (US 59, MP 19.5); District 11, Texas

Layer Thickness (ft)	Shear Wave Velocity (fps)	Poisson's Ratio	Mass Density (Slugs)	Unit Weight (pcf)	Young's Modulus (ksi)
0.667	4,200	0.288*	4.35	140	1,372
1.50	900	0.330	4.03	130	60
5.00	750	0.330	3.73	120	39
7.00	800	0.330	3.73	120	44
Half-Space	1,100	0.330	3.73	120	83

* Assumed from resonance tests on asphalt cylinders presented in Fig. 5.32

Table 6.20. Shear Wave Velocities and Young's Moduli Determined from SASW Measurements at Site 3 (US 59, MP 23.2); District 11, Texas

Layer Thickness (ft)	Shear Wave Velocity (fps)	Poisson's Ratio	Mass Density (Slugs)	Unit Weight (pcf)	Young's Modulus (ksi)
0.167	3,600	0.300*	4.35	140	1,017
0.583	950	0.330	4.03	130	67
1.00	1,000	0.330	4.03	130	75
5.00	700	0.330	3.73	120	34
8.00	650	0.330	3.73	120	29
Half-Space	950	0.330	3.73	120	62

* Assumed from resonance tests on asphalt cylinders presented in Fig. 5.32

Table 6.21. Shear Wave Velocities and Young's Moduli Determined from SASW Measurements at Site 4 (FM 2864); District 11, Texas

Layer Thickness (ft)	Shear Wave Velocity (fps)	Poisson's Ratio	Mass Density (Slugs)	Unit Weight (pcf)	Young's Modulus (ksi)
0.083	2,800	0.285*	4.35	140	608
0.790	1,000	0.330	4.03	130	75
2.00	680	0.330	3.73	120	32
8.00	590	0.330	3.73	120	24
Half-Space	1,100	0.330	3.73	120	83

* Assumed from resonance tests on asphalt cylinders presented in Fig. 5.32

Table 6.22. Shear Wave Velocities and Young's Moduli Determined from SASW Measurements at Site 5 (SH 7); District 11, Texas

Layer Thickness (ft)	Shear Wave Velocity (fps)	Poisson's Ratio	Mass Density (Slugs)	Unit Weight (pcf)	Young's Modulus (ksi)
0.083	3,600	0.292*	4.35	140	1,011
2.00	1,400	0.330	4.03	130	146
12.00	770	0.330	3.73	120	41
Half-Space	1,000	0.330	3.73	120	69

* Assumed from resonance tests on asphalt cylinders presented in Fig. 5.32

Table 6.23. Shear Wave Velocities and Young's Moduli Determined from SASW Measurements at Site 7 (FM 2259); District 11, Texas

Layer Thickness (ft)	Shear Wave Velocity (fps)	Poisson's Ratio	Mass Density (Slugs)	Unit Weight (pcf)	Young's Modulus (ksi)
0.166	3,900	0.311*	4.35	140	1,204
0.667	1,000	0.330	4.03	130	75
1.00	900	0.330	3.73	120	58
8.00	650	0.330	3.73	120	29
5.00	1,200	0.330	3.73	120	99
Half-Space	1,700	0.330	3.73	120	199

* Assumed from resonance tests on asphalt cylinders presented in Fig. 5.32

Table 6.24. Shear Wave Velocities and Young's Moduli Determined from SASW Measurements at Site 8 (FM 355); District 11, Texas

Layer Thickness (ft)	Shear Wave Velocity (fps)	Poisson's Ratio	Mass Density (Slugs)	Unit Weight (pcf)	Young's Modulus (ksi)
0.083	2,300	0.306*	4.35	140	417
0.667	900	0.330	4.03	130	60
5.00	550	0.330	3.73	120	21
10.00	750	0.330	3.73	120	39
10.00	950	0.330	3.73	120	62
Half-Space	1,100	0.330	3.73	120	83

* Assumed from resonance tests on asphalt cylinders presented in Fig. 5.32

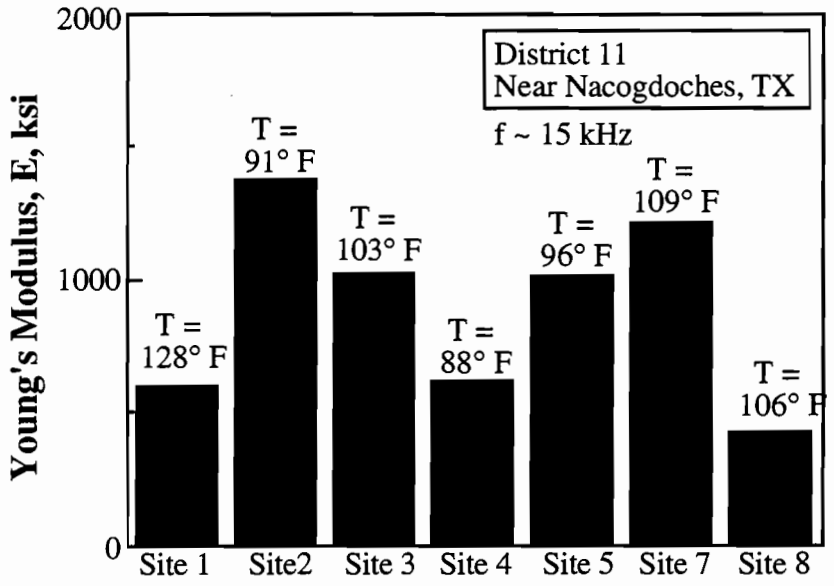

Fig 6.34. Young's Moduli of the AC Layer As Determined from SASW Measurements; District 11, Texas.

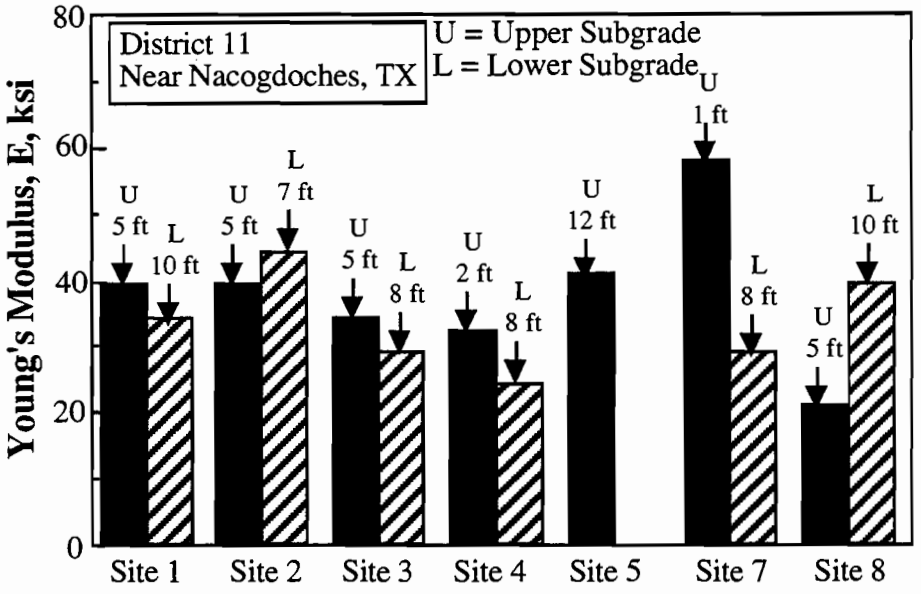

Fig 6.35. Young's Moduli of the Subgrade As Determined from SASW Measurements; District 11, Texas.

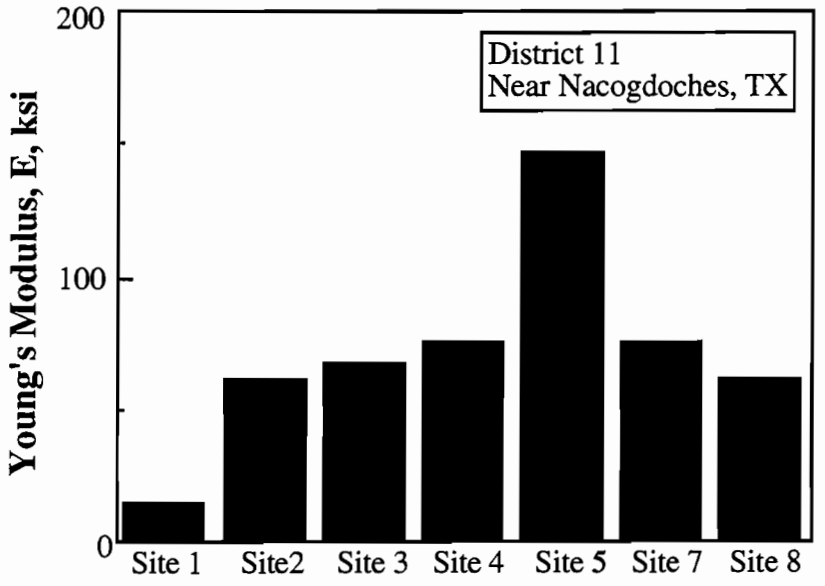

Fig 6.36. Young's Moduli of the Base As Determined from SASW Measurements; District 11, Texas.

6.5 Tests in District 21, Texas

6.5.1 P-Wave Measurements

P-wave measurements were performed at Sites 1 through 6 in District 21 using source-receiver spacings of 0.15 m (0.5 ft), 0.3 m (1.0 ft) and 1.5 ft (0.46 m). The WR Model F-7 shaker was used as the source and a WR Model 736 accelerometer was used as a receiver. The source and receiver were calibrated in the field to determine the initiation time for each component. The measured time delay of 23.4 μs (Fig. 6.14) was subtracted from all direct travel times measured in the source-to-receiver tests, and a measurement frequency of about 15 kHz was used just as in the District 8 tests.

A plot of the source-receiver distances versus the travel times (calibration factor of 23.4 μs is already subtracted) of propagating compression waves for Sites 1 through 6 is shown in Fig. 6.37. The compression wave velocities for the six sites in District 21 were calculated from the slopes of the lines shown in Fig. 6.37. Equation 2.2 was used in the calculations of Young's moduli of the AC layer assuming a unit weight of 22 kN/m^3 (140 pcf). The calculated moduli of the AC layer at the six sites are presented in Table 6.25.

Table 6.25. Young's Moduli of the AC Layer Determined from P-wave Measurements; Sites 1 through 6, District 21, Texas

Site No.	Surface Temperature (° F)	Compression Wave Velocity (fps)	Young's * Modulus (ksi)
1	108	5,300	848
2	115	4,700	667
3	88	8,200	2,030
4	100	6,300	1,198
5	123	5,900	1,051
6	145	3,950	471

* Measurement frequency is approximately 15 kHz

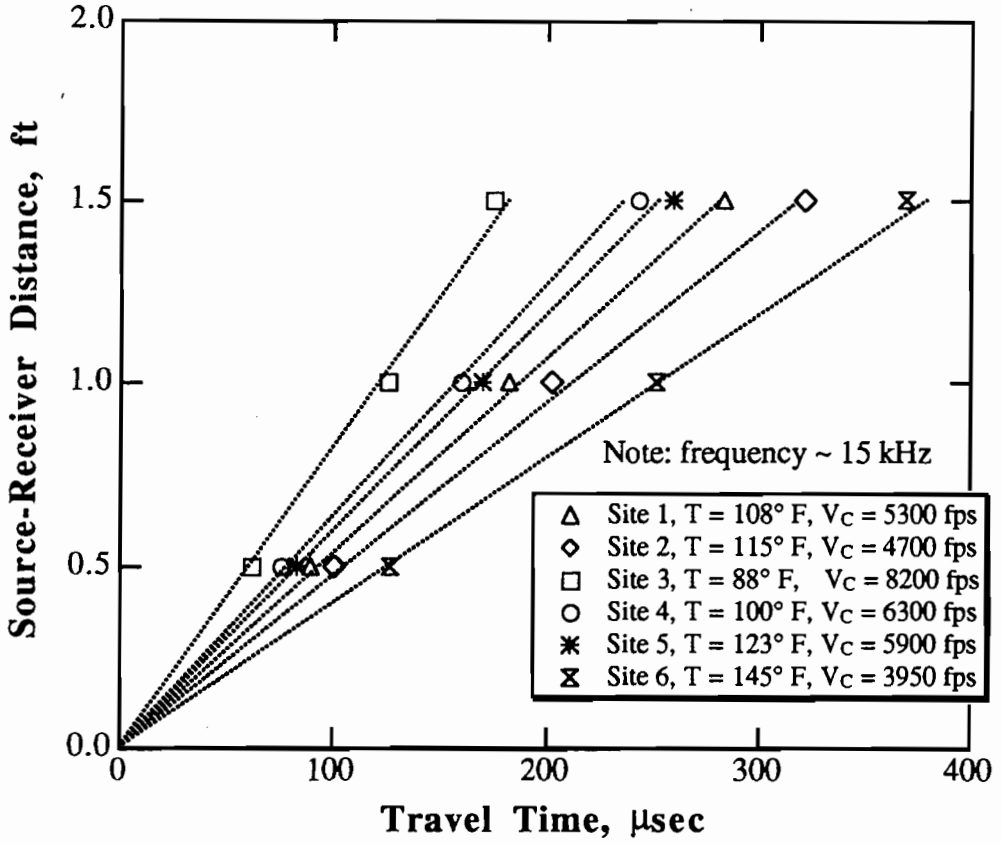

Fig 6.37. Travel Distances Versus Travel Times for P-Waves Measured at Sites 1 through 6; District 21, Texas.

6.5.2 SASW Measurements

SASW measurements were performed at six sites in District 21 using receiver spacings ranging from 0.15 to 9.1 m (0.5 to 30 ft). A comparison between the experimental and theoretical dispersion curves determined from SASW measurements is presented in Figs. 6.38 through 6.43 for Sites 1 through 6, respectively. Layer thicknesses used in the forward modeling were taken from the construction drawings and agreed well with the modeling results. The shear wave velocity profiles corresponding to the theoretical dispersion curves shown in Figs. 6.38 through 6.43 are presented in Tables 6.26 through 6.31, respectively.

Forward modeling of the SASW data showed that bedrock was not encountered at any of the test sites.

Young's moduli of the AC surface layer determined from P-wave and SASW measurements are compared in Fig. 6.44. At Sites 1, 2 and 6, Young's moduli were determined only from P-wave measurements. At Sites 3, 4 and 5, Young's moduli from both tests compare reasonably well (average within 5%). Note that Young's moduli of the AC layer represent values at high frequencies (on the order of 15 kHz for both tests). Frequency-adjusted values are presented and discussed in Section 6.7.3.

Young's moduli of the subgrade and base layers for the six sites in District 21 are presented in Figs. 6.45 and 6.46, respectively. The SASW tests showed that the subgrade changes stiffness with depth within the top 3 to 4.6 m (10 to 15 ft). Therefore, the stiffnesses of the upper and lower sublayers of the subgrade are presented in Fig. 6.45.

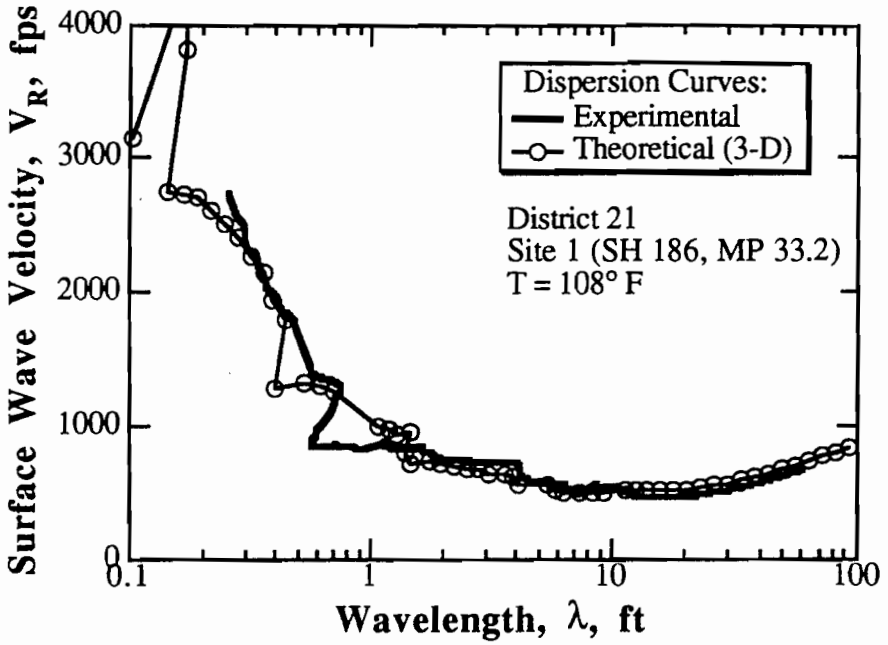

Fig 6.38. Comparison between the Experimental and Theoretical Dispersion Curves Determined at Site 1; District 21, Texas.

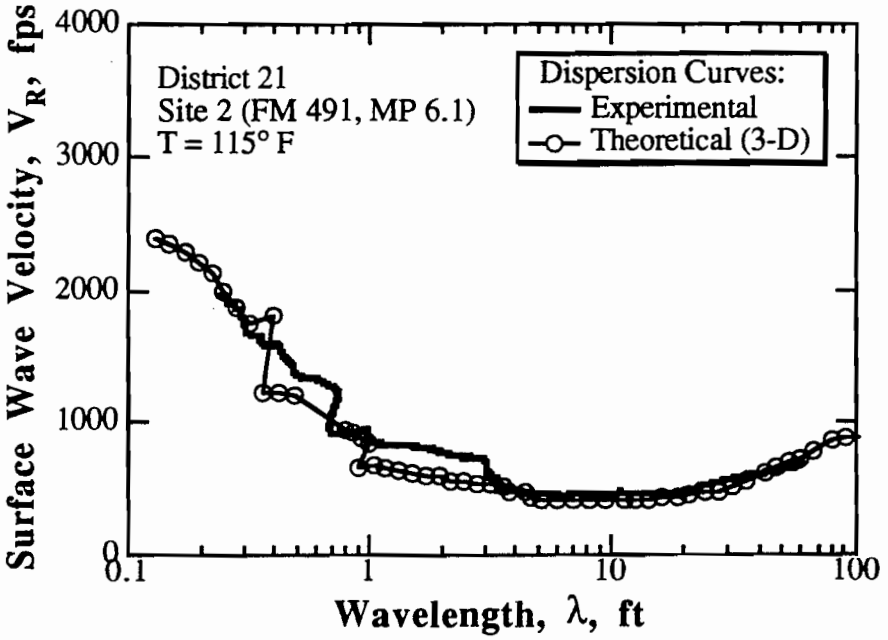

Fig 6.39. Comparison between the Experimental and Theoretical Dispersion Curves Determined at Site 2; District 21, Texas.

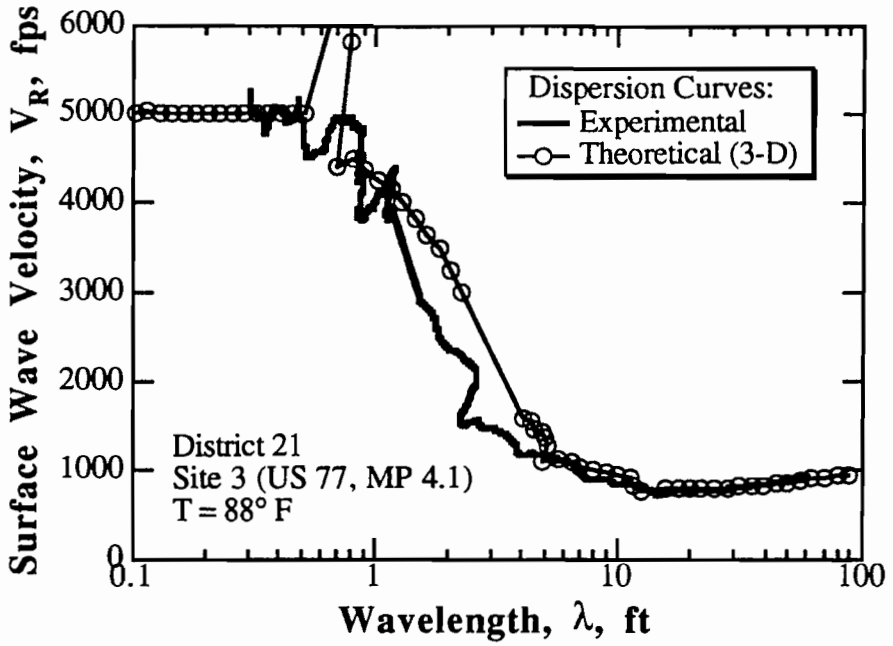

Fig 6.40. Comparison between the Experimental and Theoretical Dispersion Curves Determined at Site 3; District 21, Texas.

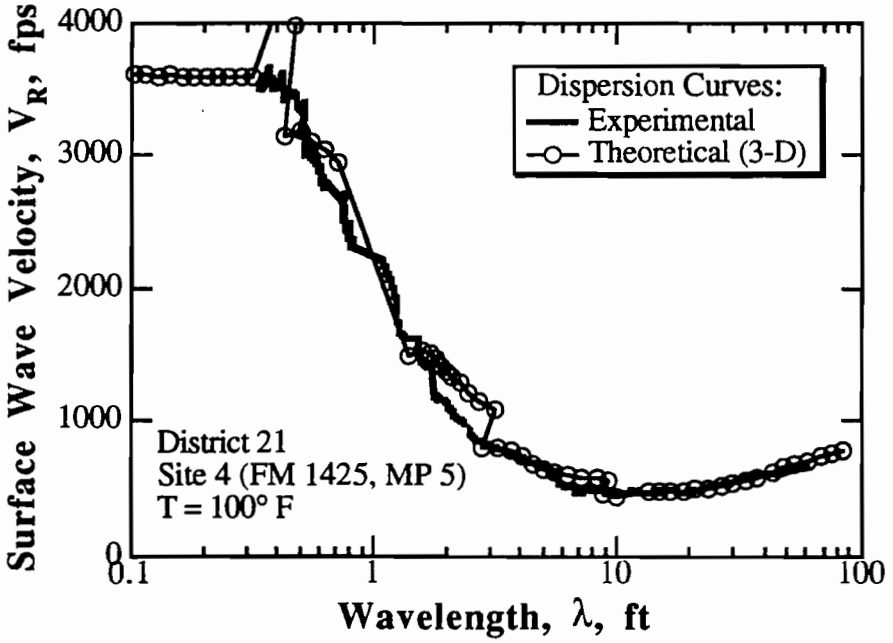

Fig 6.41. Comparison between the Experimental and Theoretical Dispersion Curves Determined at Site 4; District 21, Texas.

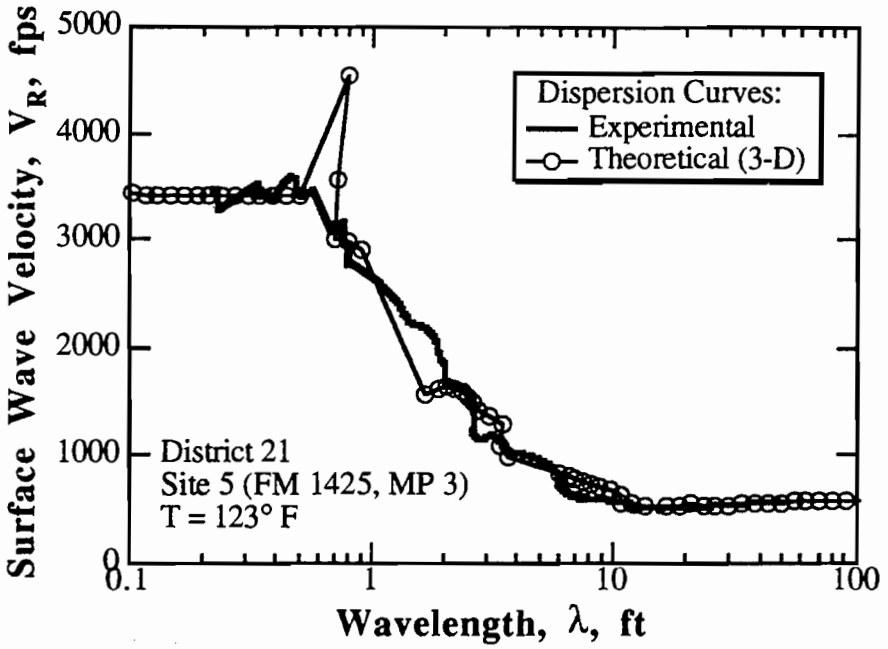

Fig 6.42. Comparison between the Experimental and Theoretical Dispersion Curves Determined at Site 5; District 21, Texas.

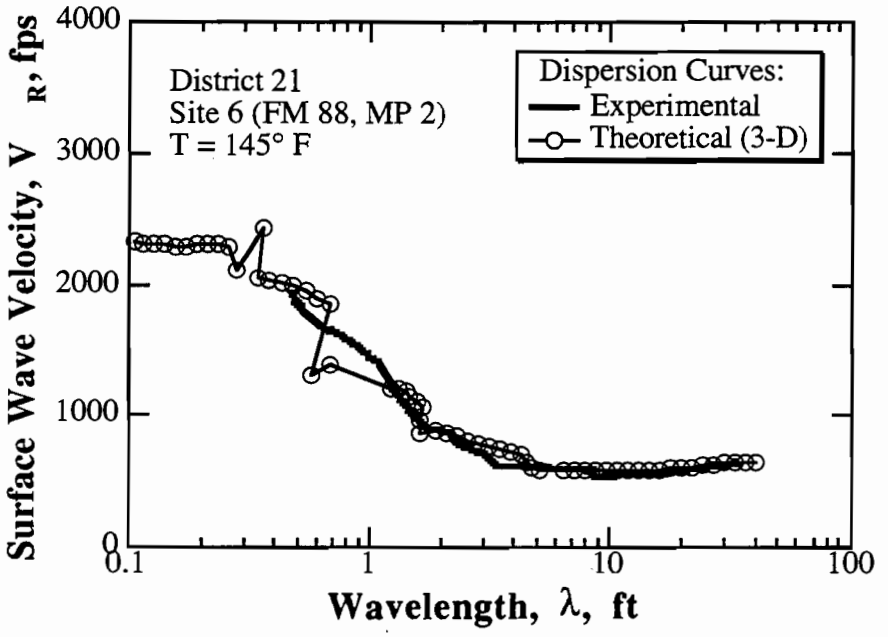

Fig 6.43. Comparison between the Experimental and Theoretical Dispersion Curves Determined at Site 6; District 21, Texas.

Table 6.26. Shear Wave Velocities and Young's Moduli Determined from SASW Measurements at Site 1 (SH 186); District 21, Texas

Layer Thickness (ft)	Shear Wave Velocity (fps)	Poisson's Ratio	Mass Density (Slugs)	Unit Weight (pcf)	Young's Modulus (ksi)
0.167	3,280*	0.309**	4.35	140	848
0.667	750	0.330	4.03	130	42
4.00	520	0.330	3.73	120	19
6.00	460	0.330	3.73	120	15
10.00	700	0.330	3.73	120	34
Half-Space	900	0.330	3.73	120	56

* Determined from the compression wave velocity measured at Site 1
** Assumed from resonance tests on asphalt cylinders presented in Fig. 5.32

Table 6.27. Shear Wave Velocities and Young's Moduli Determined from SASW Measurements at Site 2 (FM 491); District 21, Texas

Layer Thickness (ft)	Shear Wave Velocity (fps)	Poisson's Ratio	Mass Density (Slugs)	Unit Weight (pcf)	Young's Modulus (ksi)
0.083	2,890*	0.319**	4.35	140	667
0.458	700	0.330	4.03	130	37
12.00	420	0.330	3.73	120	12
10.00	900	0.330	3.73	120	56
Half-Space	1,000	0.330	3.73	120	69

* Determined from the compression wave velocity measured at Site 2
** Assumed from resonance tests on asphalt cylinders presented in Fig. 5.32

Table 6.28. Shear Wave Velocities and Young's Moduli Determined from SASW Measurements at Site 3 (US 77); District 21, Texas

Layer Thickness (ft)	Shear Wave Velocity (fps)	Poisson's Ratio	Mass Density (Slugs)	Unit Weight (pcf)	Young's Modulus (ksi)
0.541	5,300	0.285*	4.35	140	2,180
1.75	900	0.330	4.03	130	60
12.00	720	0.330	3.73	120	36
10.00	900	0.330	3.73	120	56
Half-Space	1,000	0.330	3.73	120	69

* Assumed from resonance tests on asphalt cylinders presented in Fig. 5.32

Table 6.29. Shear Wave Velocities and Young's Moduli Determined from SASW Measurements at Site 4 (FM 1425, MP 5); District 21, Texas

Layer Thickness (ft)	Shear Wave Velocity (fps)	Poisson's Ratio	Mass Density (Slugs)	Unit Weight (pcf)	Young's Modulus (ksi)
0.333	3,800	0.295*	4.35	140	1,129
0.416	800	0.330	4.03	130	48
12.00	450	0.330	3.73	120	14
10.00	800	0.330	3.73	120	44
Half-Space	900	0.330	3.73	120	56

* Assumed from resonance tests on asphalt cylinders presented in Fig. 5.32

Table 6.30. Shear Wave Velocities and Young's Moduli Determined from SASW Measurements at Site 5 (FM 1425, MP 3); District 21, Texas

Layer Thickness (ft)	Shear Wave Velocity (fps)	Poisson's Ratio	Mass Density (Slugs)	Unit Weight (pcf)	Young's Modulus (ksi)
0.50	3,600	0.327*	4.35	140	1,039
0.50	850	0.330	4.03	130	54
3.00	550	0.330	3.73	120	21
12.00	500	0.330	3.73	120	17
Half-Space	600	0.330	3.73	120	25

* Assumed from resonance tests on asphalt cylinders presented in Fig. 5.32

Table 6.31. Shear Wave Velocities and Young's Moduli Determined from SASW Measurements at Site 6 (FM 88); District 21, Texas

Layer Thickness (ft)	Shear Wave Velocity (fps)	Poisson's Ratio	Mass Density (Slugs)	Unit Weight (pcf)	Young's Modulus (ksi)
0.250	2,400*	0.350	4.35	140	471
0.583	800	0.330	4.03	130	48
5.00	550	0.330	3.73	120	21
5.00	600	0.330	3.73	120	25
Half-Space	700	0.330	3.73	120	34

* Determined from the compression wave velocity measured at Site 6

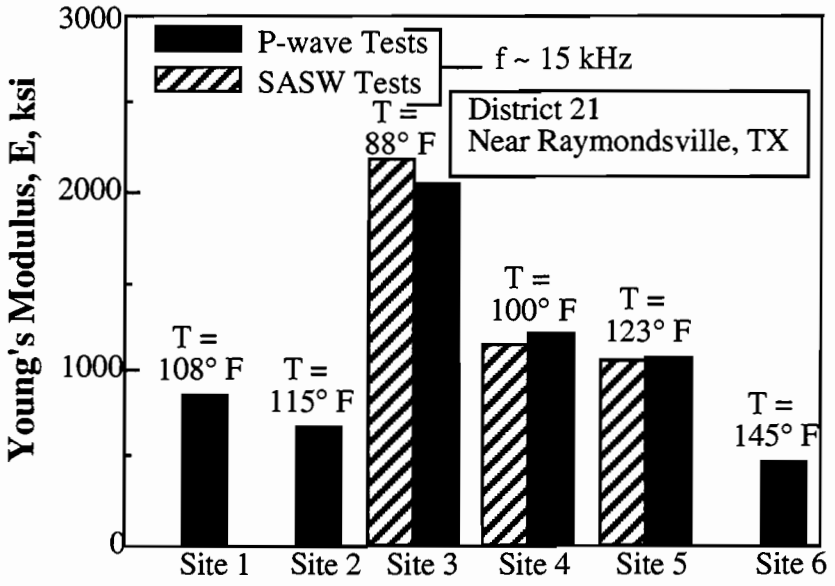

Fig 6.44. Comparison of Young's Moduli of the AC Layer As Determined from P-Wave and SASW Measurements; District 21, Texas.

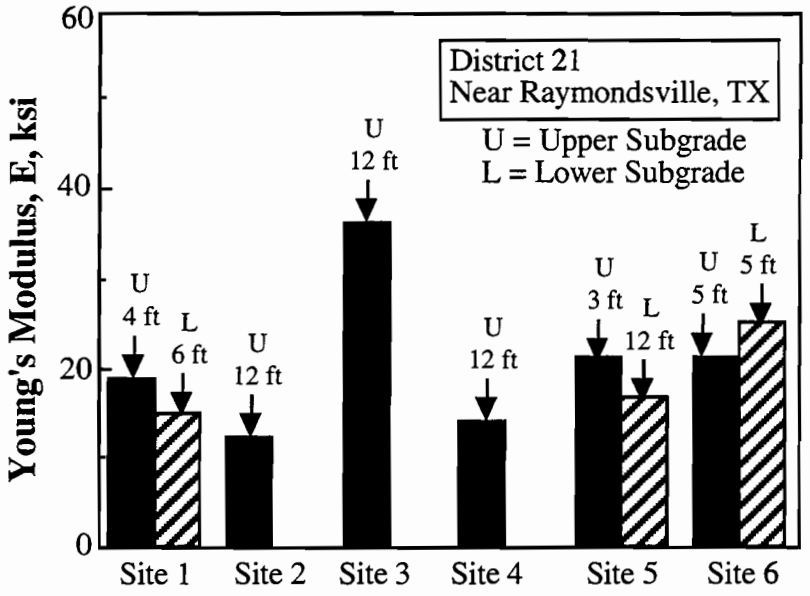

Fig 6.45. Young's Moduli of the Subgrade As Determined from SASW Measurements; District 21, Texas.

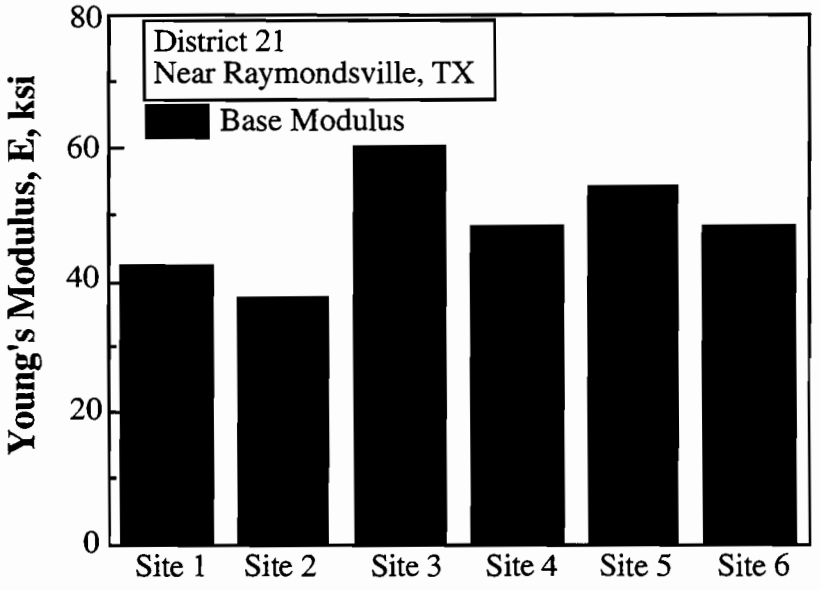

Fig 6.46. Young's Moduli of the Base As Determined from SASW Measurements; District 21, Texas.

6.6 Simplified Procedure for Determining Subgrade Stiffness

The SASW test is a nondestructive test that can be rapidly performed in the field. Development of experimental dispersion curves from the "raw" SASW data is also quite simple. However, to obtain the variation of shear wave velocity with depth, an iterative procedure is used (forward modeling). This process can be time-consuming, especially for pavement sites where use of the 3-D (Foinquinos, 1991) modeling is necessary.

Based on the authors' experience in modeling pavement sites, a simplified procedure is recommended to obtain the subgrade stiffness. However, this simplified procedure should not be considered as an alternative for the forward modeling process, especially when a detailed shear wave velocity profile for the site is desired. To obtain the stiffness of the base material in pavement sites, forward modeling of the SASW data must be performed.

In the simplified procedure, receiver spacings of 3, 6.1 and 9.1 m (10, 20 and 30 ft) are recommended. The receiver spacing of 3 m (10 ft) ensures that the influence of the surface layer on the wavelengths sampling the subgrade material is minimized. This is true only if the AC layer is no more than about 30.5 cm (12 in.) thick and the base and subgrade are not stabilized or cement-treated. The receiver spacing of 6.1 m (20 ft) generates appropriate wavelengths for sampling the subgrade. The receiver spacing of 9.1 m (30 ft) is used to possibly identify the presence of shallow bedrock, potentially a key element in the analysis of FWD data. Receiver spacings of 3, 6.1 and 9.1 m (10, 20 and 30 ft) are recommended because the SASW test can be performed in conjunction with the FWD test (performed every 3 m (10 ft) on a pavement section), using the FWD drop weight as a source. The FWD drop weight leaves no marks on the pavement surface, as opposed to sledge hammers, which can slightly damage the pavement surface if no protective pad is employed. Also, the FWD source generates appropriate frequencies for the recommended receiver spacings, depending on the weight and height of the drop. Typical phase shifts of the cross power spectra for receiver spacings of 3.0, 6.1 and 9.1 m (10, 20 and 30 ft) using the FWD drop weight as a source are shown in Figs. 6.47a through 6.47c, respectively.

Once the SASW measurements are completed, a composite dispersion curve based on receiver spacings of 3, 6.1 and 9.1 m (10, 20 and 30 ft) is calculated. Figure 6.48 shows these dispersion curves determined for Sites 1 through 5 in District 1. Also shown in Fig. 6.48 are the average surface wave velocities determined for the subgrade at Sites 1 through 5. However, the stiff surface layer makes the subgrade appear to be stiffer by about 10% (in terms of velocity) based on the forward modeling presented in Section 6.2.2. As a result, in the simplified procedure, the average surface velocities determined from the experimental dispersion curves are assumed to be the shear wave velocities of the subgrade to account for the approximately 10% increase in velocity due to the influence of the surface layer. The shear wave velocity of the subgrade, V_S, at Sites 1, 4 and 5 averaged 162 m/s (530 fps). At Sites 2 and 3, the shear wave velocities averaged 143 and 198 m/s (470 and 650 fps), respectively. Young's moduli of the subgrade determined from these shear wave velocities (simplified procedure) are compared to those obtained from the modeling process in Fig. 6.49. As shown in Fig. 6.49, Young's moduli from the two procedures compare reasonably well (average within 9%), and the simplified procedure is suggested as a rapid method for determining the average stiffness of the subgrade.

The simplified procedure described above was used to calculate Young's moduli of the subgrade at the sites tested in Districts 8, 11 and 21. Young's moduli of the subgrade determined from the simplified procedure are compared to those obtained from the modeling process in Figs. 6.50 through 6.52 for Districts 8, 11 and 21, respectively. It should be noted that the subgrade moduli obtained from the modeling process were averaged over depths ranging from 2.4 to 3.7 m (8 to 12 ft). Young's moduli of the subgrade from the two procedures compare reasonably well (average within 8%). Only at Sites 4 and 6 in District 8 does the simplified procedure yield higher values of the subgrade stiffness than the forward modeling. This happened because the subgrade layer is trapped between two stiffer layers, the AC-base layers on top and the shallow bedrock below.

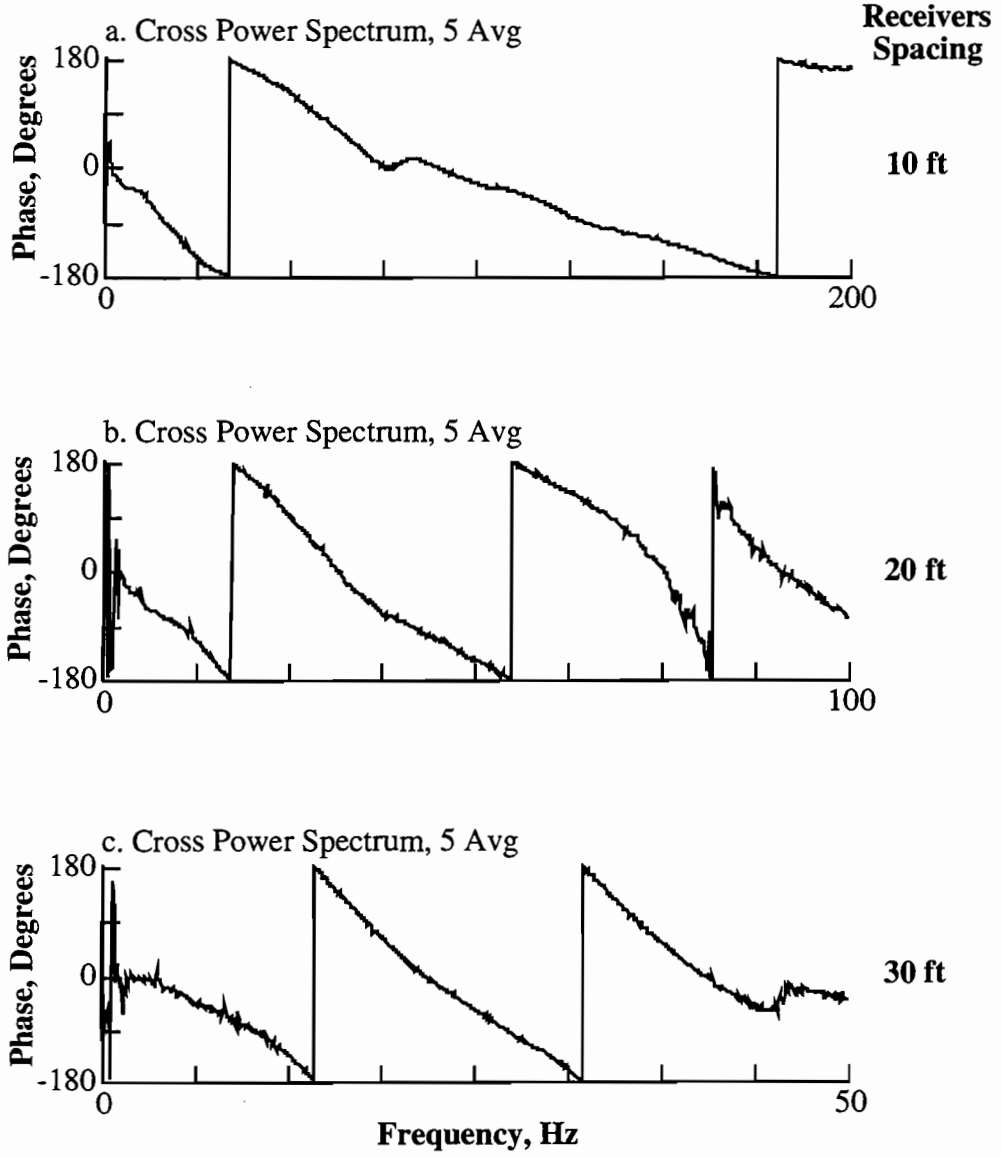

Fig 6.47. Phase Shifts of the Cross Power Spectra between the Two Receivers for Spacings of 10, 20 and 30 ft Using the FWD Drop Weight as a Source; Site 3, District 1, Texas.

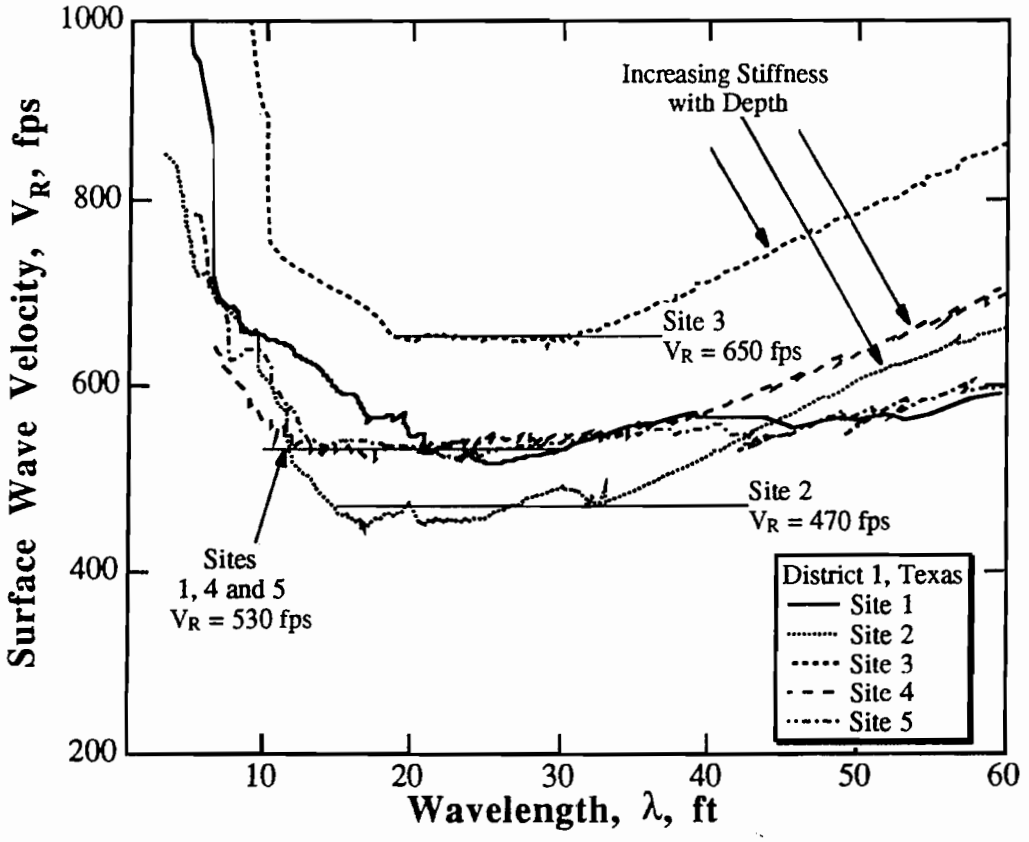

Fig 6.48. Experimental Dispersion Curves Determined from SASW Measurements Using Receiver Spacings of 10, 20 and 30 ft at Sites 1 through 5; District 1, Texas.

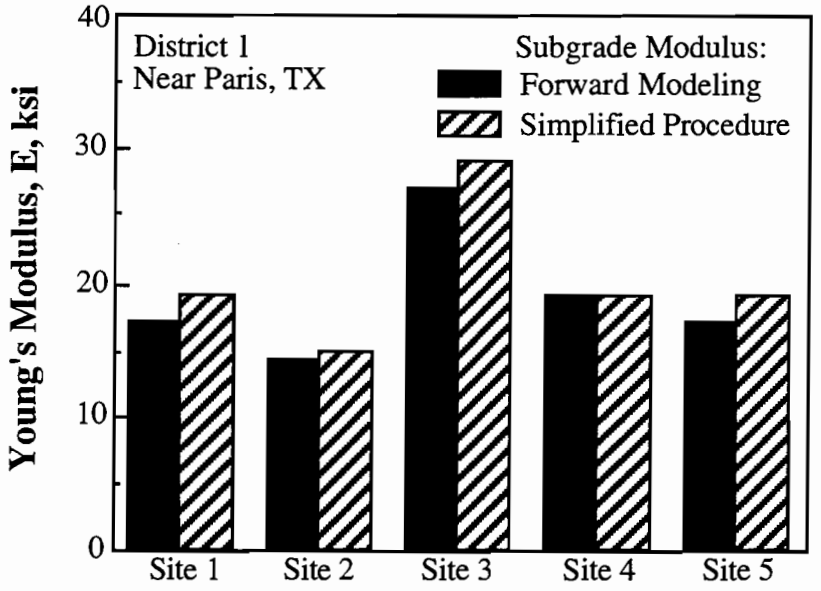

Fig 6.49. Comparison of Young's Moduli of the Subgrade As Determined from Modeling the SASW Measurements and from the Simplified Procedure; Sites 1 Through 5, District 1, Texas.

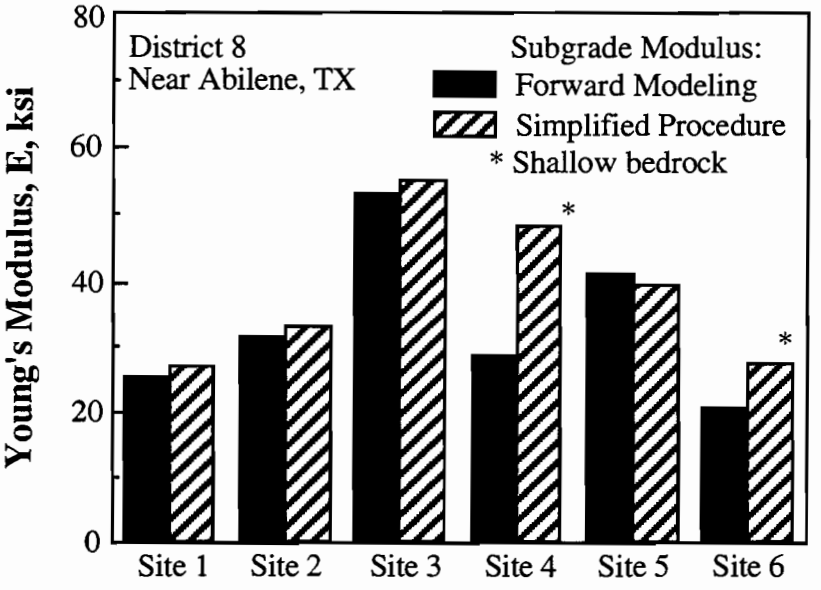

Fig 6.50. Comparison of Young's Moduli of the Subgrade As Determined from Modeling the SASW Measurements and from the Simplified Procedure; Sites 1 Through 6, District 8, Texas.

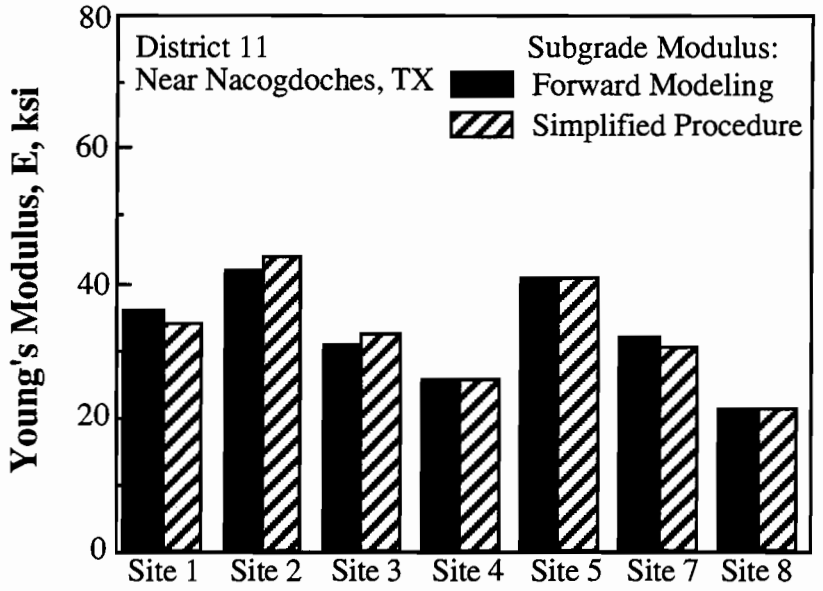

Fig 6.51. Comparison of Young's Moduli of the Subgrade As Determined from Modeling the SASW Measurements and from the Simplified Procedure; Sites 1 Through 8, District 11, Texas.

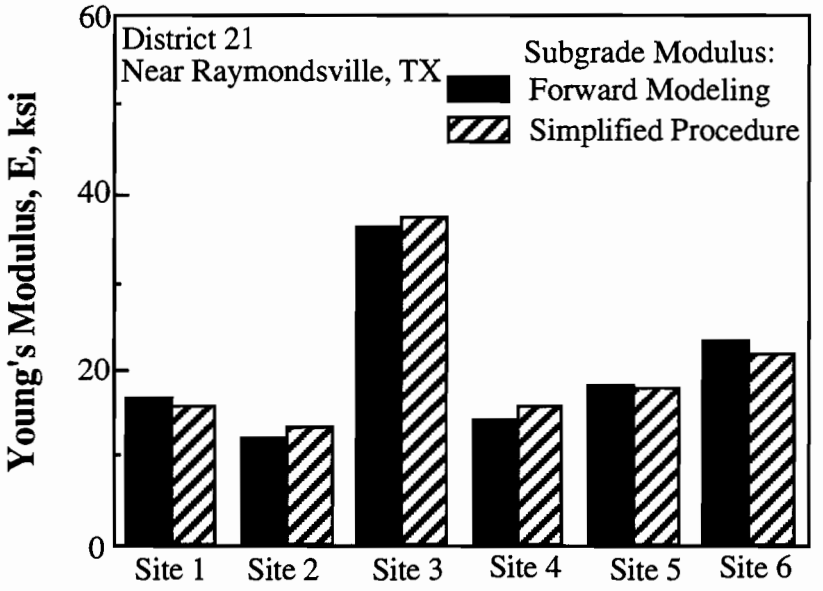

Fig 6.52. Comparison of Young's Moduli of the Subgrade As Determined from Modeling the SASW Measurements and from the Simplified Procedure; Sites 1 Through 6, District 21, Texas.

6.7 Comparison of Layer Moduli from SASW and FWD Tests

FWD tests were performed and analyzed by personnel from Texas A&M University in conjunction with Project 1175. They graciously supplied the FWD results which are presented herein. The SASW-determined subgrade moduli were calculated after completion of forward modeling by using Eq. 2.3 with assumed values of 18.9 kN/m^3 (120 pcf) for total unit weight and 0.33 for Poisson's ratio.

6.7.1 Subgrade Moduli

Young's moduli of the subgrade layers determined from SASW and FWD measurements at the 23 sites in Districts 1, 8, 11 and 21 where both types of tests were performed are compared in Figs. 6.53 through 6.56, respectively. Average values of Young's moduli from the SASW tests are presented which were weighted over a depth range from 2.4 to 3.7 m (8 to 12 ft) at each site depending on the site profile. The SASW-determined subgrade moduli were higher than those determined from the FWD tests in 22 out of the 23 sites. The one case where the FWD results yielded a higher subgrade modulus was that of Site 4 in District 11. The SASW-determined subgrade moduli ranged from 6% below to 200% above the FWD values and averaged 53% above them.

An attempt was made to determine whether the differences in subgrade moduli evaluated by the SASW and FWD tests were related in a systematic way to any measured variables at the 23 pavement sites where both tests were performed. This was done by investigating the relationship between the SASW- and FWD-determined moduli in terms of: 1) the thickness of the surface layer (which also indirectly accounts for the stiffness of the surface layer), 2) the combined thickness of the surface and base layers (and subbase layer if one existed), 3) the subgrade type, and 4) the stiffness of the subgrade. The ratio of the SASW- and FWD-

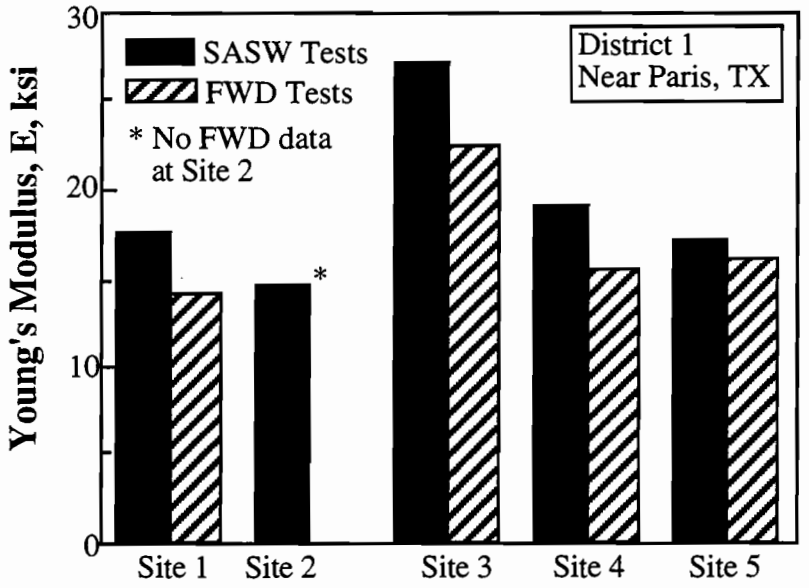

Fig 6.53. Comparison of Young's Moduli of the Subgrade As Determined from SASW and FWD Measurements; District 1, Texas.

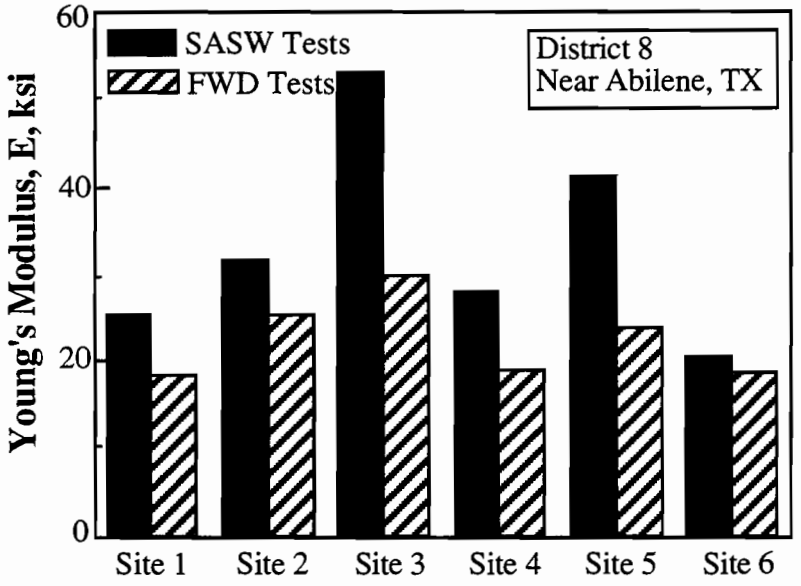

Fig 6.54. Comparison of Young's Moduli of the Subgrade As Determined from SASW and FWD Measurements; District 8, Texas.

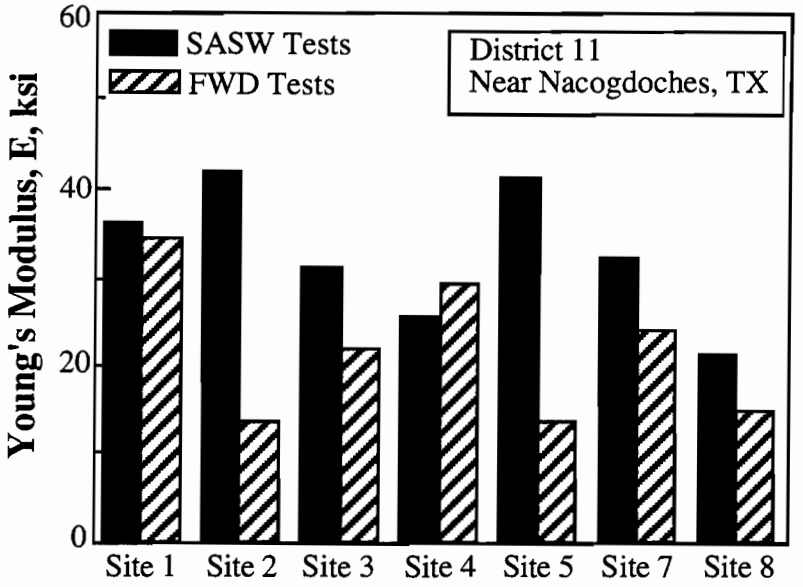

Fig 6.55. Comparison of Young's Moduli of the Subgrade As Determined from SASW and FWD Measurements; District 11, Texas.

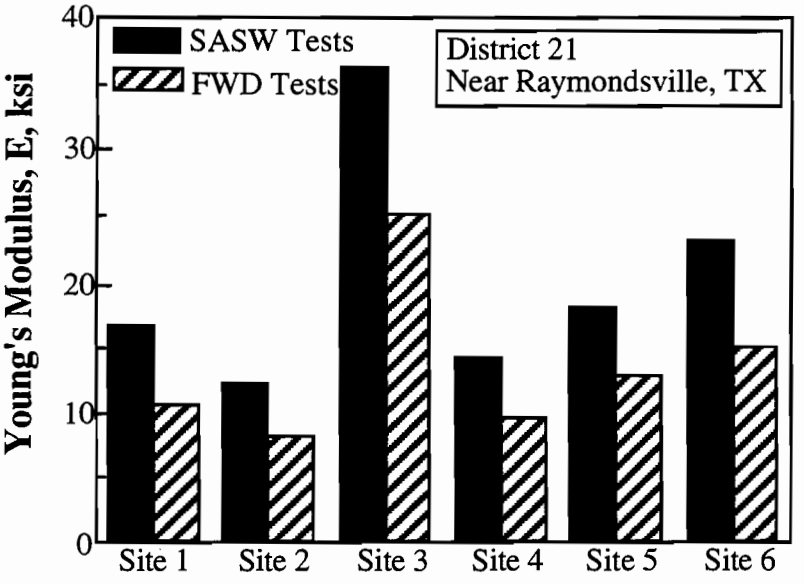

Fig 6.56. Comparison of Young's Moduli of the Subgrade As Determined from SASW and FWD Measurements; District 21, Texas.

determined subgrade moduli at each site was expressed as a normalized modulus, E_{FWD} / E_{SASW}.

The variation in normalized modulus with the four pavement variables listed above is shown in Figs. 6.57 through 6.60. Clearly there is no significant correlation in normalized modulus with surface layer thickness or with the combined thickness of the surface and base layers. Best-fit linear relationships (based on least squares) placed through the data are nearly horizontal. A slight trend of decreasing normalized modulus with increasing stiffness of the subgrade is shown in Fig. 6.59. However, the trend is rather marginal. There is also a trend of increasing values of normalized modulus as subgrade type changes from sand and silty sand to clay to sandy clay. The average values of E_{FWD} / E_{SASW} are 0.61, 0.83 and 0.74, respectively. If one simply divides the subgrade materials into two categories, sandy materials and clayey materials (by combining the sandy clay and clay categories), the respective average normalized moduli are 0.61 and 0.79, respectively, which shows the trend.

The difference between the subgrade moduli determined by the SASW and FWD tests may be due, in part, to larger strains generated during FWD testing. However, adjustment for the strain level was difficult because the strains associated with the FWD tests are not known. In addition, the nonlinear behavior of the subgrade materials was not studied. However, if an average strain level adjustment factor (a factor of 0.75 was used to adjust the SASW-determined moduli to compare with those from the FWD tests at the Loop 1 site (see Fig. 5.21)) suggested by Miner (1991) is used for adjusting the SASW-determined moduli of the subgrade at the 23 sites presented herein, then the adjusted SASW- and FWD-determined moduli values compare reasonably well except for Sites 1, 2, 4 and 5 in District 11, as shown in Fig. 6.61.

The modulus adjustment factor for strain level (0.75) suggested by Miner (1991) compares well with the average normalized modulus of 0.79 determined for clayey subgrades presented in this study. However, the average normalized

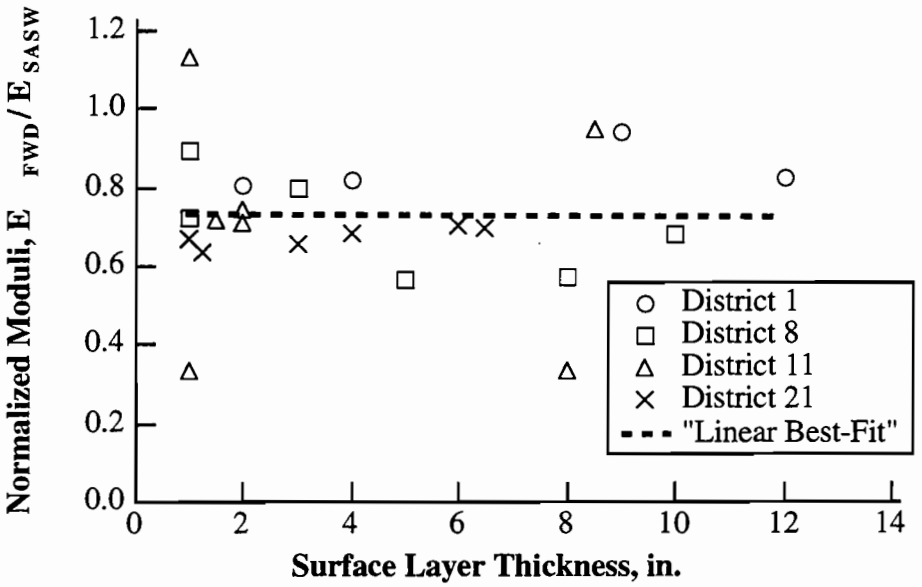

Fig 6.57. Normalized Modulus of the Subgrade Determined from FWD and SASW Tests versus Thickness of the Surface Layer.

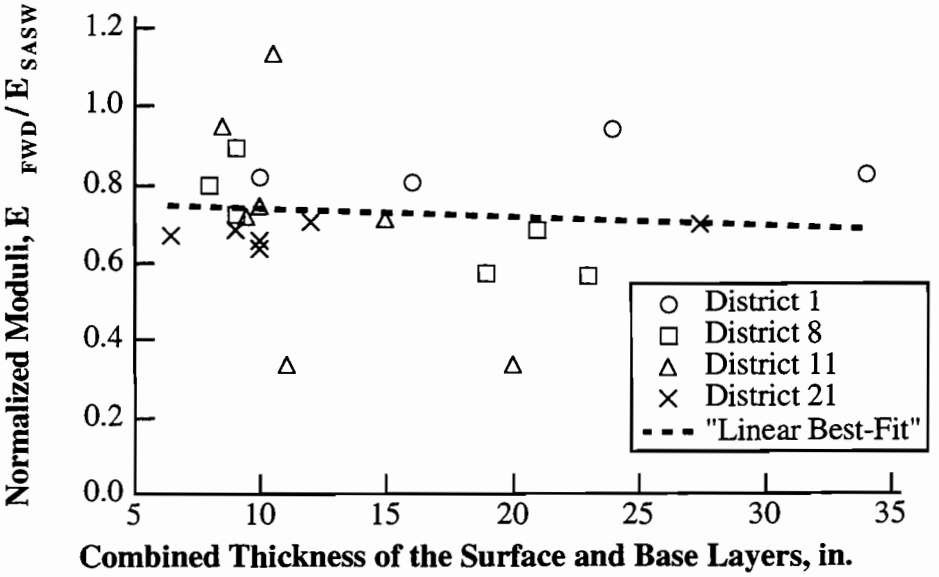

Fig 6.58. Normalized Modulus of the Subgrade Determined from FWD and SASW Tests versus Combined Thickness of the Surface and Base Layers.

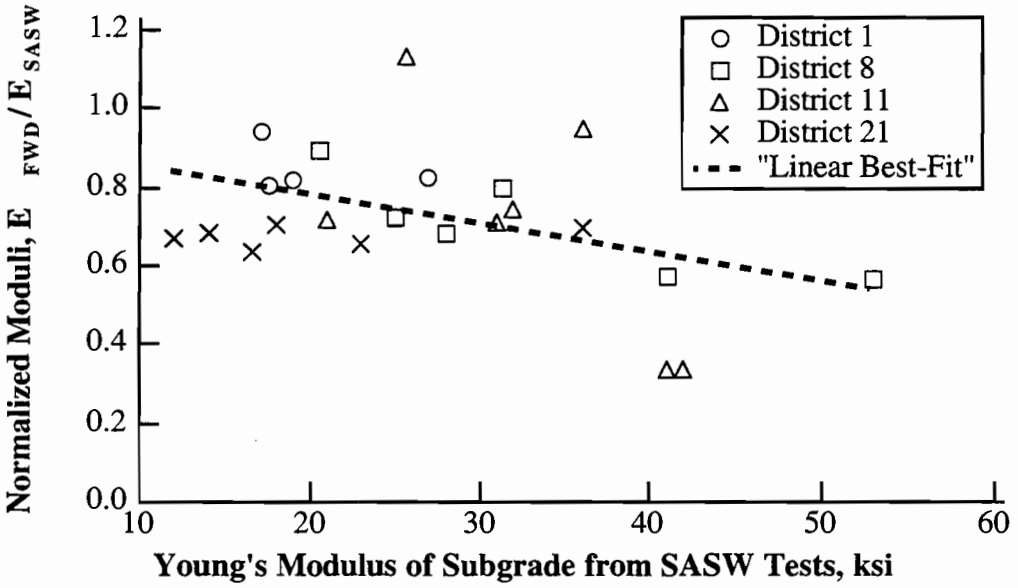

Fig 6.59. Normalized Modulus of the Subgrade Determined from FWD and SASW Tests versus Young's Modulus of the Subgrade Determined from SASW Tests.

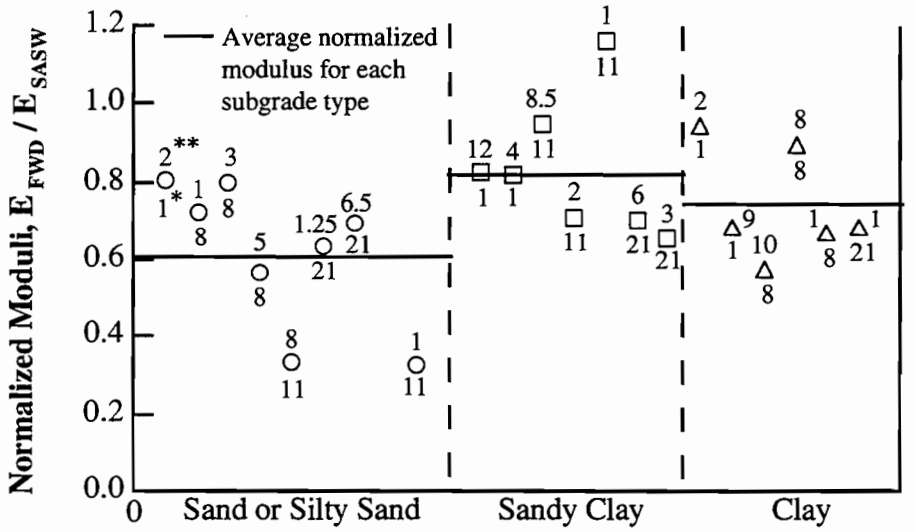

* Numbers below symbols represent district number
** Numbers above symbols represent thickness of surface layer in inches.
No correlation with surface layer thickness within each subgrade type.

Fig 6.60. Normalized Modulus of the Subgrade Determined from FWD and SASW Tests versus Subgrade Type.

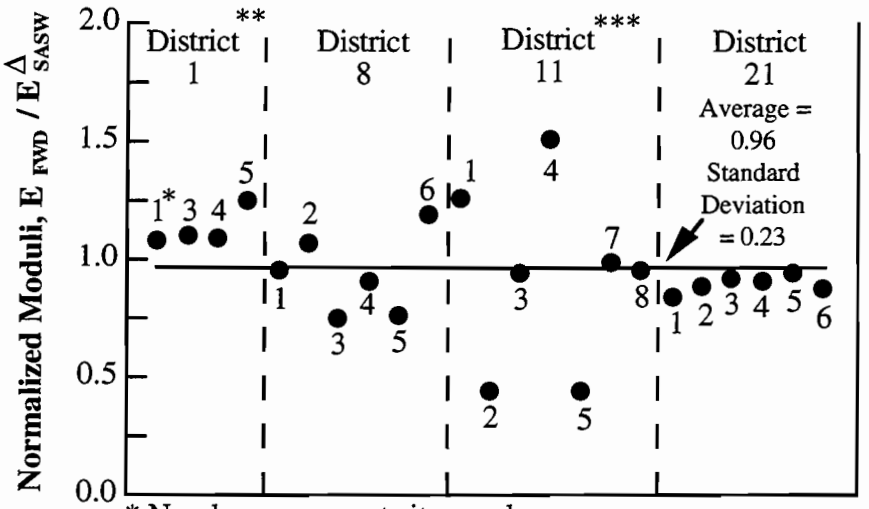

* Numbers represent site numbers

** No FWD tests at Site 2

*** No SASW tests at Site 6

Δ Adjusted to 75% of original value to correct for FWD strain level

Fig 6.61. Normalized Modulus of the Subgrade Determined from FWD and SASW Tests after Adjustment for Strain Level.

modulus for sandy subgrades presented in this study was equal to 0.61, and is suggested for adjusting the SASW-determined moduli of sandy subgrades to correct for the strain level in the FWD tests.

6.7.2 Base Moduli

Young's moduli of the granular base layers determined from SASW and FWD measurements at the 23 sites in Districts 1, 8, 11 and 21 are compared in Figs. 6.62 through 6.65, respectively. Moduli determined from the SASW tests were higher in all but three cases (Site 5 in District 1 and Sites 3 and 4 in District 21) than those determined from the FWD tests. In addition, the base and AC surface layer were combined into one layer and assigned one modulus in the analysis of the FWD data for all thin pavement sites (thickness ≤ 7.6 cm (3 in.)). Normalized values of the base moduli (E_{FWD} / E_{SASW}) for all sites are shown in Fig. 6.66. Site 3 in District 21 was excluded from Fig. 6.66 for a clearer comparison because of the unreasonably high value of the base modulus from the FWD test.

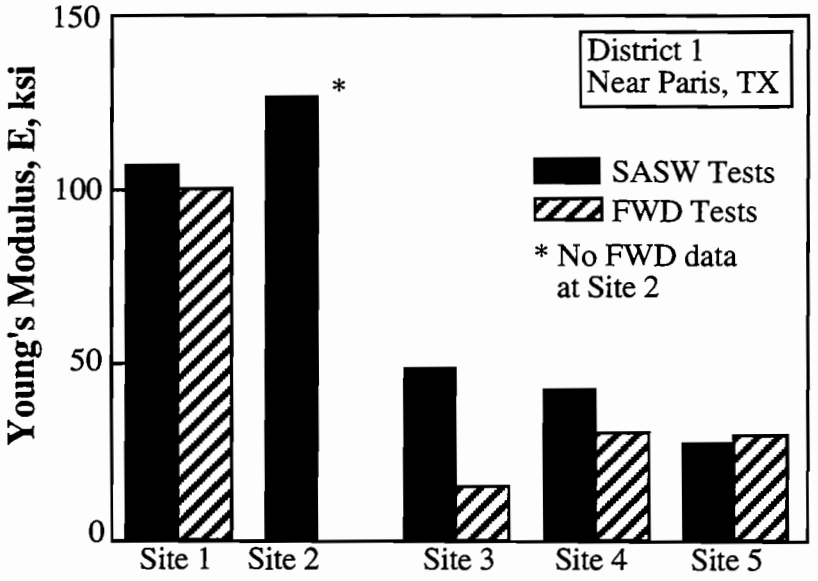

Fig 6.62. Comparison of Young's Modulus of the Base As Determined from SASW and FWD Measurements; District 1, Texas.

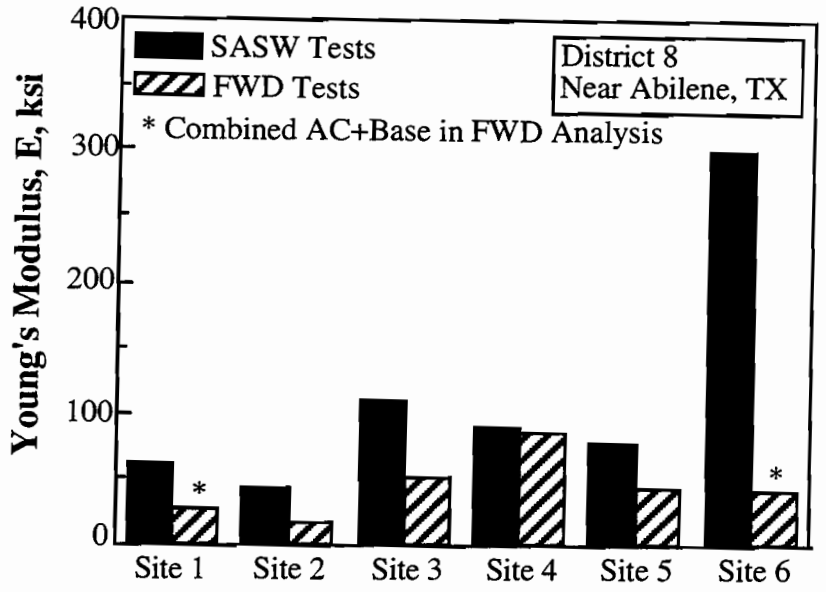

Fig 6.63. Comparison of Young's Modulus of the Base As Determined from SASW and FWD Measurements; District 8, Texas.

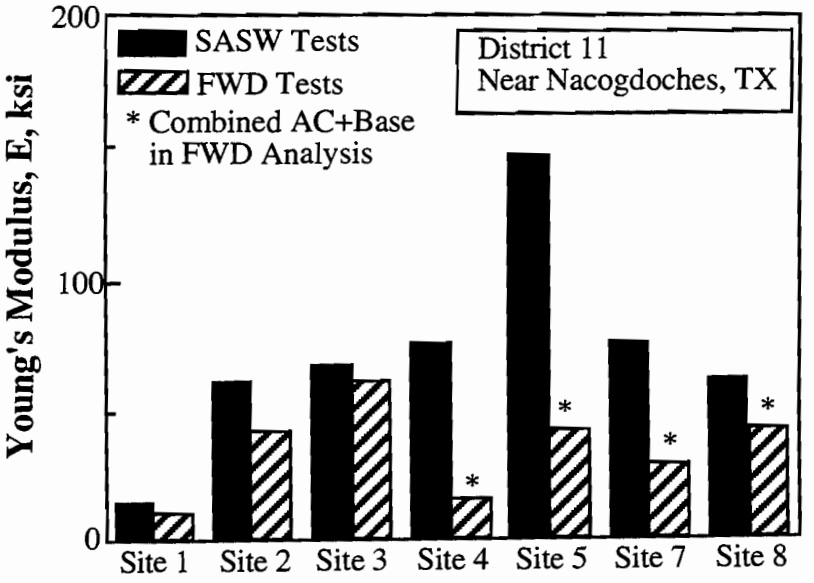

Fig 6.64. Comparison of Young's Modulus of the Base As Determined from SASW and FWD Measurements; District 11, Texas.

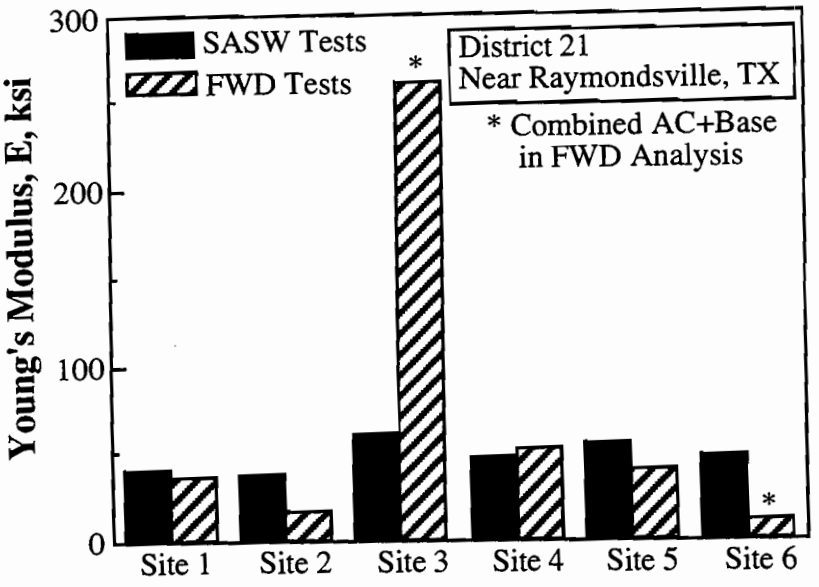

Fig 6.65. Comparison of Young's Modulus of the Base As Determined from SASW and FWD Measurements; District 21, Texas.

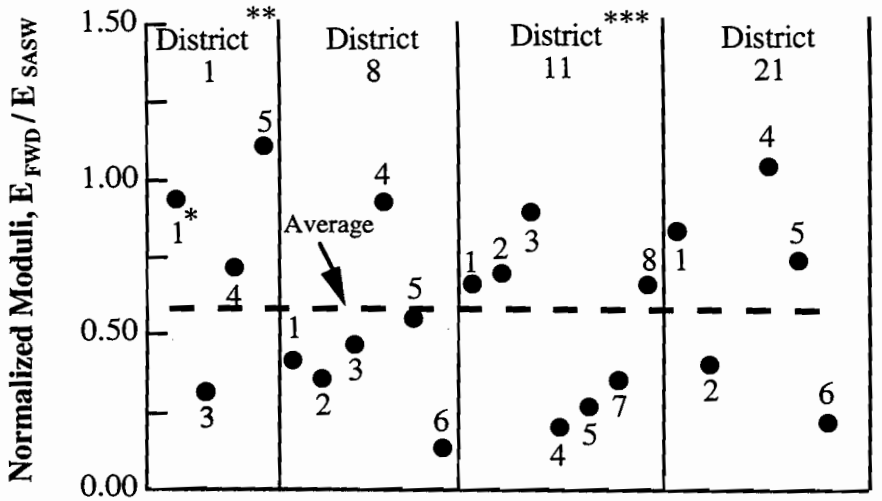

Fig 6.66. Normalized Modulus of the Base Determined from FWD and SASW Tests (excluding Site 3 in District 21).

No trend exists between normalized modulus and the pavement variables discussed in Section 6.7.1. The average value of E_{FWD} / E_{SASW} for the base materials at the 22 sites shown in Fig. 6.66 (excluding Site 3 in District 21) is equal to 0.59. If one separates pavement sites into sites with thin and with thick surface layers, then the average values of E_{FWD} / E_{SASW} are 0.48 and 0.72 for thin (thickness $\leq$ 7.6 cm (3 in.)) and thick surface layers, respectively. These values can be assumed to represent a "first-order" strain correction factor. If this is done, then the strain adjustment factor applied to the uncemented granular bases with thick AC surface layers is 0.72, and applied to uncemented granular bases with thin AC surface layers is 0.48.

6.7.3 Asphalt Concrete Moduli

Young's moduli of the AC layers determined from SASW tests at pavements with thick surface layers (t > 7.6 cm (3 in.)) are presented in Fig. 6.67 along with the best-fit curve determined from the SASW tests at the TTI test facility in Bryan, Texas. Figure 6.67 shows the general trend of decreasing values of Young's moduli with the increasing surface temperature. Young's moduli of the thick AC layers in the four districts were usually lower (except for three cases: District 1, Site 4; District 8, Site 4; District 21, Site 3) than those determined at the TTI facility. It must be remembered that different asphalt concrete materials were most likely used at the different districts and even within a district. However, the proper trend is clearly evident.

Young's moduli of the AC surface layers determined from SASW and P-wave tests at the 24 pavement sites are presented in Fig. 6.68. Note that these moduli represent values at high frequencies (on the order of 15 kHz, except the moduli from P-wave tests in District 1 (f ~ 3.5 kHz)). Also note that P-wave measurements were not performed in District 11. Young's moduli of the thin AC layers in District 11 were obtained from the initial parts of the experimental dispersion curves determined from the SASW tests. A best-fit linear relationship (based on least squares) was placed through the data. The linear relationship followed the same trend observed at the TTI test facility with lower moduli for the AC layers. It must be remembered that the TTI test facility is not open for traffic.

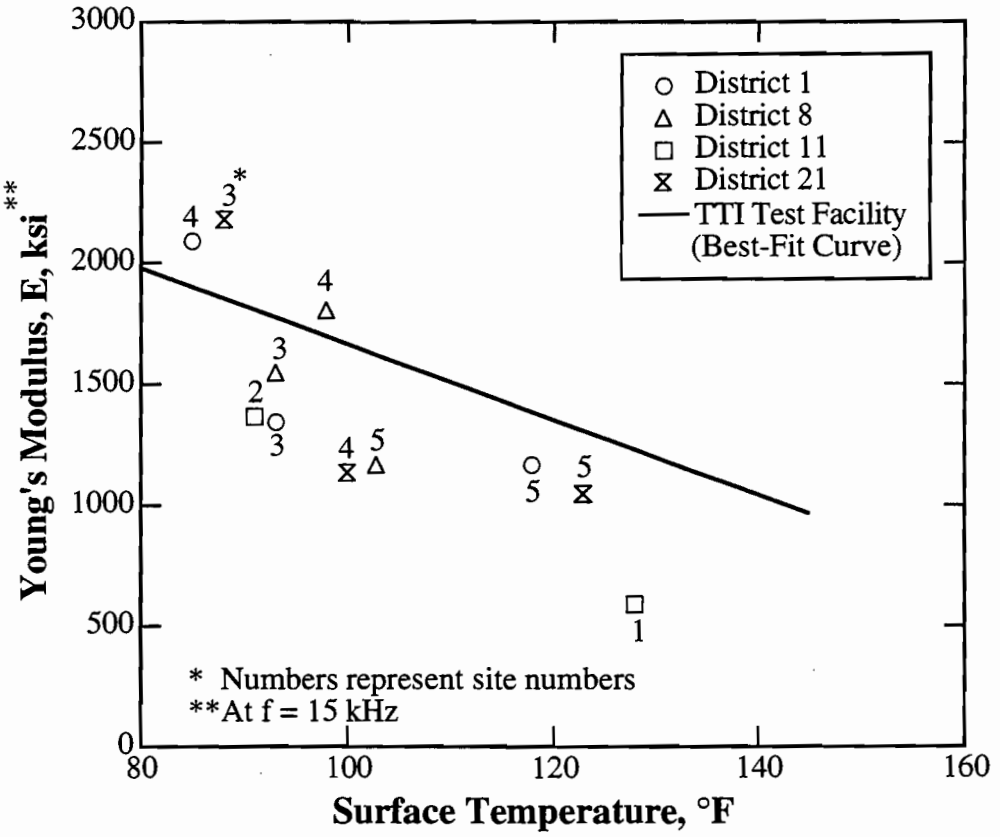

Fig 6.67. Young's Modulus of the AC Surface Layer Determined from SASW Tests at Thick Pavement Sites (t > 3 in.) in Four Districts in Texas.

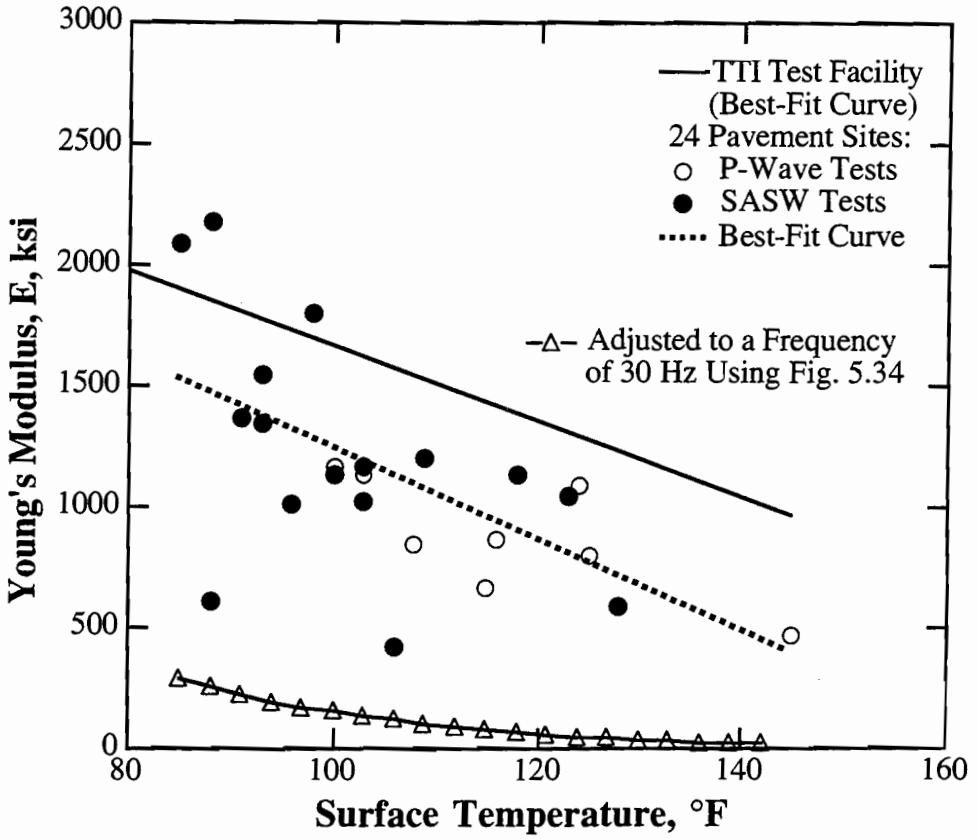

Fig 6.68. Young's Modulus of the AC Surface Layer Determined from SASW and P-Wave Tests at the 24 Pavement Sites.

This may explain the lower moduli of the AC layers observed at the 24 pavement sites as compared to those determined at the TTI test facility. Young's moduli of the AC layers at a frequency of 30 Hz were then obtained from the best-fit curve using Fig. 5.34. These moduli are shown in Fig. 6.68 in triangular symbols and are the moduli that should be used in the design of pavements.

Young's moduli of the thick AC layers in the four districts determined from SASW and FWD tests are compared in Fig. 6.69. Young's moduli determined from SASW tests are higher than those determined from FWD tests due to the effects of frequency and temperature. Figure 5.34 was then used to adjust the SASW-determined moduli to a frequency of 30 Hz to compare with the FWD moduli. It should be noted that the moduli from the SASW tests were first adjusted, using Eq. 5.8, to represent moduli at the same temperatures as those recorded during the FWD tests. A comparison between the moduli of the thick AC layers at the 11 pavement sites tests is presented in Fig. 6.70. The moduli from the SASW tests after adjustment for temperature and frequency effects compare relatively well with those determined from the FWD tests, except at Sites 3 and 4 in District 1 and at Site 3 in District 8. The average value of E_{FWD} / E_{SASW} after frequency and temperature adjustments is 1.1. This good comparison is a bit misleading because there is significant scatter in the results. It is the opinion of the authors that much of this scatter results from the lack of resolution of the surface layer inherent in FWD testing. Figure 6.70 also shows the poor comparison of the moduli from SASW and FWD tests before adjusting for temperature and frequency. The average value of E_{FWD} / E_{SASW} before any adjustment is 0.17.

6.7.4 Bedrock Depth

SASW results showed that bedrock exists at depths of 2.5 and 3 m (8.3 and 9.8 ft) at Sites 4 and 6 in District 8, respectively. The FWD tests also indicated bedrock at a depth of 2.6 m (8.5 ft) at Site 4. The bedrock depths determined from SASW and FWD measurements at Site 4 compare well. However, FWD tests showed no shallow bedrock at Site 6. It is recommended that drilling be made at Site 6 to validate the results.

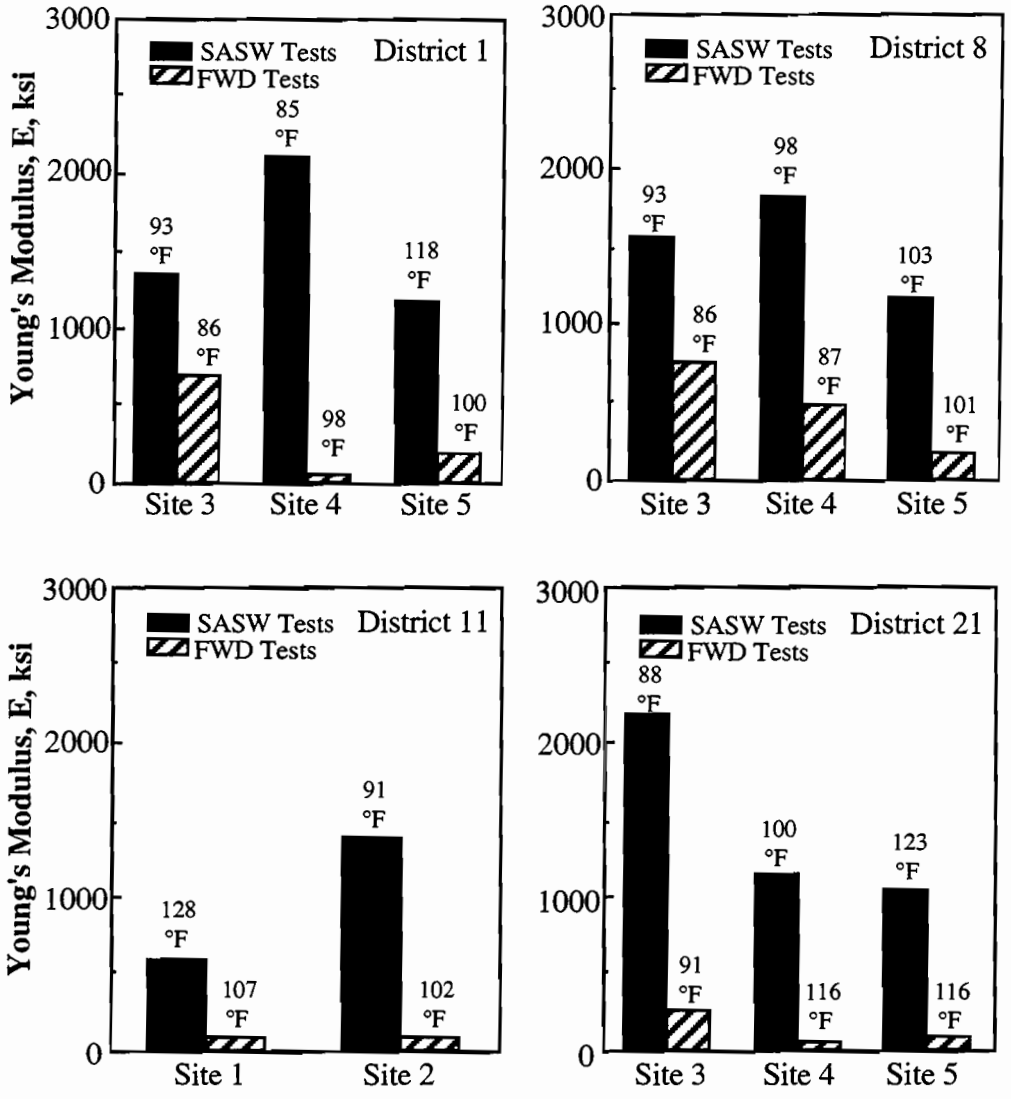

Fig 6.69. Comparison of Young's Modulus of the AC Surface Layer Determined from SASW and FWD Tests at Thick Pavement Sites (t > 3 in.) in Four Districts in Texas (without correction for frequency and temperature).

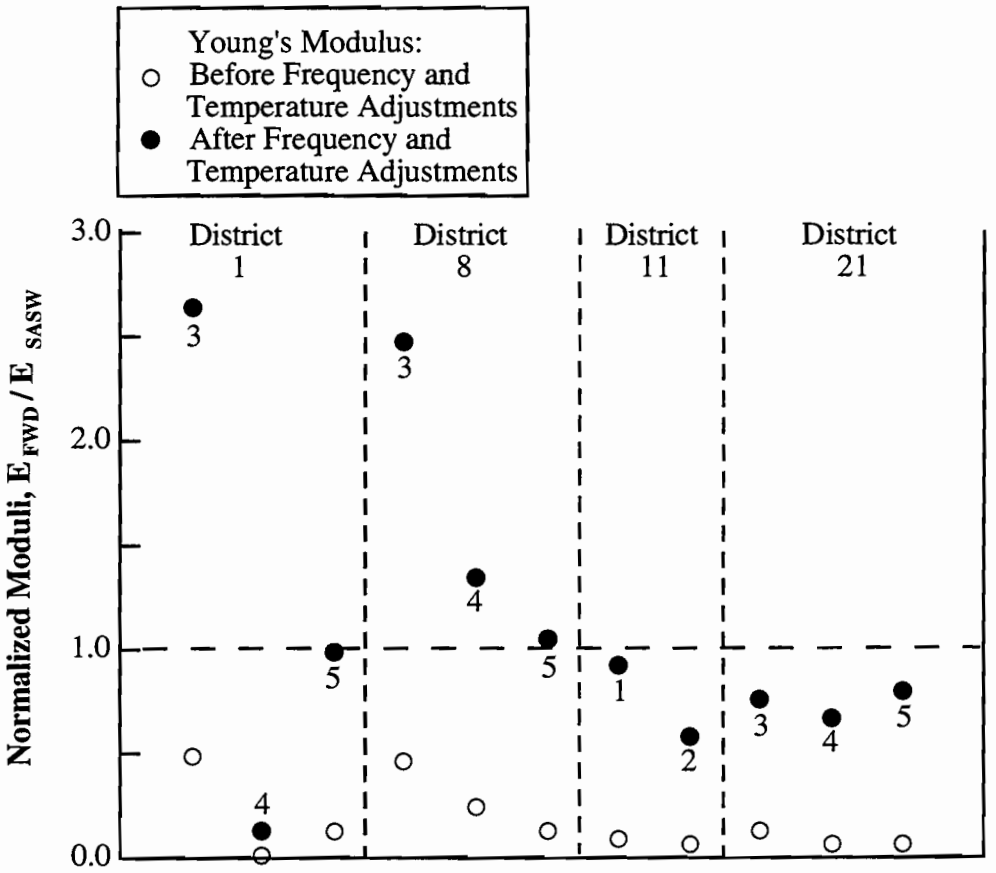

Fig 6.70. Comparison of Young's Modulus of the AC Surface Layer Determined from SASW and FWD Tests before and after Frequency and Temperature Adjustments; Thick Pavement Sites (t > 3 in.).

6.8 Summary

Twenty-four sites in four districts in Texas were tested to evaluate their material profiles. The sites were tested nondestructively using SASW, P-wave and FWD measurements. Results from the different techniques are presented in this chapter.

Results from SASW and P-wave measurements showed that the stiffness of the AC surface layer can be evaluated with confidence. The moduli values from both techniques represent moduli at high frequencies (on the order of 15 kHz, except when a chisel was used to generate the wave energy in the P-wave tests). These moduli have to be corrected for frequency if they are to be used in pavement design. The correction factor for frequency is shown in Fig. 5.34. It should be mentioned that the unconstrained wave velocity was used in the calculations of Young's moduli from the P-wave measurements. In the future, some work should be directed towards modeling the P-wave tests on AC layers as generating plate waves in the AC layer. This model might improve the correlations shown in this work because plate waves in AC layers will have slightly higher velocities than the unconstrained compression waves assumed in this work.

Young's moduli of the subgrade determined from SASW measurements were consistently higher than those determined from FWD tests. This difference seems to be due, in large part, to the larger strains involved with the FWD test (nonlinear behavior). The subgrade moduli from SASW and FWD tests compare reasonably well after adjusting the moduli for the effect of strain as suggested by Miner (1991). A factor of 0.75 was used to adjust (lower) the subgrade moduli from SASW tests to compare with those from FWD tests.

Young's moduli of the uncemented granular base layers determined from SASW measurements were also higher than those determined from FWD tests. However, scatter in the data prevented a meaningful comparison's being made. The average value of the normalized modulus, E_{FWD} / E_{SASW}, was equal to 0.59. It seems reasonable that this difference is also due, in part, to the higher strains generated in the FWD test.

Young's moduli of thick AC layers (t > 7.6 cm (3 in.)) from SASW and FWD tests compare relatively well after adjusting for temperature and frequency effects (average within 10%). At pavement sites with thin AC surface layers (t ≤ 7.6 cm (3 in.)), a comparison of Young's moduli of the AC layers from SASW and FWD tests could not be made due to the insensitivity of the FWD method in evaluating the stiffness of the AC layer. Although high frequencies were not generated to sample the AC layer in the SASW tests at thin pavement sites, one could still obtain a reasonable estimate of the stiffness of the AC layer from the initial (short wavelength) part of the experimental dispersion curve. However, at many sites with thin AC layers, P-wave measurements were successfully used to evaluate the surface layer.

CHAPTER SEVEN
SUMMARY, CONCLUSIONS AND RECOMMENDATIONS

7.1 Summary

Nondestructive tests are used in engineering practice to evaluate the material stiffnesses of pavement systems and soil sites. Nondestructive tests include wave propagation methods and deflection basin methods. An extensive amount of research has been conducted in recent years to understand the applicability and limitations of these methods. This work continues in this area of research and deals primarily with the Spectral-Analysis-of-Surface-Waves (SASW) method, a wave propagation method, and the Falling Weight Deflectometer (FWD) method, a deflection basin method. The thrust of this work is the use of these methods as reliable tools to nondestructively test pavement systems.

The SASW method relies on the generation and detection of dispersive surface waves. This is achieved by placing two (or more) vertical receivers on the ground/pavement and monitoring the response of the surface due to the passage of surface waves. Thus, the method is nondestructive and nonintrusive in nature. In addition, SASW testing can be performed directly on either the subgrade or the base before the surface layer is placed. On the other hand, the FWD method involves measurements of a deflection basin at specified receiver spacings from the source after placement of the surface layer. The modulus of elasticity of the existing layers is backcalculated by matching the measured deflection basin with an analytically calculated one.

In this research study, SASW, FWD and compression wave (P-wave) tests were employed at flexible pavement sites: 1) at the Texas Transportation Institute test facility in Bryan, Texas, 2) at a newly constructed site on Loop 1 in Austin, Texas, and 3) at 24 pavement sites in Districts 1, 8, 11 and 21 in Texas. The

objective was to improve field testing capabilities in relation to testing flexible pavement systems and to compare SASW results with those of other in situ techniques such as the FWD method. The elements which were primarily investigated were: 1) the selection and performance of high-frequency sources and receivers for SASW testing of asphalt concrete (AC) pavements, 2) the effect of temperature and frequency on the SASW and FWD measurements of AC pavements, and 3) the effect of shallow depth to bedrock on the backcalculated moduli of the subgrade layer from each method.

7.2 Conclusions

The following conclusions are based on SASW, FWD and P-wave tests performed on AC pavements in Texas.

1. High-frequency sources are needed to sample the asphalt concrete surface layer. Piezoelectric sources (V-meter and WR Model F-7 shaker) generated higher frequencies than impact sources (small hammers) did, especially at elevated pavement temperatures (T > 27° C (80° F)). Under these conditions, piezoelectric sources are recommended as high-frequency sources to sample the AC layer.

2. The SASW method is sensitive to the variation in stiffness of the AC surface layer. The method can be applied to evaluate the stiffness of the AC layer under different climatic conditions, and the variation of stiffness of the AC layer with time. However, the SASW method cannot be used to evaluate the stiffness of thin (thickness < 5.1 cm (2 in.)) AC surface layers.

3. Reflections from pavement boundaries are manifested by fluctuations in the experimental SASW dispersion curves at wavelengths sampling the surface layer. Employment of exponential windows reduces the fluctuations generated by the reflected waves. However, care should be exercised when applying exponential windows to preserve the signal associated with the direct surface waves. It is

recommended that a measurement with a uniform window be performed in conjunction with a measurement using exponential windowing to identify the general trend of the phase shift of the cross power spectrum between the two receivers.

4. In many instances, the phase shifts of the cross power spectra between the two receivers for the forward and reverse profiles showed a mismatch over a limited frequency range in the frequency span used to test. This may be due to a difference in the resonant frequencies of the coupled receiver/pavement systems. It is recommended that the phase shifts for the forward and reverse profiles be averaged in the frequency domain before calculating the average experimental dispersion curve. This averaging process produces a smoother dispersion curve which is felt to more accurately represent the pavement system.

5. In the case of pavements with thin AC surface layers (thickness < 5.1 cm (2 in.)), SASW measurements did not sample the surface layer. Under these conditions, it is recommended that compression wave tests be performed to evaluate the stiffness of the AC surface layer. This stiffness is a key element in the forward modeling process of the SASW test for stiffness evaluation of the base but not of the subgrade.

6. Comparison of Young's moduli of the AC surface layer from SASW and P-wave tests on Loop 1 and other sites showed that, for all practical purposes, the unconstrained compression wave velocity is being measured in the P-wave tests.

7. Comparison of Young's moduli (E) of the AC material from SASW, FWD and resonance tests on cylindrical specimens showed that the stiffness of the AC material is frequency (f) dependent. A log(E)-log(f) plot showed a nearly linear relationship between the stiffness of the AC material and the measurement frequency. The stiffness of the AC material is more frequency dependent at higher temperatures. A potential frequency adjustment curve (Fig. 5.34) is suggested.

The corrected values of moduli using Fig. 5.34 compare closely with normalized moduli suggested by the AASHTO guide (1986) at temperatures equal to or less than 38° C (100° F). However, at temperatures above 38° C (100° F), the AASHTO guide underestimates the in-situ moduli which have been evaluated by the SASW test and are corrected for frequency. This difference is thought to result from a strain effect which is probably inherent in the tests used to develop the AASHTO guide.

8. The subgrade moduli determined from SASW tests are usually higher than those which have been determined from FWD tests. The subgrade moduli from the two techniques compare reasonably well if the moduli are adjusted for the effect of strain (nonlinear effect). The suggested adjustment factor for SASW moduli is equal to 0.75 to represent moduli at a strain of 0.007% associated with FWD tests as proposed by Miner (1991).

9. The depth to bedrock can be predicted from SASW measurements as was the case for measurements on Loop 1. The depths to bedrock determined from SASW tests compare reasonably well with the depths determined from the FWD tests using the procedure suggested by Chang (1992) and Seng (1992). However, the depth to bedrock can be determined from the FWD time histories provided the shear wave velocity of the subgrade is known and the FWD time history is recorded for about 200 ms; both of these are not usually the case. As a result, SASW tests can be employed as an independent measurement for predicting the depth to bedrock which is sometimes required in the analysis of the FWD data. The depth to bedrock should be taken into account when bedrock is within about 1.5 to 12 m (5 to 40 ft) of the surface for proper backcalculation of Young's modulus of the subgrade from FWD tests (dynamic amplification).

10. For pavement systems where a stiff layer is encountered on the surface, the 2-D model based on plane Rayleigh wave propagation is not a good model from which to obtain the shear wave velocity profile, particularly the shear wave velocity of the base layer. The fundamental mode of vibrations is often not the one

measured in the field. Under these conditions, a 3-D model (Chang, 1991; Foinquinos, 1991) should be used to obtain the shear wave velocity profile. The 3-D model takes into account all of the types of waves generated during SASW testing, and it models more realistically the field setup involved in SASW testing.

11. Based on the authors' experience in SASW testing on pavement sites, a simplified procedure is suggested to obtain the average subgrade stiffness without performing the forward modeling process. In the simplified procedure, the measured wave velocities of the subgrade from receiver spacings of 3, 6.1 and 9.1 m (10, 20 and 30 ft) are averaged and reasonably represent the shear wave velocity of the subgrade layer. There is approximately a 10% increase in the apparent wave velocity of the subgrade due to the stiffer AC surface layers, which fortuitously adjusts the surface wave velocity to the shear wave velocity.

7.3 Recommendations

The authors believe that future work is needed in the following areas:

1. An experimental model for SASW tests under carefully controlled conditions should be constructed. The model should consist of horizontal layers of known and varying stiffnesses and thicknesses. The model would serve to study the following aspects:

a. the effect of reflected waves from the interfaces between the existing horizontal layers on the measured dispersion curves,

b. the behavior of the measured dispersion curve at wavelengths where there is a large velocity contrast between two adjacent layers,

c. the employment of exponential windowing as a tool to minimize the fluctuations observed in the measured dispersion curve, and

d. the performance of theoretical models used in the generation of theoretical dispersion curves for an assumed material profile.

2. The stiffness of the asphalt concrete material is frequency dependent. The suggested frequency adjustment curve (Fig. 5.33) needs more research to validate. This can be achieved in two ways:

a. Asphalt concrete cylinders under temperature-controlled conditions can be tested in a torsional resonant column device at a variable frequency to cover the low-frequency range. SASW measurements should be performed in the field on the same asphalt at different times of the year (wide range in temperatures) to cover the high-frequency range.

b. Longitudinal and torsional resonance tests can be performed on asphalt concrete cylinders of different lengths under temperature-controlled conditions. The resonant frequencies of the cylinders are a function of their lengths at a specific temperature. Using cylinders of different lengths, one ensures the determination of Young's and shear moduli of the AC material under a wide range of frequencies.

3. More SASW and FWD tests should be performed on pavement sites where the bedrock depth is believed to be shallow. The objective is to validate the determination of the bedrock depth from SASW and FWD tests as suggested by Chang (1992) and Seng (1992). The time record length in the FWD tests should be extended beyond the 60-ms time length used in FWD tests by the Texas Department of Transportation (TxDOT).

REFERENCES

Alexander, D.R., S. D. Kohn, and W. P. Grogan (1989), "Nondestructive Testing Techniques and Evaluation Procedures for Airfield Pavements," in *Nondestructive Testing of Pavements and Back-calculation of Moduli*, STP 1026, A. J. Bush III and G. Y. Baladi (eds.), ASTM, Philadelphia, pp. 502-524.

American Association of State Highway and Transportation Officials, (1986), "Temperature-Deflection Corrections for Asphalt Concrete," Appendix L, *AASHTO Guide for Design of Pavement Structures*, Washington, D.C.

Ballard, R. F., Jr., (1964), "Determination of Soil Shear Moduli at Depth by In Situ Vibratory Techniques," Waterways Experiment Station, Miscellaneous Paper No. 4-691, December.

Bay, J. A., and K. H. Stokoe, II, (1990), "Field Determination of Stiffness and Integrity of PCC Slabs Using the SASW Method," *Proceedings*, Nondestructive Evaluation of Civil Structures and Materials, University of Colorado, pp. 71-85.

Bay, J. A., and K. H. Stokoe, II, (1992), "Field and Laboratory Determination of Elastic Properties of PCC Using Seismic Techniques," *Transportation Research Record*, Washington, D.C.

Bolt, B. A., (1976), *Nuclear Explosions and Earthquakes*, W. H. Freeman and Co., San Francisco, 309 pp.

Chang, D. W., (1991), "Nonlinear Effects on Dynamic Response of Pavements Using the Nondestructive Testing Techniques," doctoral dissertation, The University of Texas at Austin.

Chang D. W., J. M. Roesset, and K. H. Stokoe, II, (1992), "Nonlinear Effects in Falling Weight Deflectometer Tests," *Transportation Research Record*, Washington, D.C.

Chang D. W., Y. V. Kang, J. M. Roesset, and K. H. Stokoe, II, (1992), "Effect of Depth to Bedrock on Deflection Basins Obtained with Dynaflect and FWD Tests," *Transportation Research Record*, Washington, D.C.

Dobrin, M. B., (1988), *Introduction to Geophysical Prospecting*, 4th Edition, McGraw-Hill, New York.

Elmore, W. C., and M. A. Heald, (1969), *Physics of Waves*, Dover Publications, Inc., New York, 477 pp.

Ewing, W. M., W. S. Jardetsky, and F. Press, (1957), *Elastic Waves in Layered Media*, McGraw-Hill Book Co. Inc., New York, 380 pp.

Foinquinos, R. M., (1991), "Analytical Study and Inversion for the Spectral Analysis of Surface Waves Method," master's thesis, The University of Texas at Austin.

Fuhriman, M. D., (1993), "Crosshole Seismic Tests at Two Northern California Sites Affected by the 1989 Loma Prieta Earthquake," master's thesis, The University of Texas at Austin.

Fry, Z. B., (1965), "Dynamic Soils Investigations Project Buggy, Buckboard Mesa Nevada Test Site, Mercury, Nevada," Waterways Experiment Station, Miscellaneous Paper No. 4-666, January.

Haskell, N. A., (1953), "The Dispersion of Surface Waves in Multilayered Media," *Bulletin of the Seismological Society of America*, Vol. 43, pp. 17-34.

Heisey, J. S., K. H. Stokoe, II, W. R. Hudson, and A. H. Meyer, (1982), "Determination of In Situ Shear Wave Velocities from Spectral Analysis of Surface Waves," Research Report 256-2, Center for Transportation Research, The University of Texas at Austin.

Henkelom, W., and C. R. Foster, (1960), "Dynamic Testing of Pavements," *Journal of the Soil Mechanics and Foundations Division*, ASCE, Vol. 86, No. SM1, pp. 1-28.

Henkelom, W., and J. G. Klomp, (1962), "Dynamic Testing as a Means of Controlling Pavements During and After Construction," *Proceedings*, International Conference on Structural Design of Asphalt Pavements, Ann Arbor, Michigan, pp. 495-510.

Hiltunen, D. R., and R. D. Woods, (1990), "Variables Affecting the Testing of Pavements by the Surface Waves Method," *Transportation Research Record No. 1260*, Washington, D.C., pp. 42-52.

Hoar, R. J., (1982), "Field Measurement of Seismic Wave Velocity and Attenuation," doctoral dissertation, The University of Texas at Austin.

Jones, R., (1958), "In Situ Measurements of the Dynamic Properties of Soil by Vibration Methods," *Geotechnique*, Vol. 8, No. 1, March.

Kausel, E., and J. M. Roesset, (1981), "Stiffness Matrices for Layered Soils," *Bulletin of the Seismological Society of America*, Vol. 71, No. 6, pp. 1743-1761.

Kim, D. S., (1991), "Deformational Characteristics of Soils at Small to Intermediate Strains from Cyclic Tests," doctoral dissertation, The University of Texas at Austin.

Lee, S. W., J. P. Mahoney, and N. C. Jackson, (1988), "Verification of Backcalculation of Pavement Moduli," *Transportation Research Record No. 1196*, Washington, D.C., pp. 85-95.

Mamlouk, M. S., (1985), "Use of Dynamic Analysis in Predicting Field Multilayer Pavement Moduli," *Transportation Research Record No. 1043*, Washington, D.C., pp. 113-119.

Miner, R. F., (1991), "The Falling Weight Deflectometer and Spectral Analysis of Surface Waves Test for Characterizing Pavement Moduli: A Case Study," master's thesis, The University of Texas at Austin.

Mok, Y. J, (1987), "Analytical and Experimental Studies of Borehole Seismic Methods," doctoral dissertation, The University of Texas at Austin.

Nazarian, S., K. H. Stokoe, II, and W. R. Hudson, (1983), "Use of Spectral Analysis of Surface Waves Method for Determination of Moduli and Thicknesses of Pavement Systems," *Transportation Research Record No. 930*, Washington, D.C, pp. 38-45.

Nazarian, S., (1984), "In Situ Determination of Elastic Moduli of Soil Deposits and Pavement Systems by Spectral-Analysis-of-Surface-Waves Method," Dissertation submitted in partial fulfillment of the Doctor of Philosophy Degree, The University of Texas at Austin.

Nazarian, S., and K. H. Stokoe, II, (1985), "In Situ Determination of Elastic Moduli of Pavement Systems by Spectral-Analysis-of-Surface-Waves Method (Practical Aspects)," Research Report 368-1F, Center for Transportation Research, The University of Texas at Austin.

Nazarian, S., and K. H. Stokoe, II, (1986), "In Situ Determination of Elastic Moduli of Pavement Systems by Spectral-Analysis-of-Surface-Waves Method (Theoretical Aspects)," Research Report 437-2, Center for Transportation Research, The University of Texas at Austin.

Nazarian, S., and K. H. Stokoe, II, (1986), "Effect of Seasonal Prediction on the Moduli of Farm-to-Market Roads," Technical Memorandum, Study No. 936-2, Center for Transportation Research, The University of Texas at Austin.

Patel, N. S., (1981), "Generation and Attenuation of Seismic Waves in Downhole Testing," master's thesis, The University of Texas at Austin.

Rayleigh, L., (1885), "On Waves Propagated along the Plane Surface of an Elastic Solid," *Proceedings*, London Mathematical Society, Vol. 7, pp. 4-11.

Richart, F. E., Jr., J. R. Hall, Jr., and R. D. Woods, (1970), *Vibration of Soils and Foundations*, Prentice-Hall, Inc., Englewood Cliffs, New Jersey, 414 pp.

Rix, G. J., (1988), "Experimental Study of Factors Affecting the Spectral-Analysis-of-Surface-Waves Method," doctoral dissertation, The University of Texas at Austin.

Rix, G. J., J. A. Bay, and K. H. Stokoe, II, (1990), "Assessing In Situ Stiffness of Curing Portland Cement Concrete with Seismic Tests," *Transportation Research Record No. 1084*, Washington, D.C., pp. 8-15.

Roesset, J. M., and K. Shao, (1985), "Dynamic Interpretation of Dynaflect and Falling Weight Deflectometer," *Transportation Research Record No. 1022*, Washington, D.C., pp. 7-16.

Roesset, J. M., D. W. Chang, K. H. Stokoe, II, and M. F. Aouad, (1990), "Modulus and Thickness of the Pavement Surface Layer from SASW Tests," *Transportation Research Record No. 1260,* Washington, D.C, pp. 53-63.

Rwebangira, T., R. G. Hicks, and M. Truebe, (1987), "Sensitivity Analysis of Selected Backcalculation Procedures," *Transportation Research Record No. 1117*, Washington, D.C.

Sánchez-Salinero, I., (1987), "Analytical Investigation of Seismic Methods Used for Engineering Applications," doctoral dissertation, The University of Texas at Austin.

Scrivner, F., and C. H. Michalak (1974), "Linear Elastic Layered Theory as a Model of Displacements Measured within and Beneath Flexible Pavement Structures Loaded By the Dynaflect," Research Report 123-25, Texas Transportation Institute, Texas A&M University, College Station, Texas.

Seng, C. R., (1992), "Effect of Depth to Bedrock on the Accuracy of Backcalculated Moduli Obtained with Dynaflect and FWD Tests," master's thesis, The University of Texas at Austin.

Sheu, J. C., (1987), "Applications and Limitations of the Spectral-Analysis-of-Surface-Waves Method," doctoral dissertation, The University of Texas at Austin.

Sharma, P. V., (1986), *Geophysical Methods in Geology*, 2nd Edition, Elsevier Science Publishing Co., New York, 442 pp.

Sousa, J. B., and C. L. Monismith, (1988), "Dynamic Response of Paving Materials," *Transportation Research Record No. 1136*, Washington, D.C., pp. 57-68.

Stokoe, K. H., II, and R. J. Hoar, (1978b), "Variables Affecting In Situ Seismic Measurements," *Proceedings of the Conference on Earthquake Engineering and Soil Dynamics*, ASCE, Pasadena, California, Vol. II, pp. 919-939.

Stokoe, K. H., II, W. M. Isenhower, and J. R. Hsu, (1980), "Dynamic Properties of Offshore Silty Samples," *Proceedings*, Offshore Technology Conference, OTC 3771, Houston, Texas, pp. 289-302.

Stokoe, K. H., II, S. Nazarian, G. J. Rix, I. Sánchez-Salinero, J. C. Sheu, and Y. J. Mok, (1988), "In Situ Seismic Testing of Hard-to-Sample Soils by Surface Wave Method," *Proceedings*, American Society of Civil Engineers, Specialty Conference on Earthquake Engineering and Soil Dynamics II — Recent Advances in Ground Motion Evaluation, Park City, Utah, pp. 264-278.

Stokoe, K. H., II, W. R. Hudson, and B. F. Miner, (1991), "The Falling Weight Deflectometer and Spectral Analysis of Surface Waves Test for Characterizing Pavement Moduli: A Case Study," Center for Transportation Research, The University of Texas at Austin.

Thomson, W. T., (1950), "Transmission of Elastic Waves Through a Stratified Solid," *Journal of Applied Physics*, Vol. 21, pp. 89-93.

Uddin, W., A. H. Meyer, W. R. Hudson, and K. H. Stokoe, II, (1983), "A Structural Evaluation Methodology for Pavements Based on the Dynamic Deflection," Center for Transportation Research, The University of Texas at Austin.

Uzan, J., R. L. Lytton, and F. P. Germann, (1988), "General Procedures for Back-Calculating Layer Moduli," *First Symposium on NDT of Pavements and Back-Calculation of Moduli*, American Society for Testing and Materials, Baltimore, Maryland.